N72 30000

NASA CR-120961

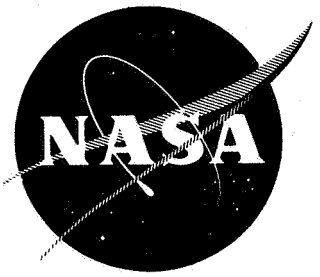

CASE FILE
COPY

FLIGHT VELOCITY INFLUENCE ON JET NOISE OF CONICAL EJECTOR, ANNULAR PLUG AND SEGMENTED SUPPRESSOR NOZZLES

by

J. F. Brausch

GENERAL ELECTRIC COMPANY

prepared for

NATIONAL AERONAUTICS AND SPACE ADMINISTRATION

NASA-Lewis Research Center
Contract NAS 3-15773

1. Report No.	2. Government Accession No.	3. Recipient's Catalog No.
NASA CR-120961		

4. Title and Subtitle	5. Report Date
FLIGHT VELOCITY INFLUENCE ON JET NOISE OF CONICAL EJECTOR, ANNULAR PLUG AND SEGMENTED SUPPRESSOR NOZZLES	August 1972
	6. Performing Organization Code
7. Author(s)	8. Performing Organization Report No.
J. F. Brausch	
	10. Work Unit No.
9. Performing Organization Name and Address	
General Electric Company Aircraft Engine Group Evendale, Ohio 45215	11. Contract or Grant No. NAS 3-15773
	13. Type of Report and Period Covered Contractor Report
12. Sponsoring Agency Name and Address	
National Aeronautics and Space Administration Washington, D. C. 20546	14. Sponsoring Agency Code

15. Supplementary Notes

Project Manager, F. A. Wilcox, Wind Tunnel and Flight Division, NASA Lewis Research Center, Cleveland, Ohio

16. Abstract

An F106 aircraft with a J85-13 engine was used for static and flight acoustic and aerodynamic tests of a conical ejector, an unsuppressed annular plug, and three segmented suppressor nozzles. Static 100 ft. arc data, corrected for influences other than jet noise, were extrapolated to a 300 ft. sideline for comparison to 300 ft. altitude flyover data at M = 0.4. Data at engine speeds of 80 to 100% (max dry) static and 88 to 100% flight are presented. Flight acoustic data are presented both as measured and corrected to standard day (59°F, 70% RH) to consistent 300 ft. altitude and to consistent flight speed of M = 0.4. Flight velocity influence on noise is shown on peak OASPL & PNL, PNL directivity, EPNL & chosen spectra. General trends of flight velocity influence, applicable to all nozzles, are not present. Peak OASPL & PNL plus EPNL suppression levels are included showing slightly lower flight than static peak PNL suppression but greater EPNL than peak PNL suppression. Aerodynamic performance was as anticipated and closely matched model work for the 32-spoke nozzle.

17. Key Words (Suggested by Author(s))	18. Distribution Statement
Jet Noise Flight Noise Noise Suppression Noise - External Flow Plug Nozzle Segmented Nozzle	Unclassified - unlimited

19. Security Classif. (of this report)	20. Security Classif. (of this page)	21. No. of Pages	22. Price*
Unclassified	Unclassified	267	

* For sale by the National Technical Information Service, Springfield, Virginia 22151

FOREWORD

The data acquisition, reduction and analysis work reported herein was sponsored by the Department of Transportation Contract No. FA-SS-67-7. Preparation of the report was funded by NASA, Lewis, Cleveland Contract NAS3-15773. The author wishes to thank Mr. Barry Horton of General Electric for his work in obtaining the noise measurements and for inputs in description of the data acquisition and reduction systems within this report.

Some of the requirements of NASA Policy Directive NPD 2220.4 (September 14, 1970) regarding the use of SI units have been waived in accordance with the provisions of paragraph 5d of that Directive by the Director of Lewis Research Center. Principle measurements and calculations were made in English units.

TABLE OF CONTENTS

TABLE OF CONTENTS (Concluded)

LIST OF ILLUSTRATIONS

LIST OF ILLUSTRATIONS - Continued

LIST OF ILLUSTRATIONS - Continued

LIST OF ILLUSTRATIONS - Continued

LIST OF ILLUSTRATIONS - Concluded

LIST OF TABLES

SUMMARY

An F106 aircraft with a J85-13 turbojet engine was used for static and flight acoustic and aerodynamic tests of a conical ejector, unsuppressed baseline plug, 32 spoke, 64 spoke, and 12 chute nozzle. The study objective was to evaluate flight velocity influence on noise, primarily on suppression capability in terms of peak PNL and EPNL. In addition, comparisons would be made to the SAE prediction technique for the conical ejector and sufficient information would be accumulated to further investigate the details of flight velocity effect. The purposes of the report were a) to document the method and procedure of test and data acquisition/reduction, b) to disseminate the measurements and c) to show flight velocity influence on gross noise parameters.

Static 100 ft. arc measurements were taken at seven angular locations for engine speeds of 80 through 100% (max dry), corrected for influences other than jet noise and to standard day, then extrapolated to a 300 ft. sideline. Flight measurements were taken with flightline and sideline microphones, for engine speeds of 88 to 100% (max dry) with the aircraft in level 300 ft. altitude flight and at M = 0.4. Flight acoustic data are presented both as measured and corrected to standard day (59° F, 70% RH), to consistent altitude and to consistent flight speed. Comparisons are made on PNL and selected spectra between the 300 ft sideline static data and the measurements under the flight path. Influence of noise sources other than pure jet, including background noise of the J75 at idle, are discussed. Several of the flight measuring days varied considerably from a standard meteorological day and influence of corrections to standard day are discussed. Flight velocity influence on noise is shown in terms of peak OASPL and PNL, PNL directivity, EPNL and chosen spectra.

In general, lower peak PNL suppression was attained in flight than statically when compared on a jet velocity basis. If compared at relative velocity, the 64 and 32 spoke nozzles show only minor suppression loss in flight. All suppressed nozzles experienced greater EPNL suppression than peak PNL suppression due to their more favorable PNL(T) directivity.

Change in noise levels from static to flight is very inconsistent between nozzles, between speed settings and even between angles at the same speed settings for each nozzle. The mechanics of change are varied and complex, generally categorized into major areas of a) change in source noise generation, b) change in directivity, c) Doppler shift and d) dynamic effect. If all changes from static to flight are considered as flight velocity effects, no general conclusions, applicable to all nozzles, can be formed. In some instances, such as the conical ejector nozzles, the full V_R effect as suggested by the SAE prediction procedure is present at peak noise location. However, a much larger effect is seen at inlet angles and a large shift in noise directivity from static to flight is present. In others, as for the 32 spoke high velocity, the static noise levels match the flight, indicating no influence of flight velocity. At low jet velocity the trend is for flight noise to exceed static measurements, indicating a reverse V_R effect or an increase of noise in flight.

The Doppler shift and flight dynamic effect are discussed. Correction by the dynamic effect, in some instances, makes the static data agree more closely to flight, but in others it suggests an even greater V_R and reverse V_R effects must be present to compensate for the dynamic effect.

The static and flight aerodynamic performance losses were fairly high, as anticipated, since the nozzles were not refined for optimum aerodynamic performance. The 32 spoke performance was within $\pm$ 1% of the results from model static and wind tunnel tests.

INTRODUCTION

Need For Technology

One of the most undefined technology regions in the complex problem of jet engine noise is flight velocity effects, particularly in application to mechanically suppressed jet noise. The need for technology is critical. State of the art understanding of noise generation mechanisms and static suppression techniques continually advances as governmental agencies and industry sponsor new research programs. However, little effort has been expended to develop suppressed jet technology in the final flight application.

During development of the American Supersonic Transport, it became evident that jet noise suppressors were required to allow the turbojet powered aircraft to meet noise levels equivalent to those imposed by federal regulations on subsonic aircraft. (ref. 1) Suppression technology was principally developed employing static engine and model test vehicles. The high cost of acquiring flight technology prohibited large scale test programs. Predictions of flight acoustic performance were accomplished by use of static suppressor designs with application of either theoretical flight effects or a combination of theoretical and emperical effects, backed by measurements from current unsuppressed jet powered aircraft.

Both General Electric and NASA recognized the need for additional investigatory programs. Test programs were necessary to develop data to aid in understanding flight velocity effects and to be more cognisant of their implications in flight noise predictions. This becomes particularly evident in considering federal regulations imposing the subjective response ratings of Effective Perceived Noise Level (EPNL). EPNL is a function not only of peak noise but also its tone content and time duration. Thus an understanding of flight velocity effects on directivity of unsuppressed and suppressed noise is required, as well as at the peak noise value.

Purpose of Program

Under the Department of Transportation sponsored Supersonic Transport program (Contract FA-SS 67-7) a three phase study was initiated by General Electric, with the cooperation of NASA, Lewis. The program was to investigate not only flight effects on unsuppressed and suppressed jet noise, but also scaling requirements from model (static) to engine (static). Model acoustic measurements were to be taken using two unsuppressed baseline nozzle geometries and several segmented jet suppressors within an annular plug system. These measurements were to be scaled to J85 engine size and compared to engine measurements on geometrically similar hardware. The engine static measurements would be compared to flight test data acquired using the same J85 engine and jet suppressors on the F106 test vehicle. The engine static and flight noise would be measured by both NASA (Lewis Research Center) and General Electric. NASA would sponsor and conduct the test program and General Electric would take the piggy-back measurements working within the original DOT/SST contract and a follow-on contract after termination of the SST program.

Thus a three phase test effort would complete the study. Data would be available to establish whether baseline and suppressed model jet noise measurements could be scaled directly to engine size. (This is to be documented in a report to DOT late in 1972.) In addition, static and flight engine data would be available to investigate the characteristic influences of flight velocity on baseline and segmented jet suppressor noise.

Objectives of the flight velocity influence study were basically:

a) To determine the magnitude of suppression change from static to flight, particularly with respect to peak perceived noise levels.

b) To determine the level of change from peak PNL suppression to EPNL suppression.

c) To assess the flight velocity influence on an unsuppressed baseline nozzle geometry in relation to the relative velocity effect prescribed by the SAE AIR 876 peak noise prediction procedure (ref. 2).

d) To accumulate data sufficient to further investigate the more detailed flight velocity effects on noise generated by baseline nozzles and segmented jet suppressors.

Purpose of Report

The static and flight test program with the F106 aircraft and J85 engine is part of a continuing NASA, Lewis research effort. General Electric (within the DOT sponsored Program) supplied several nozzle hardware sets and took piggy-back acoustic measurements. As NASA's primary responsibility is technology development and reporting to the scientific community, a contractors report agreement was established, allowing the work effort to be reported in this NASA CR, in lieu of a direct report to the Department of Transportation. Within this context, purposes of the report were defined as follows:

a) To disseminate static and flight basic measurements for baseline and suppressed nozzles.

b) To document test method and procedure.

c) To document method of data acquisition and reduction.

d) To show flight velocity changes on gross parameters such as peak OASPL and peak PNL.

TEST VEHICLE

The acoustic data presented in this report were measured during the operation of an F106 aircraft at the Selfridge Air Force Base, located about 25 miles northeast of Detroit, Michigan. The aircraft was equipped with two auxiliary GE J85-13 engines, one mounted under each wing. Only the right side J85 engine was used for this acoustic test. Figure 1 shows the aircraft in flight with the wing mounted engines. The general test program and operation of the aircraft were under the control and direction of the Lewis (Cleveland) Research Center of NASA.

The J85 engine provides a functional test vehicle for ease of adaptation to various exhaust nozzle geometries, necessary for jet noise research work. Figure 2 is a schematic of the engine with a chart of compressor and turbine blading. Design speed is 16,500 rpm. The photograph in Figure 3 shows the engine mounted in its functional position under the aircraft delta wing. Its cycle is characteristic of basic turbojets and is a good representation of exhaust conditions in the low to medium jet velocity range anticipated of turbojet powerplants considered for SST application.

FIGURE 1 F106 TEST VEHICLE ; J75 MAIN POWERPLANT ; J85'S UNDER WINGS

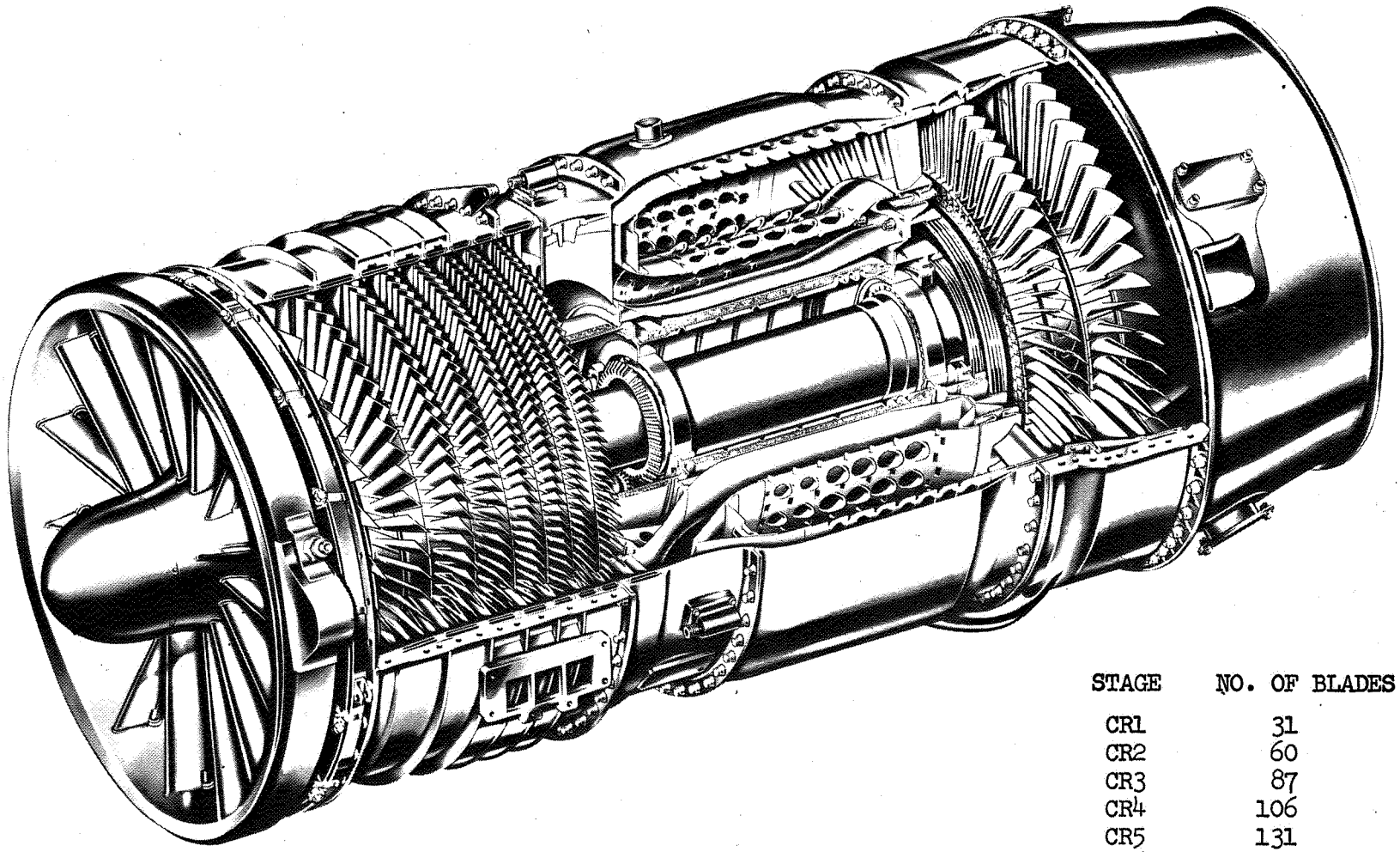

STAGE	NO. OF BLADES
CR1	31
CR2	60
CR3	87
CR4	106
CR5	131
CR6	132
CR7	140
CR8	120
TR1	75
TR2	55

FIGURE 2 CROSS SECTION OF J85 ENGINE

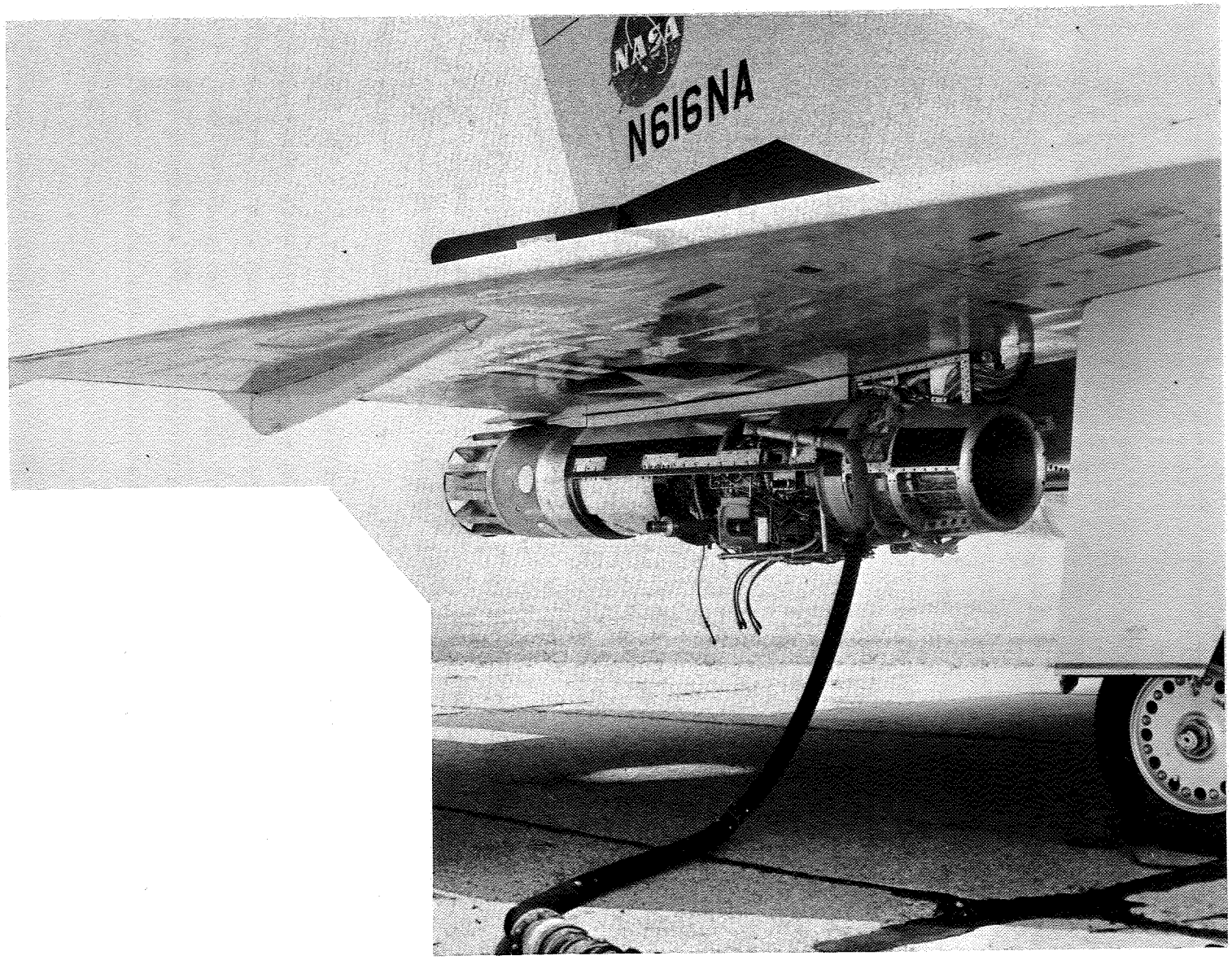

FIGURE 3 J85 ENGINE MOUNTED UNDER F106 WING

SELECTION OF SUPPRESSOR SYSTEM

During the latter phase of the SST program, a high air flow, low take off velocity engine design was identified which was anticipated to meet the FAR-PART 36 subsonic aircraft noise requirements when utilizing a segmented suppressor nozzle. The nozzle system would be similar to the schematic of Figure 4, with the suppressor stowable within the plug. The unsuppressed nozzle throat area would be controlled by variable plug geometry. At takeoff, the suppressor would be deployed from the plug and mate with the translating shroud to form the new throat.

To determine the noise suppression characteristics and corresponding aerodynamic penalties associated with segmented suppressor systems, scale model (approximately .6"D_8) acoustic and aerodynamic test programs were initiated. Within the programs a number of models were tested, not chosen specifically to be the best aero/acoustic performers but to evaluate geometric parameters such as a) number of suppressor elements, b) compactness of element spacing and c) solid spoke versus ventilated chute.

During this same time period, NASA, Lewis was conducting a flight test program, investigating flight acoustics of unsuppressed and suppressed nozzles. With NASA's approval, several of the model designs were selected to be made into engine hardware for J85 static and flight measurements. Those chosen were 32 and 64 spoke suppressors within an annular plug system and a baseline unsuppressed annular plug. Selection was done while the model parametric investigation was in progress, therefore, model suppression levels were not known and refinement was not possible to configure an optimum spoke/plug suppressor design.

Acoustic suppression levels, therefore, were neither expected to be the highest possible within this system, nor were the suppressors anticipated to show high $\Delta PNL/\Delta C_{f_g}$ results. The nozzle designs in themselves were selected by anticipating which would produce good characteristic acoustic data. They represented a suppression concept and a variation of the concept and were only to substantiate the viability of the system in application to the SST.

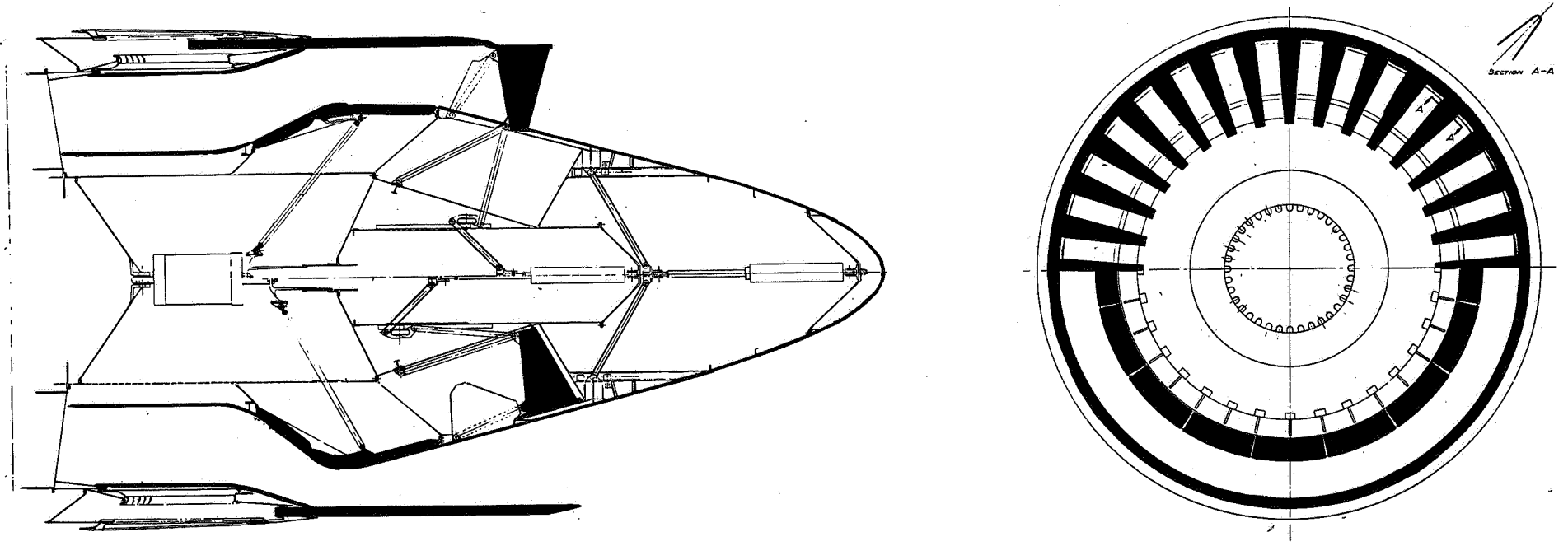

FIGURE 4 ENGINE SCHEMATIC INCORPORATING 32 CHUTE SUPPRESSOR WITHIN AN ANNULAR PLUG NOZZLE

General Electric supplied the new hardware pieces required for the spoke and baseline plug configurations. NASA's available cylindrical ejector nozzle, described in reference 11, when fitted to the conical convergent primary nozzle of the J85 engine, was chosen as the baseline configuration. In addition, NASA had fabricated a 12 chute/plug nozzle with a pointed plug end. It was included in the study and General Electric made a duplicate model nozzle for use in the scaling study.

At the end of the model parametric program (around the time period flight tests were beginning) acoustic performance of the nozzles was known. The model data were scaled to GE4 size (approximate scale factor of 8:1). 300 ft sideline peak PNL suppression is shown as a function of jet velocity in Figure 5, indicating good static performance for the three suppressors and slight PNL suppression for the baseline annular plug. If the model data were scaled to the J85 engine size (approximate scale factor of 2:1) the anticipated suppression levels for the engine velocity range to maximum dry would be as shown in Figure 6. Changes in suppression from the GE4 to the J85 size are due to shifting of spectra levels to areas of different PNL weighting.

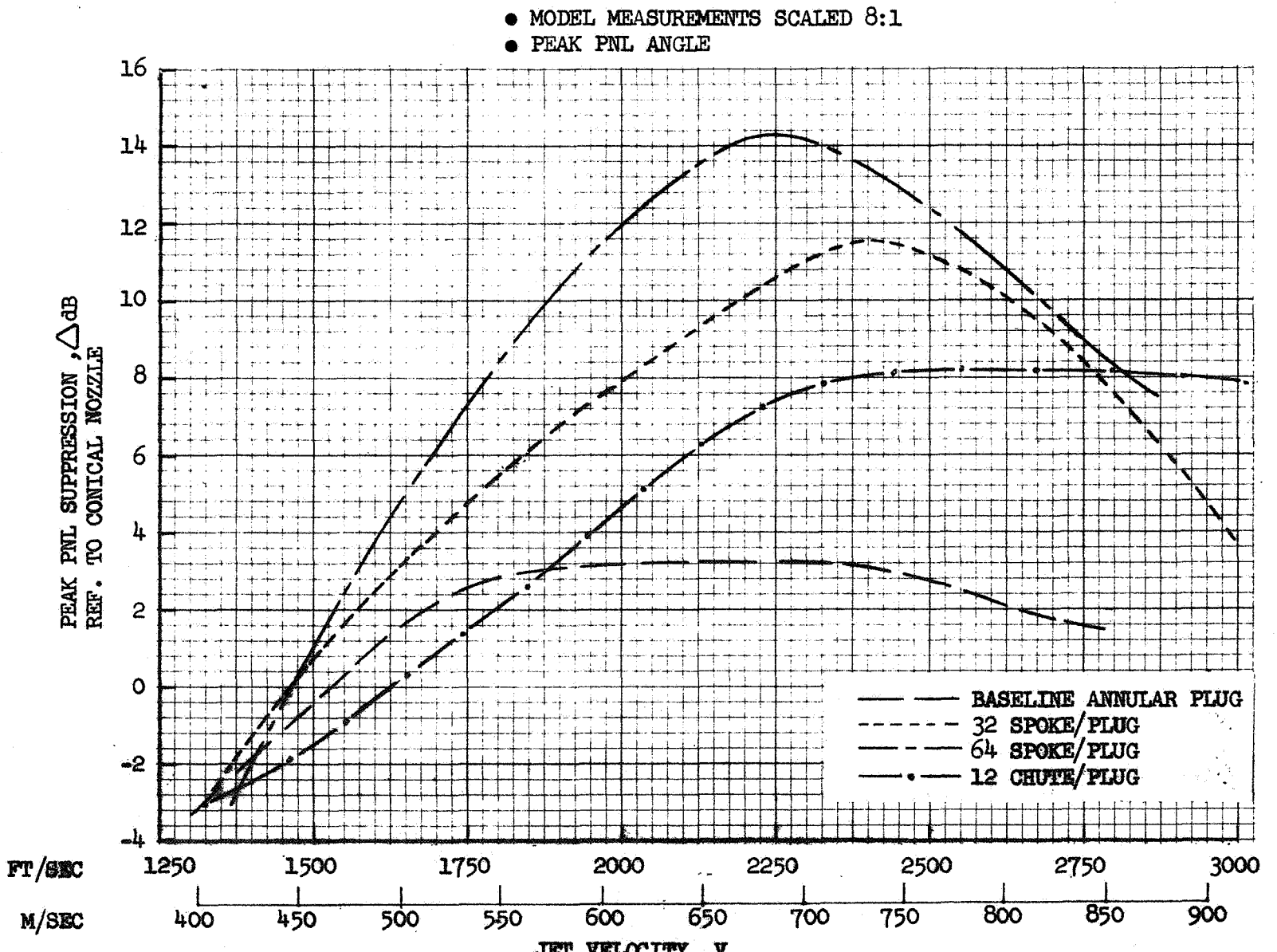

FIGURE 5 MODEL STATIC 300 FT. SIDELINE PEAK PNL SUPPRESSION

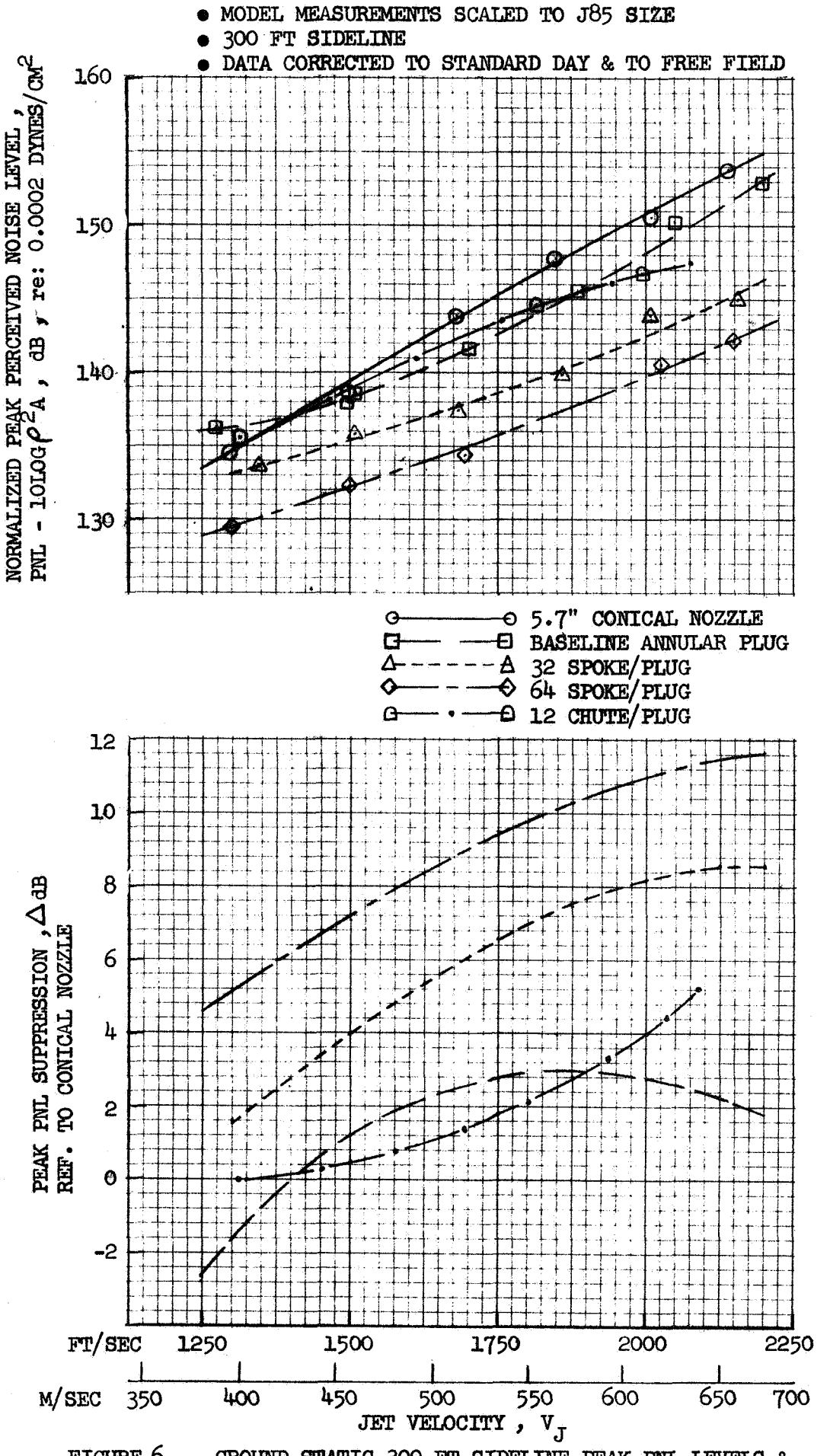

FIGURE 6 GROUND STATIC 300 FT. SIDELINE PEAK PNL LEVELS & SUPPRESSIONS , MODEL MEASUREMENTS SCALED TO J85 SIZE

DESCRIPTION OF TEST HARDWARE

The engine nozzle systems were designed to have a fixed throat area of approximately 110 square inches, selected for T_5 requirements at 100% speed. Each was designed to operate up to maximum dry exhaust cycle, therefore, no special cooling techniques were employed. As the discharge coefficients were different for each nozzle, the effective throat areas changed and varied the attained cycle. Figure 7 shows measured cycle curves, P_{T8}/P_o versus T_{T8}, for each nozzle during static and flight tests.

The nozzle which will be termed, for simplicity throughout this report, as a conical ejector is shown in Figure 8. The system was comprised of a conical convergent primary nozzle with a cylindrical secondary ejector. It pumped cooling flow, equivalent to a corrected 4 to 6% of the primary flow, over the primary nozzle during flight. This nozzle was designed and built by NASA for use in calibrating the thrust measuring system as described in reference 11, and was chosen as baseline unsuppressed reference for this study.

A schematic of the baseline annular plug nozzle is shown in Figure 9a. The throat of the nozzle is just aft of the maximum plug diameter location. A 10° half angle afterbody was chosen with a contoured plug end. The plug forebody (ref. 12) and outer annular nozzle were NASA's hardware. The contoured plug end was supplied by General Electric. This is also the basic plug geometry of the suppressor nozzles.

Figure 9b is a schematic of the 32 and 64 spoke configurations, the annular nozzle of the baseline plug geometry being replaced by a shroud with the segmented suppressor pieces. Geometric throat location is at the exit of the spokes, considerably aft of the baseline plug nozzle throat, to allow the same flow area at the larger annulus area location. Photographs of the 32 and 64 spoke nozzles are shown in Figures 10a and 10b, respectively. Both nozzles were area ratio of 2.0 designs, meaning the total annulus area divided by the flow area equals two, or the blocked area is equivalent to the flow area.

The 32 spoke nozzle has blocker elements of shallow 'V' design with radially tapered sides and therefore each flow element is nearly rectangular in shape. The 64 spoke nozzle elements are solid and radially parallel sided for the

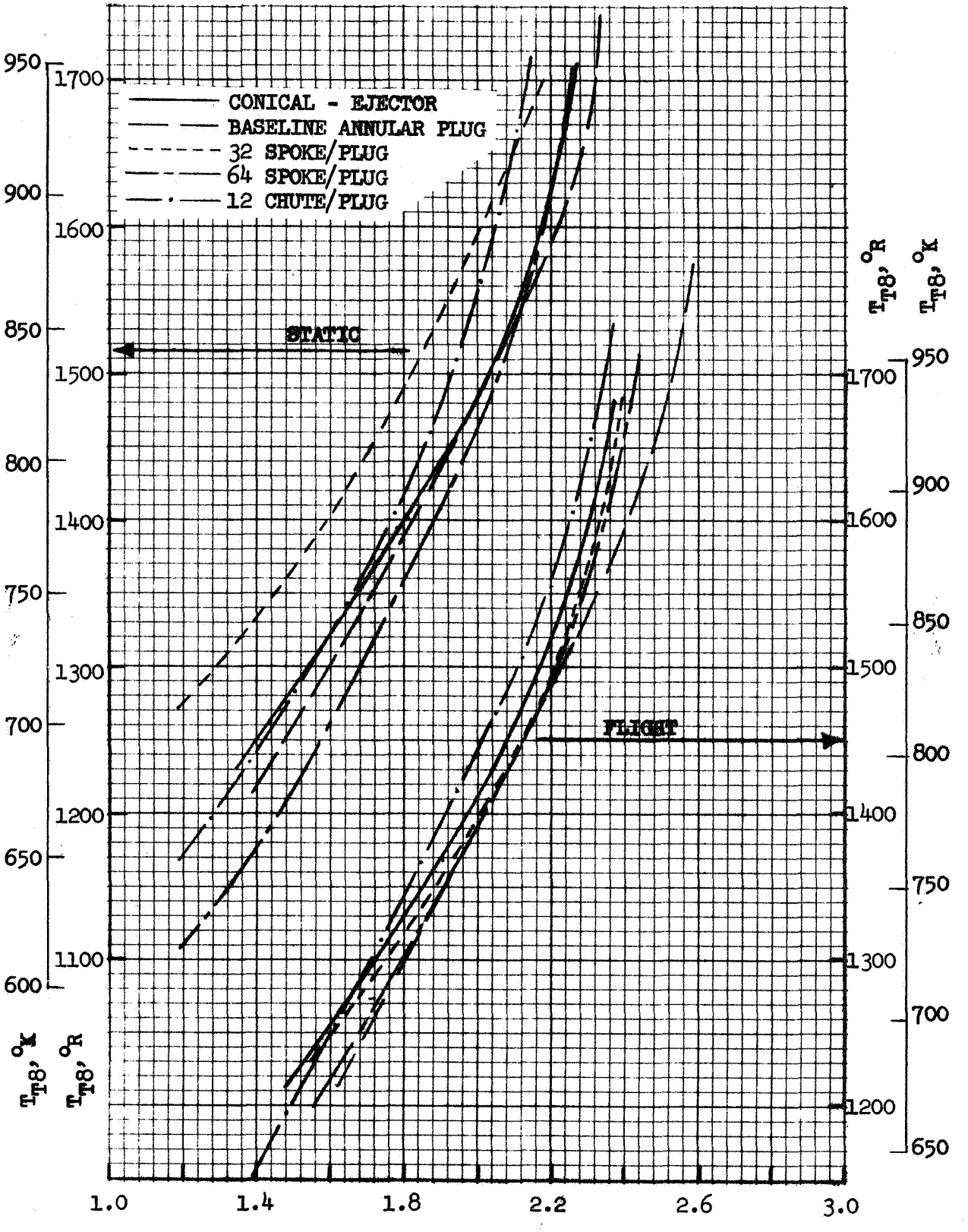

FIGURE 7 J85 STATIC & FLIGHT CYCLES

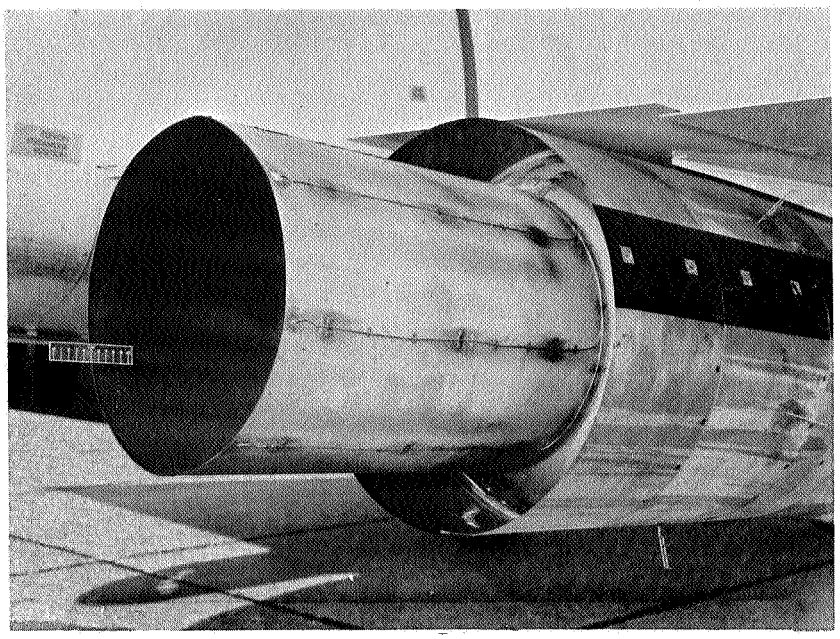

A) REFERENCE NOZZLE ON J85 ENGINE

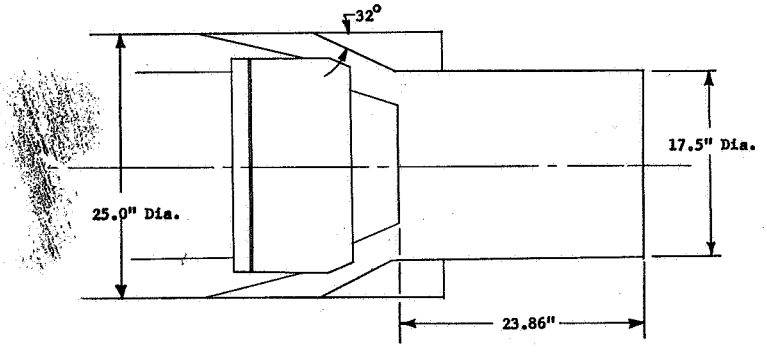

B) SCHEMATIC OF REFERENCE NOZZLE

FIGURE 8 REFERENCE NOZZLE ; CONICAL PRIMARY WITH CYLINDRICAL EJECTOR

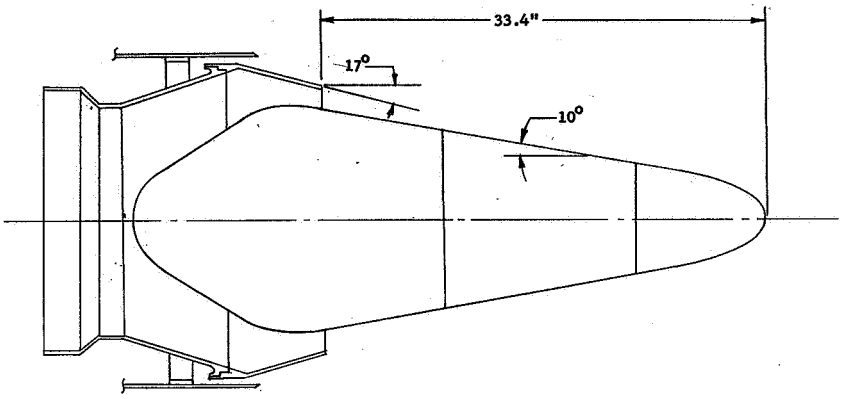

A) BASELINE ANNULAR PLUG NOZZLE

B) 64 SPOKE/PLUG NOZZLE

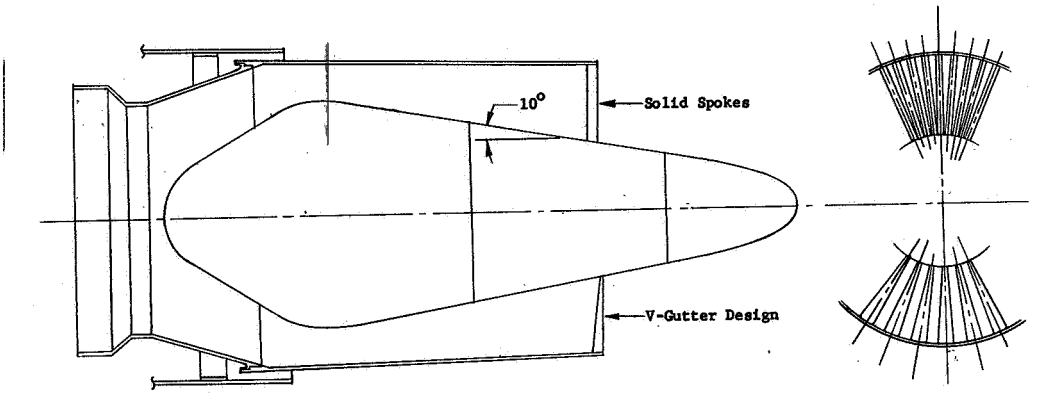

C) 32 SPOKE/PLUG NOZZLE

FIGURE 9 SCHEMATIC OF ANNULAR PLUG , 32 SPOKE/PLUG & 64 SPOKE/PLUG NOZZLES

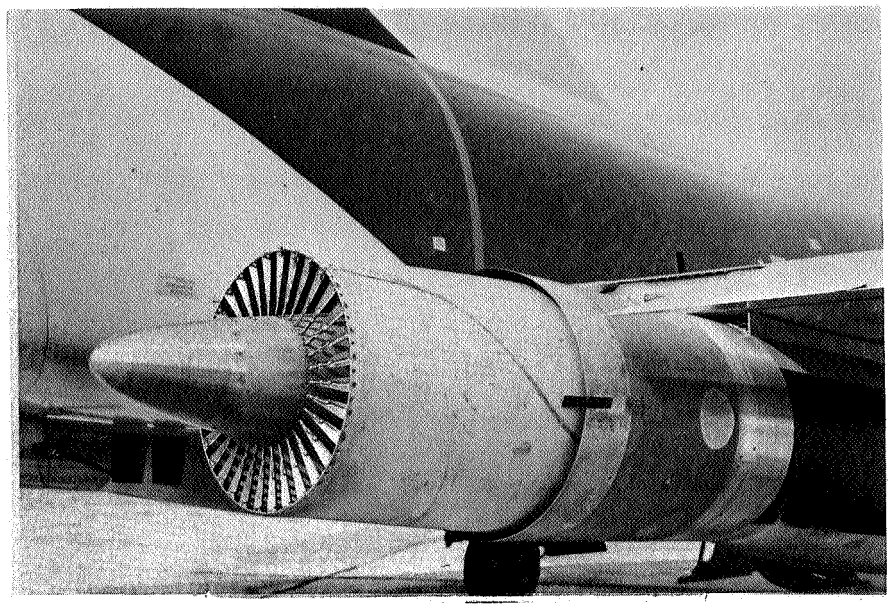

A) 32 SPOKE/PLUG NOZZLE

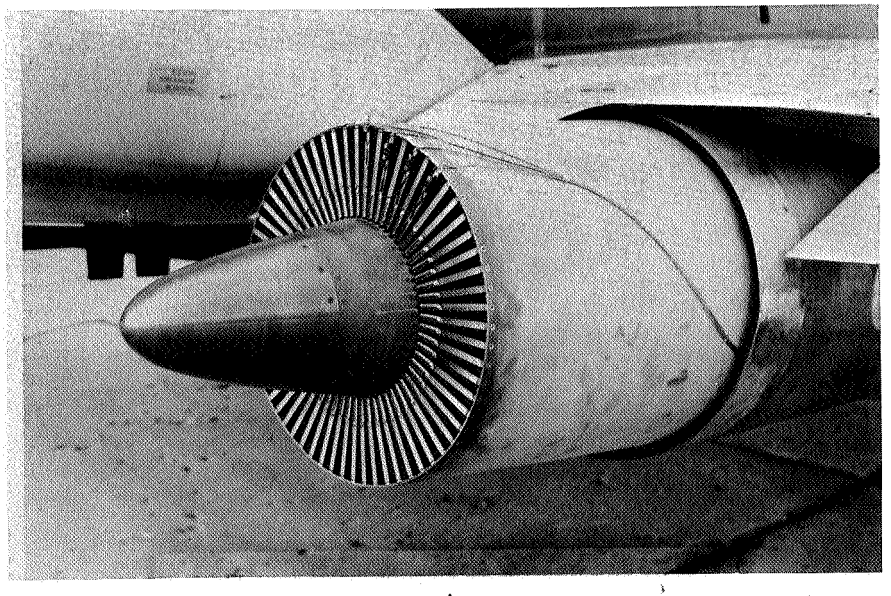

B) 64 SPOKE/PLUG NOZZLE

FIGURE 10 32 & 64 SPOKE/PLUG NOZZLES ON J85 ENGINE

required physical strength of the small cross section, therefore, the flow sections are radially tapered. For both nozzles the elements were designed as blockers rather than chutes. Aerodynamic loss of the nozzles was anticipated to be high as the base areas of the spokes would not be well ventilated. Base pressures would be low, resulting in high base drag loss. As was found from the model program, design of the elements to entrain large amounts of ambient air, as can be done with chutes open to ambient, would ventilate the base area and reduce base drag loss by several percent of the total ΔC_{f_g} loss.

The fifth test nozzle was a 12 chute/plug design shown schematically in Figure 11a and as a photograph in Figure 11b. This nozzle was designed and built by NASA. The internal plug was the same as for the other nozzles but had a pointed plug end, continuing the 10° half angle, in place of the contoured plug end. The nozzle was of area ratio = 3.0, meaning the total annulus area/primary flow area = 3.0 or the blocked area is twice that of the primary flow area. The chutes were of shallow slope in design to allow an easy entrance ramp for entraining ambient flow.

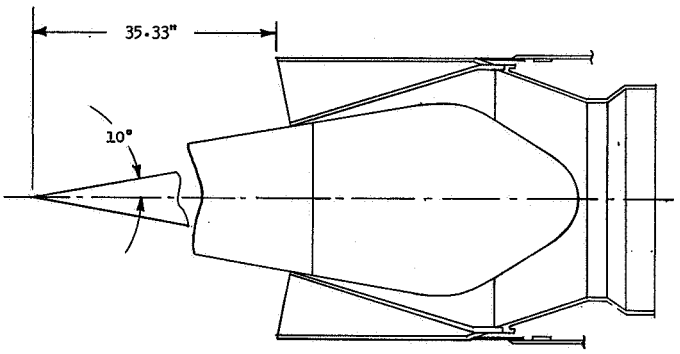

A) SCHEMATIC OF 12 CHUTE/PLUG NOZZLE

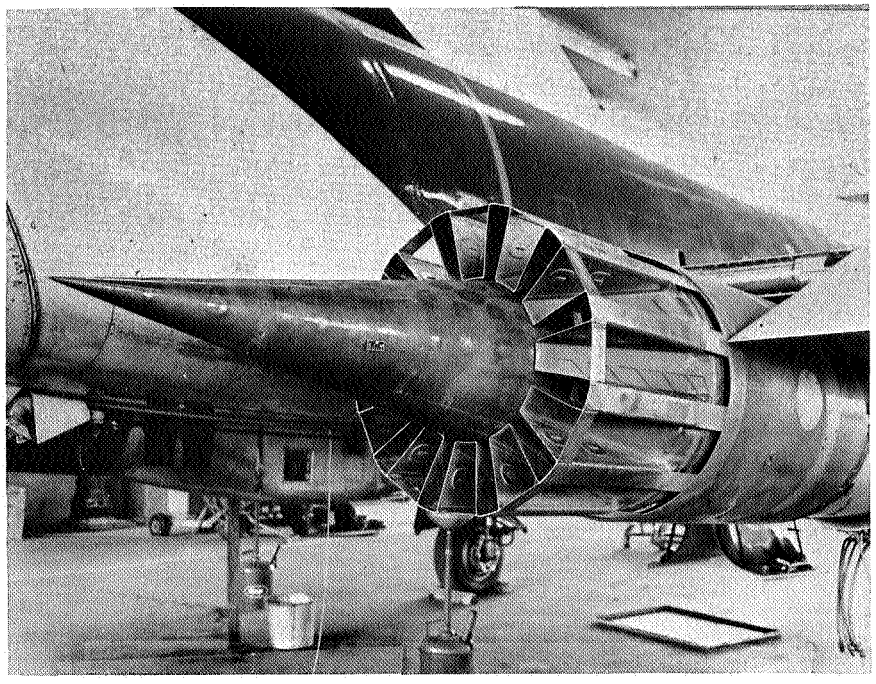

B) 12 CHUTE/PLUG NOZZLE ON J85 ENGINE

FIGURE 11 12 CHUTE/PLUG NOZZLE

TEST PLAN

For each ground static run-up test, a bellmouth inlet was installed on the J85 engine. With the J75 at idle, sound data was to be recorded with the J85 engine operating at nominal speeds of 100, 96, 92, 88, 84, and 80%. These speeds were chosen to provide a sufficiently low engine static jet exhaust velocity to compare to the relative velocity ($V_R = V_{jet} - V_{aircraft}$) of the lowest flight engine speed setting of 88%. The J85 engine was normally held on each point for a period of approximately 2 minutes during which gain levels were set and about 1-1/2 minutes of data were recorded. Repeat power settings were set as special circumstances of the day warranted. Since the J75 furnished power for the aircraft data recording system and for fuel supply pressure to the J85 engine, it was maintained at idle power setting for all of the sound tests. On occasion the J75 was run by itself at idle to establish the background noise levels at all measuring angles.

For flight testing, the bellmonth inlet was replaced by a flight inlet. Test plan for each nozzle was to set nominal J85 engine speeds of 100, 96, 92 and 88% with the J75 at idle and to fly three repetitive passes at each speed while tape monitoring the noise. Background noise levels of the J75 at idle would be measured using only the J75; the J85 shut off.

Altitude of 300 ft. was chosen to minimize variances in noise propagation due to wind gradients and thermal layers. In addition, the fairly short acoustic path lengths (from source to receiver) would help control variance due to high frequency atmospheric absorption.

A consistent flight speed of 260 knots (438 ft/sec) was desired, as it was in the range of lift off/climbout speed considered for the supersonic transport aircraft to which the study results would be applied and was near the minimum drag condition for the F106.

TEST SET-UP

Ground Static Run-Up

The F106 aircraft was positioned on an all concrete taxiway with the exhaust plane of the right hand J85 engine at the center of a 100 ft. arc as shown in Figure 12. Seven microphones were located on the 100 ft. arc at 40°, 80°, 110°, 120°, 130°, 140°, and 150° from the engine inlet axis and at a height equivalent to the exhaust plane centerline height of approximately 63 inches. Portable folding, tripod microphone stands were used with the microphones clamped such that the heads were approximately 6 inches from the stand. In the ground static position of the aircraft, the J85 was canted approximately 4 1/2° with the engine inlet centerline about 14 inches lower than the exhaust centerline. Figure 12 also shows the proximity of the J75 engine and F106 fuselage to the J85 test engine. A photograph of the F106 during ground run-up up test is shown in Figure 13.

Prior to each static of flight test, a frequency response through each microphone system was recorded before going to the field. Upon arrival in the field, the equipment was setup as it would be used during the test and a pre-test pistonphone calibration (124 dB @ 250 Hz) was recorded on each system utilizing a B&K model 4220 pistonphone calibrater. As the test proceeded, the signal gain levels were adjusted for maximum signal to noise ratio for each power setting. A post pistonphone calibration was also recorded immediately following the completion of each test.

Flight

Sound data was recorded at two stations during the level flyovers as per the typical microphone layout in Figure 14a. One microphone was located directly under the flight path and the second was at a 492 ft. (150m) sideline position. Both were positioned 4 ft. above the concrete surface of the taxiways. Two different physical locations on the air force base were used for flight measurements to minimize interference from other aircraft and thereby causing the sideline microphone offset location to change. For flights 146 and 159 the

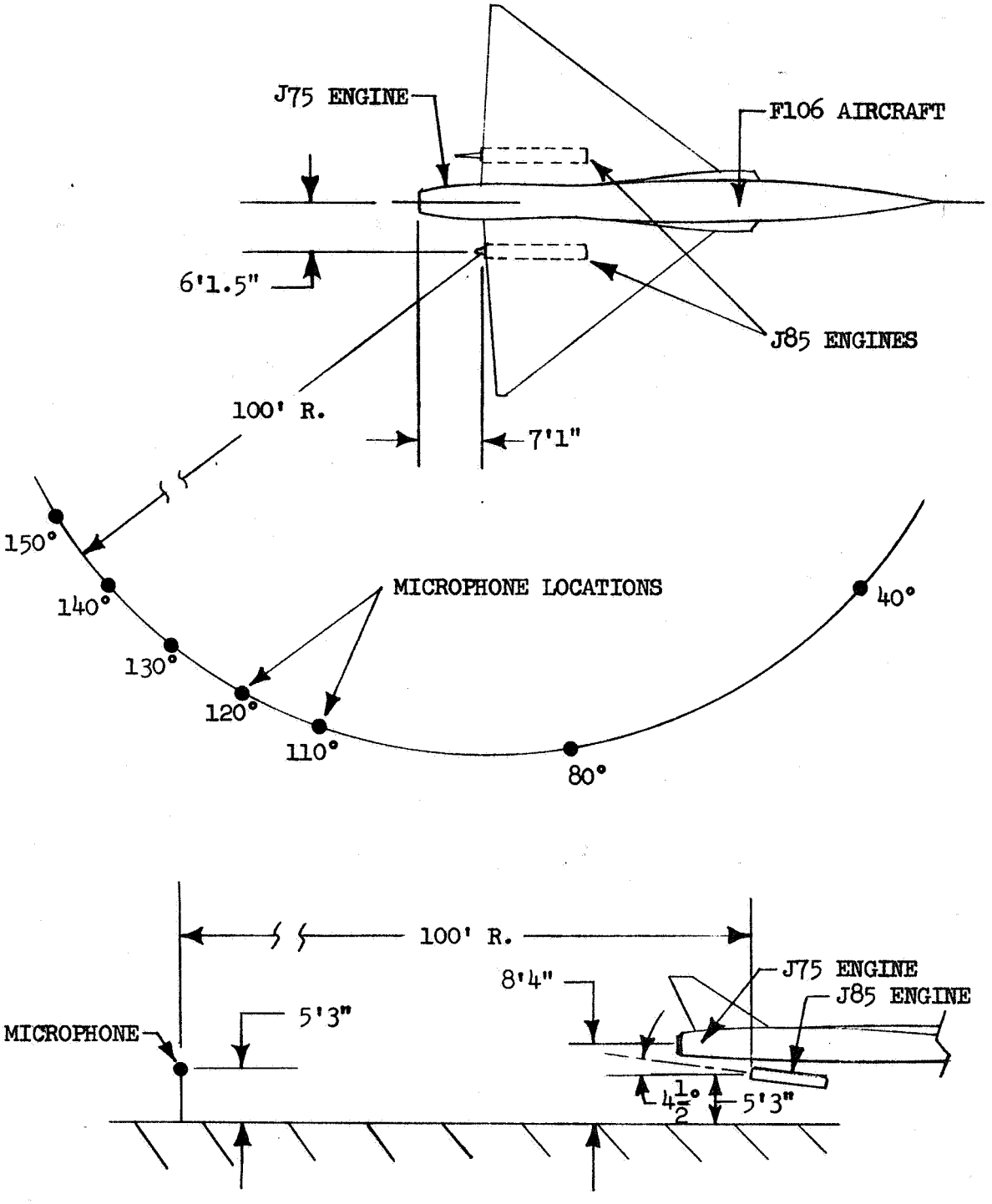

FIGURE 12 F106/J85 GROUND STATIC MICROPHONE LAYOUT

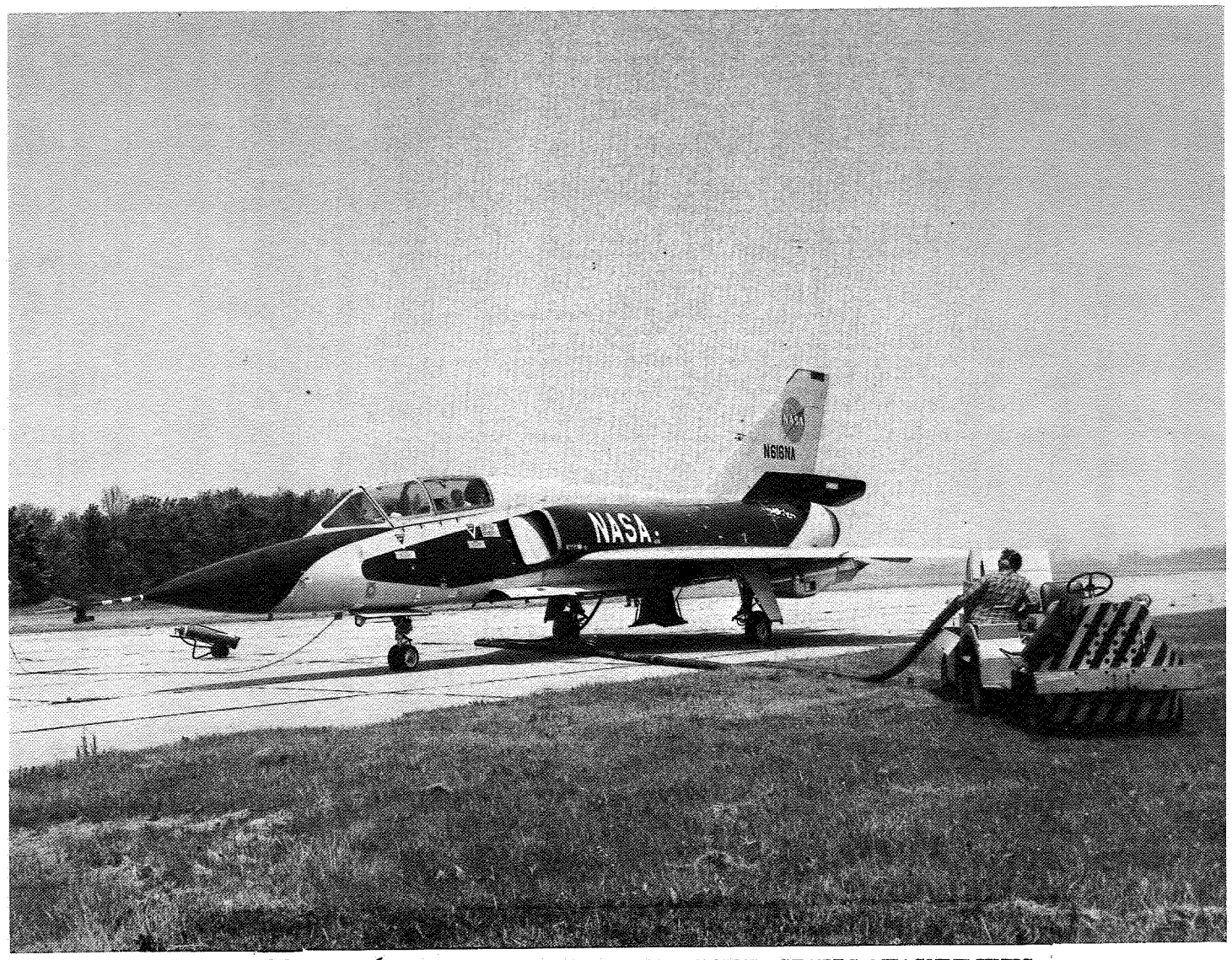

FIGURE 13 F106 AIRCRAFT LOCATED FOR GROUND STATIC MEASUREMENTS

a) LOCATION OF MICROPHONES FOR FLIGHT ACOUSTIC MEASUREMENTS

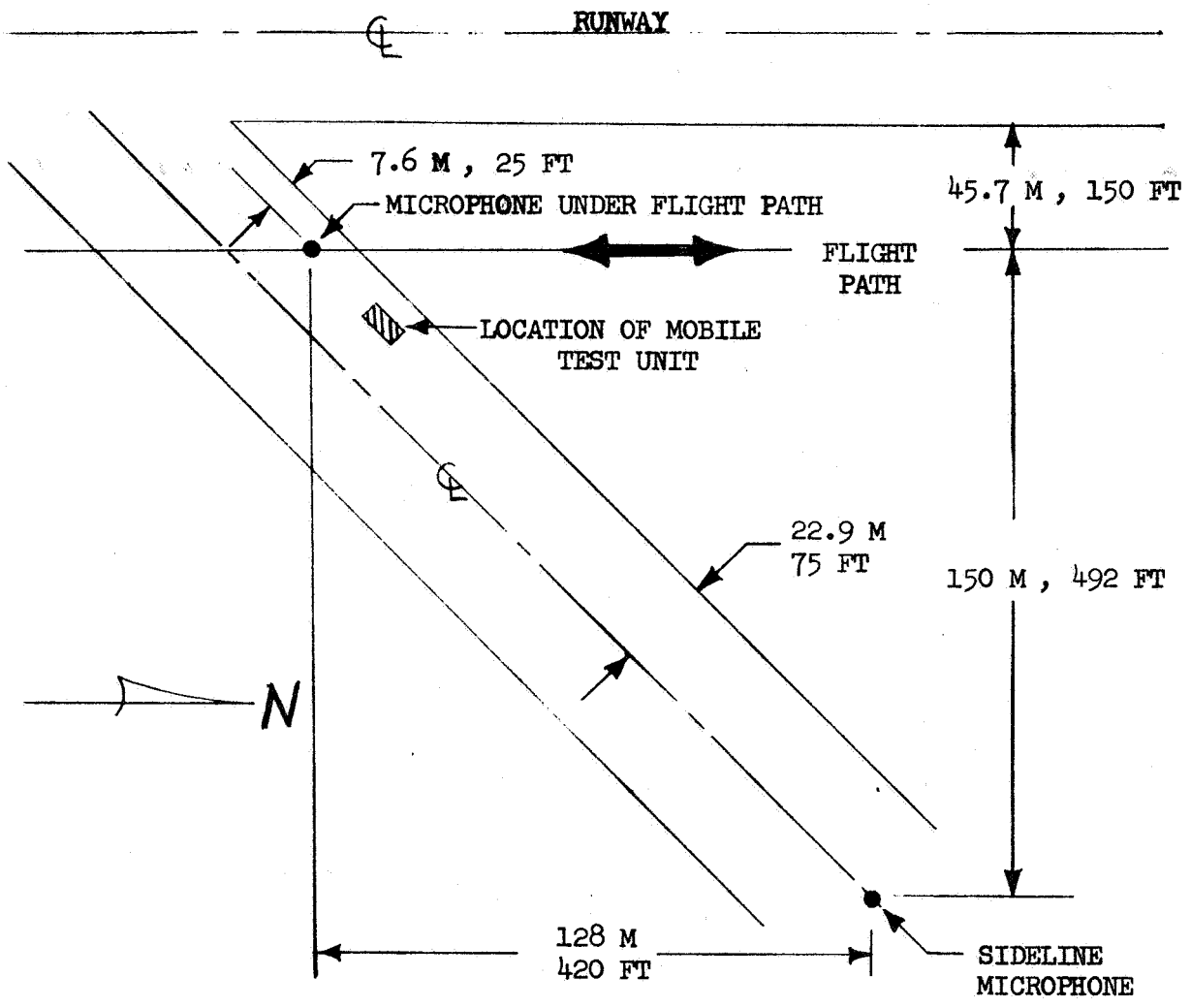

b) AIRCRAFT & ENGINE ANGULAR ORIENTATION IN FLIGHT

A°= 7° AIRCRAFT ANGLE OF ATTACK TO FLIGHT PATH
B°= 4 1/2° ENGINE MOUNT ANGLE RELATIVE TO AIRCRAFT ℄
C°= 2 1/2° RESULTANT ANGLE OF ENGINE RELATIVE TO HORIZON

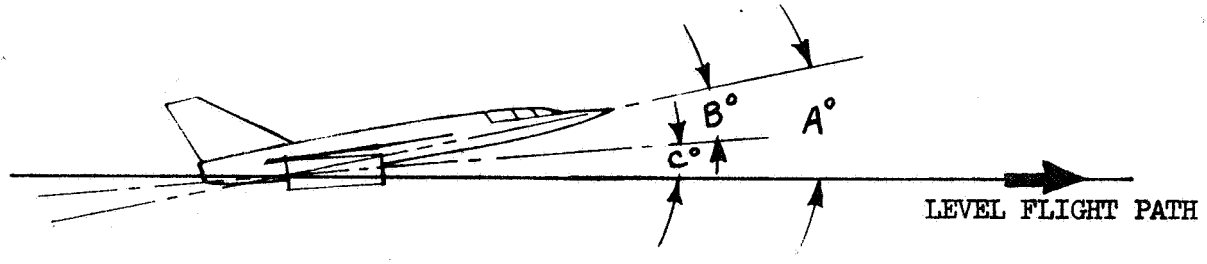

FIGURE 14 MICROPHONE LOCATIONS & AIRCRAFT ORIENTATION FOR FLIGHT MEASUREMENTS

sideline microphone location was in line with the flight path microphone and at a right angle to the flight path. (No sideline data, however, was obtained for flight 146 due to equipment malfunction.) For flights 152, 155 and 170, the sideline microphone was offset 420 ft. (128m) north of the flight path microphone as per Figure 14a to position it over the concrete of the angled taxiway.

The aircraft flight path paralleled the runway, the pilot being guided by concrete markers under the flight path. Direction of flight was consistent during flights, either north to south or south to north, but was changed for different flights.

Figure 14b shows the aircraft and engine angular orientations in flight mode. During level flyover the aircraft was nominally flown at a positive 7° angle of attack to the flight path. The engine being permanently fixed under the wing at a negative 4-1/2 degrees; a final angle of +2-1/2° of the engine centerline relative to the horizon resulted. This resultant angle became important when comparing static noise measurements to equivalent acoustic angle flight measurements.

ENGINE CYCLE MEASUREMENTS

Cycle parameters of the J85 engine, required for acoustic data correlation, were monitored by an onboard data system described in references 11 and 13 during both static and flight tests for each speed setting. These measurements, including thrust, were reduced and supplied by NASA. Cycle parameters of P_{T8} and T_{T8} are quite accurate measurements (ref. 13), and therefore produced accurate ideal jet velocity calculations. V_J is the parameter against which most of the acoustic data was compared.

AIRCRAFT ALTITUDE AND VELOCITY MEASUREMENTS

The aircraft altitude and velocity were taken from the NASA flight data sheets. These parameters were recorded by the front seat pilot immediately after each data pass. The altitude is reported to be the average of information from three sources during the pass:

- o From AFB radar
- o From onboard radio altimeter
- o From onboard pressure altimeter

The indicated airspeed was read as the aircraft passed over the flight path microphone. The estimated accuracy of the reported aircraft velocity and altitude is within $\pm$ 5 knots and $\pm$ 10 ft., respectively.

The aircraft velocity, as indicated by an onboard Mach meter, was also monitored on the aircraft recorder. Accuracy of this parameter is significant because when it is used with overhead time, flight altitude and ambient temperature, it establishes the acoustic angles of noise generation with respect to the receiving microphone. Unsteadiness in aircraft velocity or error in its measurement would accumulate error in the assigned angular locations as the aircraft passes through the more shallow angles approaching or receding from the overhead location. The total error in aircraft axial location would be a maximum of about 40 ft. for a typical 10 ft/second aircraft variance, for the range of distance for which acoustic measurements are used. This is due to the high flight speed and short noise duration and would mislocate acoustic angles by only several degrees.

AIRCRAFT OVERHEAD LOCATION

When recording flight noise data, a separate data channel was used to simultaneously record a 400 Hz voltage pulse. The signal was used, when correlated with the recorded "real time" from the time code generator, to indicate the time at which the aircraft was directly overhead the flight path microphone. The voltage pulse or "blip", induced using an oscillator, was actuated based on visual judgment of a ground observer stationed at the flight path microphone. The system is based purely on human judgment and response and therefore has limitations in accuracy. Variations which may have been introduced are, however, felt not to have any significant influence on the accuracy of results of the acoustic study. Procedural steps in data reduction and assignment of overhead aircraft location tended to eliminate any major human error and average the inconsistencies of aircraft positioning between successive passes at the same engine power setting. This procedure is explained in more detail under ACOUSTIC DATA REDUCTION - FLIGHT.

ACOUSTIC MEASUREMENTS INSTRUMENTATION

Ground Static Run-Up

Each microphone system for the seven ground stations was composed of a one-half inch Bruel & Kjaer (B&K) 4133 microphone cartridge, a 2615 cathode follower, a 2801 power supply, and 300 ft. of coax cable utilizing the 7 pin matching impedence 50 ohm output of the power supply. The type 4133 microphones were pointed at the exhaust plane of the J85 engine, subject to normal incidence of the radiating sound, and with flat response characteristics within the 10KHz frequency range of interest. The output of each 300 ft. coax cable was fed to a 7-channel A-C coupled dB step amplifier, serving to condition the signal gain for maximum signal-to-noise ratio on the recorder. A Lockheed 7-channel FM recorder was used with data recorded at 30-inches per second tape speed. An oscilloscope was used to monitor signal input levels to the tape recorder.

All the static and flight acoustic equipment were operated from a General Electric Company station wagon. The 110V AC power for operation of the microphone systems and recording equipment was provided by a DC to AC converter, operated off the battery/generator system of the station wagon.

Voice identification of each data point was alternated with noise recording of the 40° to inlet microphone.

Flight

Two battery powered field microphone systems (B&K Type 141B) were used to record the flyby data. They were designed to drive the signal over long cable lengths without appreciable loss in amplitude and with a relatively flat frequency response. System features include 200 volt polarization voltage, preemphasis signal conditioning, microphone cartridge "K" factor adjustment, and line length compensating adjustment for flatter frequency response. Each system consists of a 1/2 inch B&K diffuse field microphone (Model 4134 having a frequency characteristic for grazing incidence which is flat up to 20K Hz), a microphone preamplifier (Model 2619 which is a solid state device), a 0 to 40 dB signal amplifier (in 10 dB steps), a line drive amplifier for sending the microphone signal over the long cable distance, a preemphasis filter (which effectively provides 10-12 dB/octave gain in the higher frequencies starting at about 1000 Hz),

and a battery pack which supplies the remote operating power. The units can be operated with or without the preemphasis filter in the circuit.

Without the preemphasis signal conditioning, recording of aircraft flight data can become a problem due to the large dynamic range requirement created during a complete fly-by. The maximum noise, which occurs when the aircraft is near or past overhead, limits the signal gain levels for driving the tape recorder; but for shallow acoustic angles, during approaching or receding from overhead, the higher frequency generated noise rolls off quickly before reaching the microphone, mainly due to atmospheric attenuation over the long distances.

The preemphasis filter effectively provides the tool required to insure that the true aircraft generated noise in the higher frequency range is recorded above the tape recorder and/or equipment electrical noise floor. All fly-by data were recorded with preemphasis. The data were deemphasized with a matched de-emphasis filter at the time of tape recorder playback for data reduction. Sponge type wind screens (B&K Type UA0237) were used on both microphones for all flight tests. Figure 15 is a typical flight acoustic setup showing both General Electric and NASA systems.

The specially designed conductor cable for the 141B battery powered microphone units is provided in 1000 ft. reels; therefore, 1000 ft. of cable was used on both units, even though the station wagon was located only 80 to 100 ft. from the flight path microphone. The 141B microphone units are, however, designed to drive the signal over cable lengths of up to 6000 ft. The data from the two battery operated microphone systems was FM recorded at 30 IPS on the Lockheed 7-channel recorder. A time code generator signal was also recorded (on AM) for the purpose of triggering the timing mechanism of the analyzer/computer for real time data analysis.

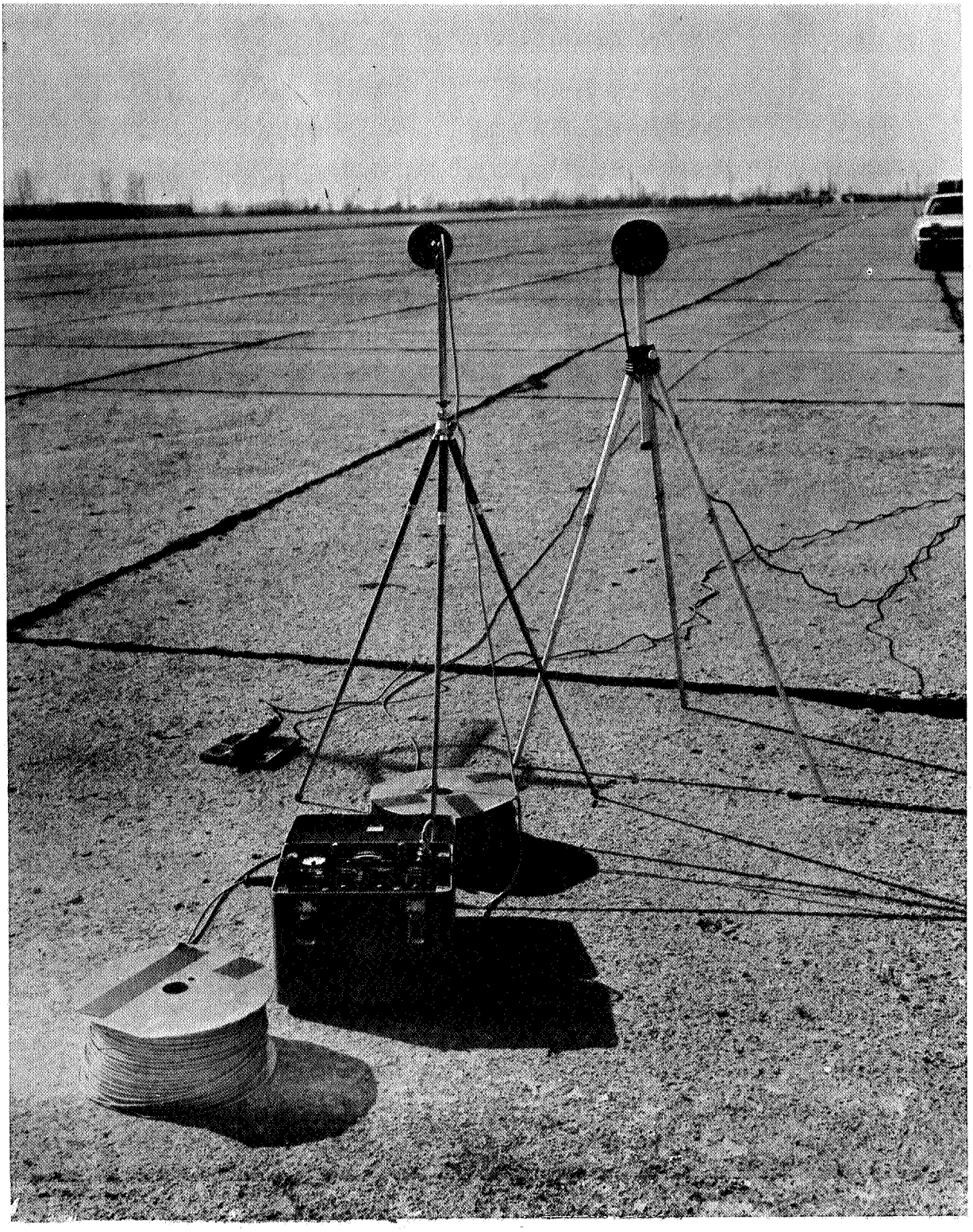

FIGURE 15 GENERAL ELECTRIC & NASA FLIGHT NOISE MONITORING INSTRUMENTATION

TEST SUMMARY

Summaries of static test points and flight test passes, for which data will be presented in this report, are included as Tables I through V as follows:

Tables	Configuration	Static	Flight
I&Ia	Conical Ejector	Run 147	FLT 146
II&IIa	Baseline Annular Plug	Run 151	FLT 152
III&IIIa	32 Spoke/Plug	Run 180 & 181	FLT 159
IV&IVa	64 Spoke/Plug	Run 150	FLT 155
V&Va	12 chute/plug	Run 168	FLT 170

The first table for each configuration is in English units and the second presents the same information in International Standard Units. Measured cycle parameters, plus calculated velocities and normalization parameters, are presented. These are used for comparing acoustic measurements. Meteorological conditions of barometric pressure (P_o), dry bulb temperature (T_o) and relative humidity are included as they are used in calculating theoretical atmospheric absorption of sound. These conditions are averages for the test day as measured by the control tower, not from the aircraft data recorder. The barometric pressure is ambient pressure corrected to sea level.

TABLE I

SUMMARY CYCLE DATA

Nozzle: CONICAL EJECTOR

GROUND STATIC

Run 147 Test Date: 2-25-71

Point No.	% Corr. RPM	W_G PPS	P_{T8}/P_o	T_8, °R	V_J Ft/Sec	10Log $\rho^2 A$
1	103.6	45.6	2.26	1692	2078	-32.2
7	102.9	45.2	2.26	1686	2072	-32.2
2	98.3	44.1	2.07	1520	1869	-31.6
3	94.2	39.8	1.82	1408	1643	-31.2
4	90.1	35.9	1.65	1344	1476	-31.0
5	85.3	31.1	1.48	1270	1275	-30.7
6	85.4	31.1	1.47	1263	1264	-30.7
8	81.4	27.5	1.36	1250	1128	-30.7

P_o = 29.90 in. Hg T_o = 39.5°F Rel. Hum. = 78%

FLIGHT

Flight 146 Test Date: 2-18-71

Pass No.	% Corr. RPM	Alt. Ft.	V_A Ft/Sec	W_G PPS	P_{T8}/P_o	T_8, °R	V_J Ft/Sec	V_R Ft/Sec	10Log $\rho^2 A$
3	100.9	300	430	48.7	2.37	1658	2107	1677	-31.9
4	101.0	305	447	48.5	2.35	1662	2100	1653	-32.0
5	95.0	300	430	46.3	2.16	1496	1901	1470	-31.3
6	95.1	295	422	46.3	2.17	1495	1906	1484	-31.3
7	95.4	300	430	46.7	2.20	1509	1931	1501	-31.3
9	90.0	310	439	39.6	1.85	1339	1622	1183	-30.7
10	91.3	305	439	41.3	1.91	1377	1686	1247	-30.9
11	87.0	305	430	36.0	1.59	1285	1390	959	-30.7
12	81.8	305	439	30.9	1.55	1234	1328	889	-30.4

P_o = 30.14 in. Hg T_o = 47°F Rel. Hum. = 67%

TABLE Ia

SUMMARY CYCLE DATA

Nozzle: Conical Ejector

GROUND STATIC

Run 147 — Test Date: 2/25/71

Point No.	% Corr. RPM	W_G kg/s	P_{T8}/P_o	T_8, °K	V_J m/s
1	103.6	20.7	2.26	940	634
7	102.9	20.5	2.26	937	632
2	98.3	20.0	2.07	844	570
3	94.2	18.1	1.82	782	501
4	90.1	16.3	1.65	747	450
5	85.3	14.1	1.48	706	389
6	85.4	14.1	1.47	702	385
8	81.4	12.5	1.36	694	348

$P_o = 10.125 \times 10^4$ n/m^2 $T_o = 277.5$ °K Rel. Hum. = 78%

FLIGHT

Flight 146 — Test Date: 2/18/71

Pass No.	% Corr. RPM	Alt. m	V_A m/s	W_G kg/s	P_8/P_o	T_8, °K	V_J m/s	V_R m/s
3	100.9	91.4	131.1	22.1	2.37	921	642	511
4	101.0	93.0	136.2	22.0	2.35	923	640	504
5	95.0	91.4	131.1	21.0	2.16	831	529	448
6	95.1	89.9	128.6	21.0	2.17	831	581	452
7	95.4	91.4	131.1	21.2	2.20	838	589	458
9	90.0	94.5	133.8	18.0	1.85	744	495	361
10	91.3	93.0	133.8	18.7	1.91	765	514	380
11	87.0	93.0	131.1	16.3	1.59	714	424	292
12	81.8	93.0	133.8	14.0	1.55	686	405	271

$P_o = 10.193 \times 10^4$ n/m^2 $T_o = 281.7$ ° K Rel. Hum. = 67%

TABLE II

SUMMARY CYCLE DATA

Nozzle: BASELINE ANNULAR PLUG

GROUND STATIC

Run 151 — Test Date: 3-17-71

Point No.	% Corr. RPM	W_G PPS	P_{T8}/P_o	T_8, °R	V_J Ft/Sec	$10\text{Log}\,\rho^2 A$
9	103.0	46.1	2.34	1734	2142	-32.2
10	103.0	46.1	2.34	1734	2142	-32.2
1	98.3	45.1	2.19	1583	1972	-31.6
8	98.3	45.1	2.19	1583	1972	-31.6
2	93.6	39.9	1.86	1421	1679	-31.1
3	93.6	39.9	1.86	1421	1679	-31.1
4	89.7	36.0	1.67	1323	1481	-30.7
5	85.2	31.7	1.50	1257	1292	-30.5
6	81.2	28.0	1.38	1230	1145	-30.5

P_o = 30.25 in. Hg T_o = 31°F Rel. Hum. = 61%

FLIGHT

Flight 152 — Test Date: 3-25-71

Pass No.	% Corr. RPM	Alt. Ft.	V_A Ft/Sec	W_G PPS	P_{T8}/P_o	T_8, °R	V_J Ft/Sec	V_R Ft/Sec	$10\text{Log}\,\rho^2 A$
1	102.3	295	439	51.1	2.58	1728	2246	1807	-31.9
2	102.2	310	447	51.1	2.58	1744	2257	1809	-32.0
3	102.4	300	430	50.2	2.53	1739	2232	1802	-32.1
4	96.6	300	439	48.1	2.31	1531	2000	1561	-31.2
5	96.7	295	430	48.2	2.30	1537	1999	1568	-31.3
6	96.6	300	430	48.2	2.31	1537	2003	1573	-31.3
7	92.3	310	430	42.6	1.96	1368	1710	1280	-30.7
8	92.8	320	439	43.0	1.98	1381	1730	1291	-30.8
9	92.5	290	439	43.1	1.97	1373	1719	1280	-30.7
10	89.0	310	439	39.1	1.76	1273	1521	1082	-30.3
11	89.0	305	430	39.0	1.75	1272	1530	1083	-30.3
12	89.0	310	439	39.2	1.76	1272	1521	1082	-30.3

P_o = 30.27 in. Hg T_o = 32°F Rel. Hum. = 45%

TABLE IIa

SUMMARY CYCLE DATA

Nozzle: BASELINE ANNULAR PLUG

GROUND STATIC

Run 151 TEST DATE: 3/17/71

Point No.	% Corr. RPM	W_G kg/s	P_{T8}/P_0	T_8, °K	V_J m/s
9	103.0	20.9	2.34	963	653
10	103.0	20.9	2.34	963	653
1	98.3	20.5	2.19	879	601
8	98.3	20.5	2.19	879	601
2	93.6	18.1	1.86	789	512
3	93.6	18.1	1.86	789	512
4	89.7	16.3	1.67	735	453
5	85.2	14.4	1.50	698	394
6	81.2	12.7	1.38	683	349

$P_o = 10.23 \times 10^4$ in/in^2 $T_o = 273$ °K Rel. Hum. = 61%

FLIGHT

Flight 152 TEST DATE: 3/25/71

Pass No.	% Corr. RPM	Alt. m	V_A m/s	W_G kg/s	P_{T8}/P_o	T_8, °K	V_J m/s	V_R m/s
1	102.3	89.9	133.8	23.2	2.58	960	685	551
2	102.2	94.5	136.2	23.2	2.58	968	688	552
3	102.4	91.4	131.1	22.8	2.53	966	681	549
4	96.6	91.4	133.8	21.8	2.31	850	610	476
5	96.7	89.9	131.1	21.9	2.30	853	610	478
6	96.6	91.4	↓	21.9	2.31	853	611	480
7	92.3	94.5	↓	19.3	1.96	760	521	390
8	92.8	97.5	133.8	19.5	1.98	766	527	397
9	92.5	88.4	↓	19.5	1.97	762	524	390
10	89.0	94.5	↓	17.7	1.76	707	464	330
11	↓	93.0	131.1	17.7	1.75	706	466	
12		94.5	133.8	17.8	1.76	706	464	

$P_o = 10.23 \times 10^4$ in/in^2 $T_o = 273$ °K Rel. Hum. = 45%

TABLE III

SUMMARY CYCLE DATA

Nozzle: 32-SPOKE/PLUG

GROUND STATIC

Run 181 — Test Date: 7-1-71

Point No.	% Corr. RPM	W_G PPS	P_{T8}/P_o	T_8, °R	V_J Ft/Sec	10Log $\rho^2 A$
6	98.4	42.8	2.02	1627	1901	-32.2
7	96.4	41.7	1.98	1553	1835	-31.8
5	93.6	39.2	1.75	1503	1645	-31.8
4	89.3	34.3	1.57	1435	1455	-31.6
8	88.5	33.3	1.60	1346	1429	-31.0
3	86.0	30.8	1.47	1391	1323	-31.5
2	82.2	27.3	1.36	1378	1189	-31.6
11	82.2	27.3	1.36	1378	1189	-31.6
1	79.0	25.2	1.30	1361	1095	-31.5

P_o = 29.90 in. Hg T_o = 83°F Rel. Hum. = 54%

Run 180 — Test Date: 6-29-71

2	≈84		1.35	1398	1179	-31.7
1	≈80		1.29	1374	1075	-31.6

P_o = 30.04 in. Hg T_o = 88°F Rel. Hum. = 48%

FLIGHT

Flight 159 — Test Date: 4-14-71

Pass No.	% Corr. RPM	Alt. Ft.	V_A Ft/Sec	W_G PPS	P_{T8}/P_o	T_8, °R	V_J Ft/Sec	V_R Ft/Sec	10Log $\rho^2 A$
1	101.7	300	447	50.2	2.42	1669	2139	1692	-31.9
2	101.8	310	430	49.6	2.37	1670	2117	1687	-31.9
3	101.9	305	439	49.9	2.38	1669	2121	1682	-31.9
4	95.8	300	439	47.6	2.19	1476	1905	1467	-31.1
5	95.8	300	430	47.5	2.19	1497	1919	1488	-31.2
6	95.5	310	447	47.9	2.20	1487	1917	1470	-31.2
7	91.4	320	439	41.9	1.89	1359	1662	1222	-30.8
8	91.6	320	439	42.2	1.91	1364	1677	1238	-30.8
9	91.4	300	439	41.7	1.90	1357	1666	1228	-30.7
10	87.7	310	447	37.7	1.69	1273	1470	1022	-30.4
11	87.8	320	439	37.7	1.69	1275	1470	1031	-30.5
12	87.8	295	430	37.3	1.68	1282	1466	1036	-30.5

P_o = 30.20 in. Hg T_o = 43°F Rel. Hum. = 39%

TABLE IIIa

SUMMARY CYCLE DATA

Nozzle: 32-SPOKE/PLUG

GROUND STATIC

Run 181 — Test Date: 7/1/71

Point No.	% Corr. RPM	W_G kg/s	P_{T8}/P_o	T_8, °K	V_J m/s
6	98.4	19.4	2.02	904	579
7	96.4	18.9	1.98	863	559
5	93.6	17.8	1.75	835	501
4	89.3	15.6	1.57	797	444
8	88.5	15.1	1.60	748	436
3	86.0	14.0	1.47	773	403
2	82.2	12.4	1.36	766	362
11	82.2	12.4	1.36	766	362
1	79.0	11.4	1.30	756	334

$P_o = 10.13 \times 10^4$ n/m^2 $T_o = 301$ °K Rel. Hum. = 54%

Run 180 — Test Data: 6/29/71

2	84		1.35	777	1179
1	80		1.29	763	1075

$P_o = 10.17 \times 10^4$ n/m^2 $T_o = 304.4$ °K Rel. Hum. = 48%

FLIGHT

Flight 159 — Test Date: 4/14/71

Pass No.	% Corr. RPM	Alt. m	VA m/s	W_G kg/s	P_8/P_o	T_8, °K	V_J m/s	V_R m/s
1	101.7	91.4	136.2	22.8	2.42	927	652	516
2	101.8	94.5	131.1	22.5	2.37	928	645	514
3	101.9	93.0	133.8	22.6	2.38	927	646	513
4	95.8	91.4	133.8	21.6	2.19	820	571	447
5	95.8	91.4	131.1	21.5	2.19	832	585	454
6	95.5	94.5	136.2	21.7	2.20	826	584	448
7	91.4	97.5	133.8	19.0	1.89	755	507	372
8	91.6	97.5	↓	19.1	1.91	758	511	377
9	91.4	91.4	↓	18.9	1.90	754	508	374
10	87.7	94.5	136.2	17.1	1.69	707	448	311
11	87.8	97.5	133.8	17.1	1.69	708	448	314
12	87.8	89.9	131.1	16.9	1.68	712	447	316

$P_o = 10.23 \times 10^4$ n/m^2 $T_o = 279°$ K Rel. Hum. = 39%

TABLE IV

SUMMARY CYCLE DATA

Nozzle: 64-SPOKE/PLUG

GROUND STATIC

Run 150 — Test Date: 3-11-71

Point No.	% Corr. RPM	W_G PPS	P_{T8}/P_o	T_8, °R	V_J Ft/Sec	$10\text{Log}\,\rho^2 A$
1	103.3	45.6	2.24	1674	2055	-32.1
7	103.3	45.6	2.24	1674	2055	-32.1
11	103.3	45.6	2.24	1674	2055	-32.1
2	97.6	44.0	2.03	1485	1827	-31.4
10	97.6	44.0	2.03	1485	1827	-31.4
3	93.2	39.0	1.71	1326	1516	-30.8
4	89.0	34.9	1.47	1203	1237	-30.2
8	89.0	34.9	1.47	1203	1237	-30.2
5	84.8	31.0	1.33	1154	1045	-30.0
9	84.8	31.0	1.33	1154	1045	-30.0
6	80.4	27.1	1.24	1123	899	-29.9

P_o = 30.00 in. Hg T_o = 31°F Rel. Hum. = 61%

FLIGHT

Flight 155 — Test Date: 4-6-71

Pass No.	% Corr. RPM	Alt. Ft.	V_A Ft/Sec	W_G PPS	P_{T8}/P_o	T_8, °R	V_J Ft/Sec	V_R Ft/Sec	$10\text{Log}\,\rho^2 A$
2	101.5	300	430	49.5	2.41	1679	2141	1711	-31.9
3	101.4	310	439	49.9	2.42	1677	2144	1705	-31.9
4	101.5	295	439	49.7	2.39	1662	2121	1682	-31.9
5	95.4	295	447	47.6	2.18	1463	1892	1445	-31.0
6	95.4	310	439	47.2	2.16	1460	1880	1441	-31.1
7	95.4	290	430	47.1	2.14	1455	1866	1436	-31.0
8	91.4	310	439	41.6	1.83	1316	1596	1157	-30.6
9	91.3	300	439	41.6	1.82	1312	1586	1148	-30.5
10	91.4	300	430	41.5	1.82	1318	1591	1160	-30.6
11	87.6	300	452	37.4	1.55	1201	1310	858	-30.1
12	87.9	300	447	37.7	1.58	1196	1331	887	-30.0

P_o = 30.22 in. Hg T_o = 46°F Rel. Hum. = 37%

TABLE IVa

SUMMARY CYCLE DATA

Nozzle: 64-SPOKE/PLUG

GROUND STATIC

Run 150 — TEST DATE: 3/11/71

Point No.	% Corr. RPM	W_G kg/s	P_{T8}/P_o	T_8, °K	V_J m/s
1	103.3	20.7	2.24	930	626
7	↓	↓	↓	↓	↓
11	↓	↓	↓	↓	↓
2	97.6	20.0	2.03	825	557
10	97.6	20.0	2.03	825	557
3	93.2	17.7	1.71	737	462
4	89.0	15.8	1.47	668	377
8	89.0	15.8	1.47	668	377
5	84.8	14.1	1.33	641	318
9	84.8	14.1	1.33	641	318
6	80.4	12.3	1.24	624	274

$P_o = 10.16 \times 10^4$ in/in^2 $T_o = 273$ °K Rel. Hum. = 61%

FLIGHT

Flight 155 — TEST DATE: 4/6/71

Pass No.	% Corr. RPM	Alt. m	V_A m/s	W_G kg/s	P_{T8}/P_o	T_8, °K	V_J m/s	V_R m/s
2	101.5	91.4	131.3	22.5	2.41	933	653	522
3	101.4	94.5	133.8	22.6	2.42	932	654	520
4	101.5	89.9	133.8	22.5	2.39	923	647	513
5	95.4	89.9	136.2	21.6	2.18	813	577	441
6	↓	94.5	133.8	21.4	2.16	811	574	439
7	↓	88.4	131.8	18.9	1.83	731	487	353
8	91.4	94.5	133.8	↓	1.83	741	487	353
9	91.3	91.4	133.8	↓	1.82	729	484	350
10	91.4	↓	131.8	18.8	1.82	732	485	354
11	87.6	↓	137.8	17.0	1.55	667	399	262
12	87.9	↓	136.2	17.1	1.58	664	406	270

$P_o = 10.23 \times 10^4$ in/in^2 $T_o = 281$ °K Rel. Hum. = 37%

TABLE V

SUMMARY CYCLE DATA

Nozzle: 12-CHUTE/PLUG

GROUND STATIC

Run 168 — Test Date: 5-13-71

Point No.	% Corr. RPM	W_G PPS	P_{T8}/P_o	T_8, °R	V_J Ft/Sec	10Log $\rho^2 A$
1	101.3	44.2	2.13	1683	2001	-32.4
2	96.4	42.6	2.00	1530	1833	-31.7
3	92.0	37.5	1.65	1345	1477	-31.0
4	96.0	42.1	1.91	1500	1759	-31.7
5	92.0	37.4	1.62	1335	1446	-31.0
6	88.1	33.3	1.46	1244	1245	-30.6
7	83.4	28.8	1.32	1213	1058	-30.6
8	79.0	25.6	1.24	1204	931	-30.6

P_o = 29.10 in. Hg T_o = 54°F Rel. Hum. = 45%

FLIGHT

Flight 170 — Test Date: 5-14-71

Pass No.	% Corr. RPM	Alt. Ft.	V_A Ft/Sec	W_G PPS	P_{T8}/P_o	T_8, °R	V_J Ft/Sec	V_R Ft/Sec	10Log $\rho^2 A$
1	99.8	300	430	47.8	2.33	1698	2114	1684	-32.2
2	99.9	300	422	48.1	2.38	1715	2151	1729	-32.2
3	100.1	290	422	47.9	2.31	1687	2100	1678	-32.1
13	99.6	290	447	48.2	2.37	1693	2132	1685	-32.1
4	94.3	300	430	45.3	2.13	1503	1890	1459	-31.4
5	94.3	300	430	45.5	2.13	1502	1890	1459	-31.4
6	94.3	300	430	45.1	2.11	1504	1883	1453	-31.4
14	94.1	300	447	45.3	2.11	1493	1876	1429	-31.3
7	90.1	300	439	38.9	1.76	1323	1549	1110	-30.7
8	90.1	300	439	39.8	1.76	1321	1549	1110	-30.7
9	90.1	300	439	39.6	1.75	1321	1542	1103	-30.7
10	86.5	295	439	35.4	1.48	1193	1241	803	-30.2
11	86.5	310	447	35.7	1.50	1193	1254	806	-30.1
12	86.8	300	447	36.0	1.51	1201	1274	826	-30.2

P_o = 29.41 in. Hg T_o = 61°F Rel. Hum. = 37%

TABLE Va

SUMMARY CYCLE DATA

Nozzle: 12-CHUTE/PLUG

GROUND STATIC

Run 168 Test Date: 5-13-71

Point No.	% Corr. RPM	W_G kg/s	P_{T8}/P_o	T_8, °K	V_J m/s
1	101.3	20.0	2.13	934	610
2	96.4	19.3	2.00	849	659
3	92.0	17.0	1.65	746	450
4	96.0	19.1	1.91	833	538
5	92.0	17.0	1.62	741	441
6	88.1	15.1	1.46	690	379
7	83.4	13.1	1.32	674	323
8	79.0	11.6	1.24	668	284

$P_o = 9.85 \times 10^4$ in/in^2 $T_o = 286$ °K Rel. Hum. = 45%

FLIGHT

Flight 170 Test Date: 5-14-71

Pass No.	% Corr. RPM	Alt. m	V_A m/s	W_G kg/s	P_{T8}/P_0	T_8, °K	V_J m/s	V_R m/s
1	99.8	91.4	131.1	21.7	2.33	943	645	513
2	99.9	91.4	128.6	21.8	2.38	952	656	527
3	100.1	88.4	128.6	21.7	2.31	938	640	512
13	99.6	88.4	136.2	21.9	2.37	940	650	514
4	94.3	91.4	131.1	20.5	2.13	834	576	445
5	↓	↓	↓	20.6	2.13	834	576	445
6	↓	↓	↓	20.5	2.11	834	574	443
14	94.1	↓	136.2	20.5	2.11	829	572	436
7	90.1	↓	133.8	17.6	1.76	735	472	338
8	↓	↓	↓	18.1	1.76	734	472	338
9	↓	↓	↓	18.0	1.75	734	470	336
10	86.5	89.9	↓	16.1	1.48	662	470	245
11	86.5	94.5	136.2	16.2	1.50	662	382	246
12	86.8	91.4	136.2	16.3	1.51	666	388	252

$P_o = 9.96 \times 10^4$ in/in^2 $T_o = 289$ °K Rel. Hum. = 37%

ACOUSTIC DATA REDUCTION - GROUND STATIC RUN-UP

Data tapes from the 100 ft. arc static measurements were reduced through a B&K 1/3 octave band parallel filter analyzer. The output of the analyzer was fed into an "analog to digital" converter from which a digital magnetic tape was generated. The digital tape was then fed into a computer program which corrected the measured data to a standard day of 59°F, 70% relative humidity from its as-measured levels on the non-standard measuring day. Correction to a 77° F, 70% relative humidity, as prescribed by federal regulation FAR PART 36 for subsonic aircraft noise certification, would not have affected the validity of acoustic results of this report. Absolute noise levels for both static and flight would have been slightly lower due to the smaller differences in the atmospheric absorption corrections necessary to apply when correcting the measured day to a 77° standard day rather than to a 59° standard day. Therefore, comparison of absolute levels between static and flight and comparison of suppressions levels reference to the baseline nozzle would have been only insignificantly altered.

Correcting the static data on the 100 ft. arc to an acoustic standard day, rather than leaving it on an as-measured day, is believed to make the data more consistent for comparisons. The corrections applied are per the SAE procedure for evaluating atmospheric absorption changes in noise levels with distance as a function of meteorological conditions. Industry recognizes that these corrections appear fairly valid and consistent for application to short distances, such as far field arc static measurements and flight measurements with reasonably short acoustic path lengths. However, application to measurements taken over long distances are believed to over correct the data, particularly so when the measuring day is quite meteorologically different than the standard acoustic day. Correction of the ground static measured data to standard day is therefore believed to be valid and necessary. Correction of flight acoustic data are described under ACOUSTIC DATA REDUCTION - FLIGHT.

Several anomalies existed in various portions of the measured ground static data and made it diverge from the pure jet noise idealy sought for this study. The influence of these non-jet noise contributors was eliminated as best possible

from the 100 ft. arc data before making final OASPL and PNL calculations on the arc and before extrapolating the arc data to the 300 ft. sideline. The noise sources and influences are discussed individually as follows:

Conical Ejector Pure Tone

The conical primary-cylindrical ejector system, when statically tested at engine speeds of approximately 94% and below, generated a pure tone centering around 300 Hz frequency. The cavity between the converging primary nozzle and the convergent portion of the ejector system is felt to have produced a resonance at this frequency whenever the primary nozzle became unchoked. See Figure 8b. Run 147, points 1, 7 and 2 at 103.6, 102.9 and 98.3% corrected speed had no tone present. See Table I and Ia. At lower speeds, the tone appeared and became more predominant as the jet noise level was lowered. The tone was then present in spectra from all seven measuring angles. The tone did not change frequency as engine speed was decreased.

To correct the 1/3 octave spectra levels for elimination of pure tone contribution the data were reduced in 10 Hz bandwidth narrowbands. This was necessary to gage the magnitude of tone contribution to the broadband jet noise. This was done for Run 147, points 3 thru 6 and 8 and is felt to have accurately eliminated the pure tone contribution to the total noise. Correction magnitude to the 1/3 octave band data was only several dB at the 94.2% speed of point 3 but increased to a range of 15 to 20 dB at the low speed setting of point 8. As the tone was of low frequency, minor inconsistencies in its removal are felt would have no influence on the resultant perceived noise levels which are strongly high frequency weighted.

The pure tone, however, is not detectable in the flight noise spectra when searched for at the doppler shifted frequency.

J85 Turbomachinery Tones

J85 turbomachinery pure tones were generated within the 10K Hz range of acoustic interest when the engine speed was low. Their acoustic levels on the 100 ft arc were sufficiently high to contribute to the measured total noise. This was particularly true during test of the segmented suppressor nozzles, when the high frequency jet noise levels were sufficiently suppressed that the blade passing tones overrode the jet broadband noise in contributing to the total noise. The engine physical speed range during static runup ranged from 13000 to 16700 rpm. Reference to the blading chart in Figure 2 and consideration of the engine speed range shows the first stage compressor rotor capable of producing blade passing frequencies from 6700 to 8600 Hz. Thus, contribution to the last three 1/3 octave bands of jet noise data could have been and was present. Stage 1 compressor had 31 blades. The high blade numbers of all other stages set their blade passing frequencies above the 10K Hz 1/3 octave band.

Generally the contribution to the 1/3 octave data was within a 3 to 5 dB range and usually localized toward the inlet angles. The maximum interference was during test of the 64 spoke nozzle at low engine speed where broadband jet noise was suppressed.

The contribution of pure tone was eliminated as best possible by lowering the particular 1/3 octave band levels within which the tones occurred to where they were felt to be equivalent to the characteristic broadband jet noise levels.

J75 at Idle - Background Noise

During ground static and flight testing it was necessary to have the J75 engine running at idle for operation of the recording system and for fuel pressure to the J85 engine. Therefore, background noise measurements with only the J75 at idle (J85 off) were necessary to gage interference with the J85 jet noise. Measurements were taken on several different test days and the average spectra at the 7 measuring stations on the 100 ft. arc are shown in Figures 16 through 19. These levels were then compared individually to the measured spectra from each respective test nozzle. For the reference conical ejector nozzle

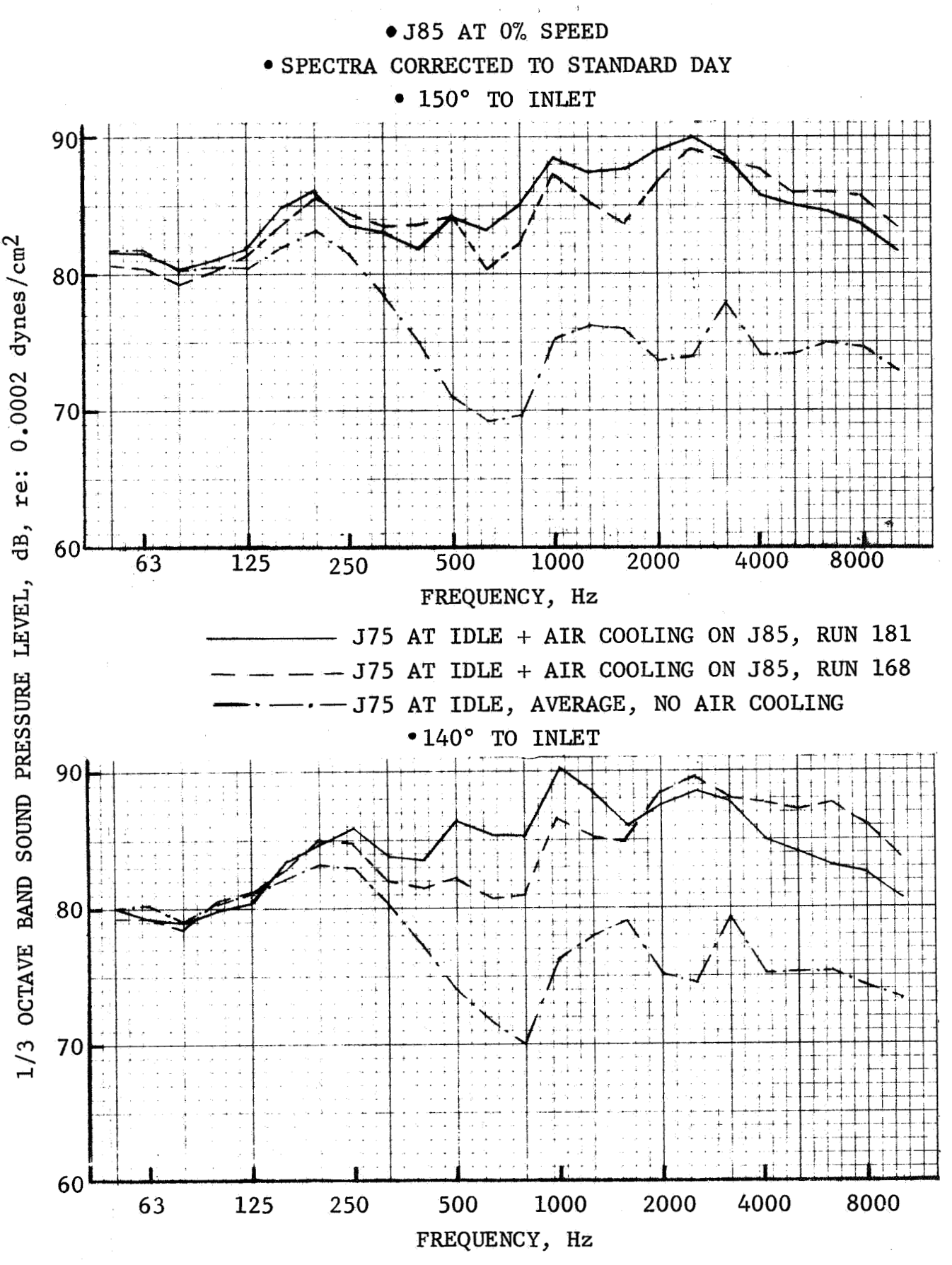

FIGURE 16 100 FOOT ARC J75 - IDLE GROUND STATIC SPECTRA WITH AND WITHOUT AIR COOLING ON J85

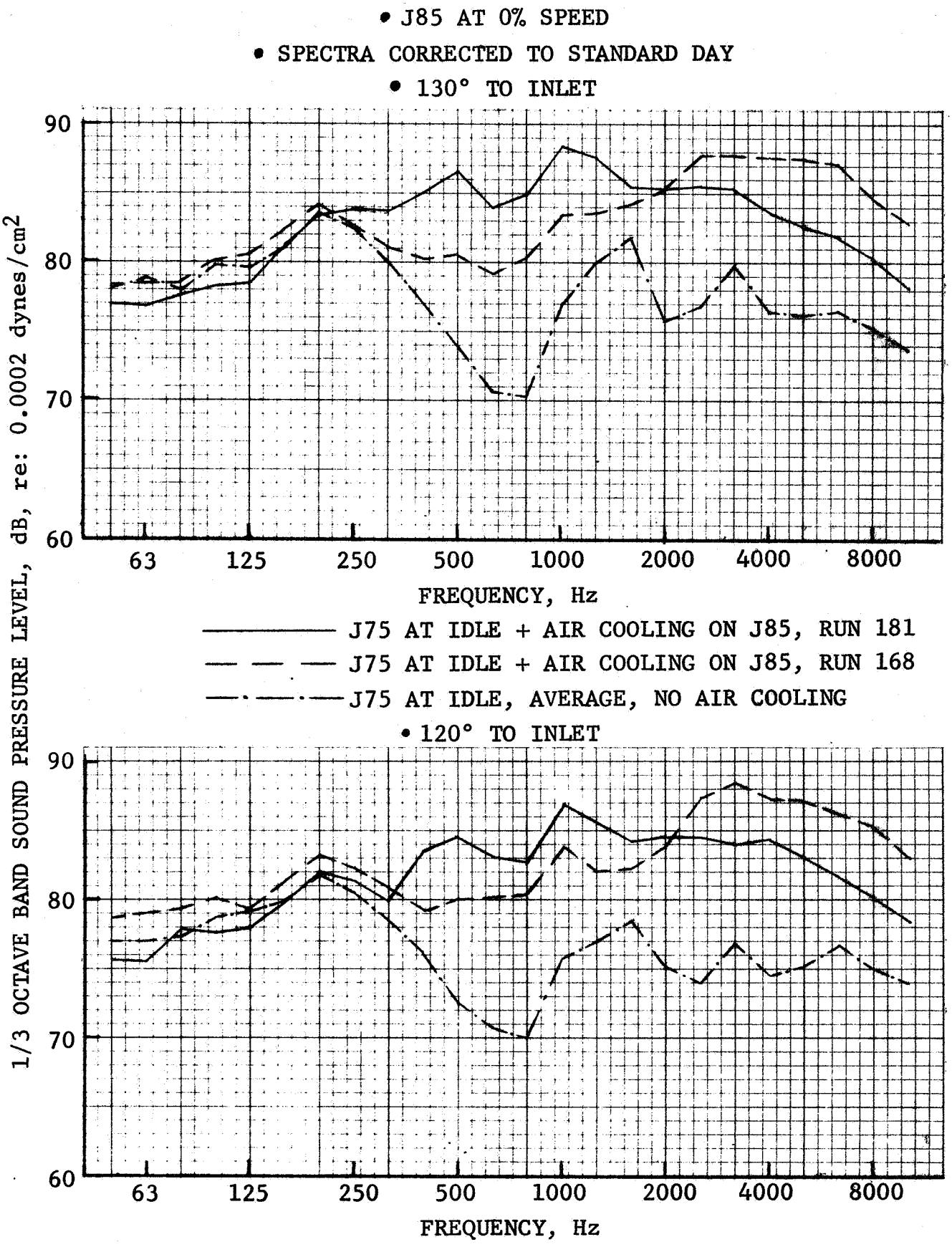

FIGURE 17 100 FOOT ARC J75 - IDLE GROUND STATIC SPECTRA WITH AND WITHOUT AIR COOLING ON J85

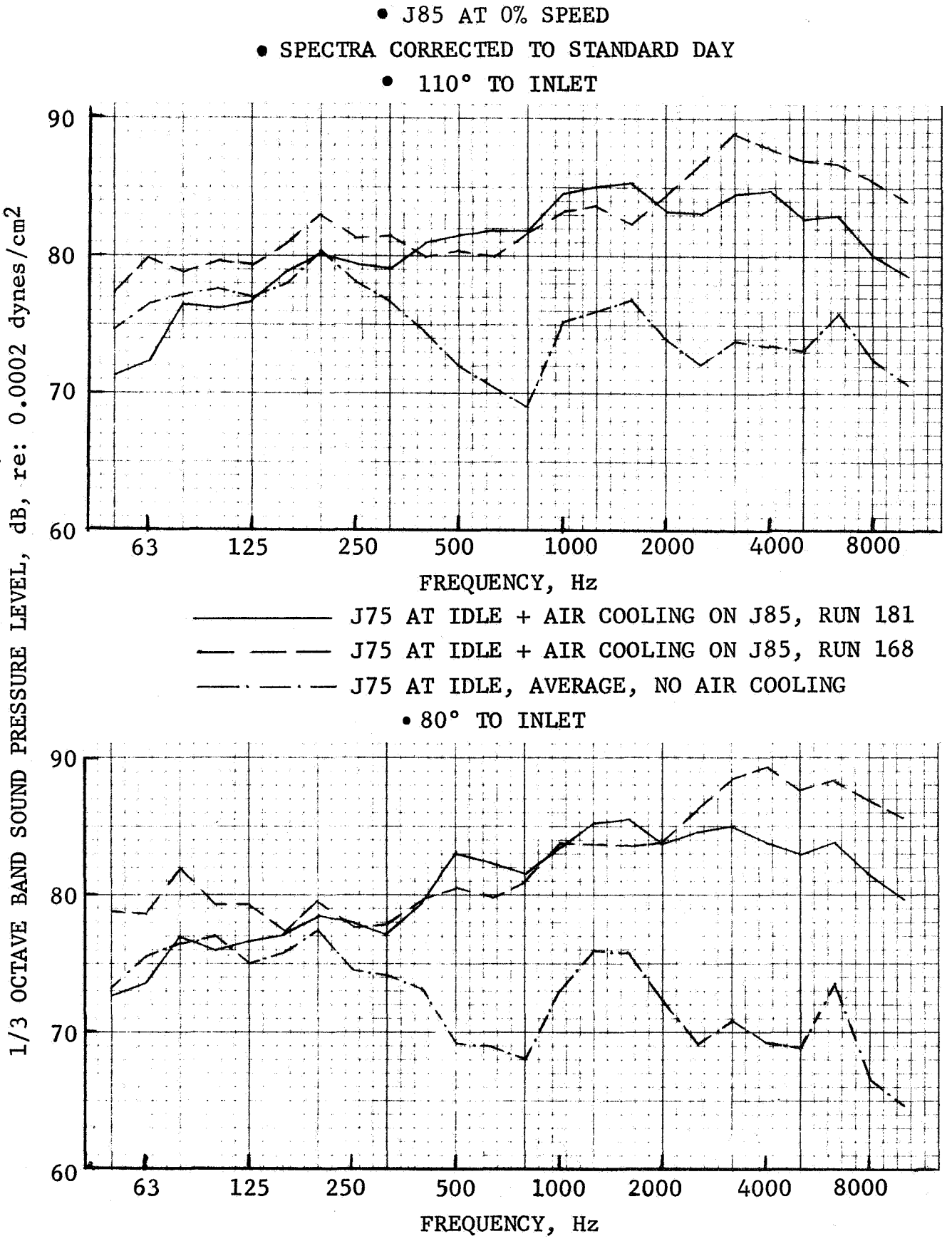

FIGURE 18 100 FOOT ARC J75 - IDLE GROUND STATIC SPECTRA WITH AND WITHOUT AIR COOLING ON J85

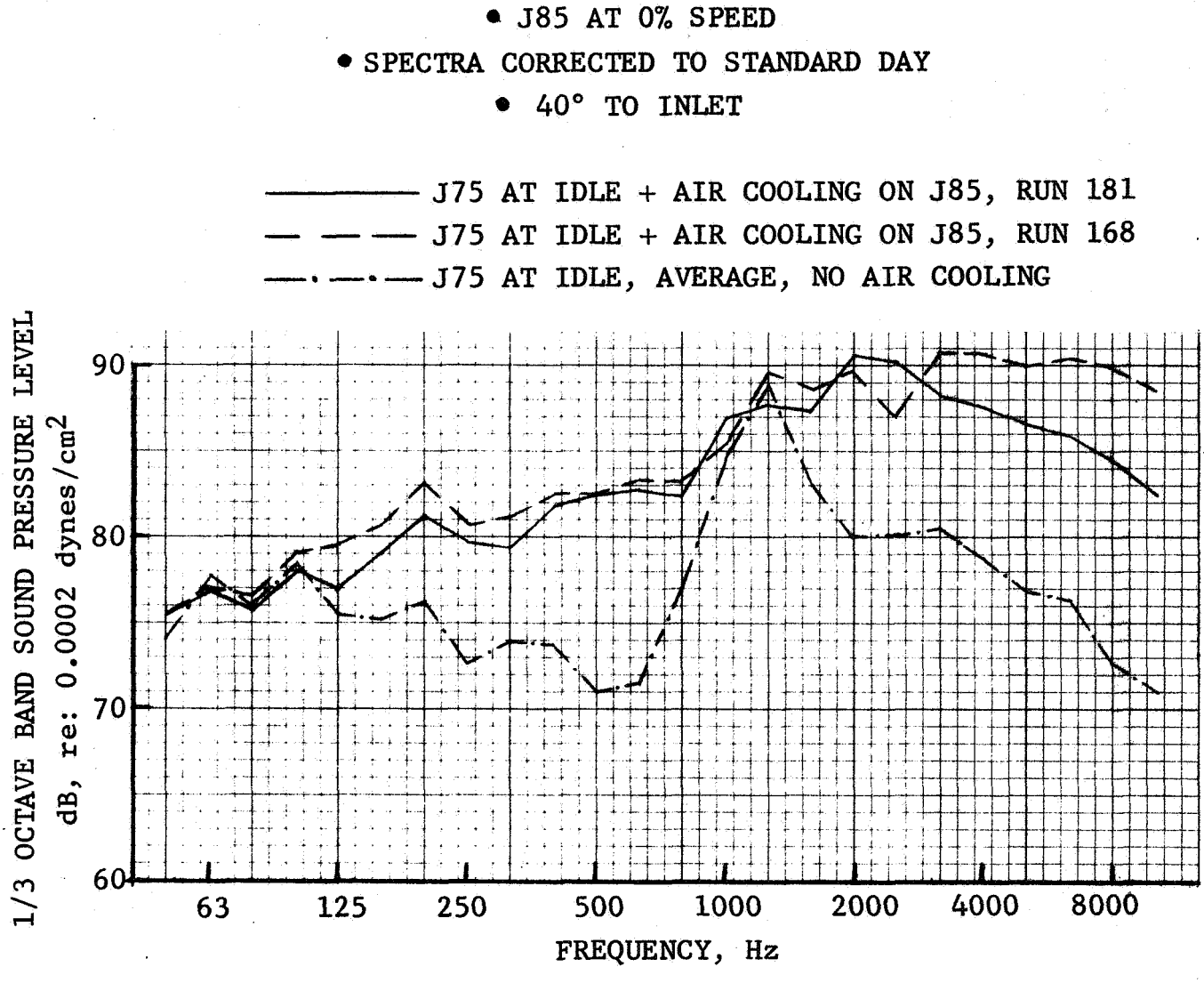

FIGURE 19 100 FOOT ARC J75 - IDLE GROUND STATIC SPECTRA WITH AND WITHOUT AIR COOLING ON J85

there was no interference. For the annular plug nozzle, only minor interference at low engine speed occurred and was readily removed. In general, for the three suppressed nozzles, no interference occurred until engine speeds in the range of 93 to 90% and lower were set. Low frequency interference then occurred generally at angles of 40, 80, 110, and 120° to the inlet. Removal of this low frequency interference was generally felt to be fairly accurate as the J75 alone noise did not over-ride the J85 jet noise and individual levels of contribution were discernible.

The only major influence of the J75 at idle for which correction was felt to be inadequate occurred near the inlet. The J75 generated a distinct blade passing pure tone which predominated the mid-frequency noise spectra when operating the J85 suppressed nozzles at low engine speeds. This occurred only at 40° to inlet angle as the tone from the long J75 inlet was fairly directional. J85 data will be presented for all angles with levels adjusted as best possible for interference, however, they will be qualified as to accuracy.

Cooling Air - Background Noise

During ground tests of several of the suppressed nozzle configurations, the J85 experienced an overheating problem which resulted in a fire warning light in the cockpit and immediate engine deceleration by the pilot. Overheating occurred due to poor secondary air circulation around the engine during static operation, only at high speed points. To circumvent this problem so that acoustic data could be acquired at high jet velocity, supplementary air cooling, utilizing an air start cart, was used. The start cart was positioned on the far side of the aircraft as seen in Figure 13 and the air supply run to the engine and directed through a pipe/nozzle as seen in Figure 3. During operation, however, the cooling air blowing through the fixed nozzle generated high frequency noise which created additional interference to the measured J85 jet spectra. The air cooling was used only on the 32 spoke nozzle at 88% speed and above (Run 181, points 5, 6, 7, and 8) and on the 12 chute nozzle at 92% speed and above (Run 168, points 1, 2, and 3). So that magnitude of interference could be gaged and possibly removed from the spectra, noise measurements were taken with the J75 at idle and with the cooling air blowing, but with the J85 off. These spectra are presented for each measuring angle in Figures 16 through 19. The cooling air background noise is lower in the high frequencies for Run 181 as

the cooling air supply line was split into two hoses and ducted on each side of the engine, thus lowering the generated noise and shadowing the noise from the one nozzle with the engine.

As the cooling air was necessary only at high speed where the basic jet noise levels were high, the background noise did not over-ride the jet noise. Thus, interference levels could be reasonably gaged and corrections made to the spectra are felt to be accurate and adequate.

In summary, all of the ground static measured spectra presented in this report have been examined for extraneous contributions above the basic engine jet noise levels. Where identified, the contributions due to conical-ejector pure tone, turbomachinery pure tone, J75 at idle background and cooling air background have been extracted as best possible from the total noise to leave remaining only the basic engine jet noise required for this study. The magnitude of corrections and resultant spectra are felt to be accurate with the exception of several areas.

- o Predominance of J75 mid-frequency pure tone in the 40° inlet angle measured spectra for suppressed nozzles at low speed.
- o Broadband turbomachinery noise contribution at low engine speed, particularly at angles near the inlet and for the suppressed nozzles. Its contribution is not readily identifiable and cannot be easily separated from the total noise.

Areas of questionable data will be qualified under discussion of static data.

300 Ft. Sideline Extrapolation

The calculated 300 ft. sideline static noise data presented in this report are extrapolated from the 100 ft. arc corrected spectra. The extrapolation is based on inverse square law, extra ground attenuation per SAE AIR 923 (ref. 3). and 59° F, 70% R/H standard day atmospheric absorption per SAE ARP 866 (ref. 4). The 300 ft. sideline reference plane was chosen so that the data could be directly compared to the measurements taken under the flight path for the 300 ft. altitude flyovers. Direct changes from static to flight could then be gaged by comparing flight data at similar acoustic angles.

PRESENTATION OF STATIC DATA

The basic ground static data are presented in this report in 1/3 octave band spectra form. The data are corrected to a 59°, 70% relative humidity standard day and for tones and interference as discussed under ACOUSTIC DATA REDUCTION - GROUND STATIC RUN-UP. The 100 ft. arc data were chosen for inclusion as they are the basic measured data and can be used in any manner chosen to establish other data reference planes. The data are not corrected to free field as no set procedure for correction is accepted industry-wide. By presenting the data in non-free field form and referring to the acoustic setup in Figure 12 for calculation of null and reinforcement points, each user of the data can apply corrections in his own preferred manner.

In addition to the basic spectra, OASPL and PNL directivity plots are included at the 100 ft. arc and 300 ft. sideline. The 300 ft sideline data are extrapolated from the non-free field 100 ft. arc data.

The data are presented for each nozzle individually per the following table. Refer to Tables I through V for individual point cycle parameters.

	100 ft. Arc			300 ft. Sideline	
Nozzle	Spectra	OASPL	PNL	OASPL	PNL
	Figure No.				
Conical Ejector	20 to 26	27	28	29	30
Baseline Annular Plug	31 to 37	38	39	40	41
32 Spoke/Plug	42 to 48	49	50	51	52
64 Spoke/Plug	53 to 59	60	61	62	63
12 Chute/Plug	64 to 70	71	72	73	74

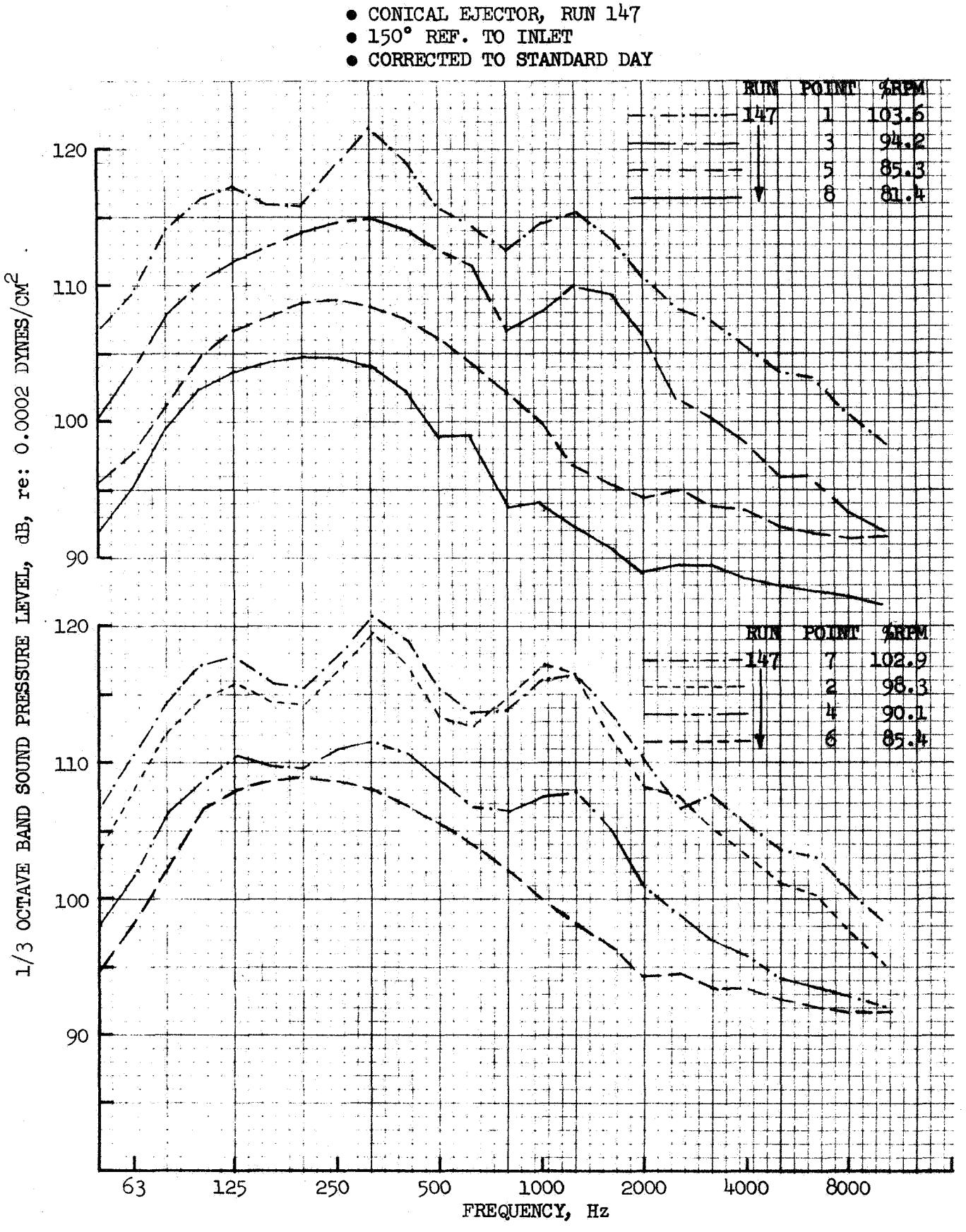

FIGURE 20 100 FT. ARC J85 GROUND STATIC SPECTRA, CONICAL EJECTOR

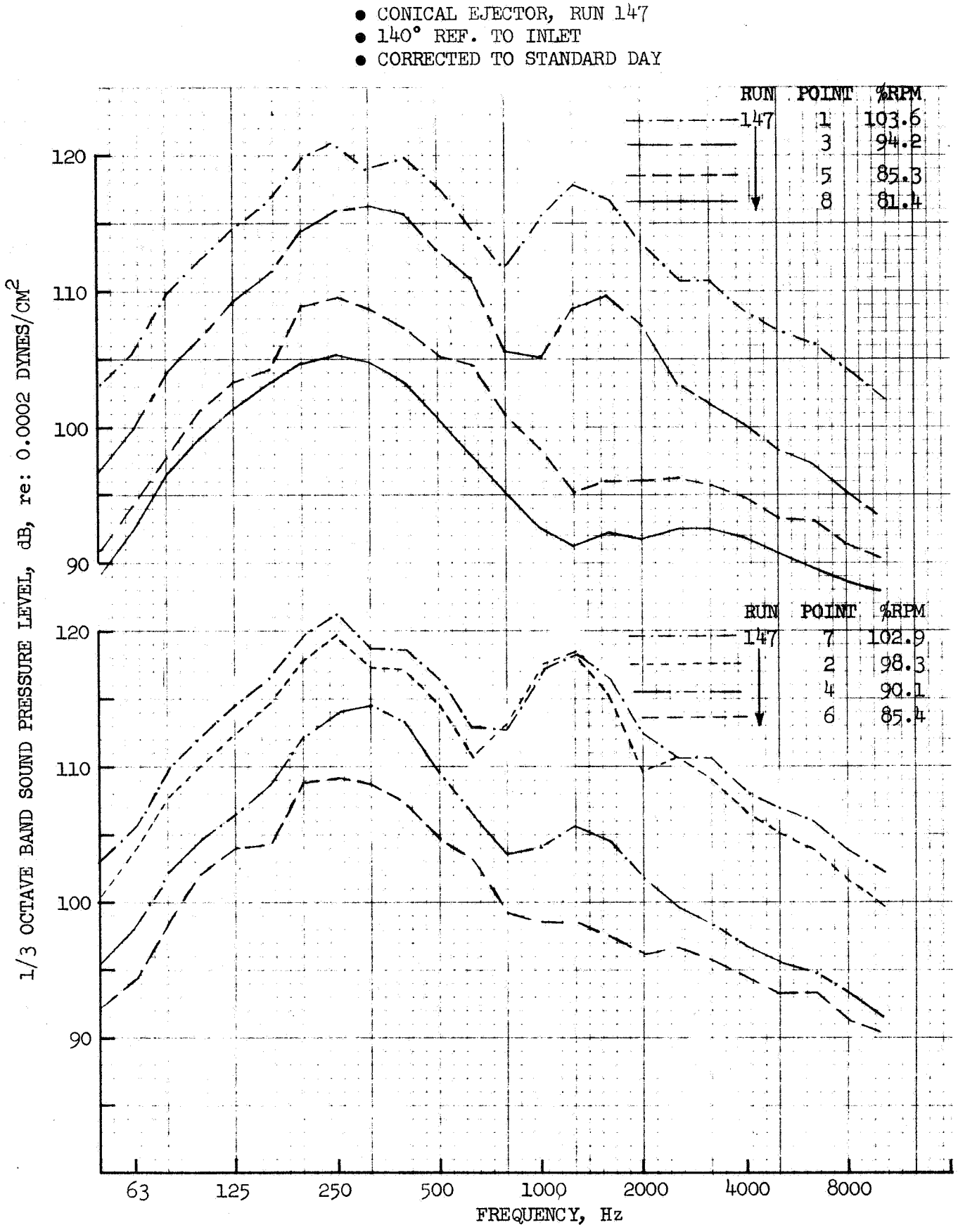

FIGURE 21 100 FT. ARC J85 GROUND STATIC SPECTRA, CONICAL EJECTOR

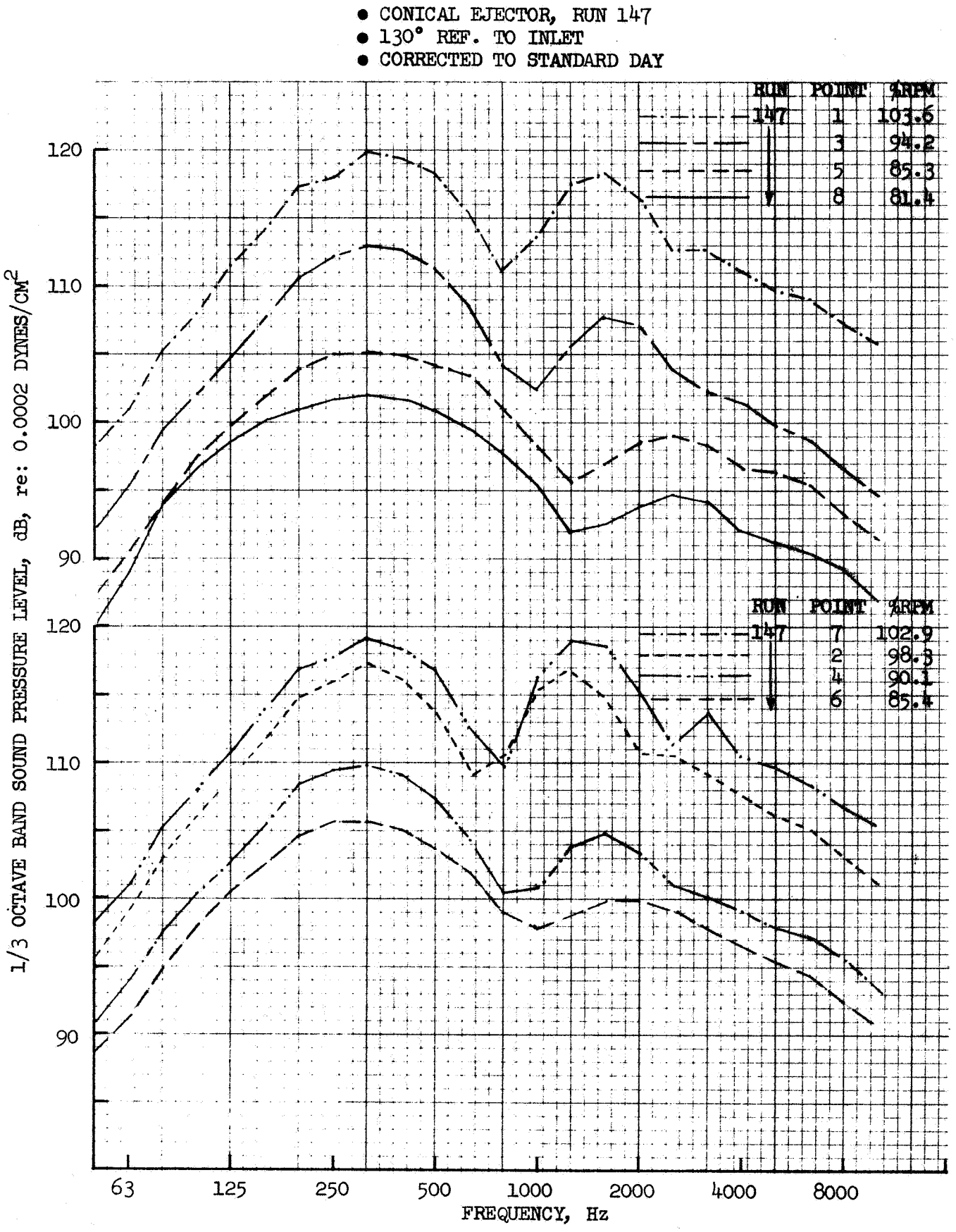

FIGURE 22 100 FT. ARC J85 GROUND STATIC SPECTRA, CONICAL EJECTOR

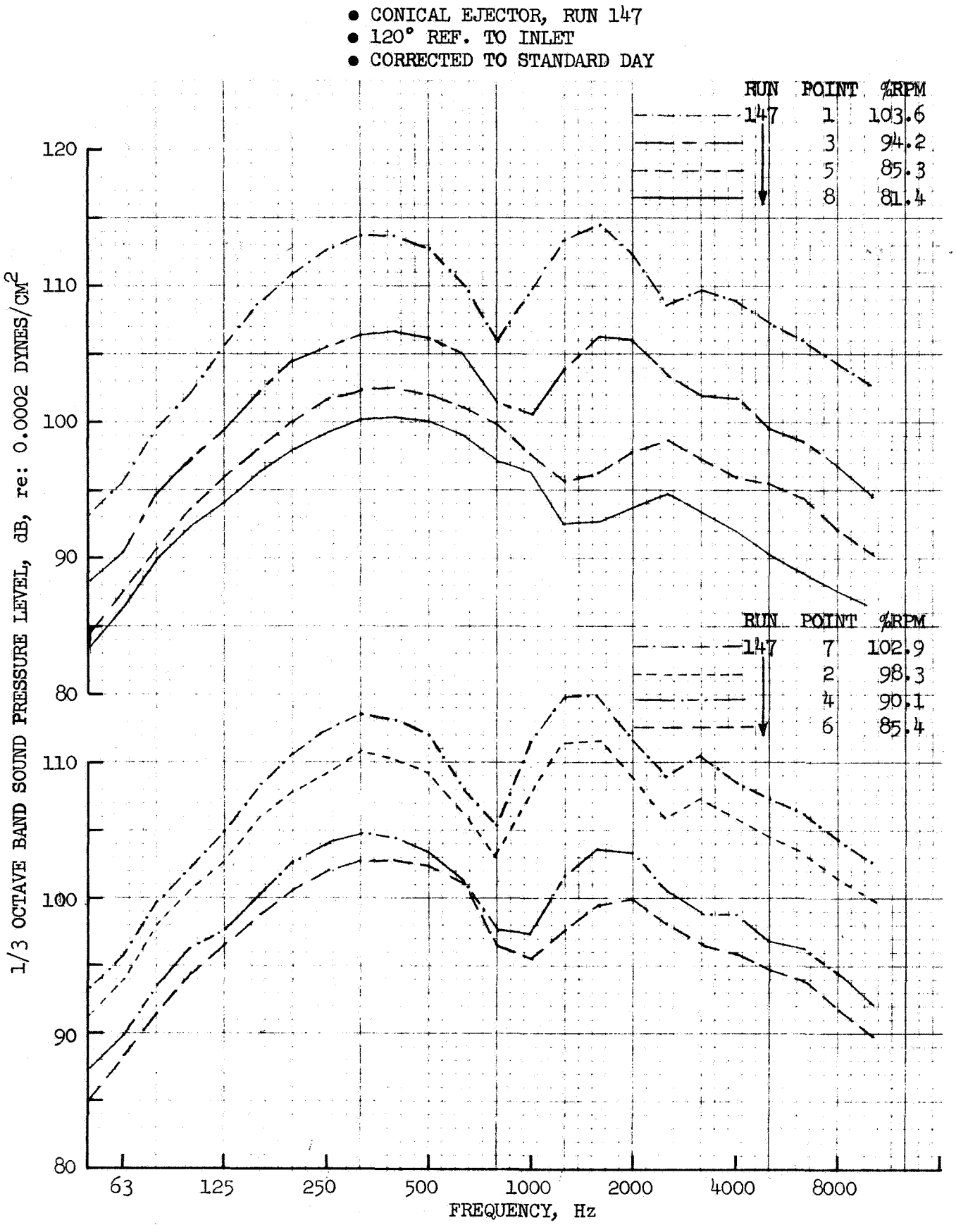

FIGURE 23 100 FT. ARC J85 GROUND STATIC SPECTRA, CONICAL EJECTOR

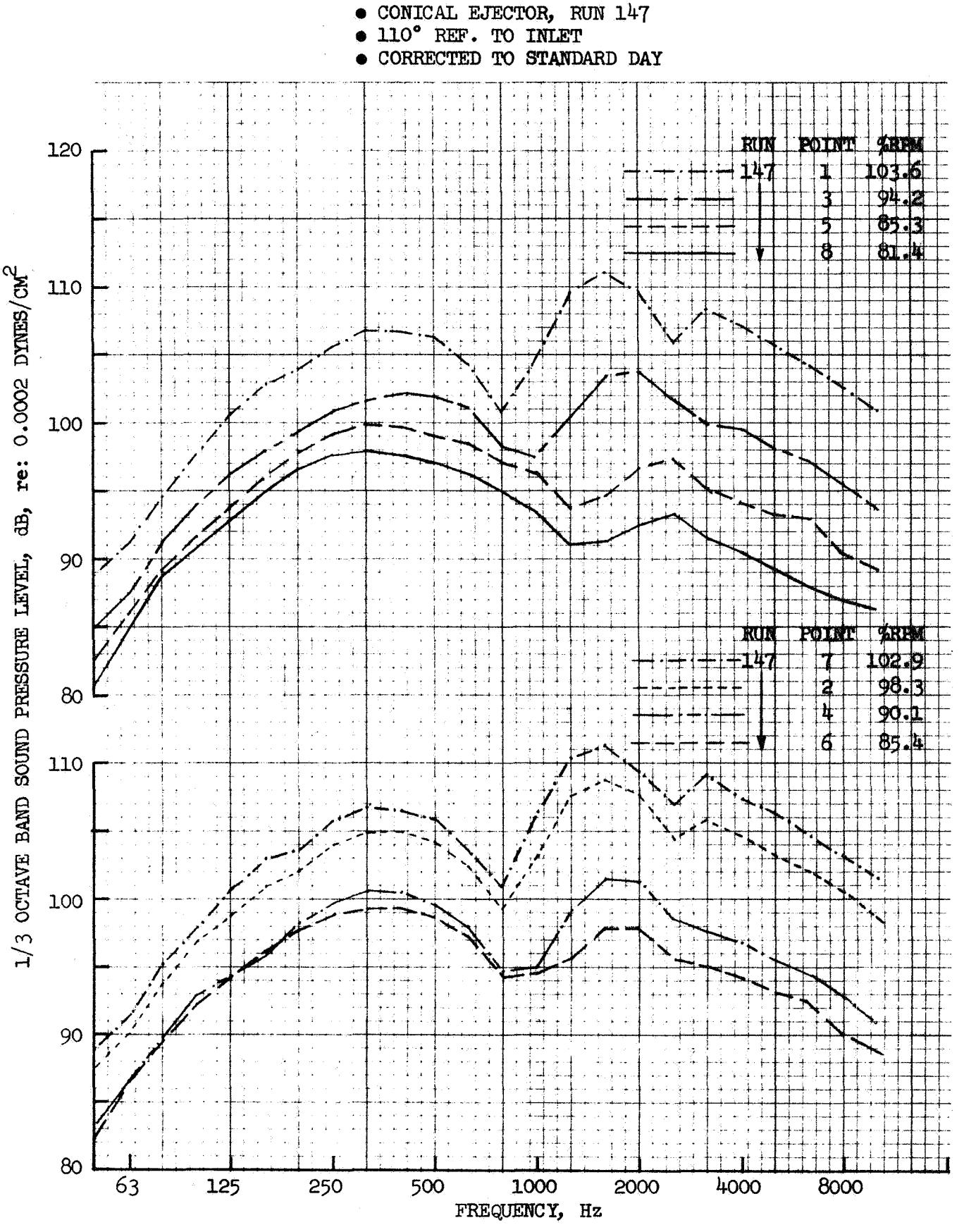

FIGURE 24 100 FT. ARC J85 GROUND STATIC SPECTRA, CONICAL EJECTOR

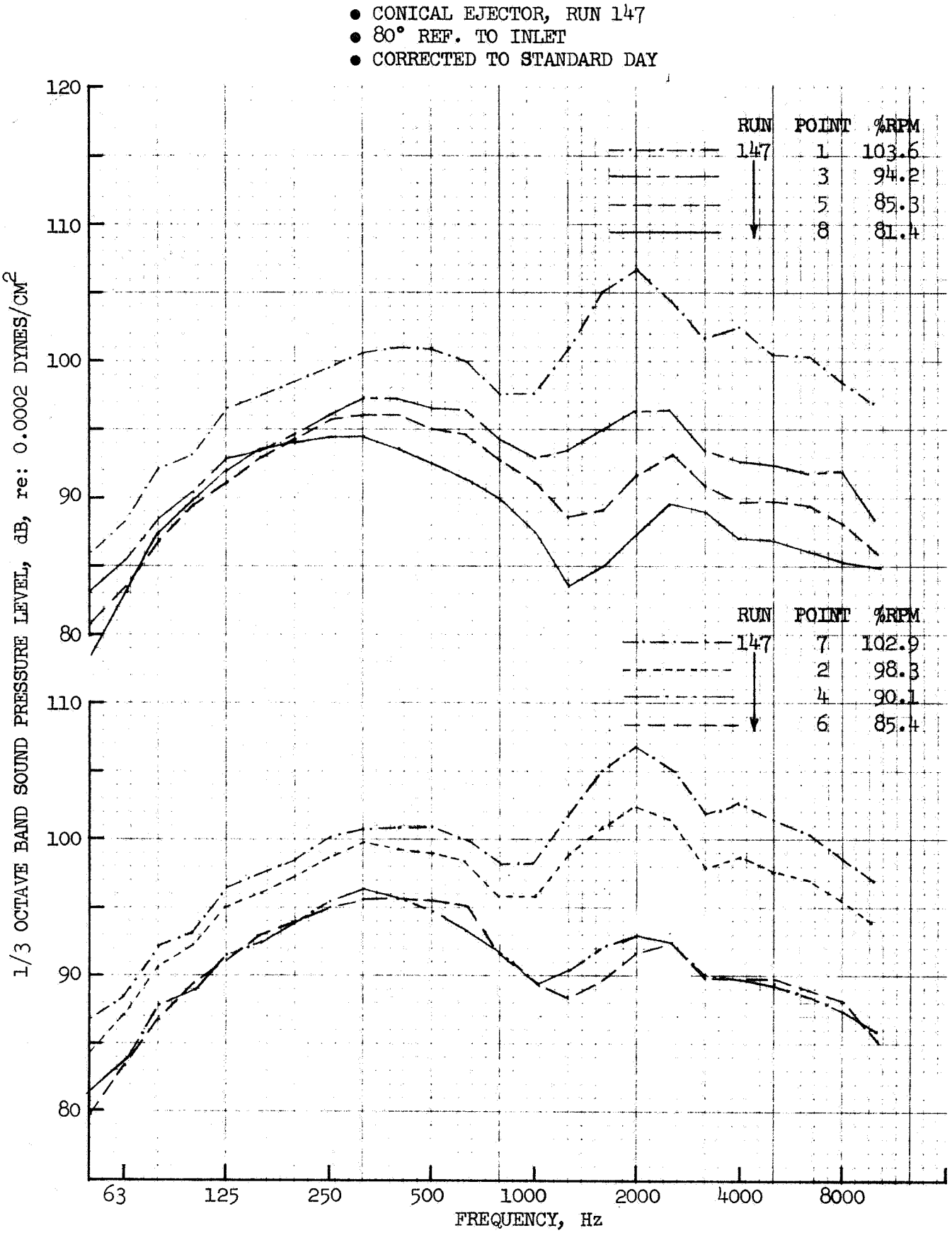

FIGURE 25 100 FT. ARC J85 GROUND STATIC SPECTRA, CONICAL EJECTOR

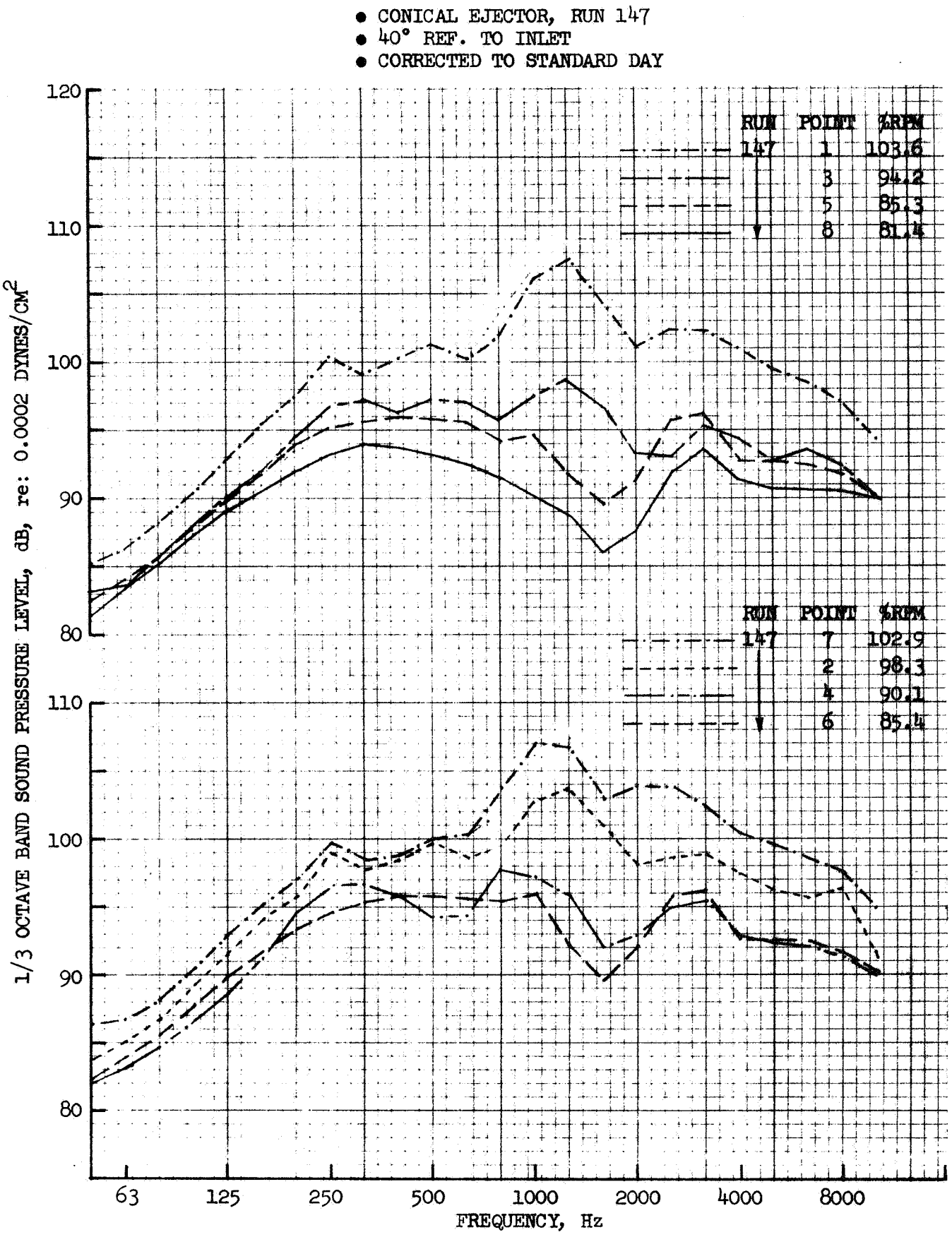

FIGURE 26 100 FT. ARC J85 GROUND STATIC SPECTRA, CONICAL EJECTOR

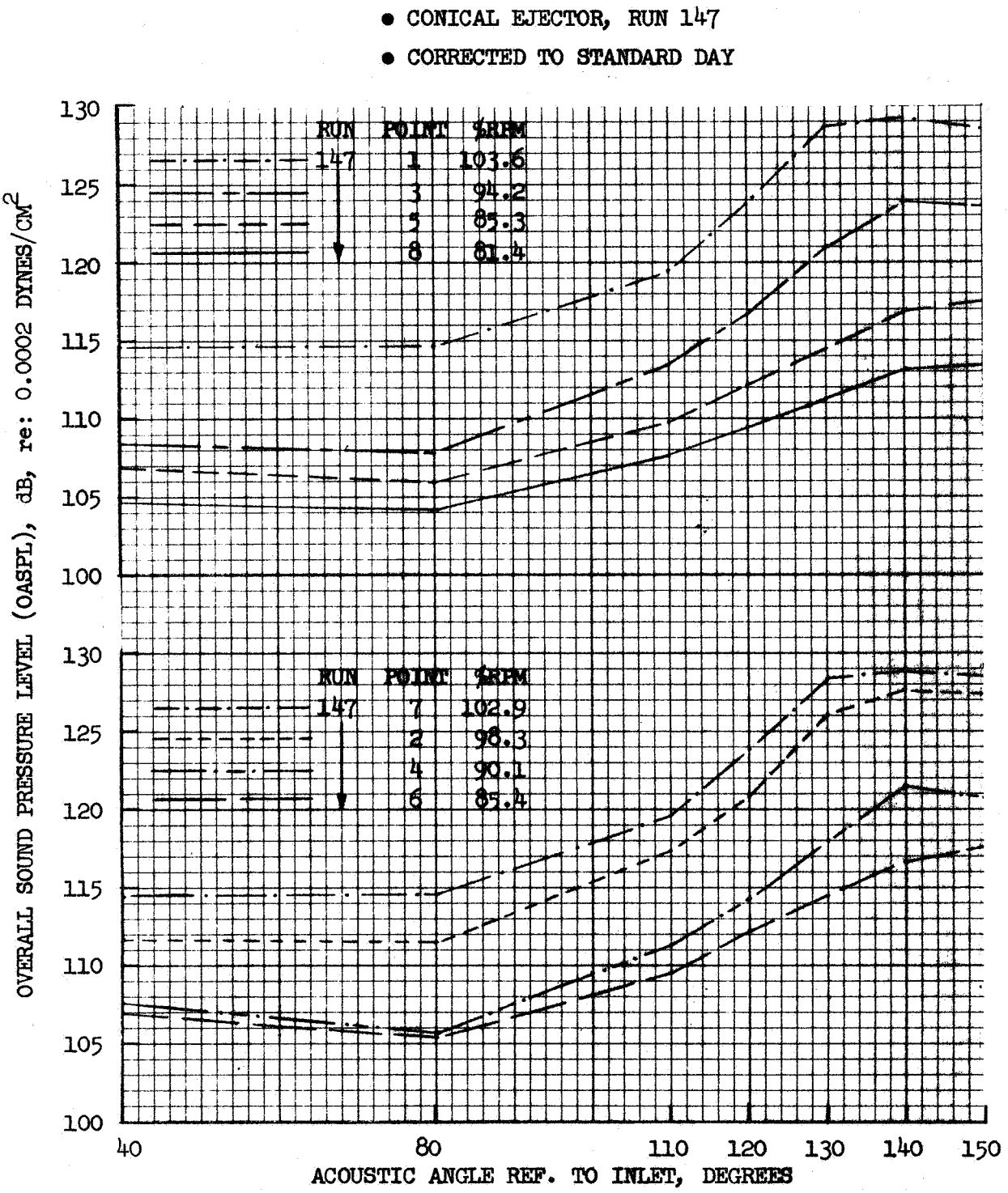

FIGURE 27 GROUND STATIC 100 FT. ARC OASPL DIRECTIVITY; CONICAL EJECTOR

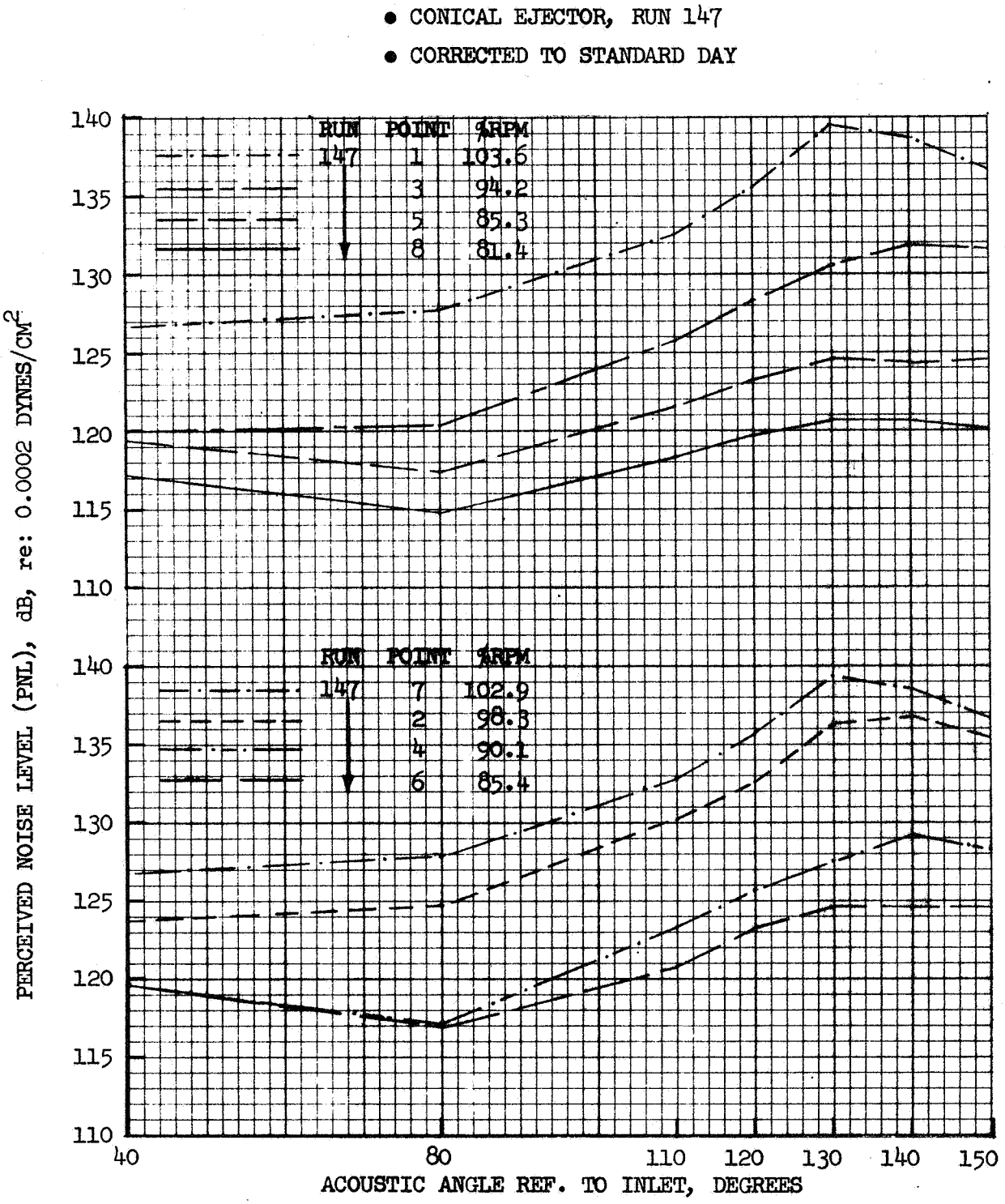

FIGURE 28 GROUND STATIC 100 FT. ARC PNL DIRECTIVITY; CONICAL EJECTOR

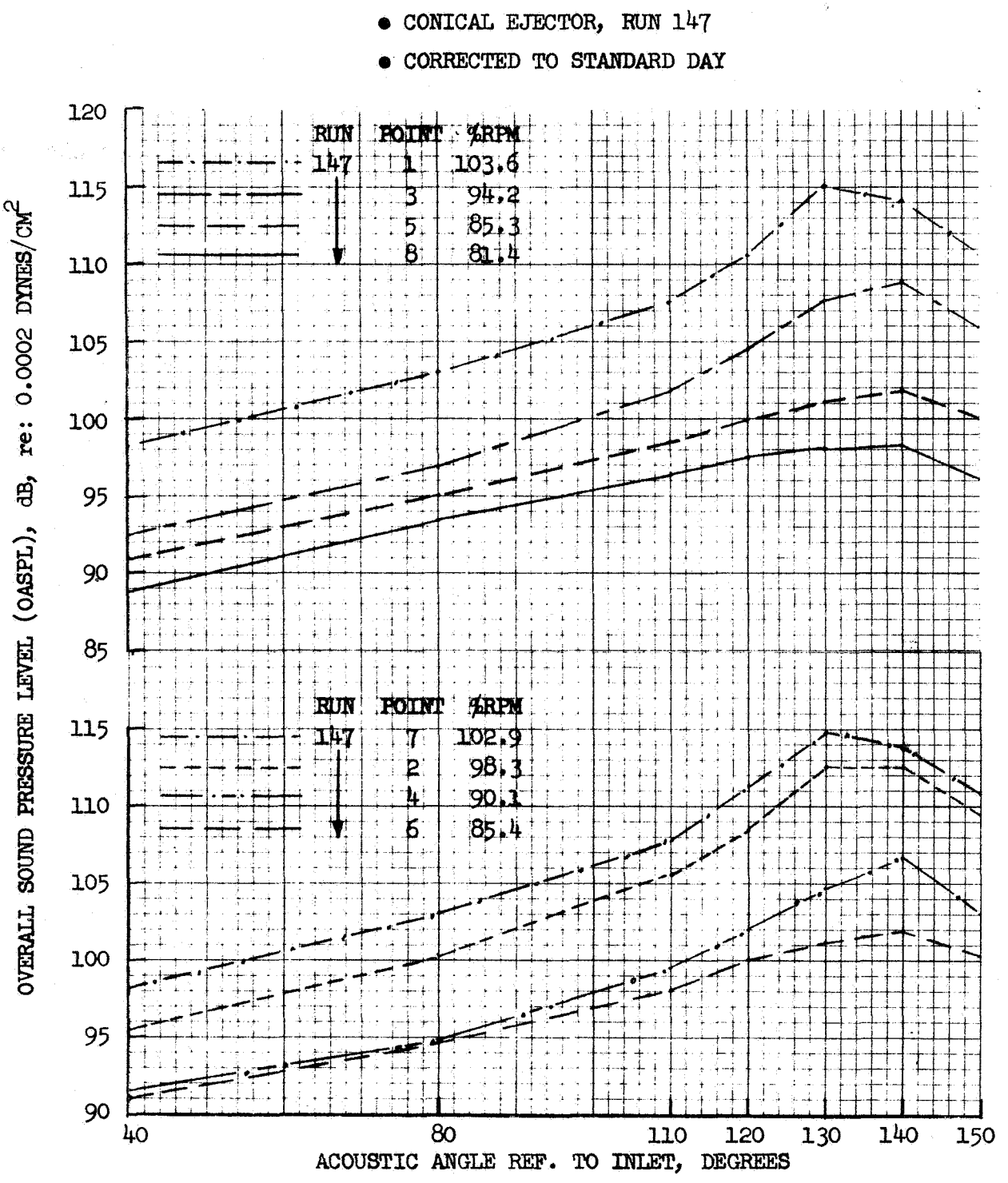

FIGURE 29 GROUND STATIC 300 FT. SIDELINE OASPL DIRECTIVITY; CONICAL EJECTOR

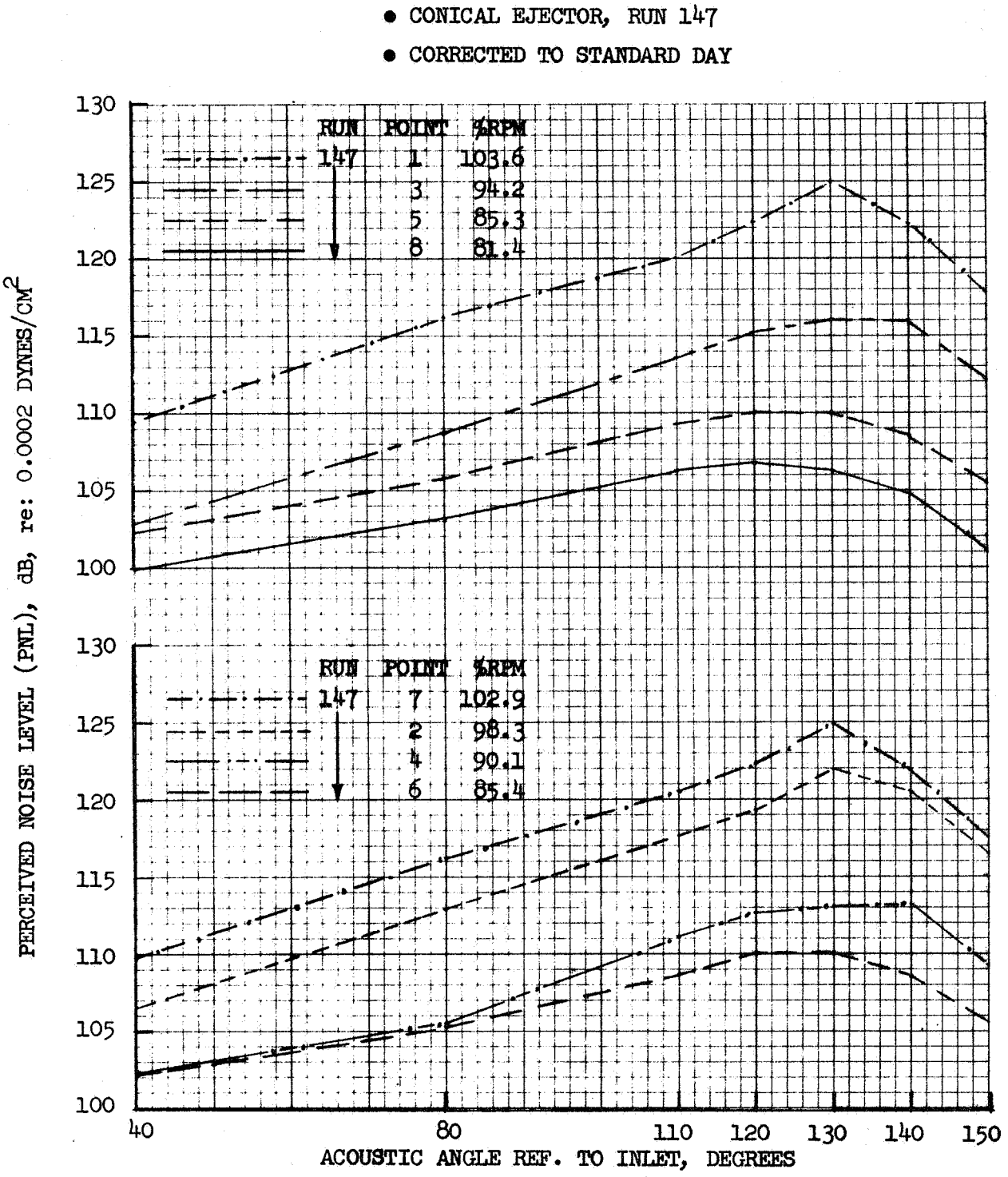

FIGURE 30 GROUND STATIC 300 FT. SIDELINE PNL DIRECTIVITY; CONICAL EJECTOR

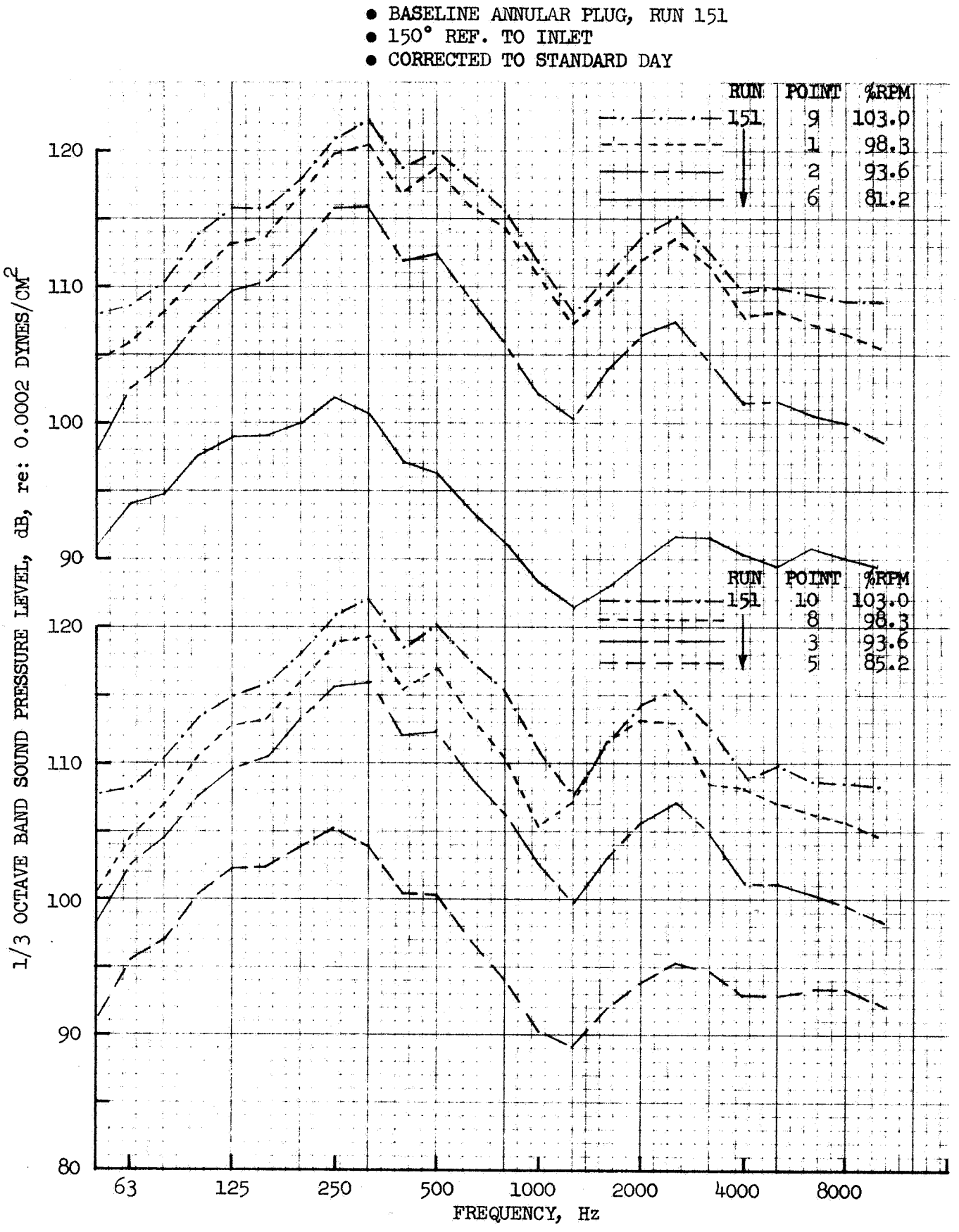

FIGURE 31 100 FT. ARC J85 GROUND STATIC SPECTRA, BASELINE ANNULAR PLUG

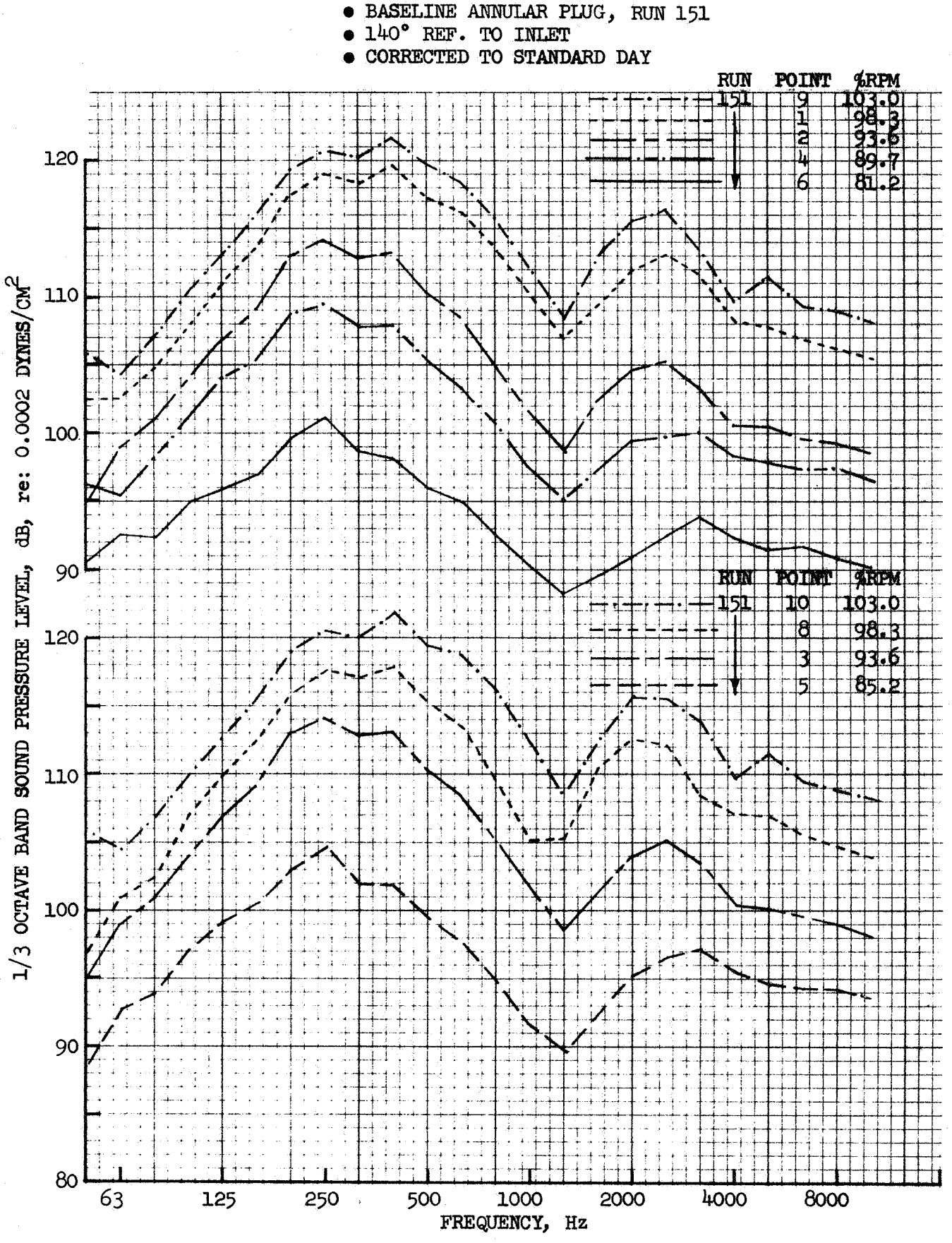

FIGURE 32 100 FT. ARC J85 GROUND STATIC SPECTRA, BASELINE ANNULAR PLUG

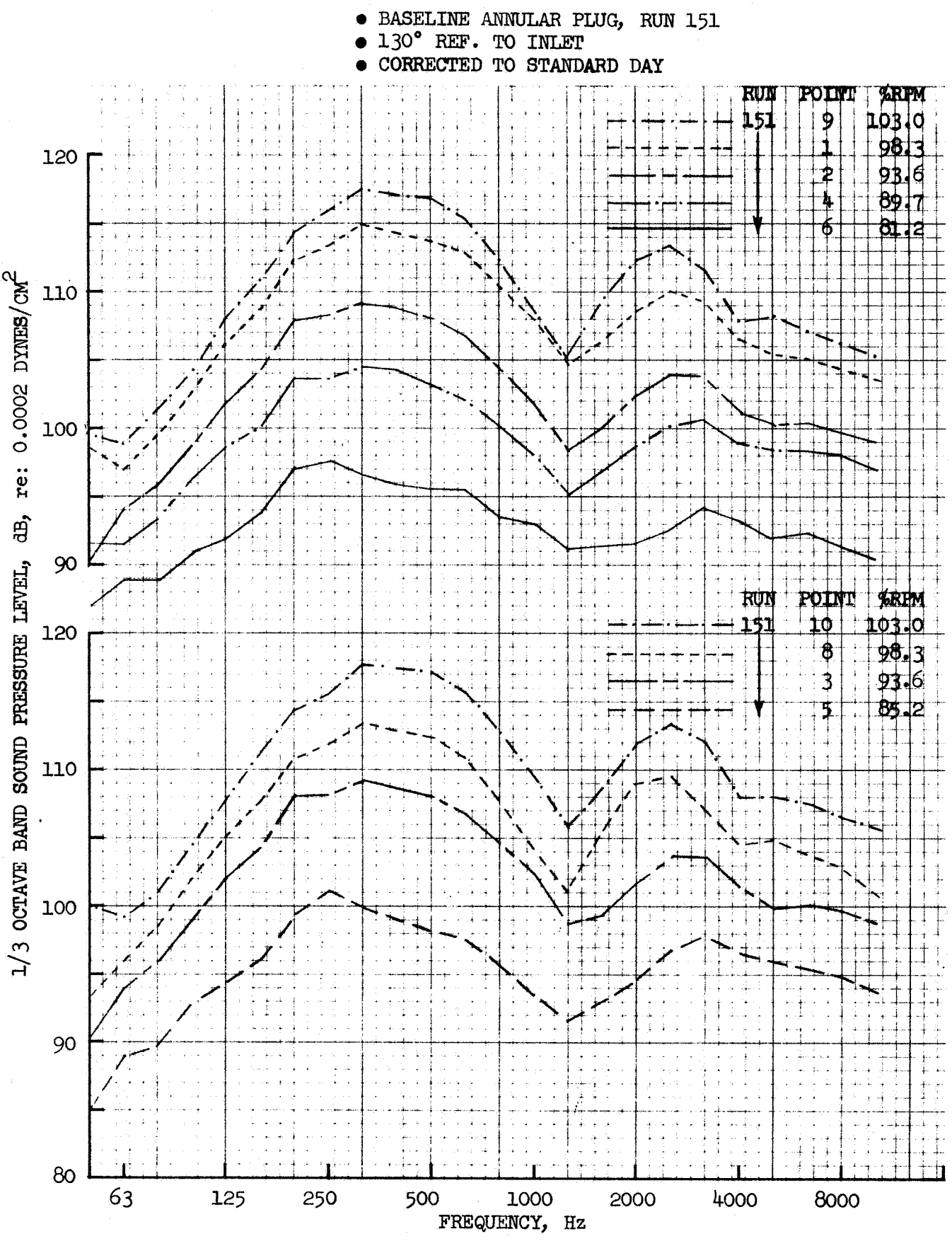

FIGURE 33 100 FT. ARC J85 GROUND STATIC SPECTRA, BASELINE ANNULAR PLUG

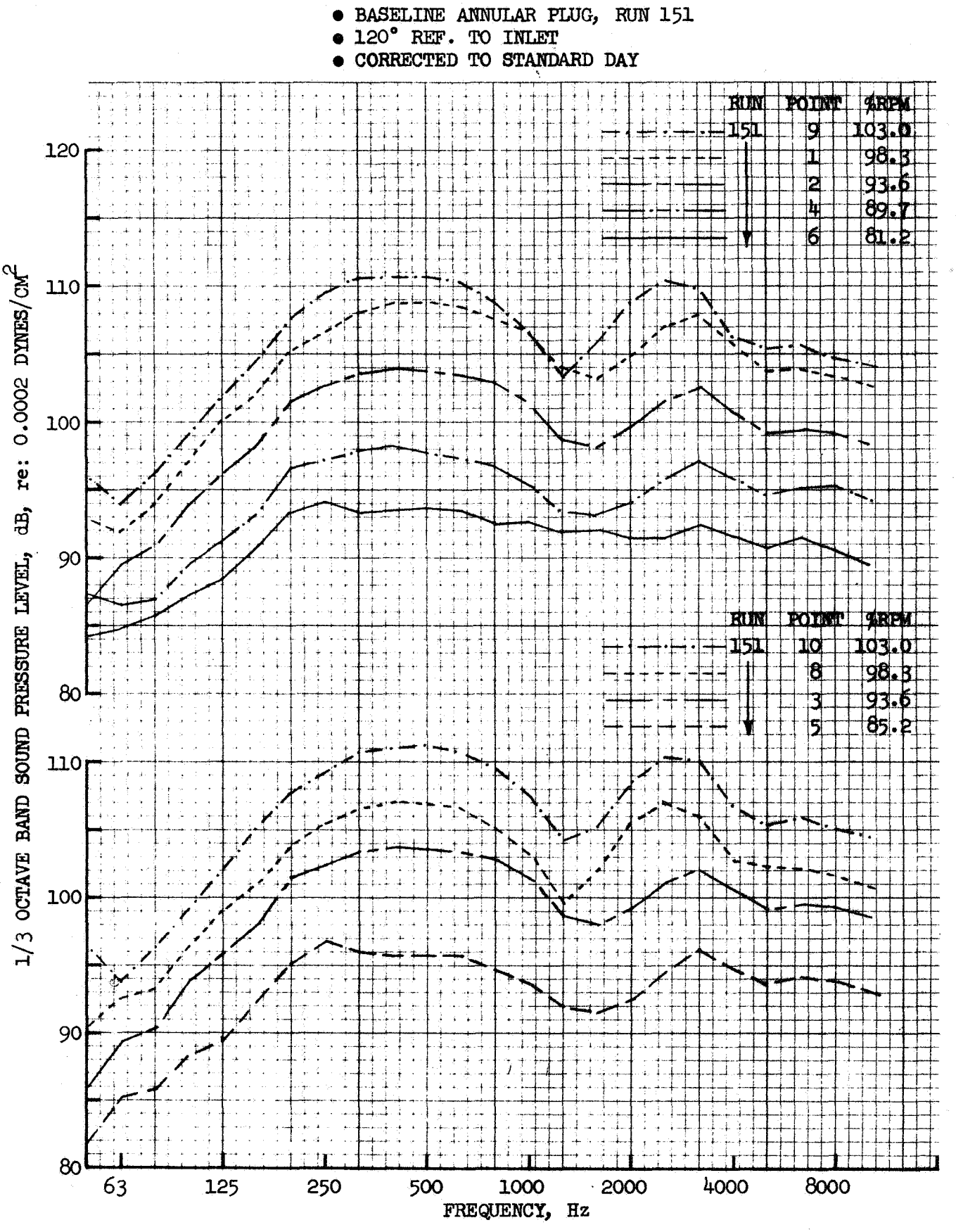

FIGURE 34 100 FT. ARC J85 GROUND STATIC SPECTRA, BASELINE ANNULAR PLUG

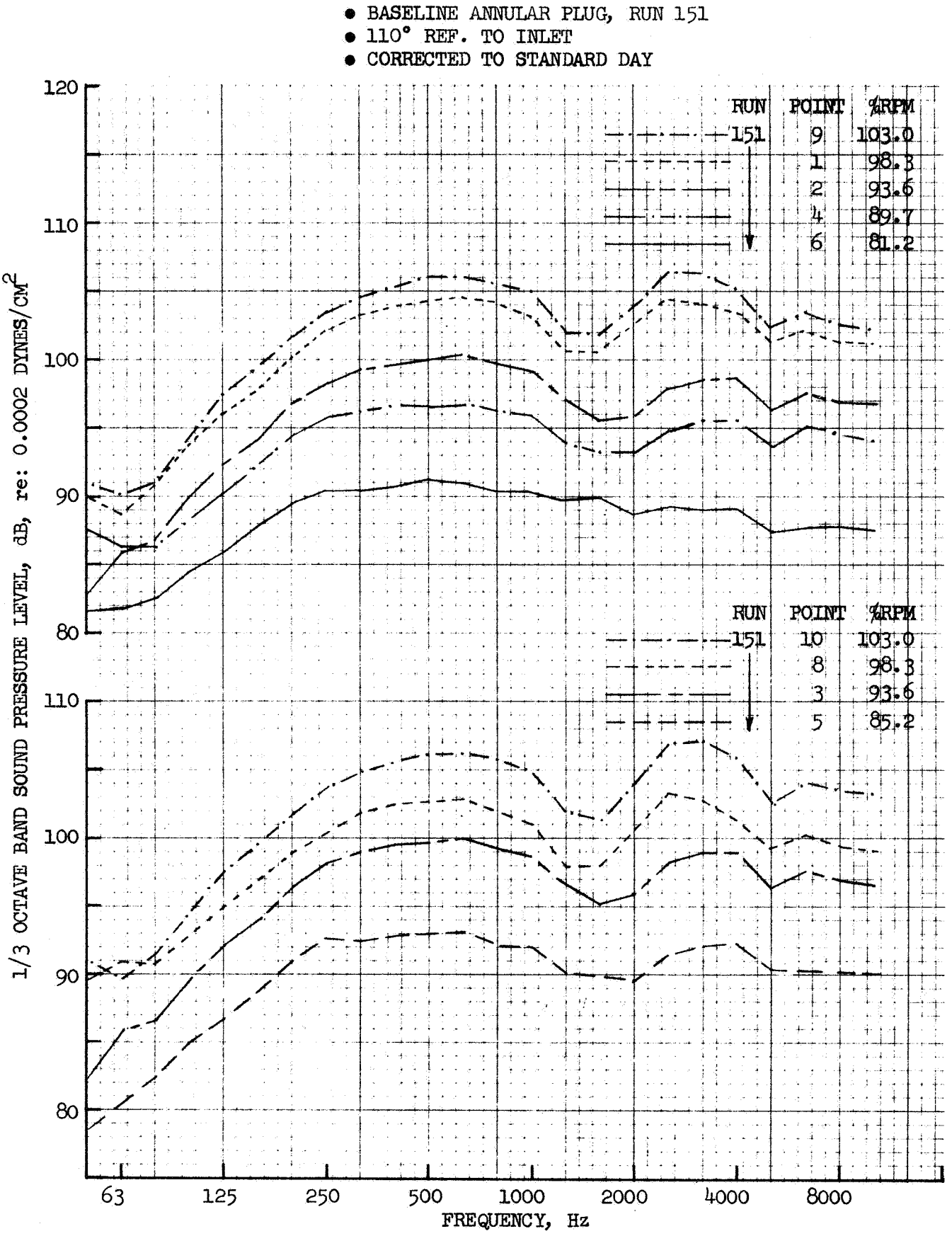

FIGURE 35 100 FT. ARC J85 GROUND STATIC SPECTRA, BASELINE ANNULAR PLUG

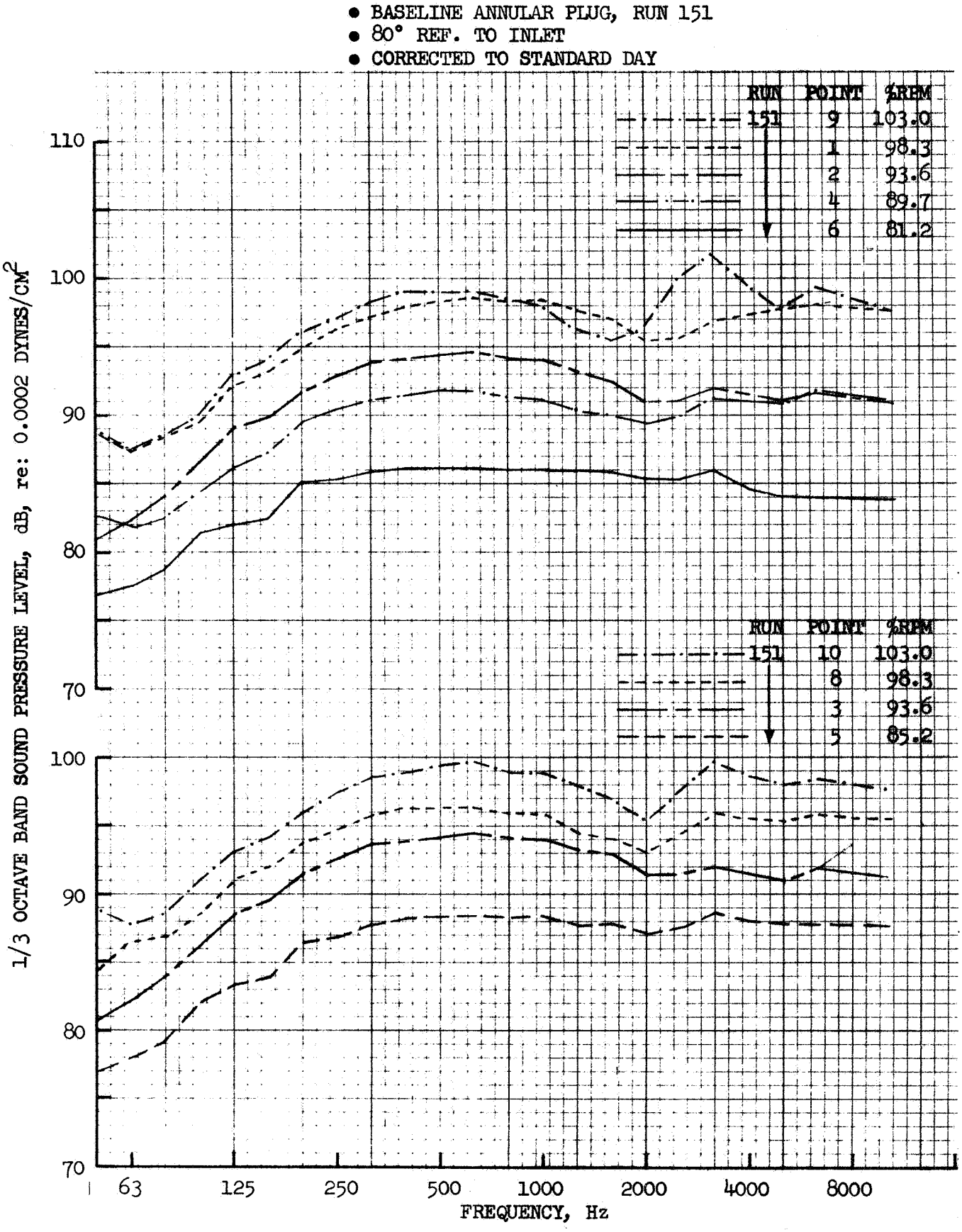

FIGURE 36 100 FT. ARC J85 GROUND STATIC SPECTRA, BASELINE ANNULAR PLUG

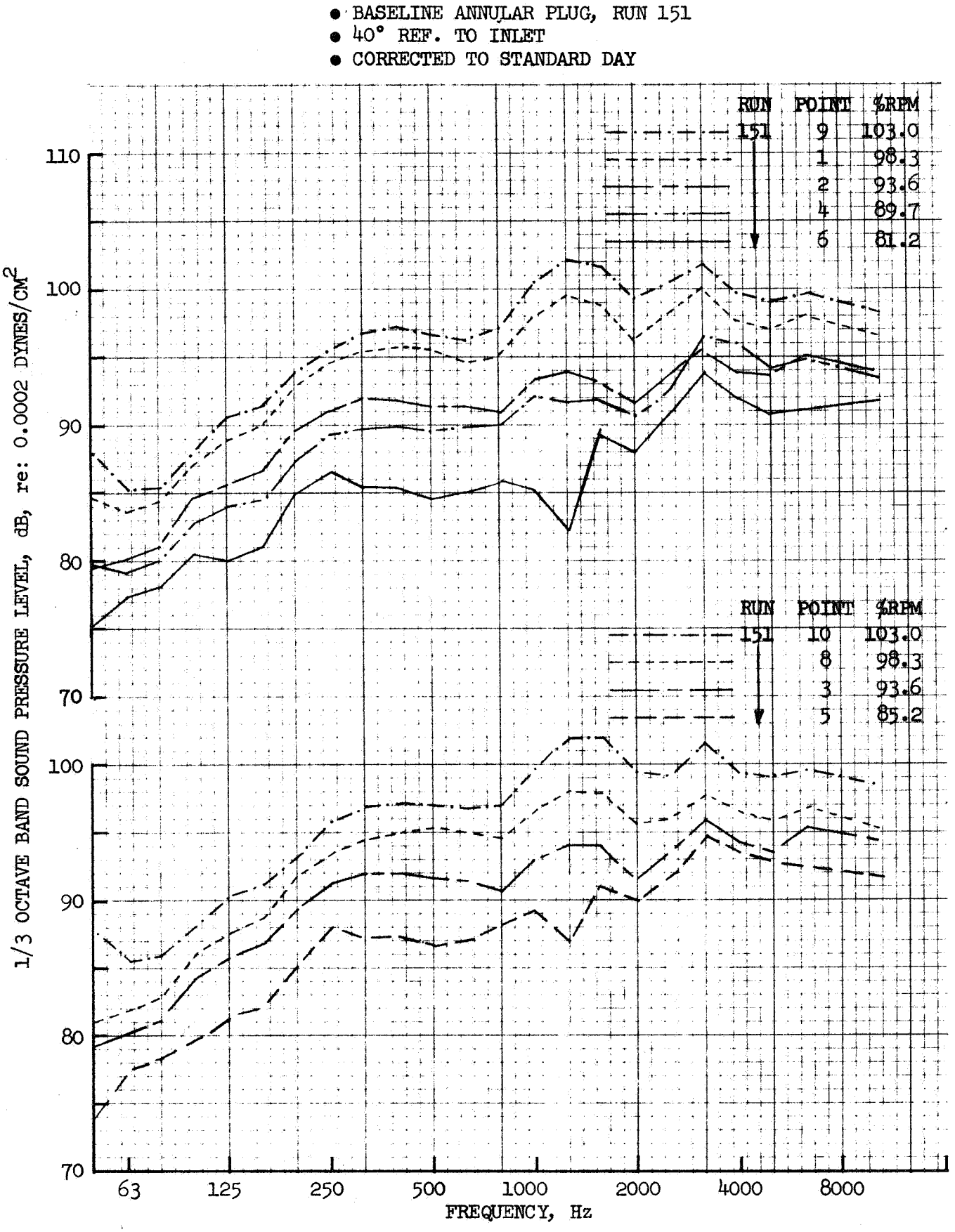

FIGURE 37 100 FT. ARC J85 GROUND STATIC SPECTRA, BASELINE ANNULAR PLUG

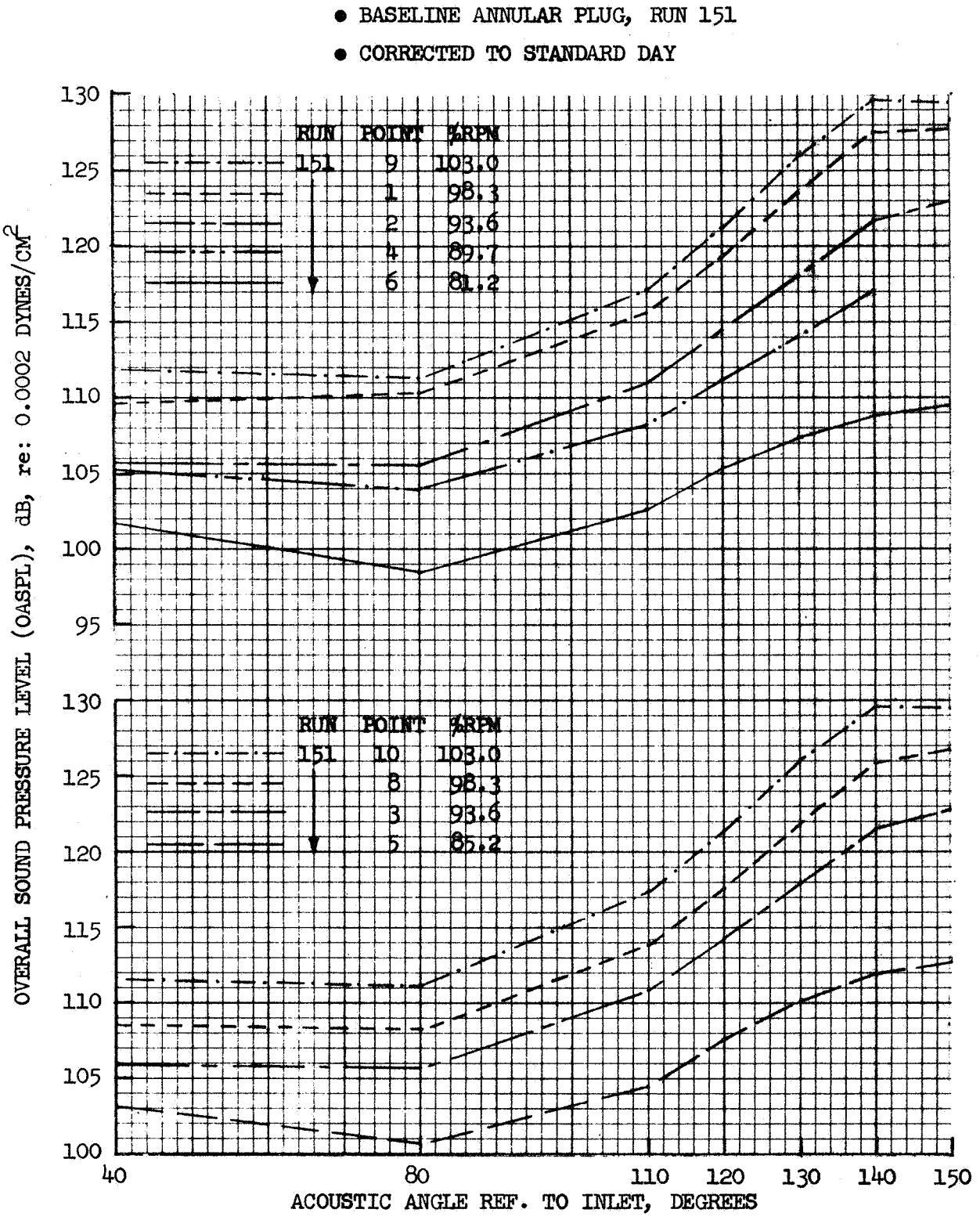

FIGURE 38 GROUND STATIC 100 FT. ARC OASPL DIRECTIVITY; BASELINE ANNULAR PLUG

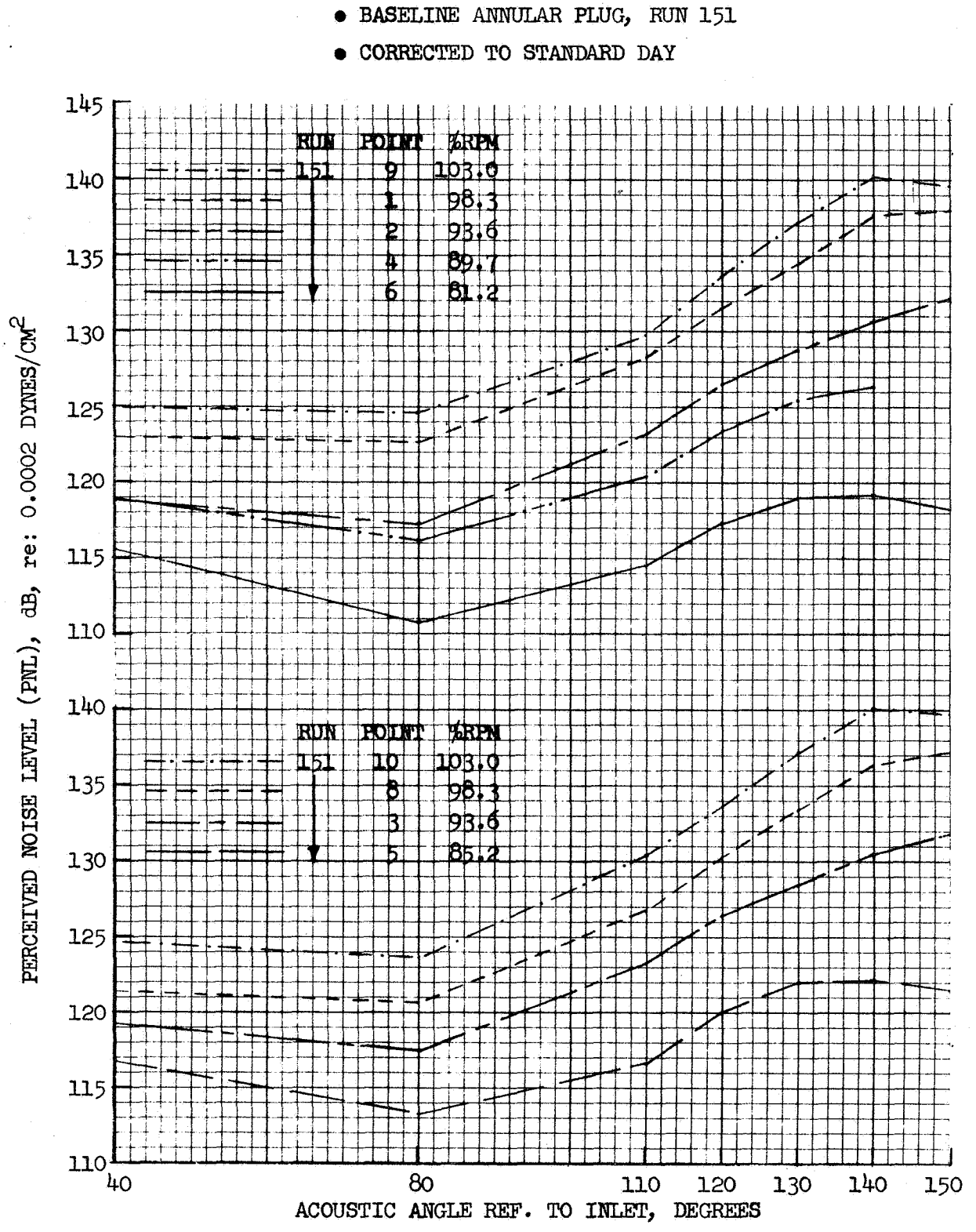

FIGURE 39 GROUND STATIC 100 FT. ARC PNL DIRECTIVITY; BASELINE ANNULAR PLUG

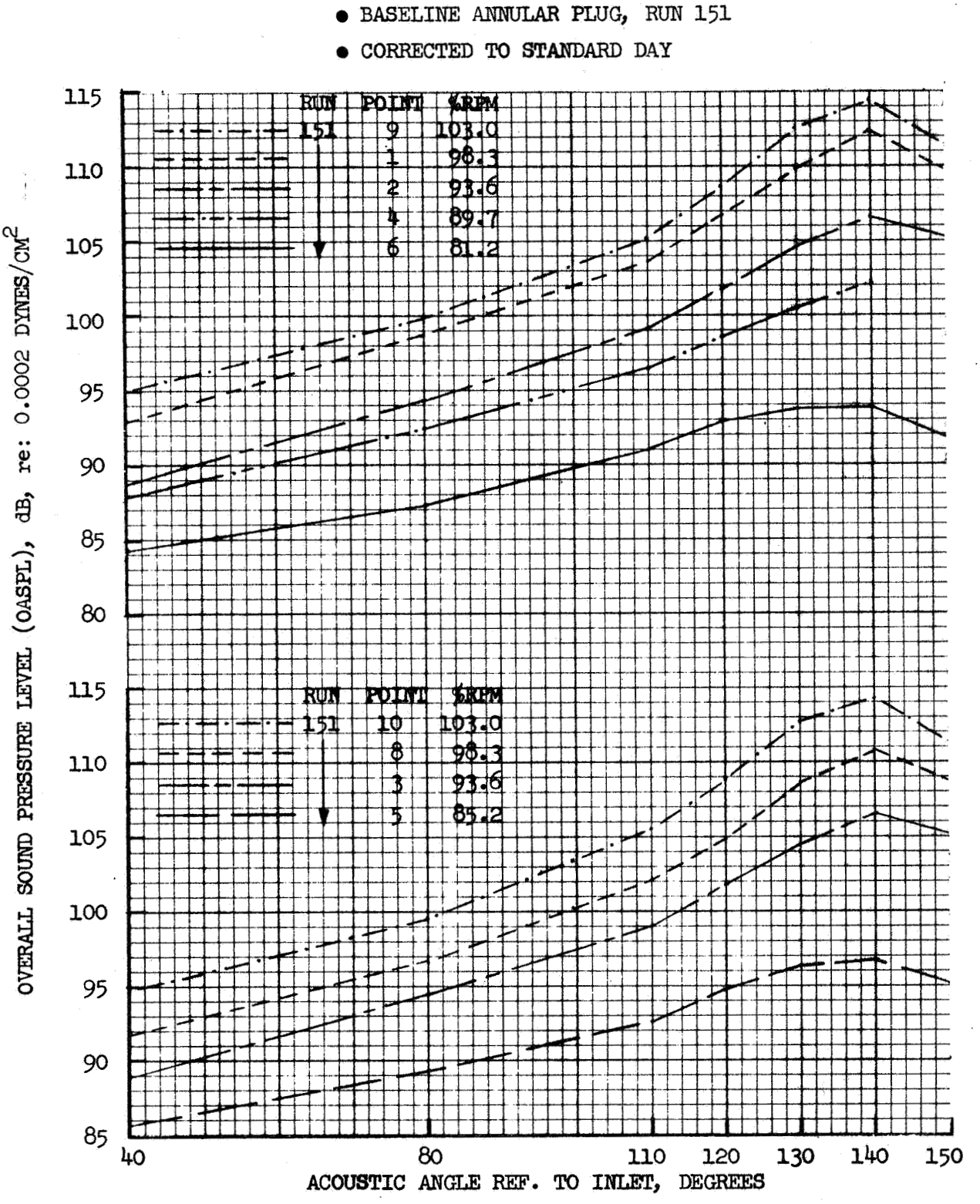

FIGURE 40 GROUND STATIC 300 FT. SIDELINE OASPL DIRECTIVITY; BASELINE ANNULAR PLUG

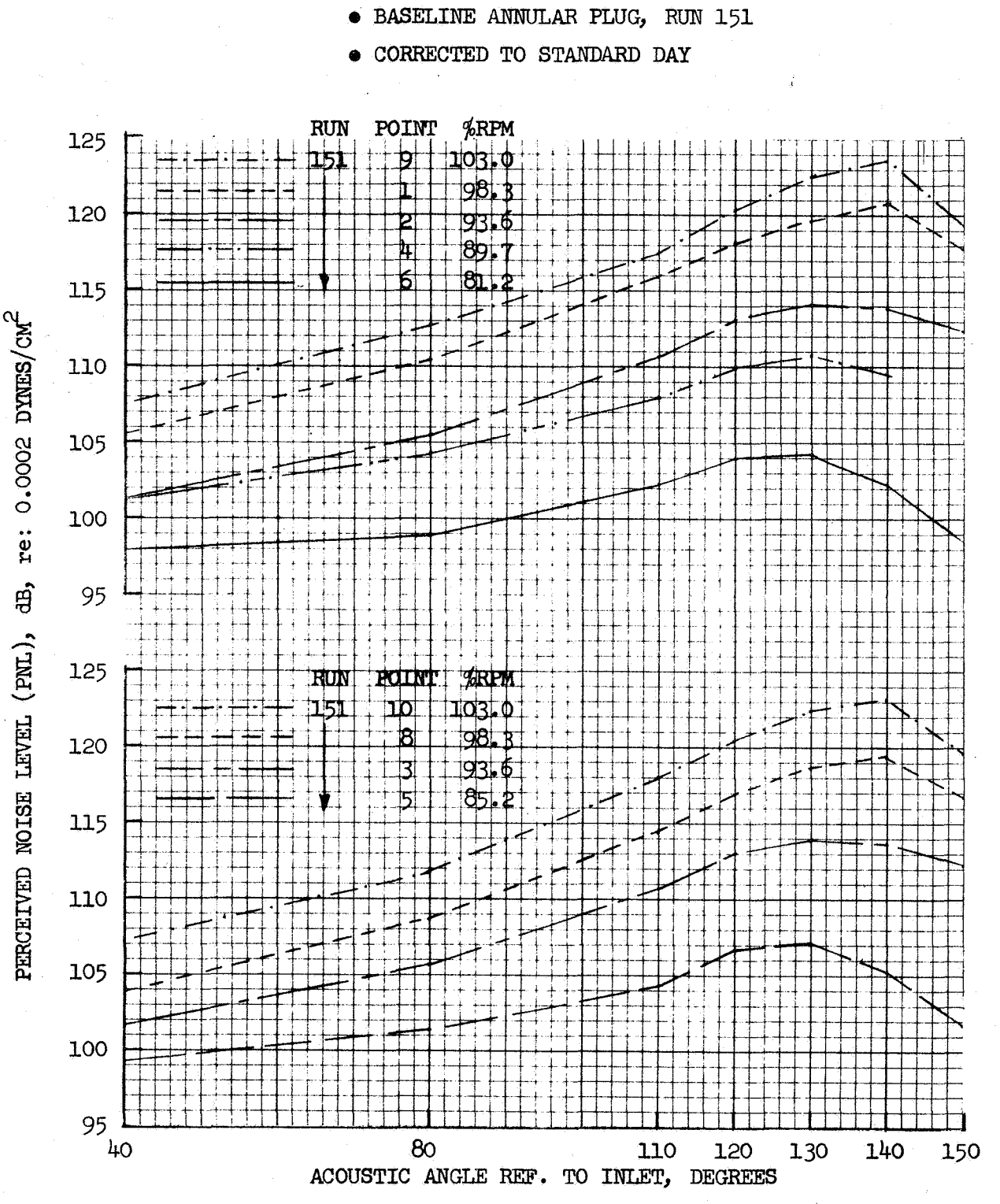

FIGURE 41 GROUND STATIC 300 FT. SIDELINE PNL DIRECTIVITY; BASELINE ANNULAR PLUG

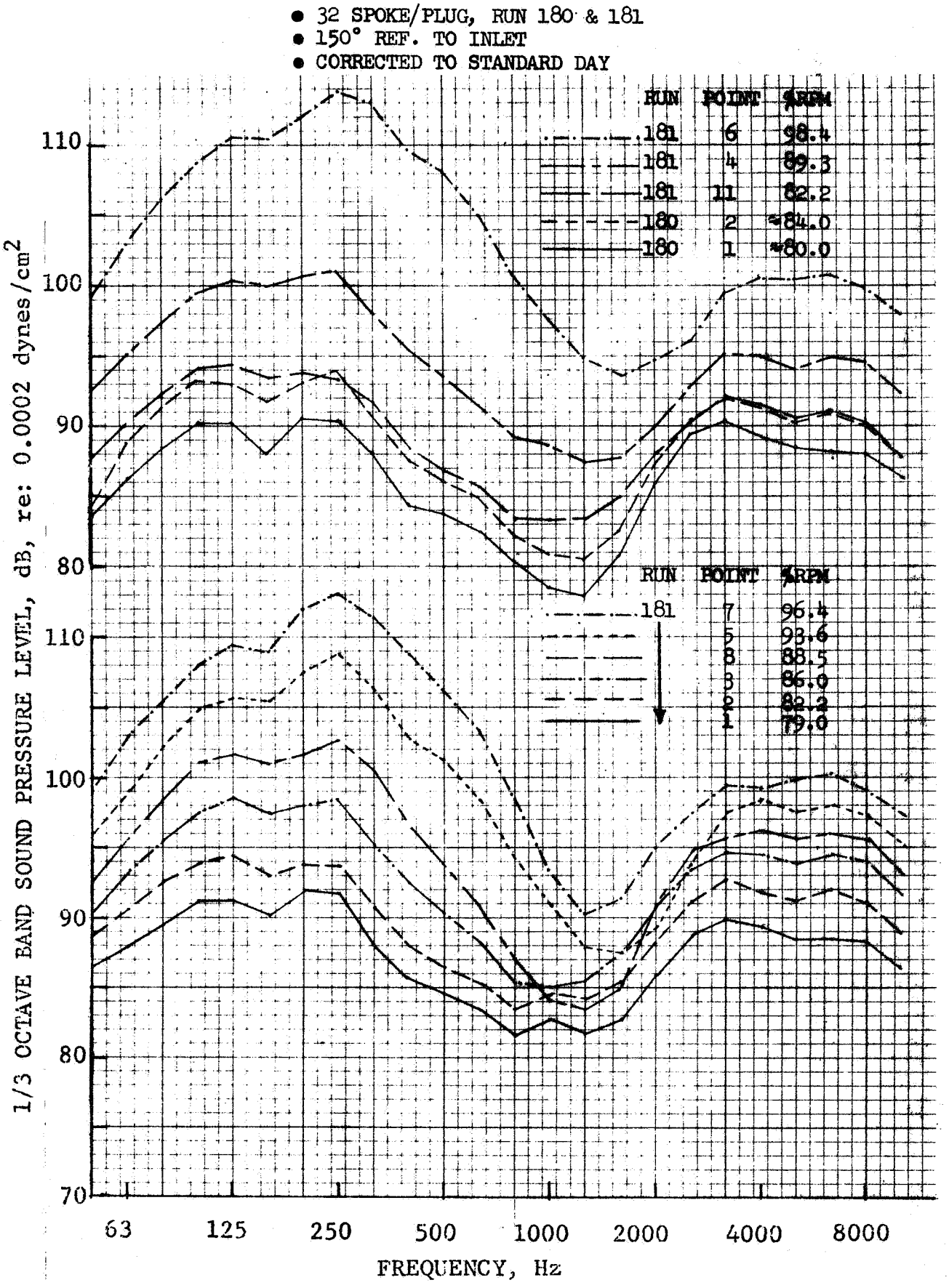

FIGURE 42 100 FT. ARC J85 GROUND STATIC SPECTRA, 32 SPOKE/PLUG

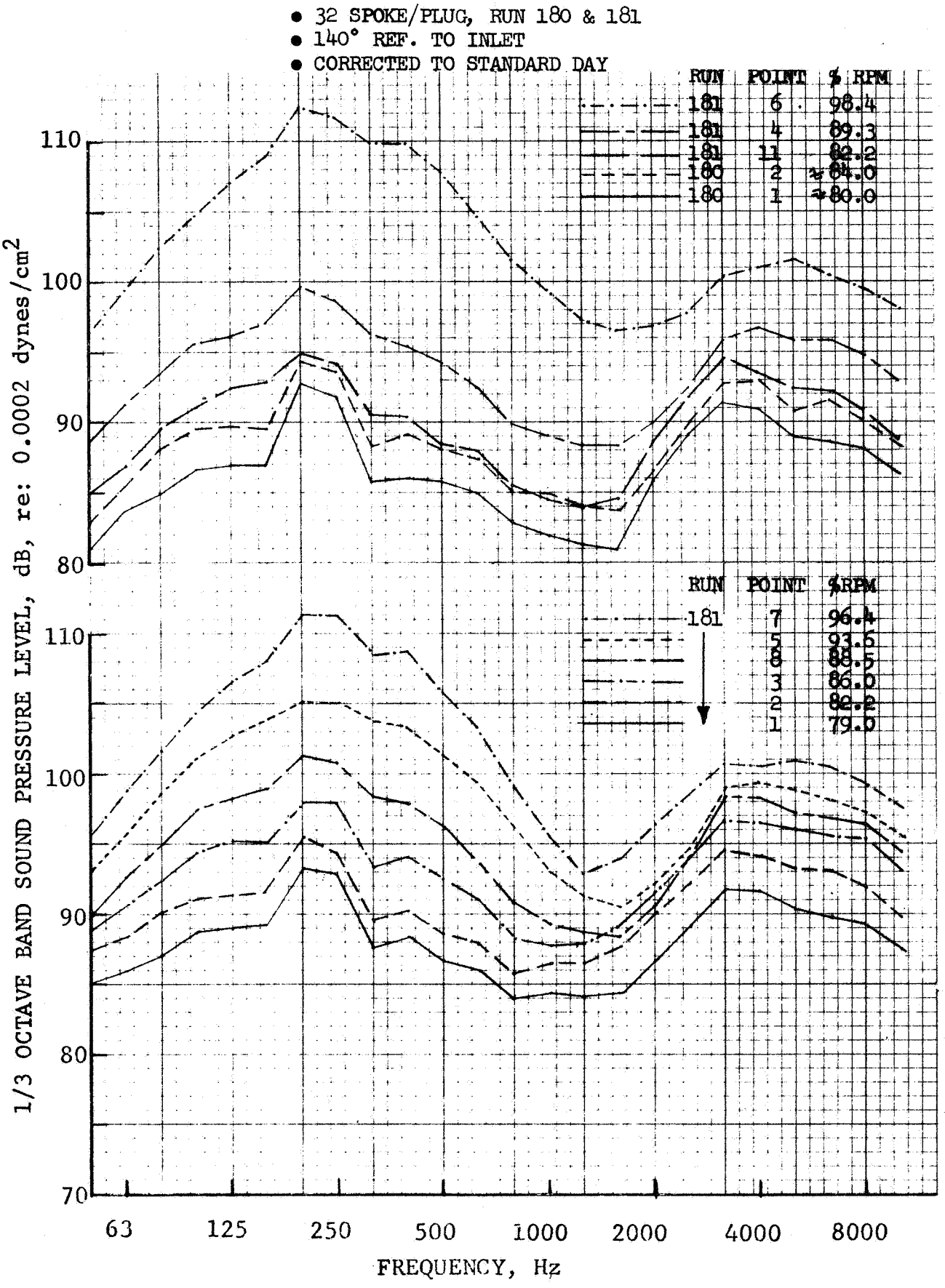

FIGURE 43 100 FT. ARC J85 GROUND STATIC SPECTRA, 32 SPOKE/PLUG

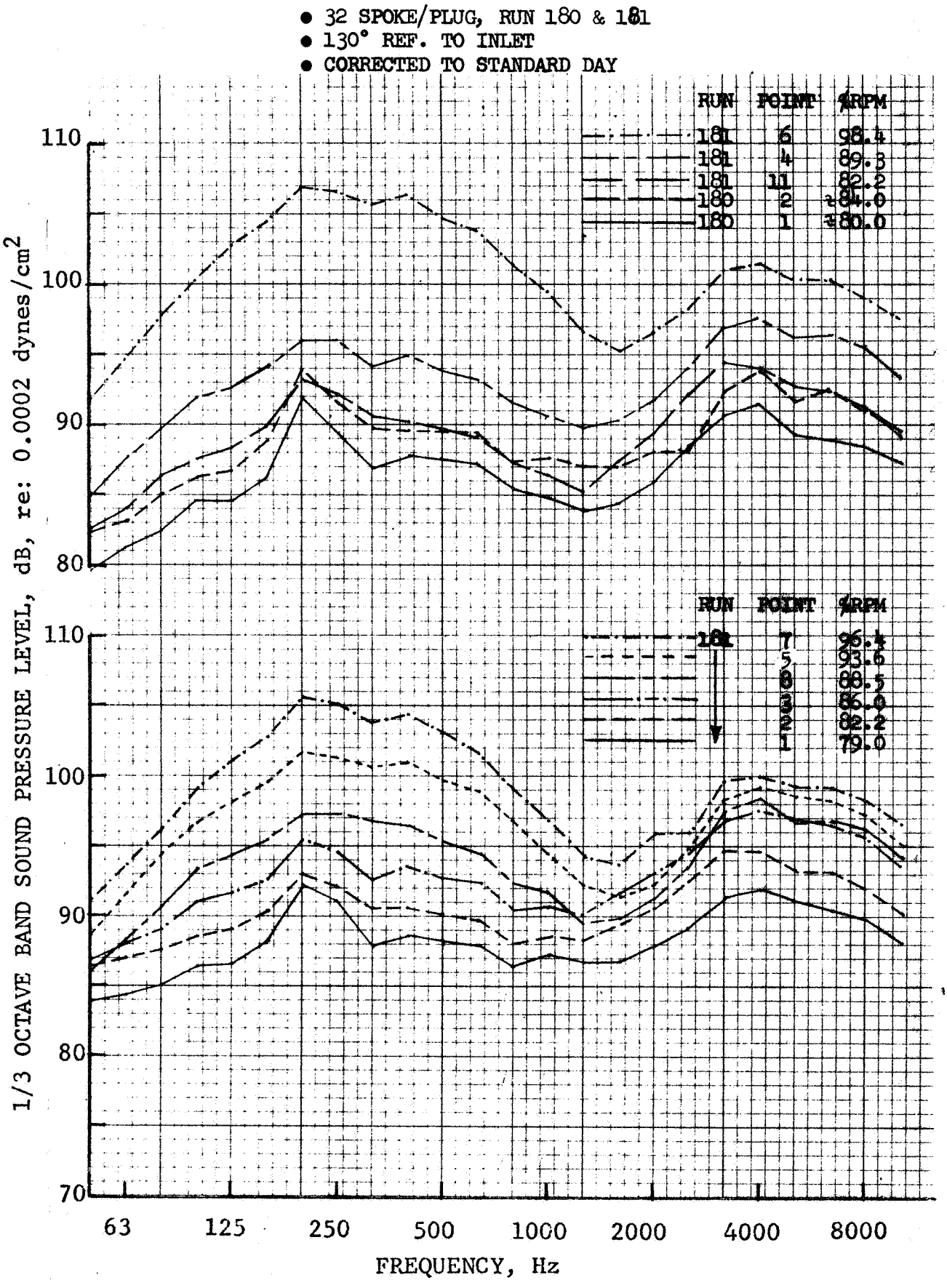

FIGURE 44 100 FT. ARC J85 GROUND STATIC SPECTRA, 32 SPOKE/PLUG

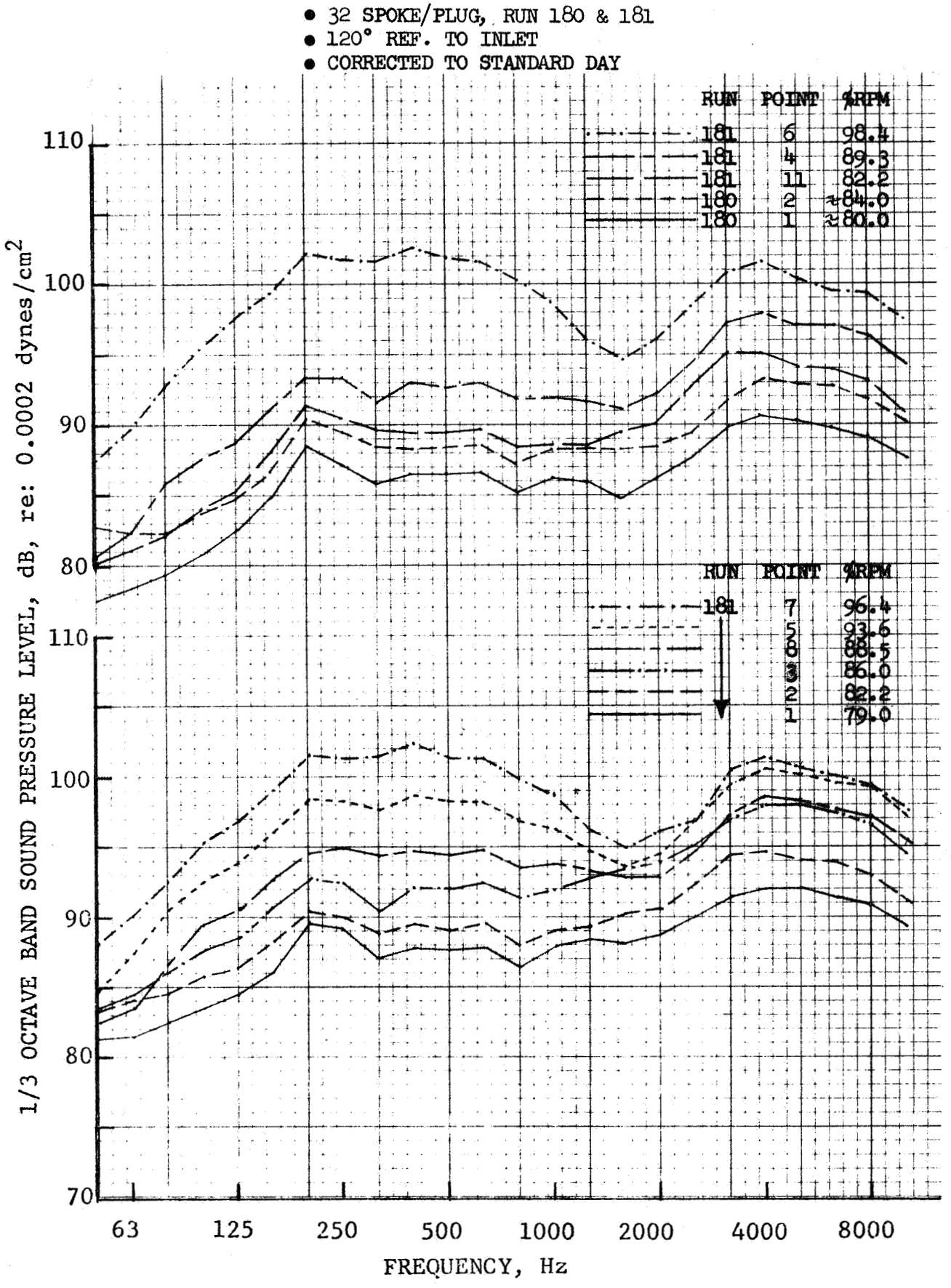

FIGURE 45 100 FT. ARC J85 GROUND STATIC SPECTRA, 32 SPOKE/PLUG

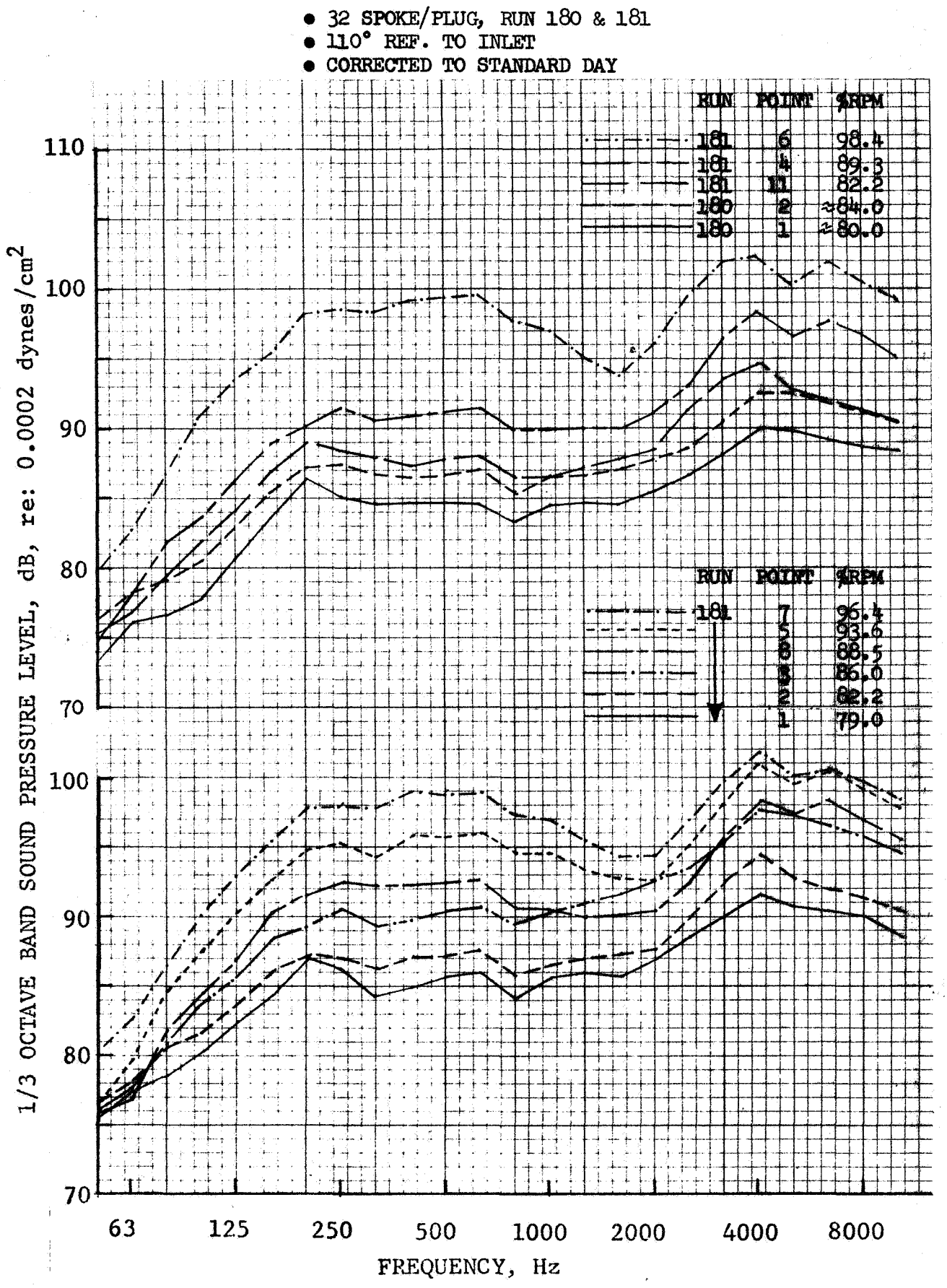

FIGURE 46 100 FT. ARC J85 GROUND STATIC SPECTRA, 32 SPOKE/PLUG

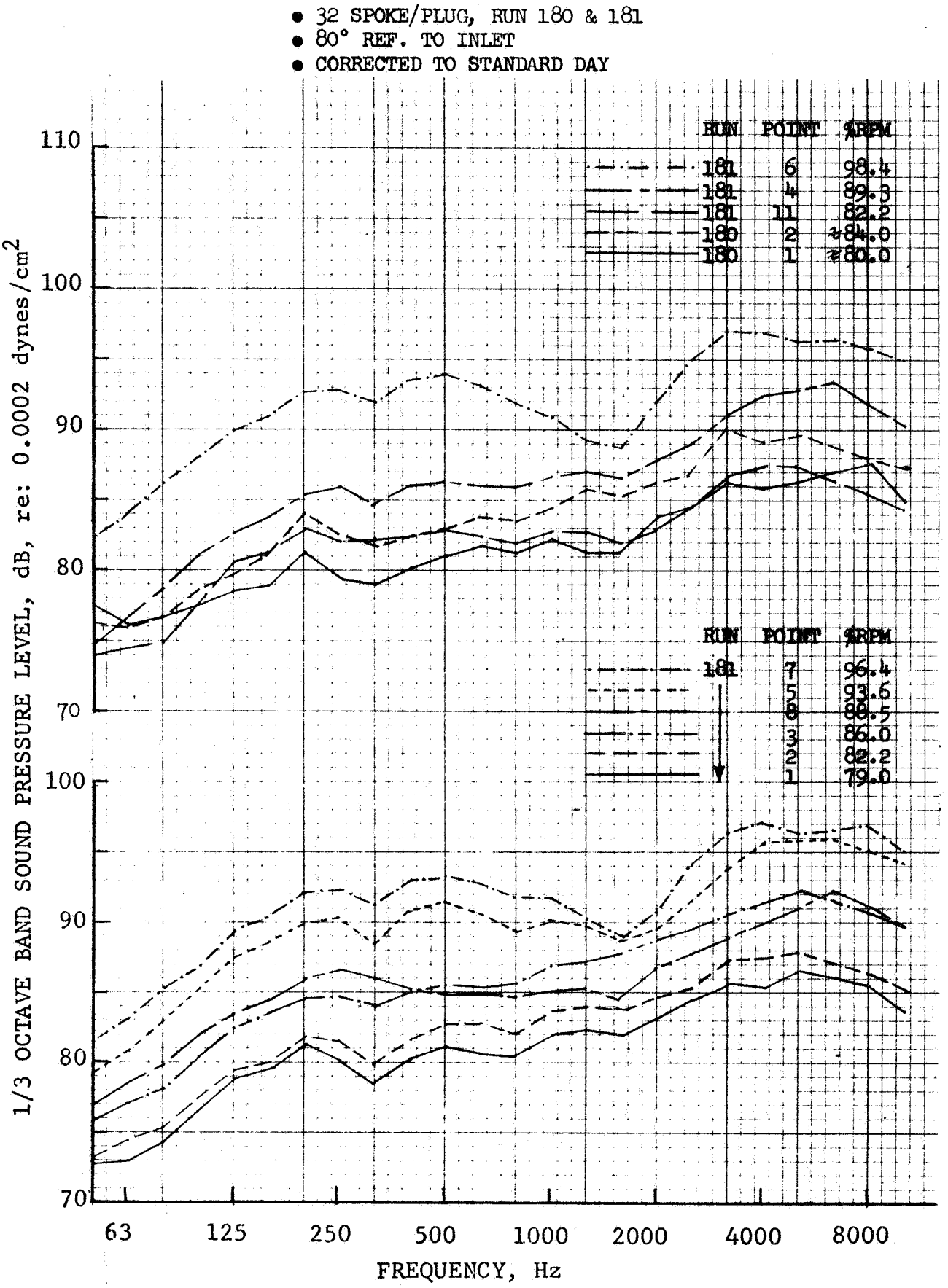

FIGURE 47 100 FT. ARC J85 GROUND STATIC SPECTRA, 32 SPOKE/PLUG

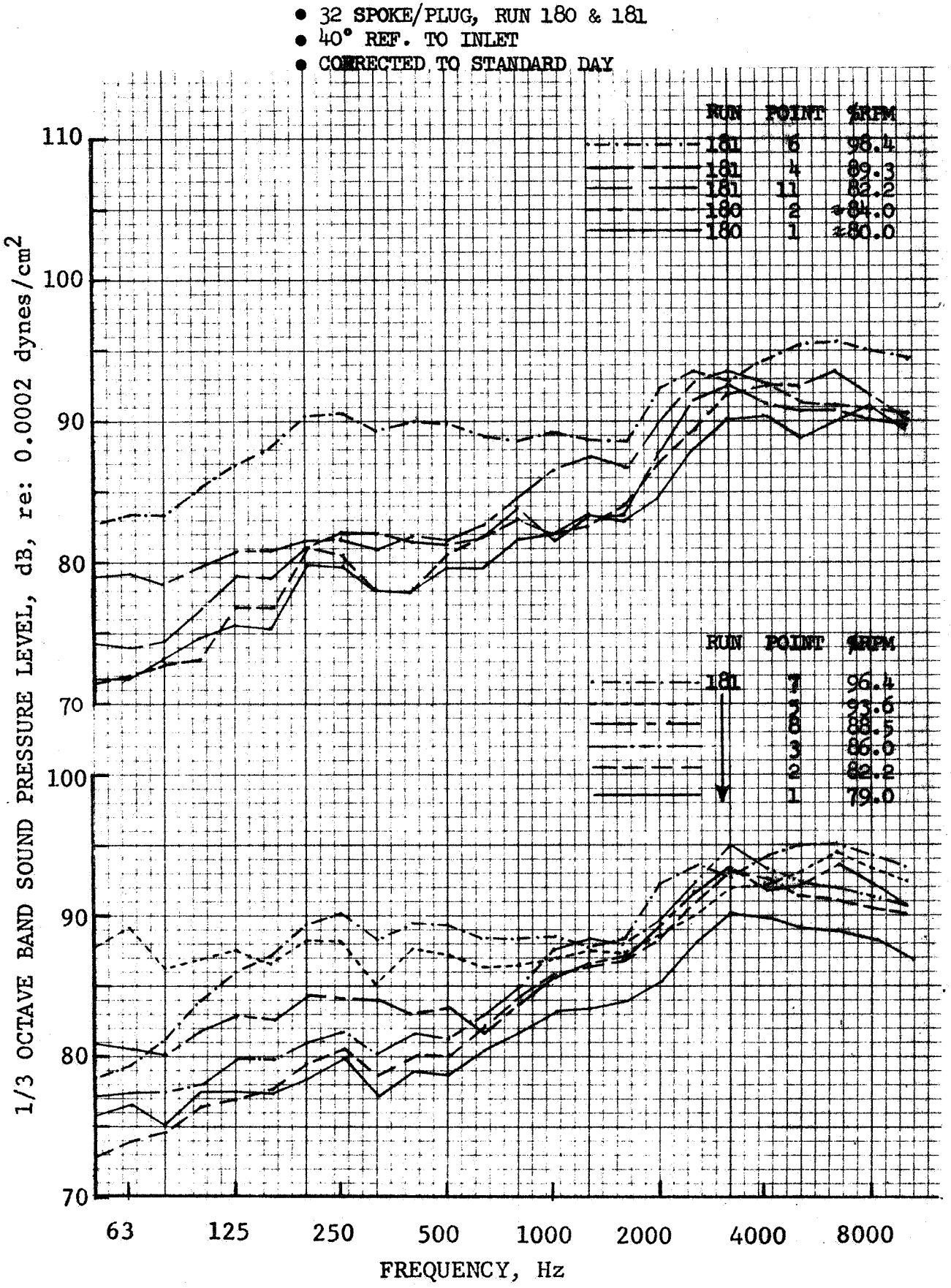

FIGURE 48 100 FT. ARC J85 GROUND STATIC SPECTRA, 32 SPOKE/PLUG

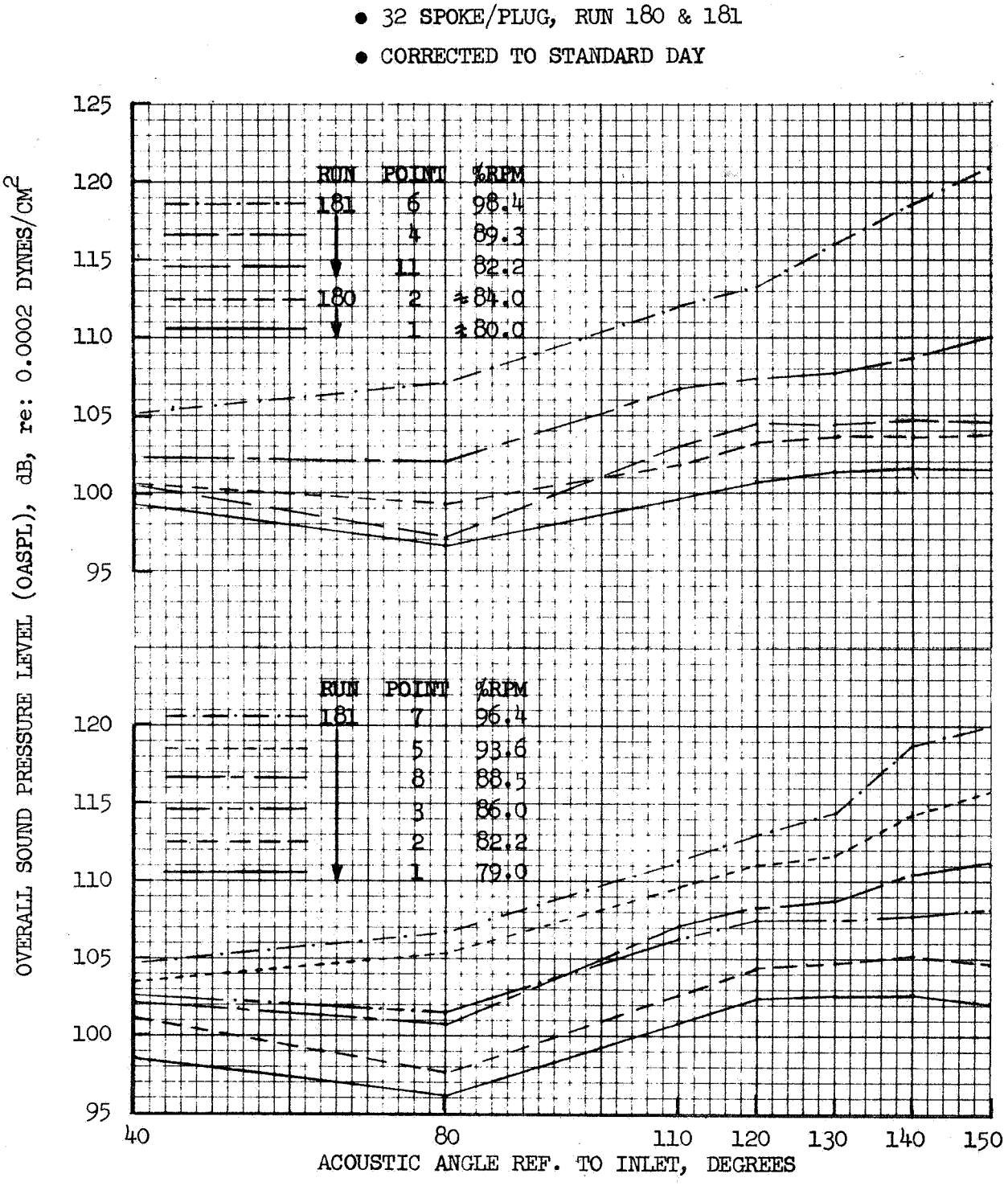

FIGURE 49 GROUND STATIC 100 FT. ARC OASPL DIRECTIVITY; 32 SPOKE/PLUG

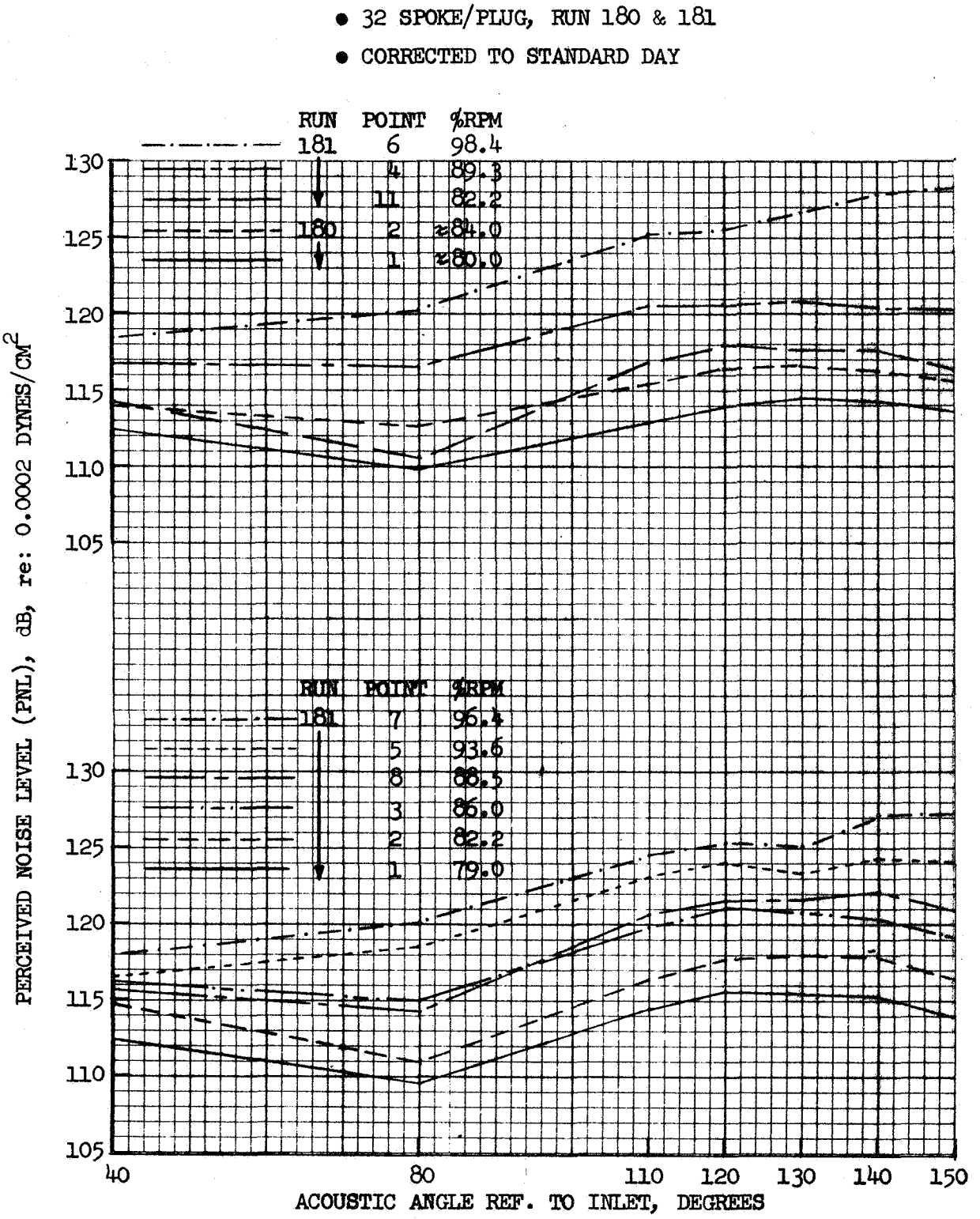

FIGURE 50 GROUND STATIC 100 FT. ARC PNL DIRECTIVITY; 32 SPOKE/PLUG

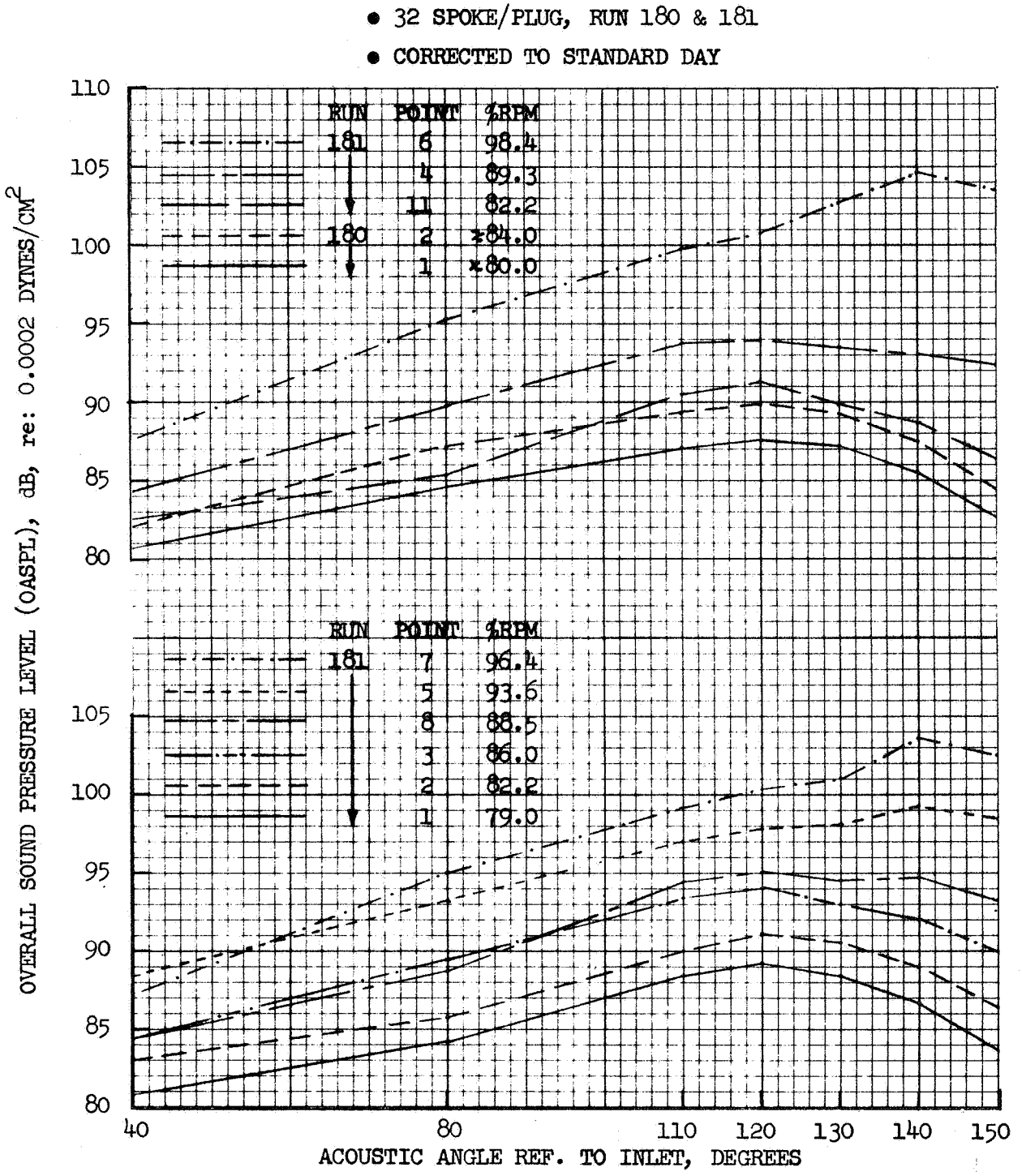

FIGURE 51 GROUND STATIC 300 FT. SIDELINE OASPL DIRECTIVITY; 32 SPOKE/PLUG

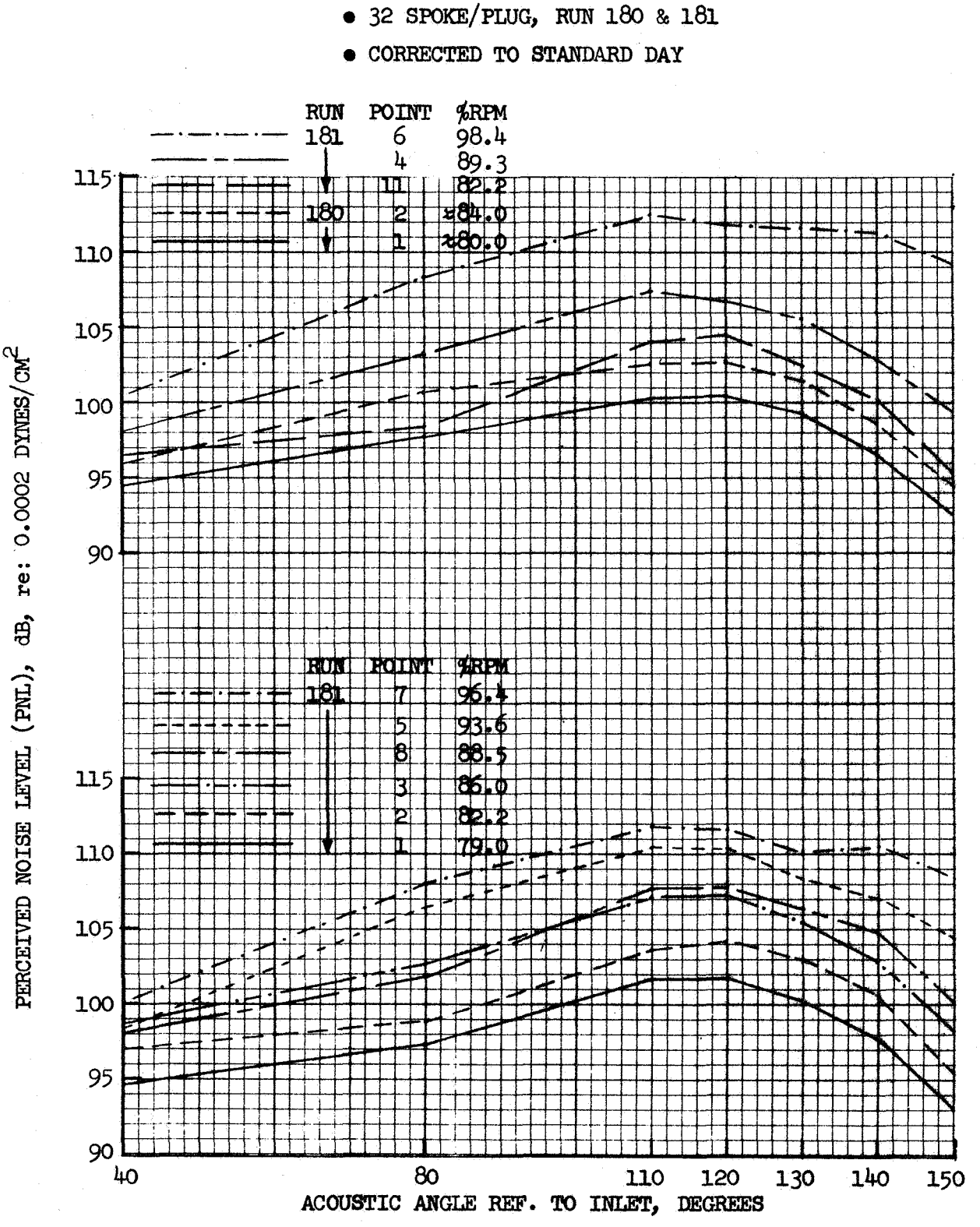

FIGURE 52 GROUND STATIC 300 FT. SIDELINE PNL DIRECTIVITY; 32 SPOKE/PLUG

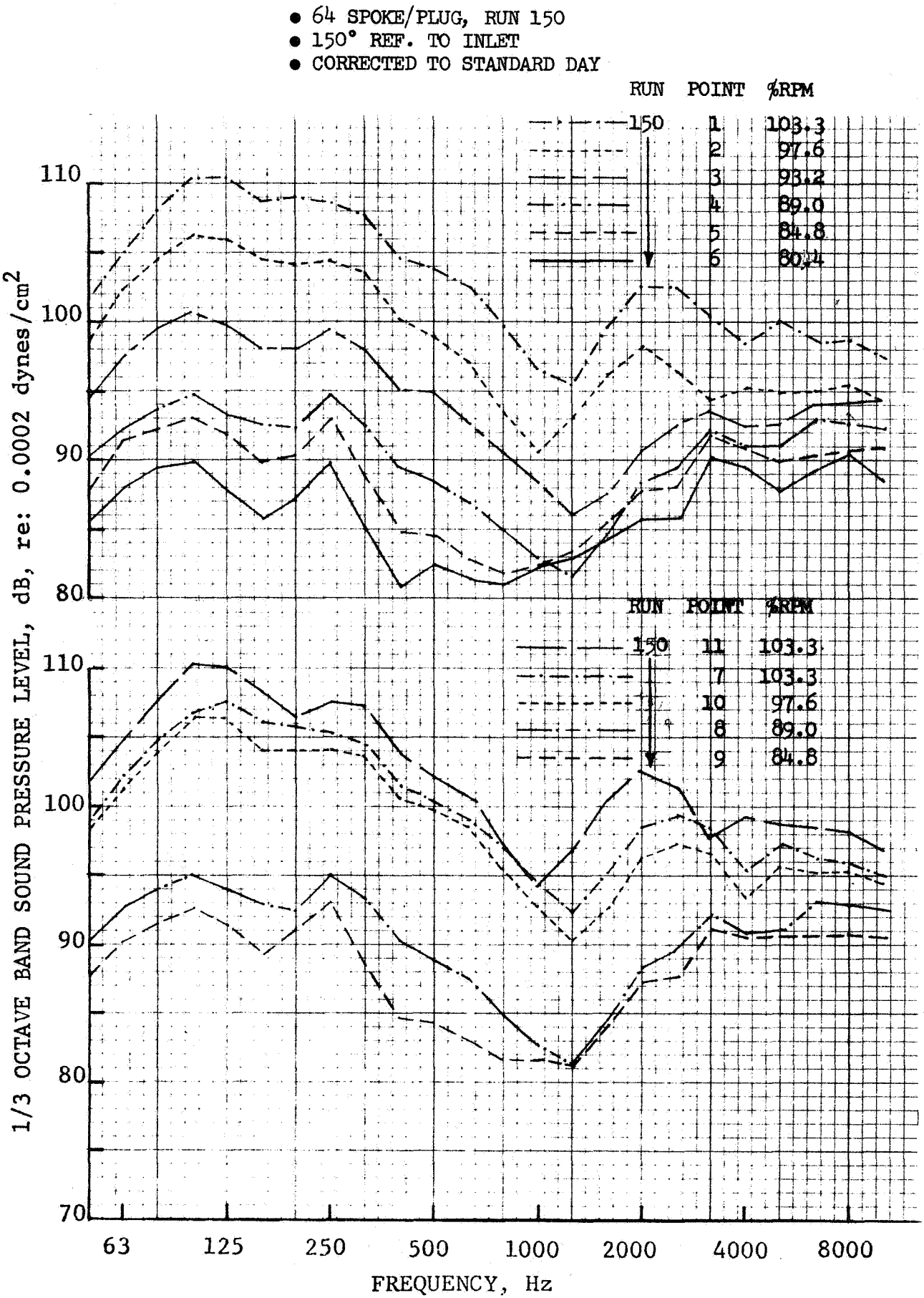

FIGURE 53 100 FT. ARC J85 GROUND STATIC SPECTRA, 64 SPOKE/PLUG

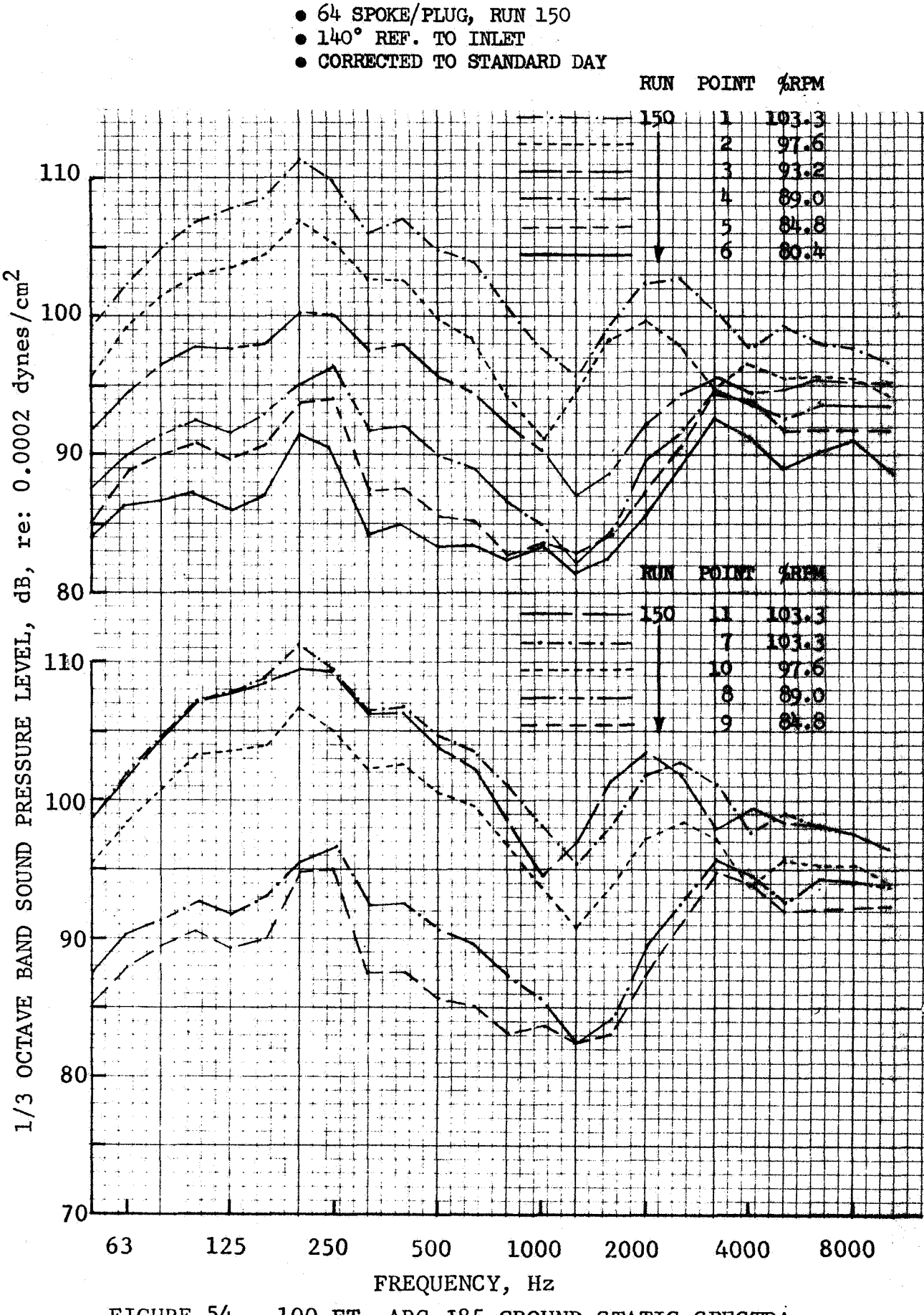

FIGURE 54 100 FT. ARC J85 GROUND STATIC SPECTRA, 64 SPOKE/PLUG

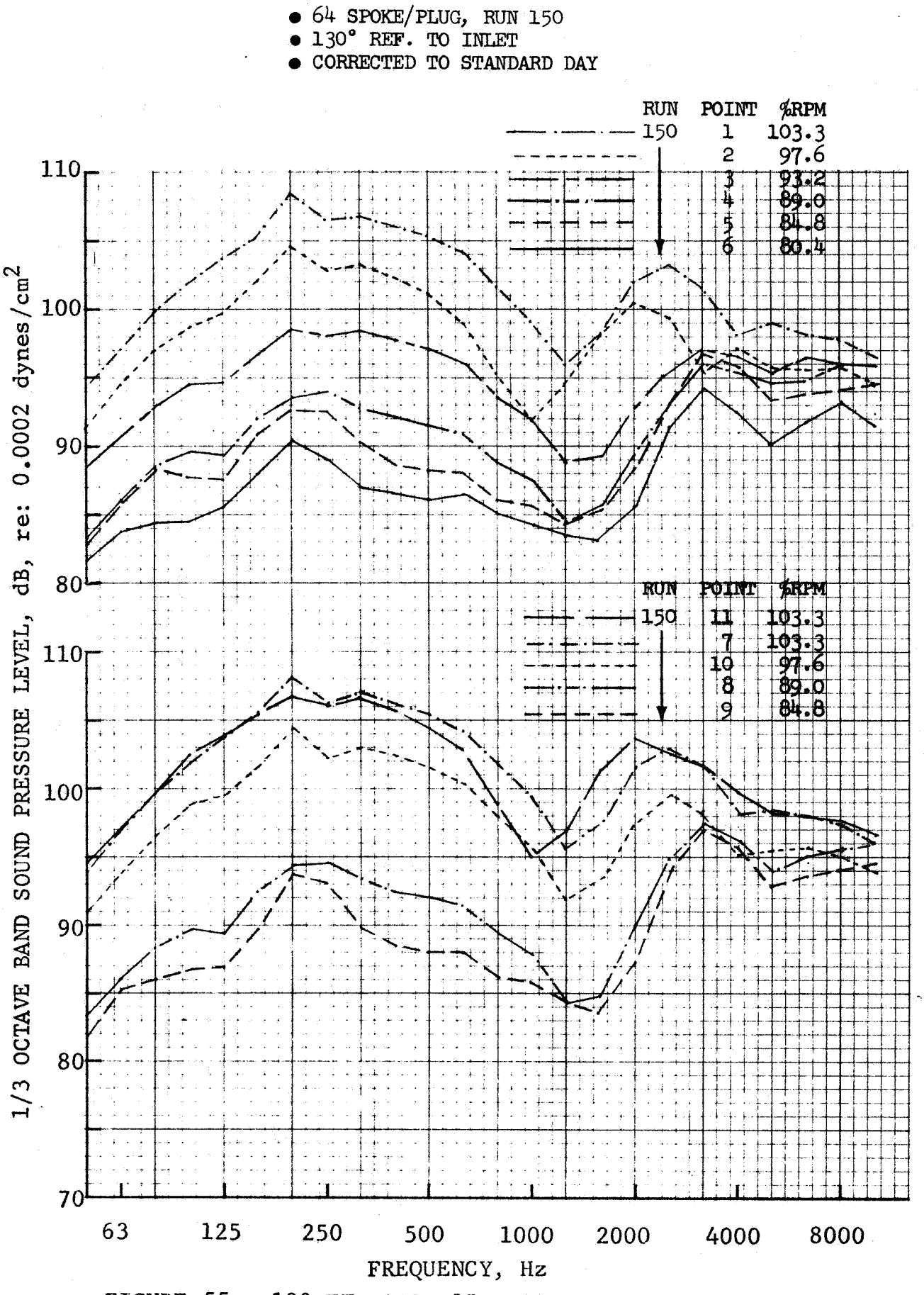

FIGURE 55 100 FT. ARC J85 GROUND STATIC SPECTRA, 64 SPOKE/PLUG

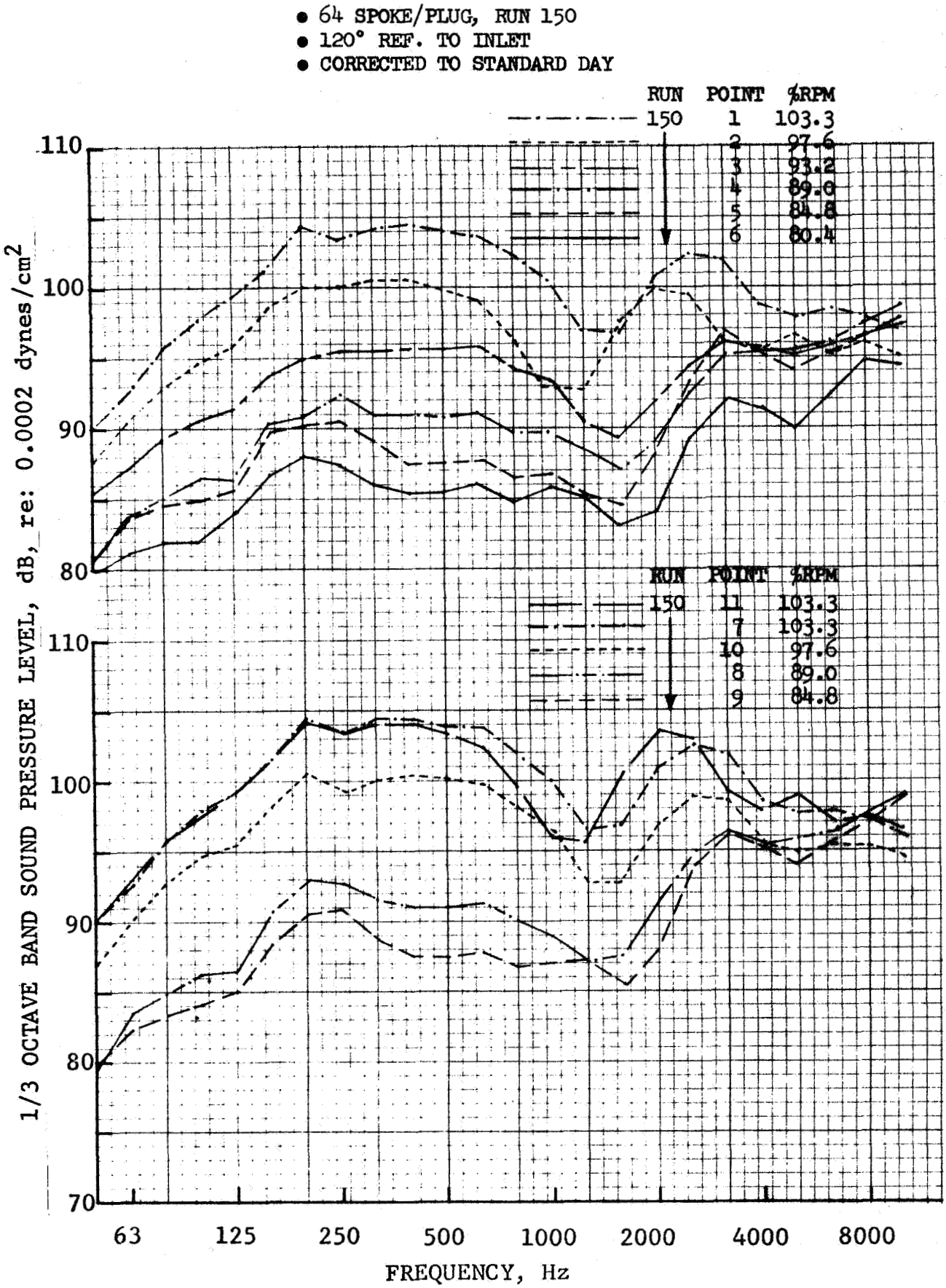

FIGURE 56 100 FT. ARC J85 GROUND STATIC SPECTRA, 64 SPOKE/PLUG

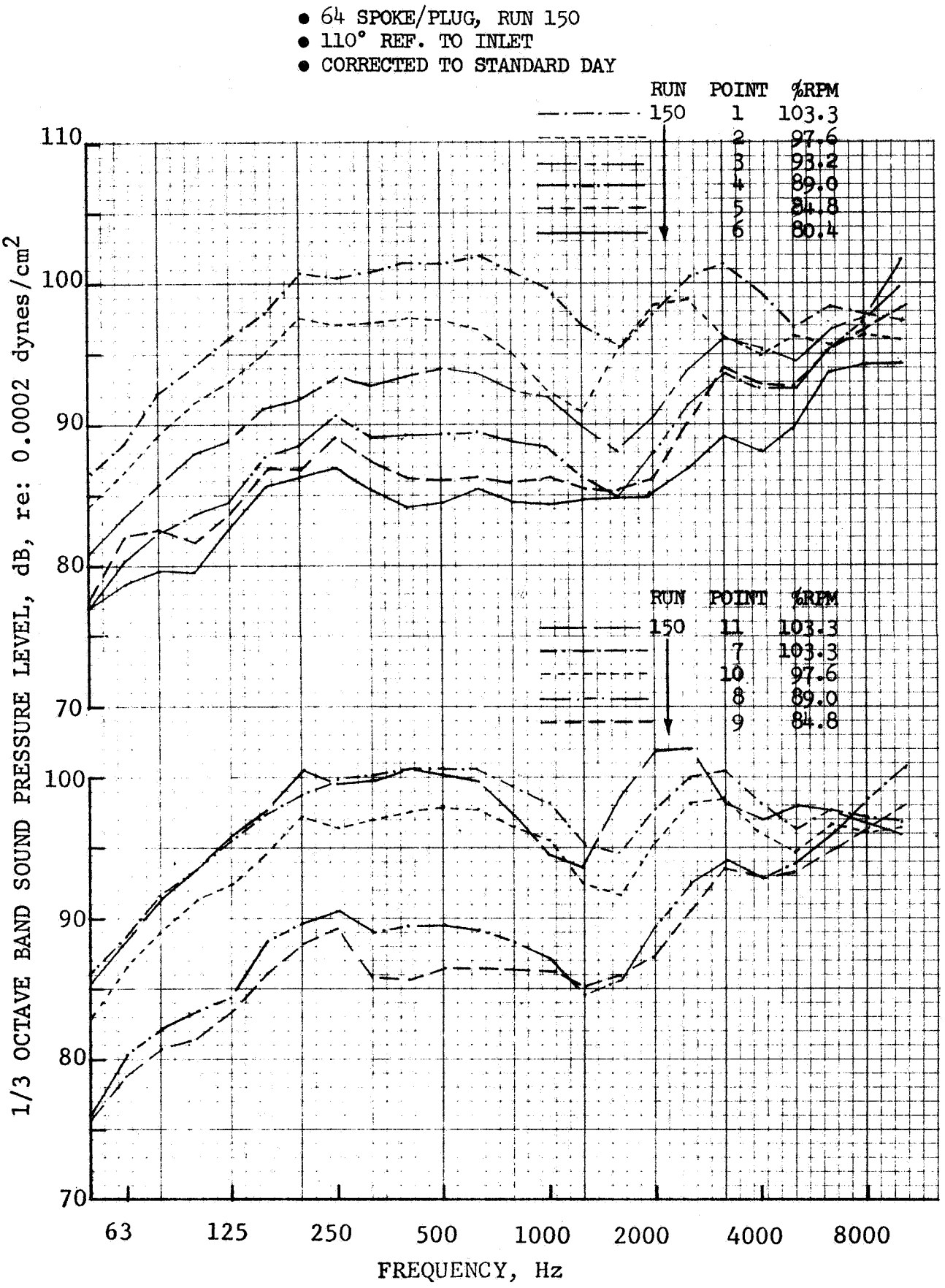

FIGURE 57 100 FT. ARC J85 GROUND STATIC SPECTRA, 64 SPOKE/PLUG

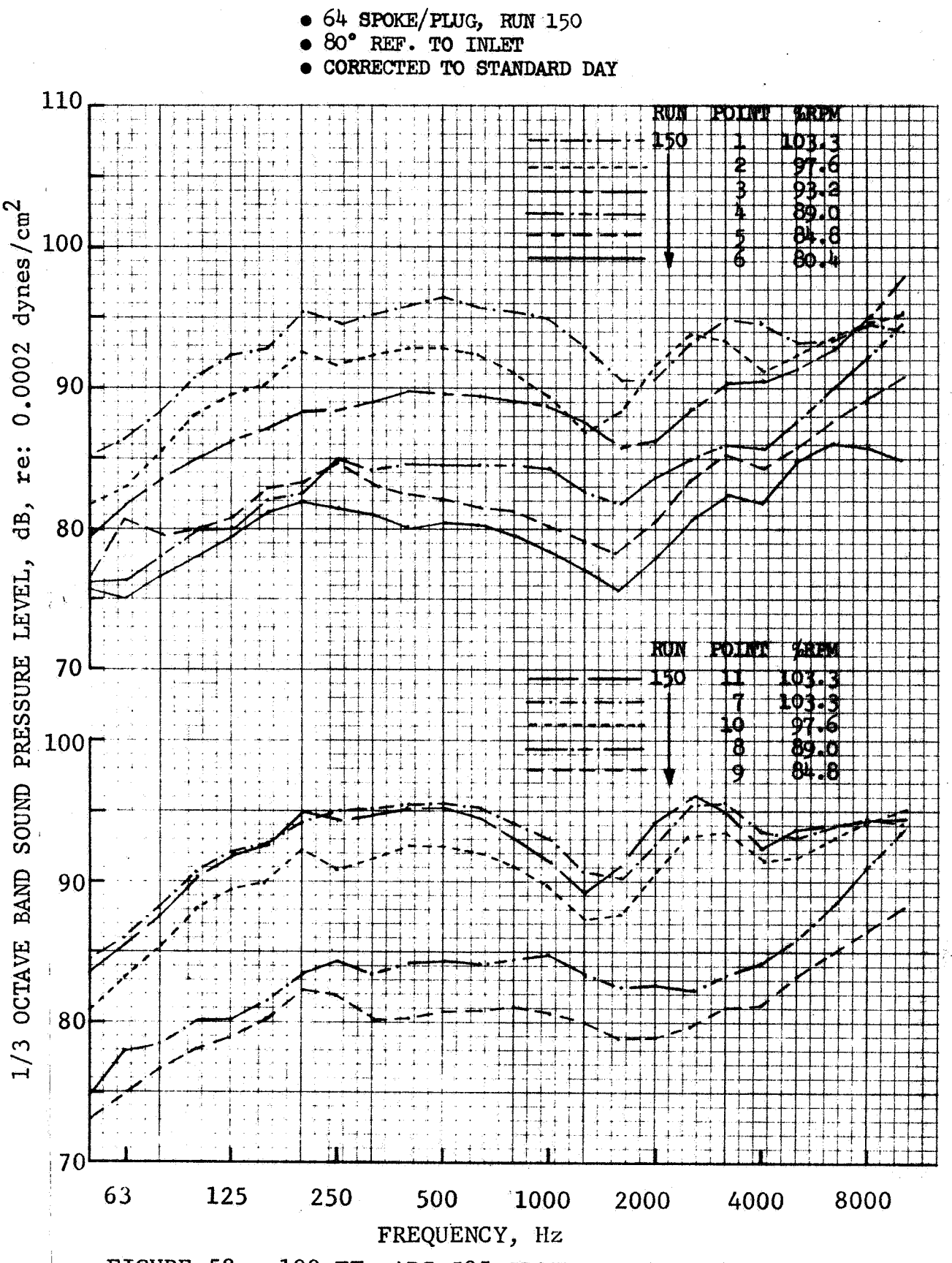

FIGURE 58 100 FT. ARC J85 GROUND STATIC SPECTRA, 64 SPOKE/PLUG

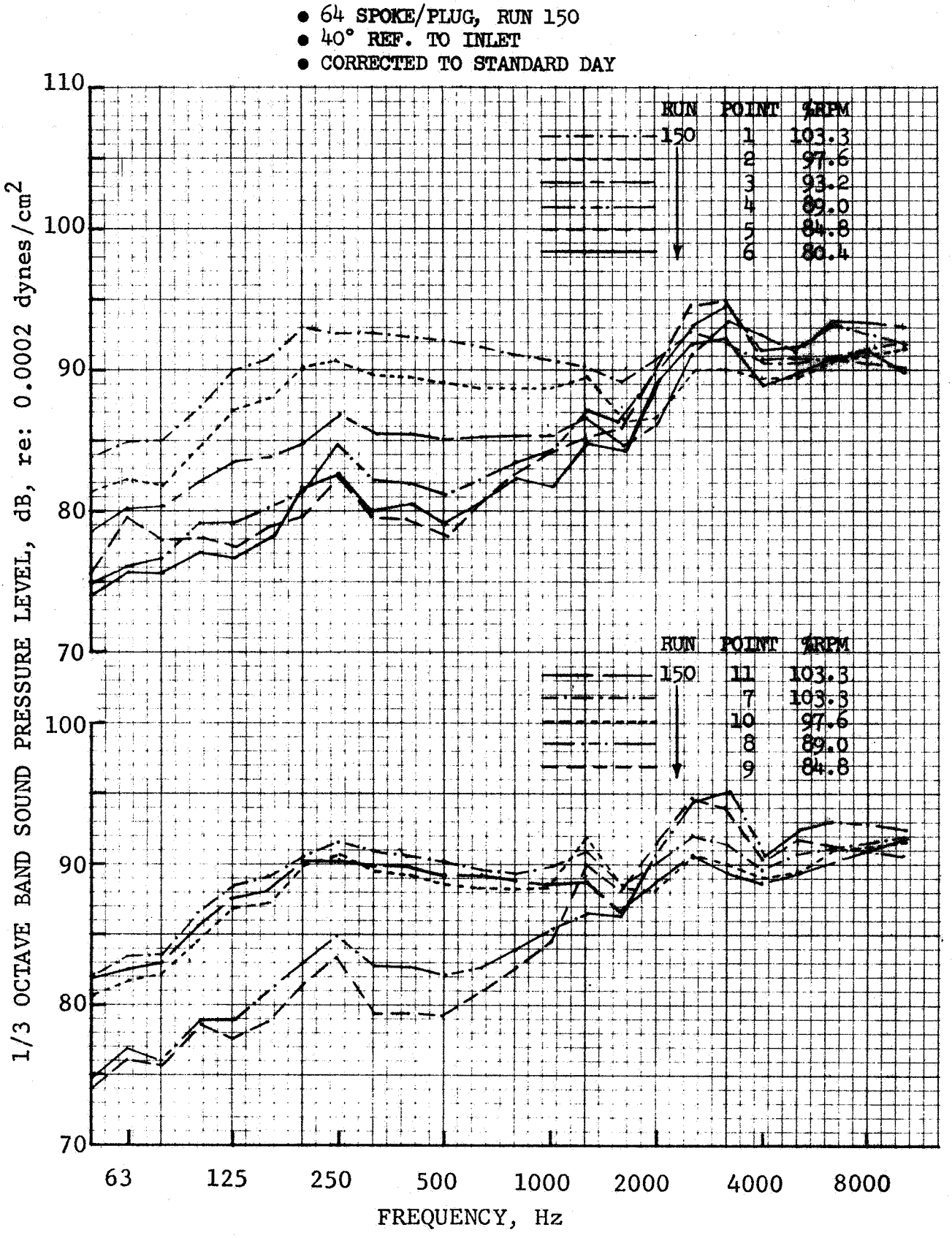

FIGURE 59 100 FT. ARC J85 GROUND STATIC SPECTRA, 64 SPOKE/PLUG

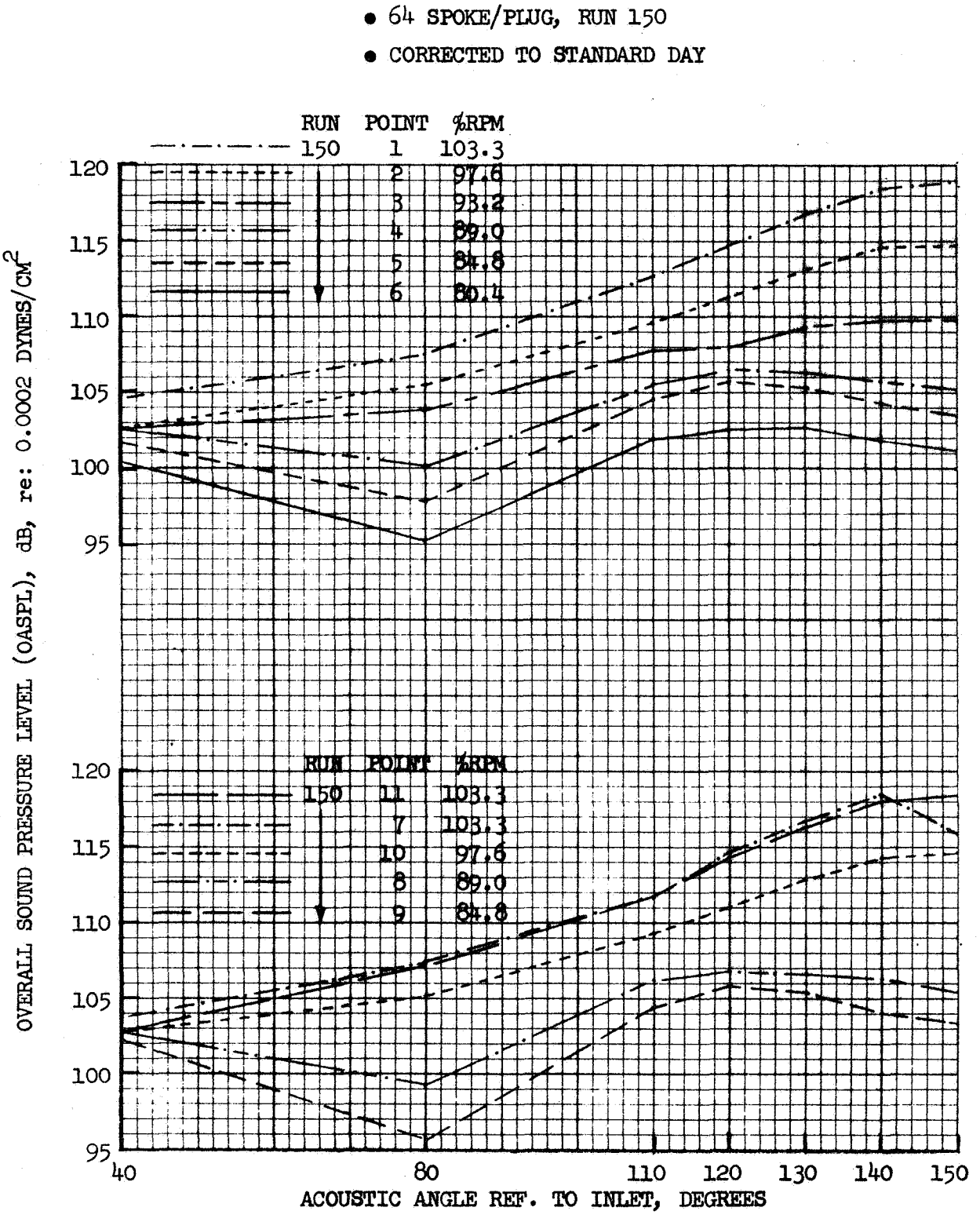

FIGURE 60 GROUND STATIC 100 FT. ARC OASPL DIRECTIVITY; 64 SPOKE/PLUG

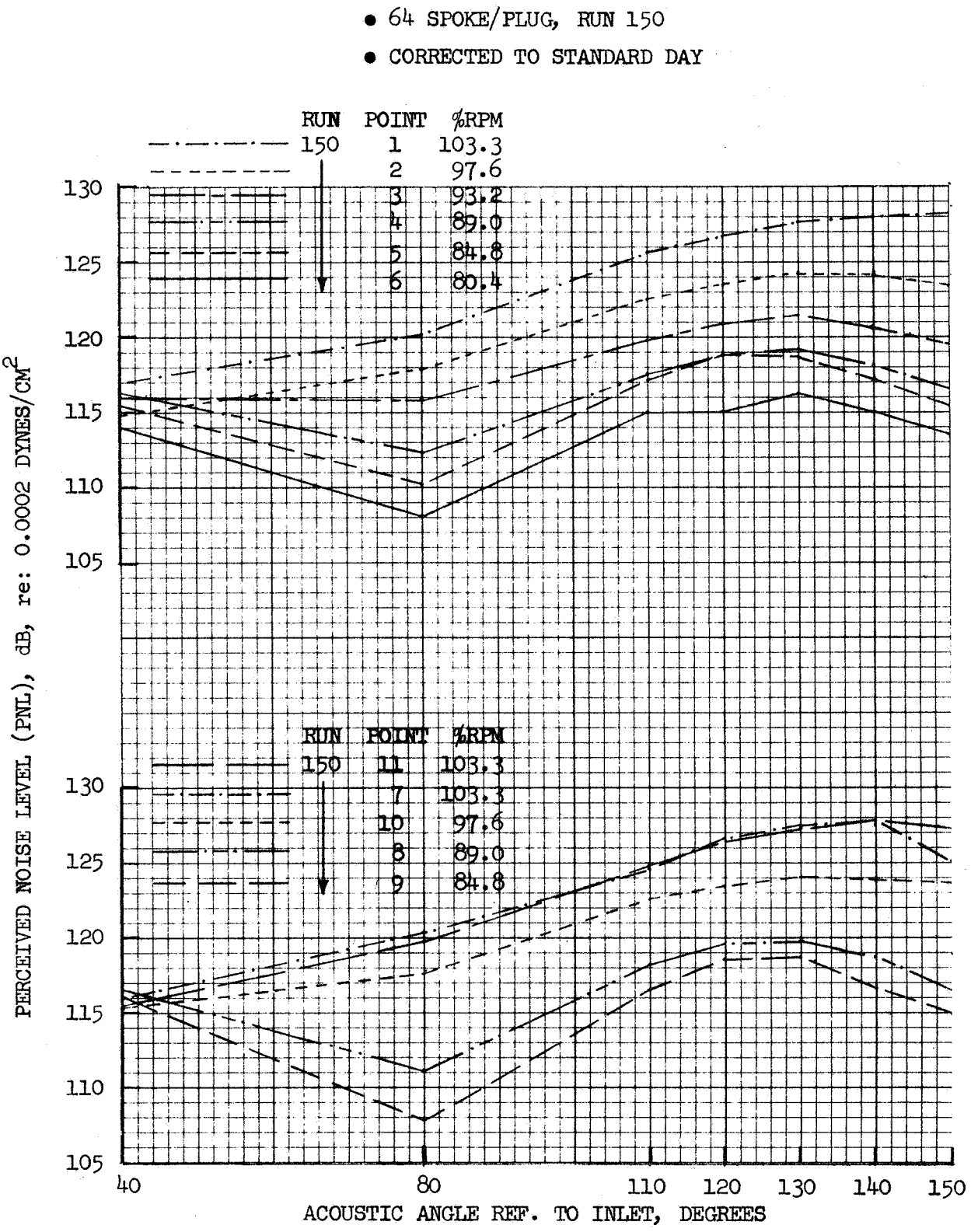

FIGURE 61 GROUND STATIC 100 FT. ARC PNL DIRECTIVITY; 64 SPOKE/PLUG

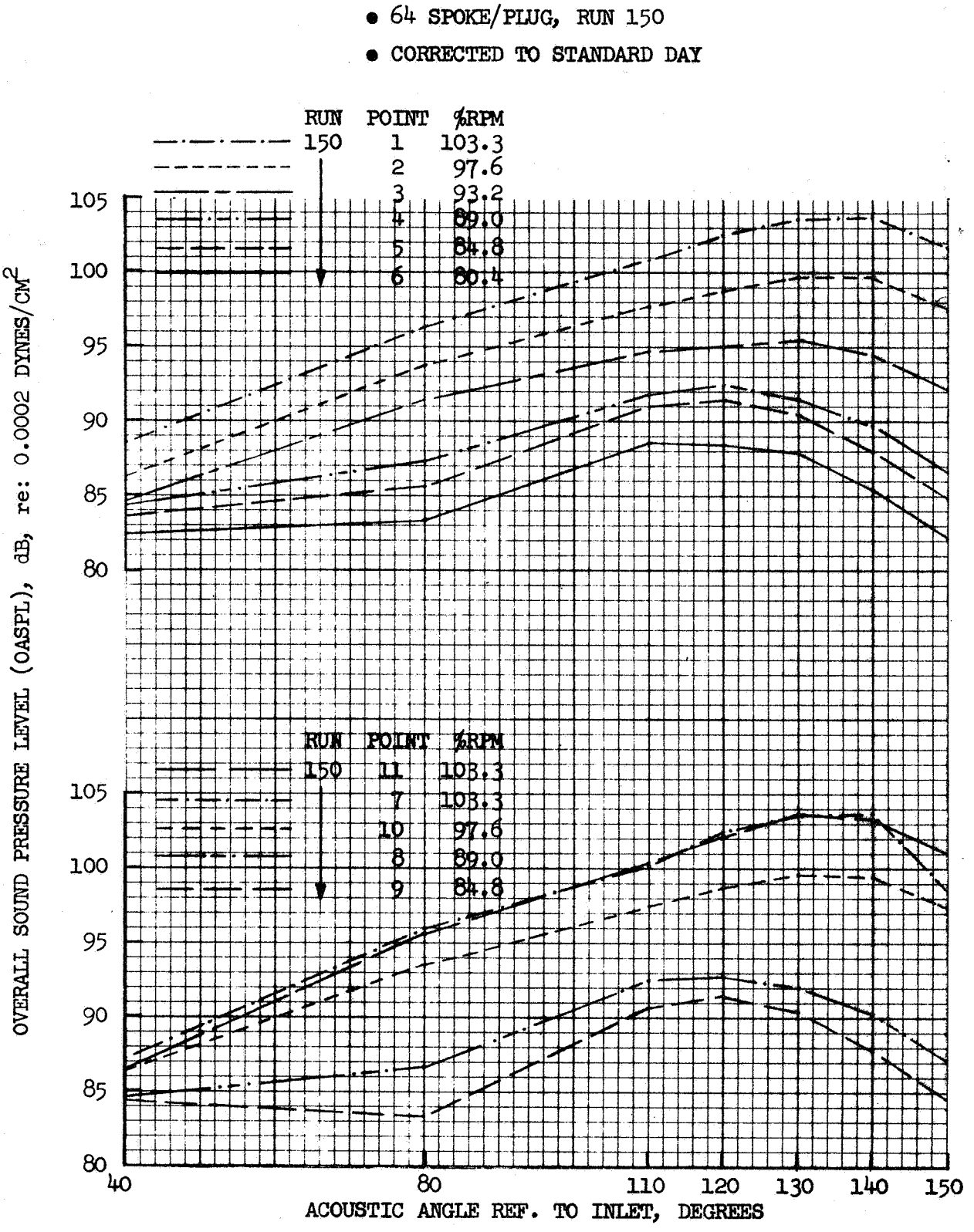

FIGURE 62 GROUND STATIC 300 FT. SIDELINE OASPL DIRECTIVITY; 64 SPOKE/PLUG

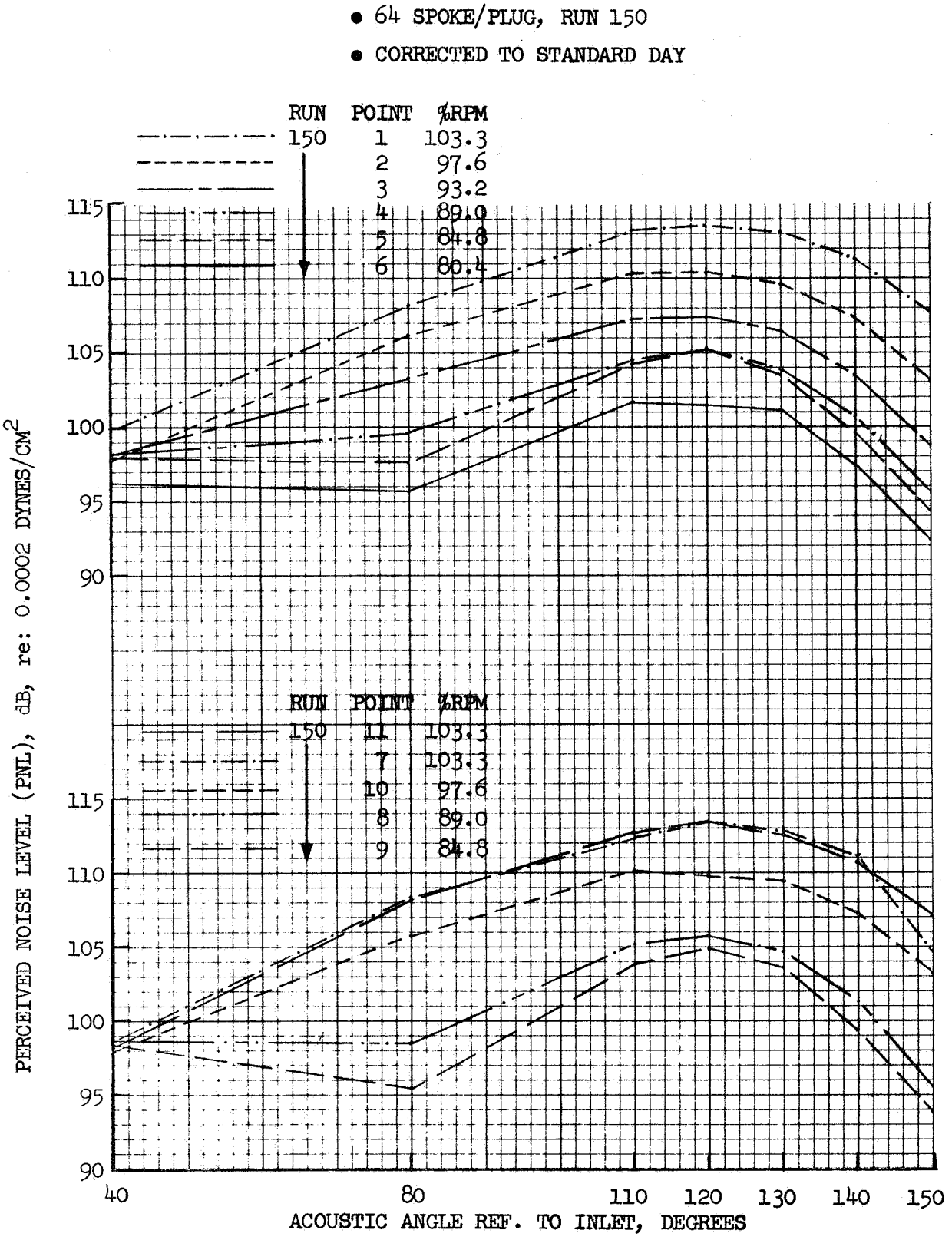

FIGURE 63 GROUND STATIC 300 FT. SIDELINE PNL DIRECTIVITY; 64 SPOKE/PLUG

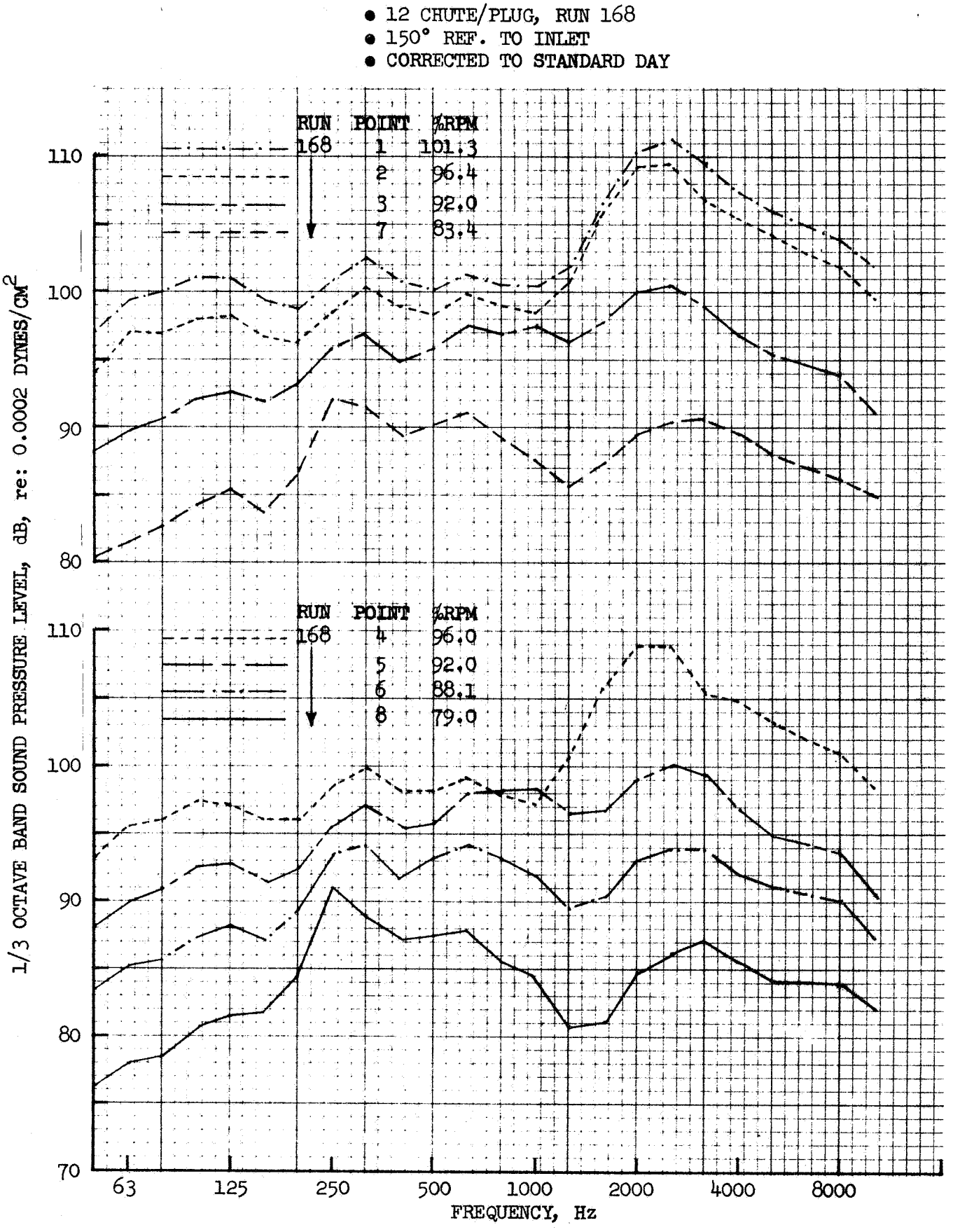

FIGURE 64 100 FT. ARC J85 GROUND STATIC SPECTRA, 12 CHUTE/PLUG

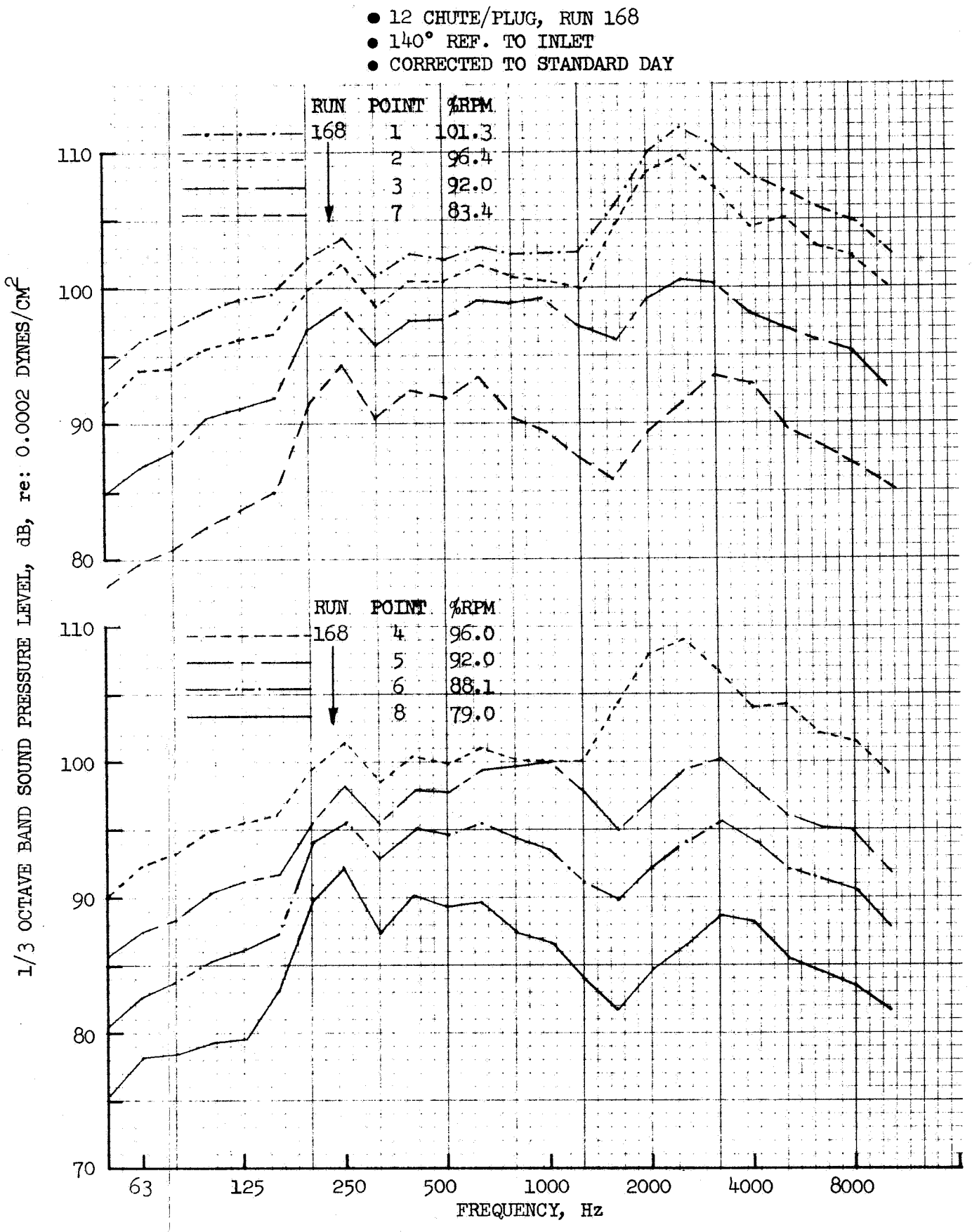

FIGURE 65 100 FT. ARC J85 GROUND STATIC SPECTRA, 12 CHUTE/PLUG

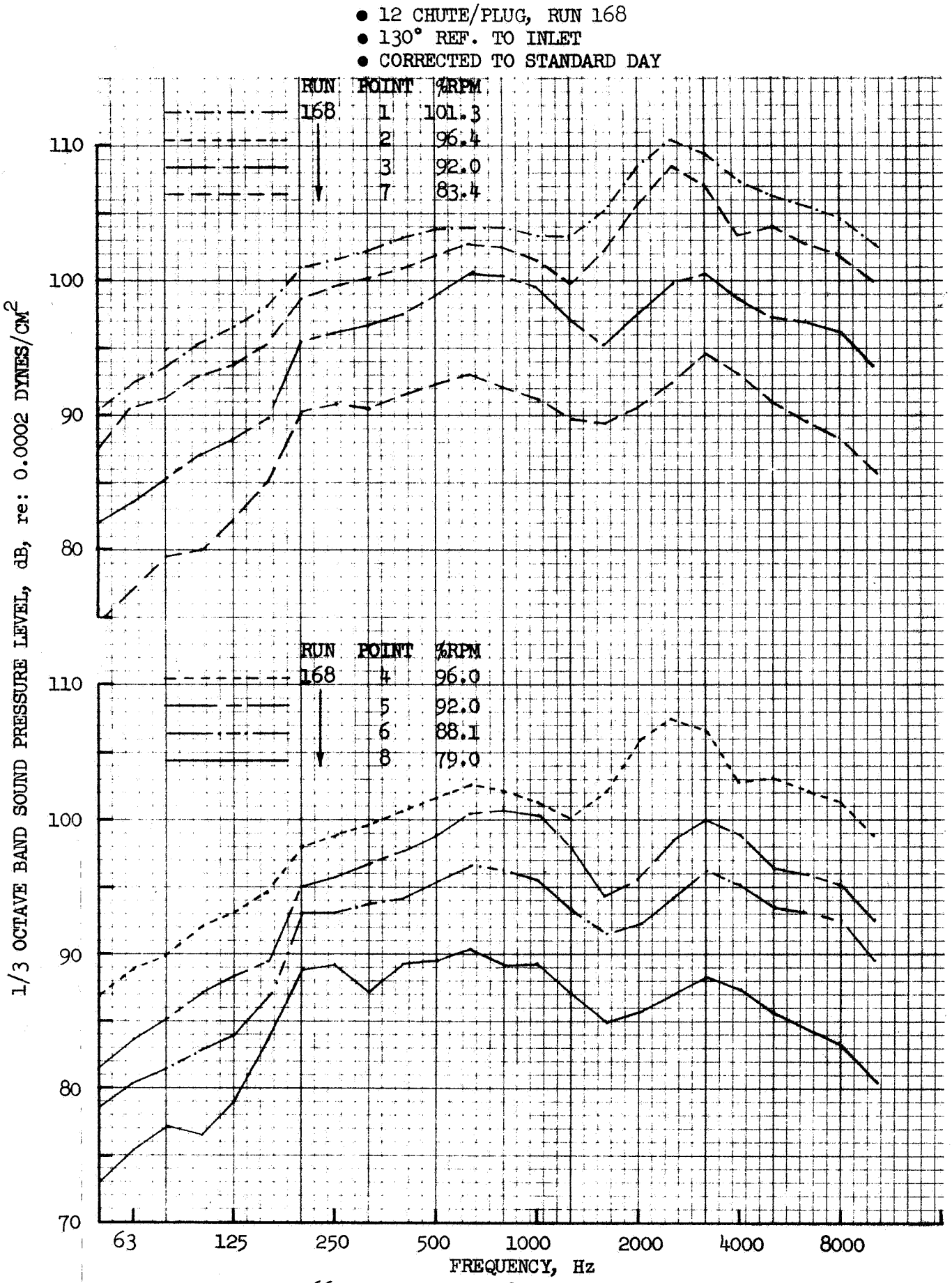

FIGURE 66 100 FT. ARC J85 GROUND STATIC SPECTRA, 12 CHUTE/PLUG

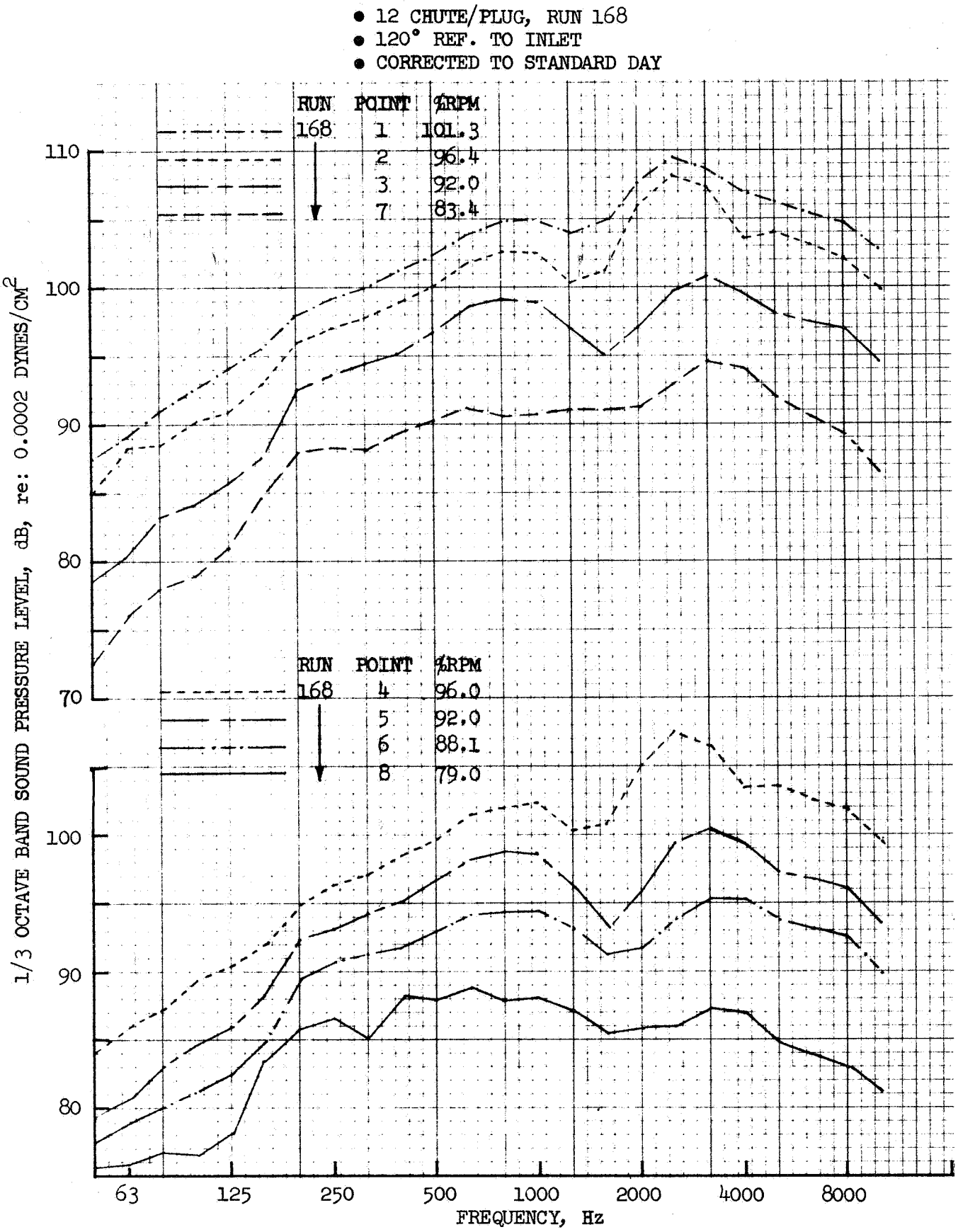

FIGURE 67 100 FT. ARC J85 GROUND STATIC SPECTRA, 12 CHUTE/PLUG

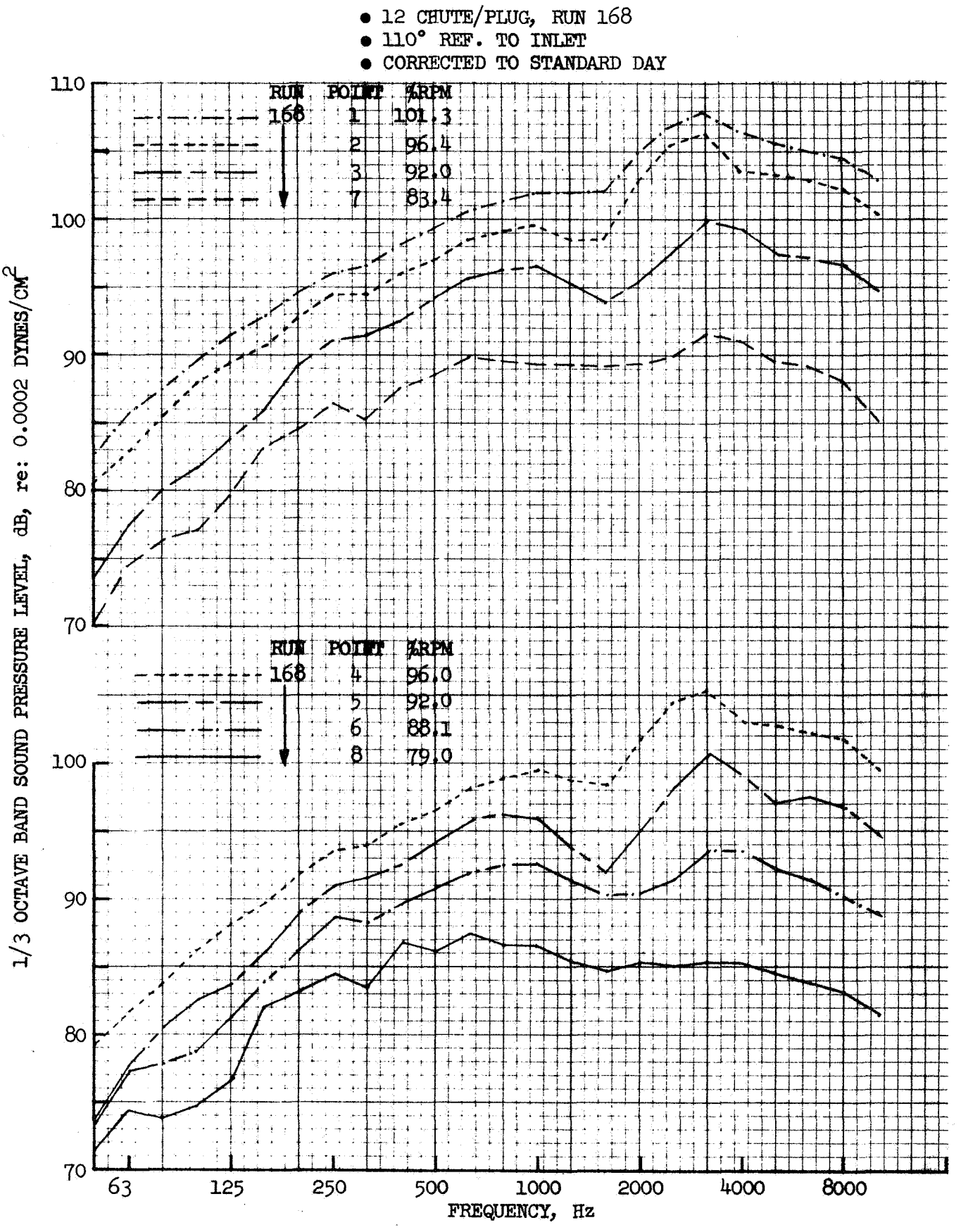

FIGURE 68 100 FT. ARC J85 GROUND STATIC SPECTRA, 12 CHUTE/PLUG

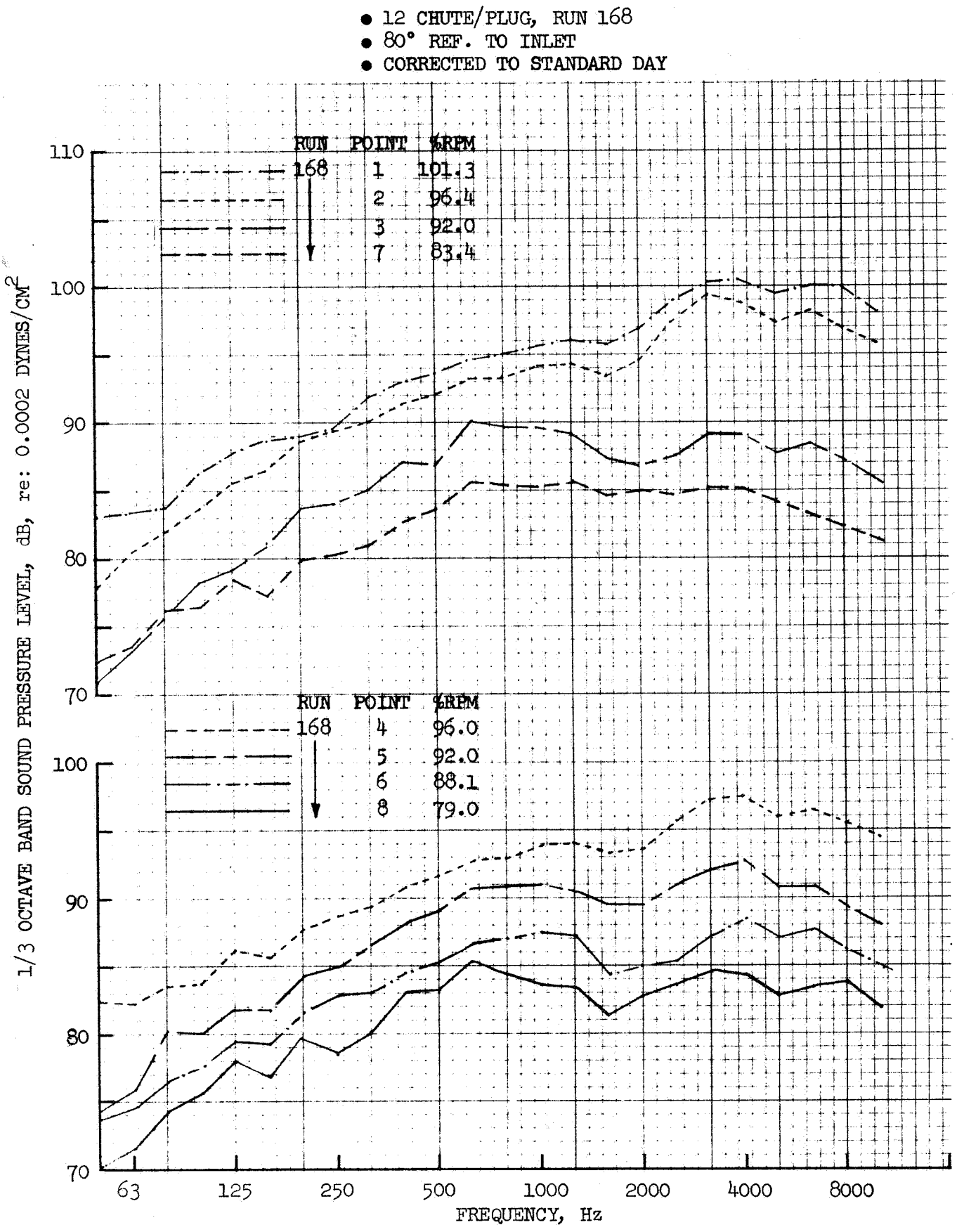

FIGURE 69 100 FT. ARC J85 GROUND STATIC SPECTRA, 12 CHUTE/PLUG

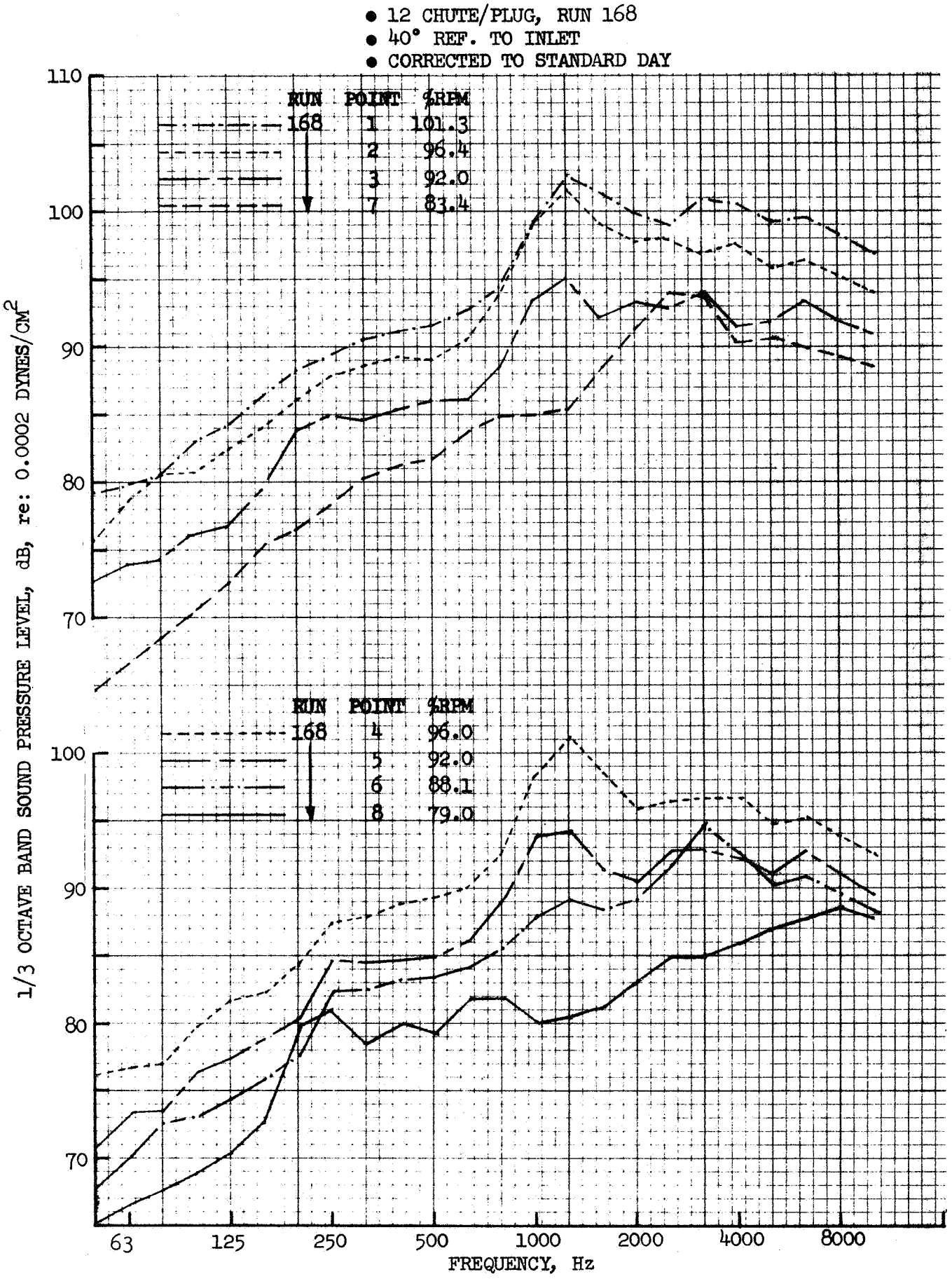

FIGURE 70 100 FT. ARC J85 GROUND STATIC SPECTRA, 12 CHUTE/PLUG

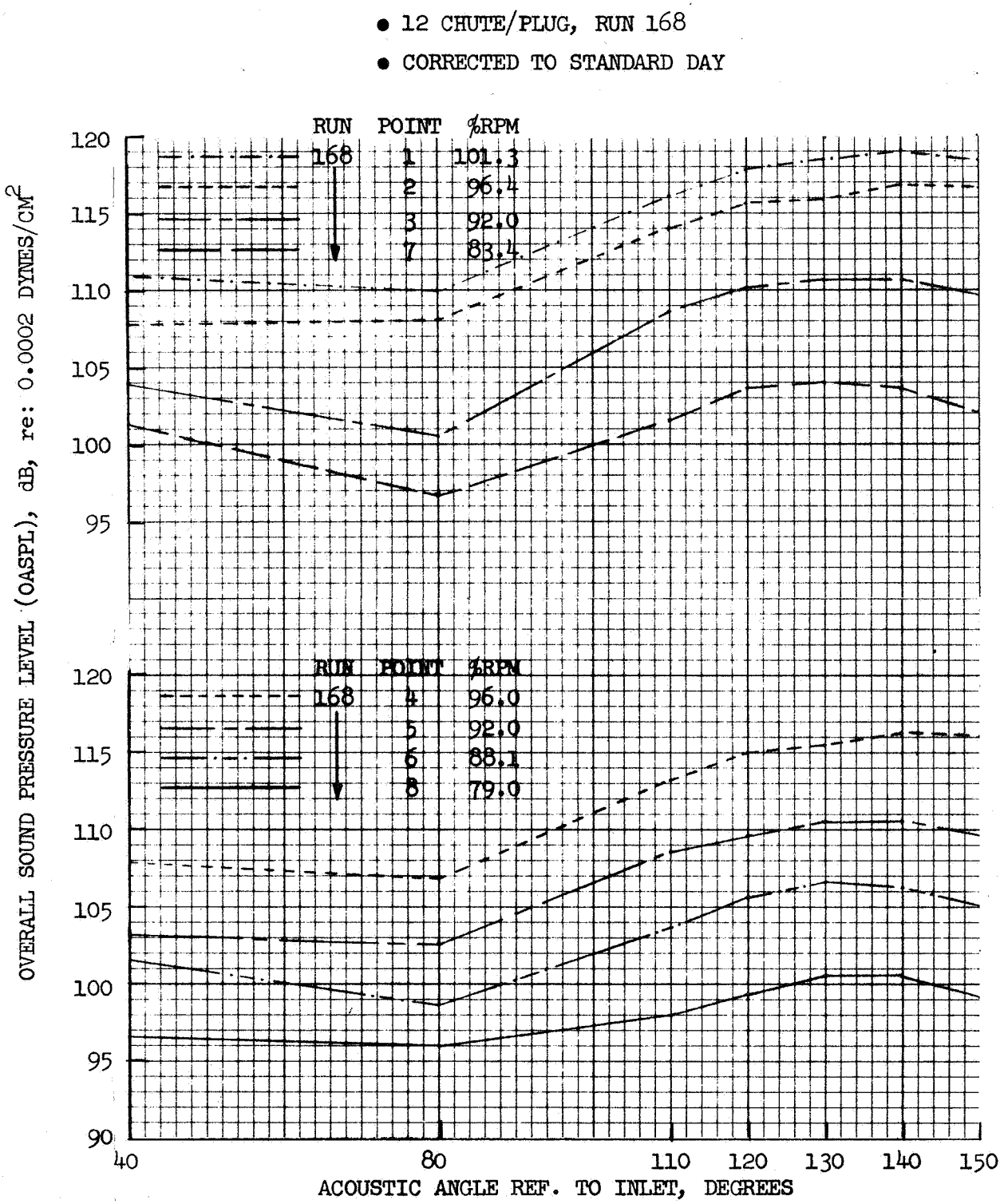

FIGURE 71 GROUND STATIC 100 FT. ARC OASPL DIRECTIVITY; 12 CHUTE/PLUG

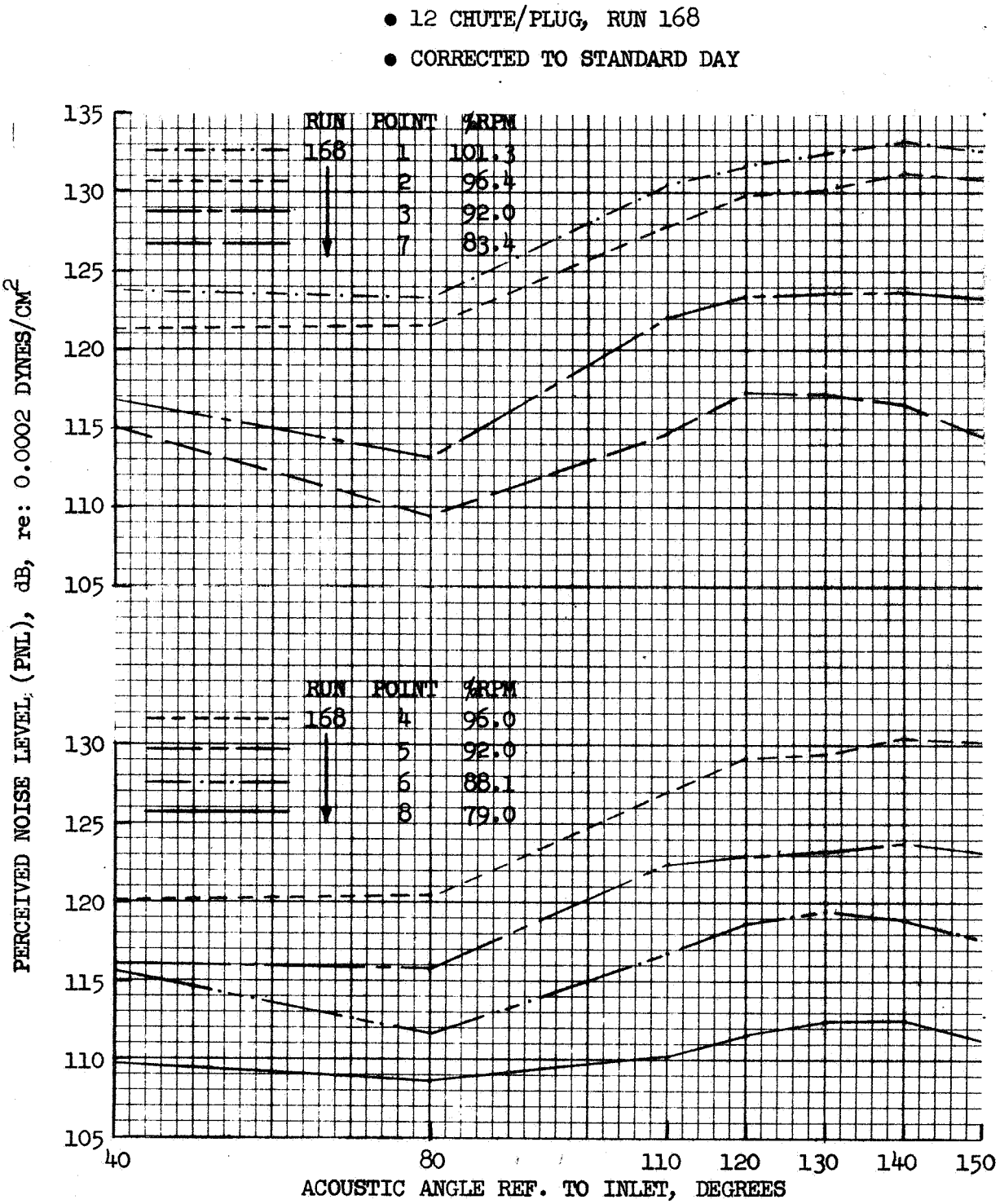

FIGURE 72 GROUND STATIC 100 FT. ARC PNL DIRECTIVITY; 12 CHUTE/PLUG

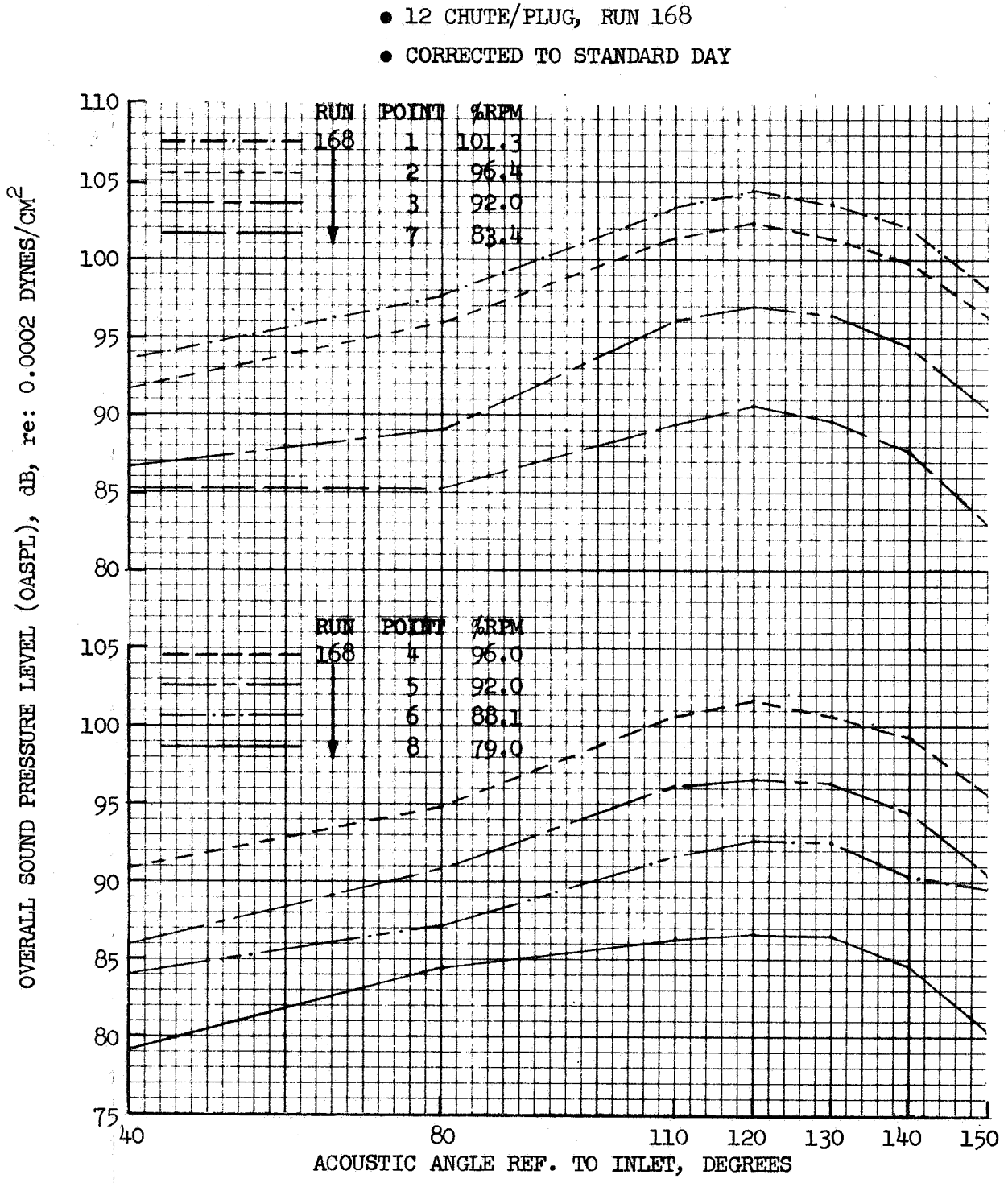

FIGURE 73 GROUND STATIC 300 FT. SIDELINE OASPL DIRECTIVITY; 12 CHUTE/PLUG

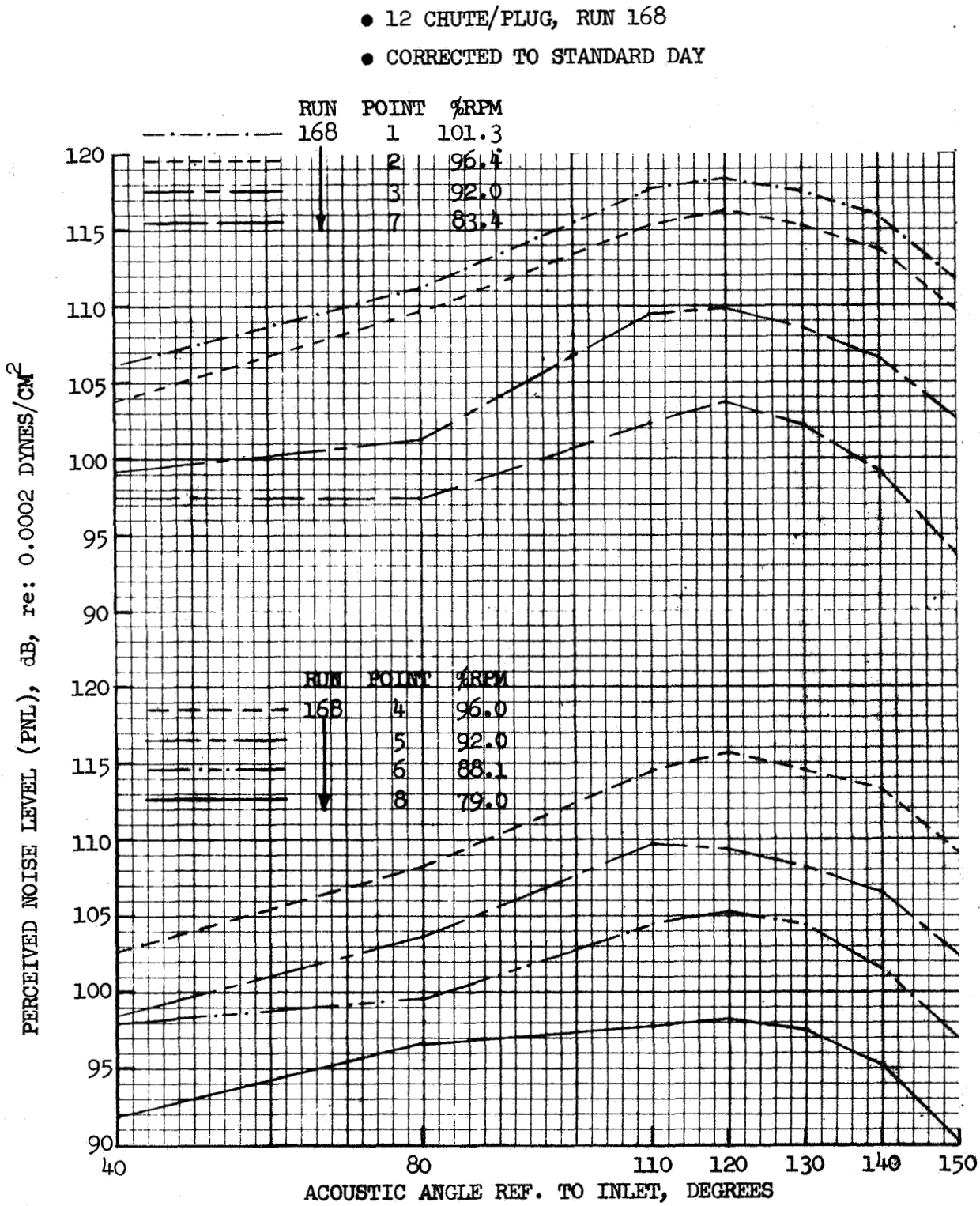

FIGURE 74 GROUND STATIC 300 FT. SIDELINE PNL DIRECTIVITY; 12 CHUTE/PLUG

DISCUSSION OF STATIC DATA

Spectral Characteristics

Examination of the general spectral characteristics of the five nozzle systems leads to an understanding as to their general noise characteristics. The conical-ejector spectra are typical of those expected from a pure convergent nozzle system as would be predicted at the peak noise angle, per the SAE procedure (ref. 2). The baseline annular plug spectra are similar to those of the conical ejector but with slightly greater high frequency content due to the annular discharge of jet flow. The 32 and 64 spoke suppressor nozzles have the characteristic double hump spectra typical of highly segmented spoke or tube nozzles with compacted spacing. The high frequency spectra hump is attributed to the individual segmented jets. The low frequency hump is characteristic of the coalesced jet region, being lower in level, as the total mixing region of the coalesced jet is shorter than that of a non-segmented convergent nozzle jet stream. The 12 chute/plug nozzle has a distinctly different spectra shape; quite low level in the lower frequency range but high level in the high frequency range. The large spacing between lobes (Area Ratio = 3) allows for predominance of the noise generated by the individual jets in the high frequency region before coalescence into a single stream. The merged jet low frequency noise contribution is low since the major part of turbulent mixing and velocity decay is complete before coalescence. The remaining region of turbulent mixing, which generates low frequency noise, is quite shortened compared to a convergent nozzle jet stream. Thus, suppression is realized from segmented nozzles not only due to the lower low frequency noise characteristic of the shorter mixing length but primarily due to fast decay rates of high frequency noise with distance.

Directivity

As is seen from the 100 ft arc OASPL and PNL directivity plots, the peak noise on the measuring arc generally occurs quite near the jet exhaust. In some instances the peak occurred closer than the location of the 150° microphone and was not measured. This is seen from the directivity plots of the conical ejector, Figures 27 and 28, baseline annular plug, Figures 38 and 39, and the

32 spoke/plug, Figures 49 and 50; particularly on OASPL. As the arc measurements are extrapolated to the 300 ft. reference sideline, the longer path lengths at shallow angles have greater noise attenuation. This generally changes the angular location of peak noise. Therefore, the 300 ft. sideline directivity plots contain the peak noise for all the nozzles. Generally the angular shift from arc to sideline is from 10° to 30° away from the jet exhaust axis, the suppressor nozzles shifting more due to the greater content of high frequency noise.

Data Validity

Examining the trends of jet noise OASPL and PNL directivity suggests that near the inlet the noise measurements are no longer J85 pure jet but are influenced by the J75 turbomachinery noise. As discussed under ACOUSTIC DATA REDUCTION - GROUND STATIC RUN-UP the J75 at idle generated a predominant blade passing tone. It was quite directional and highly influenced the mid frequency spectra at the 40° inlet measuring station. As the tone contribution overrode the jet spectra, the magnitude of interference, and thus level of correction, could not be accurately established. The noise levels at the 40° to inlet station are therefore questionable at low J85 engine speeds, particularly for the 32 and 64 spoke nozzles and the 12 chute nozzle. At high engine speed, the J85 noise is believed to have masked the J75 tone and produced valid spectra.

Peak Noise and Suppression Versus Jet Velocity

Figures 75 and 76 present the peak arc normalized OASPL and PNL as a function of jet velocity. Suppressions are also shown, referenced to the conical ejector nozzle. Figures 77 and 78 are the same type plots for the 300 ft. sideline data. Suppression levels and trends are seen to change slightly from the arc to the sideline due to shifts in peak noise locations. In general the suppression levels attained are fairly similar to magnitudes anticipated in this jet velocity region. Comparison of 300 ft. sideline PNL suppression levels of Figure 78 to those anticipated from model measurements of Figure 6 are shown in Figure 79. The model measurements were on similar scale model hardware tested on a pure jet hot flow facility and scaled to J85 engine size. Suppression levels

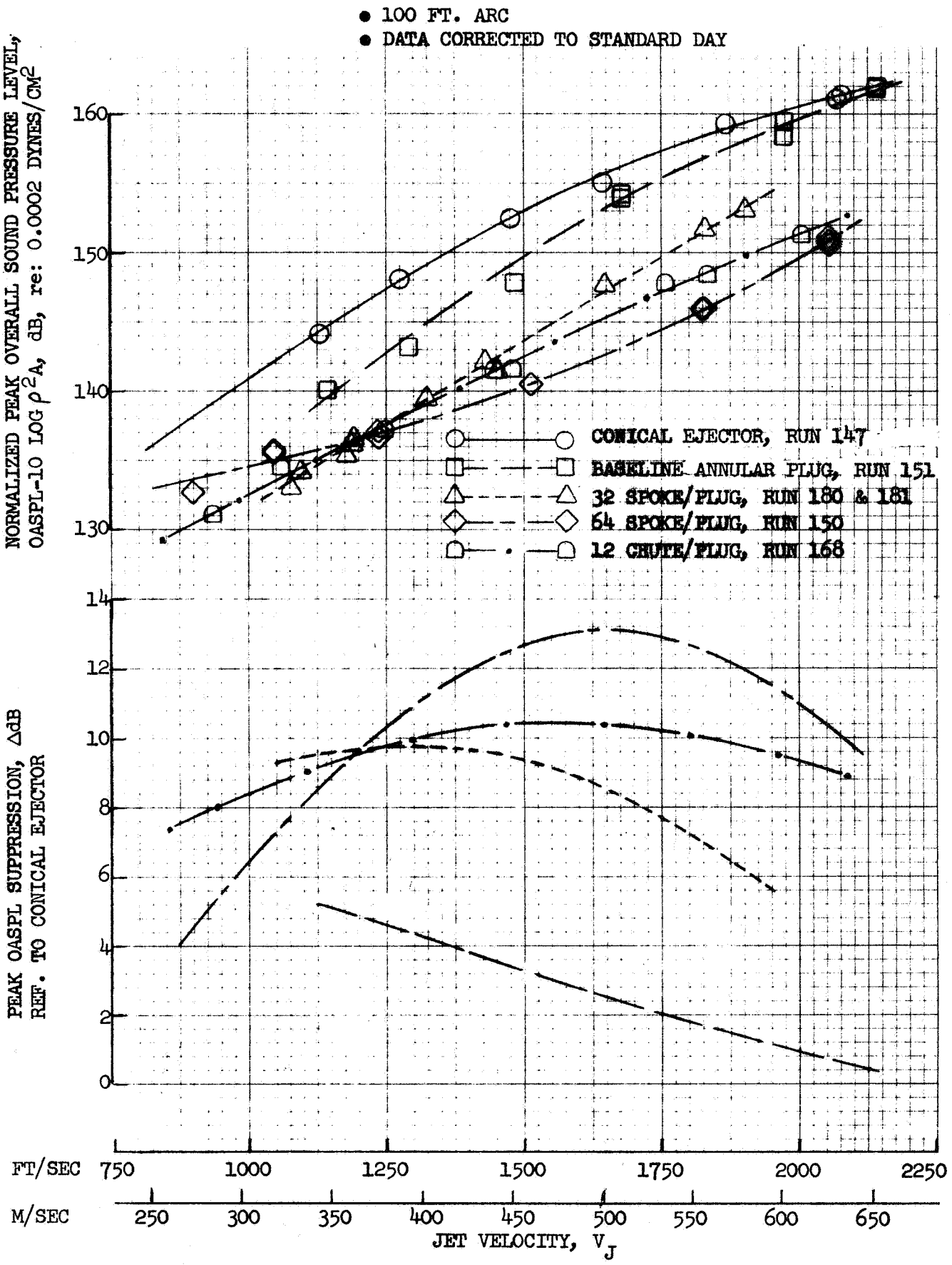

FIGURE 75 GROUND STATIC 100 FT. ARC PEAK OASPL LEVELS & SUPPRESSIONS

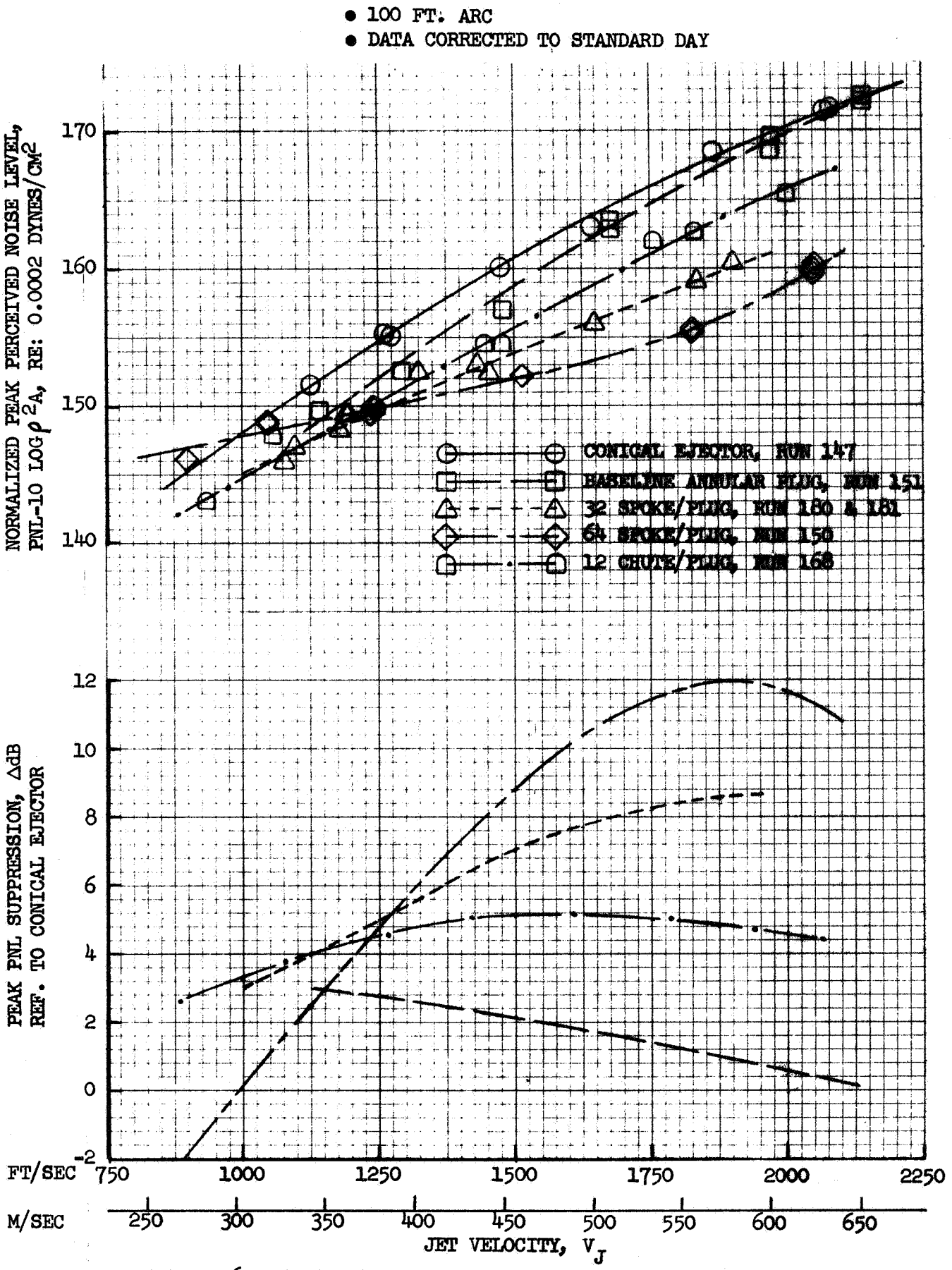

FIGURE 76 GROUND STATIC 100 FT. ARC PEAK PNL LEVELS & SUPPRESSIONS

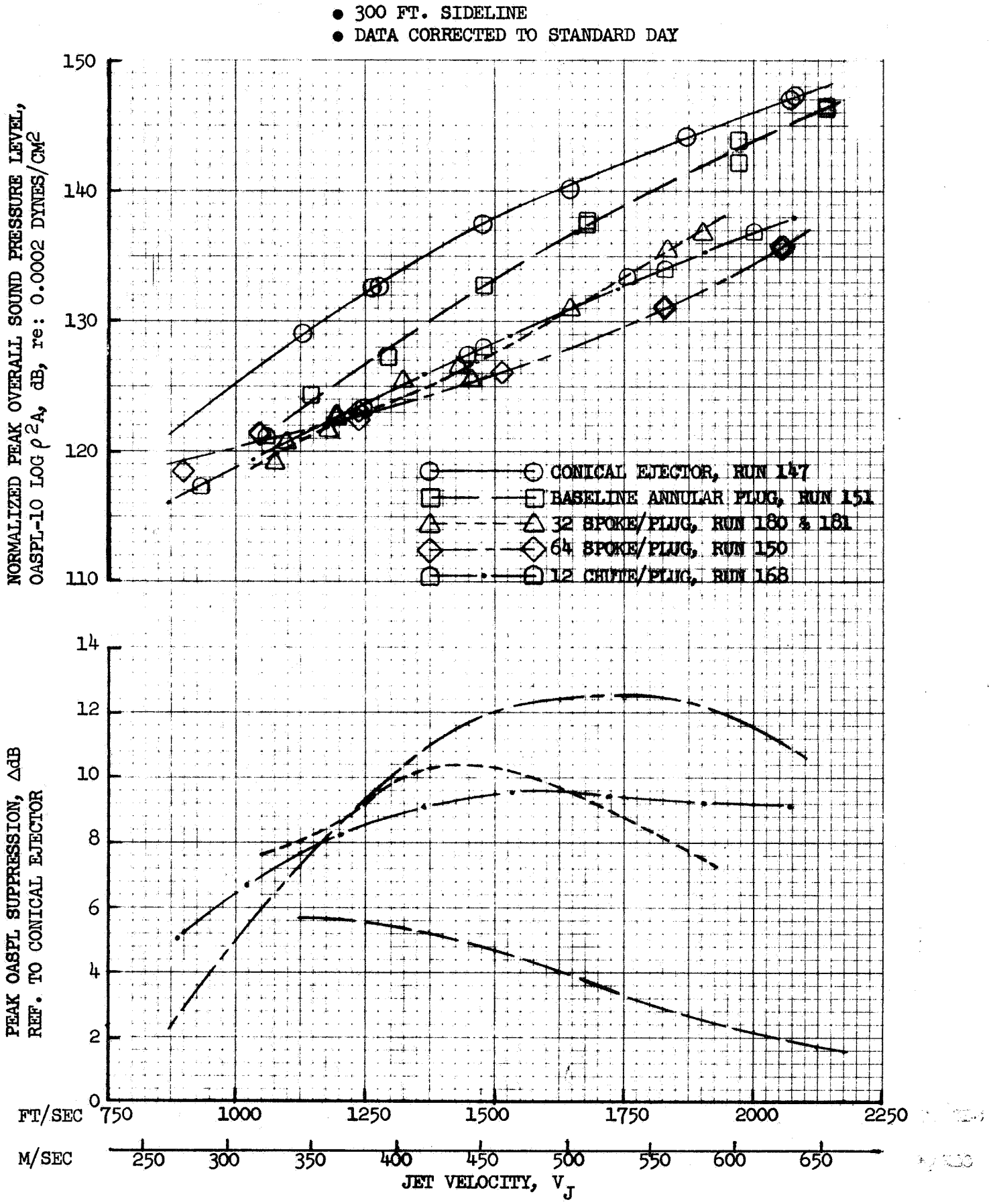

FIGURE 77 GROUND STATIC 300 FT. SIDELINE PEAK OASPL LEVELS AND SUPPRESSIONS

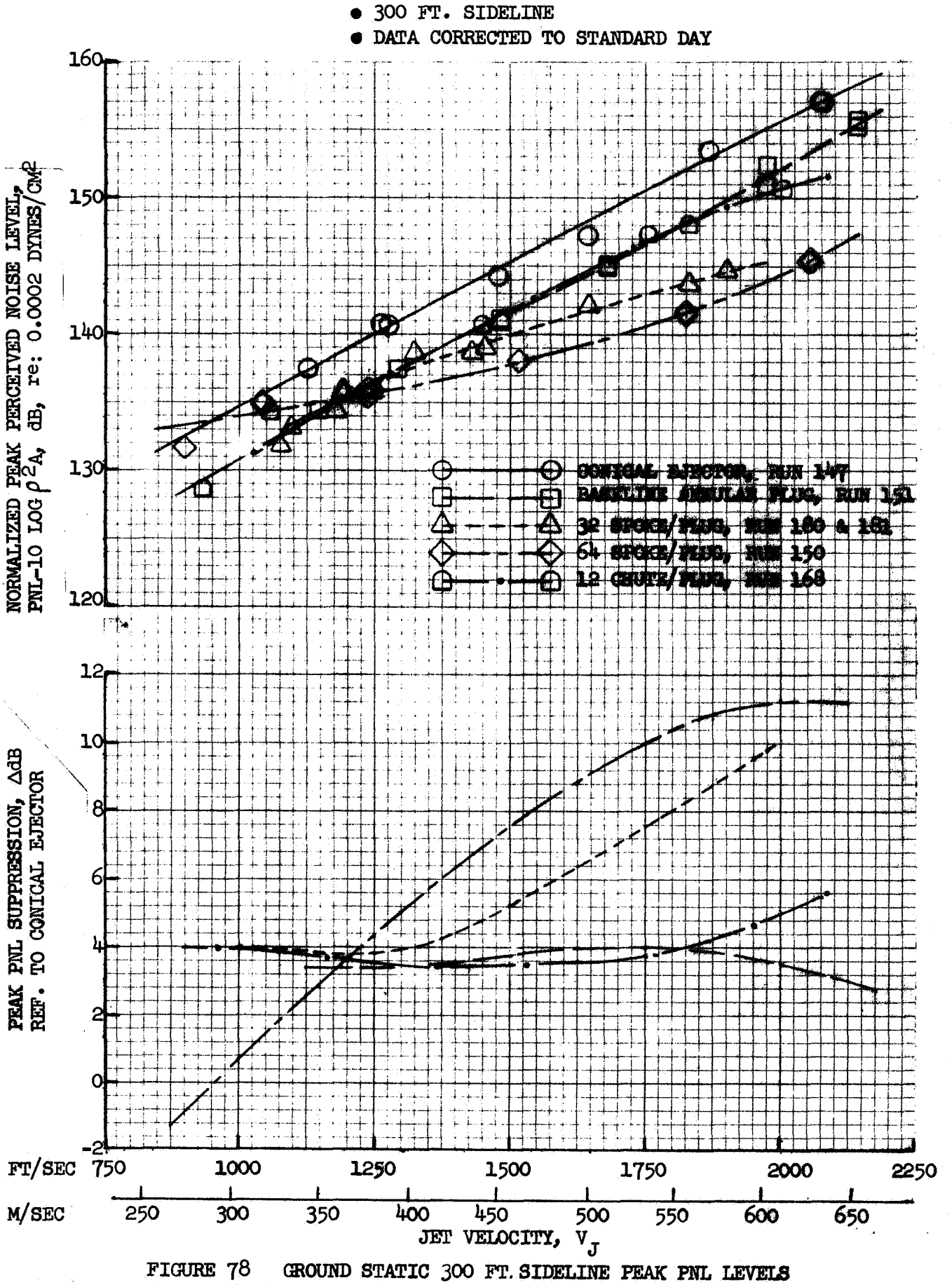

FIGURE 78 GROUND STATIC 300 FT. SIDELINE PEAK PNL LEVELS AND SUPPRESSIONS

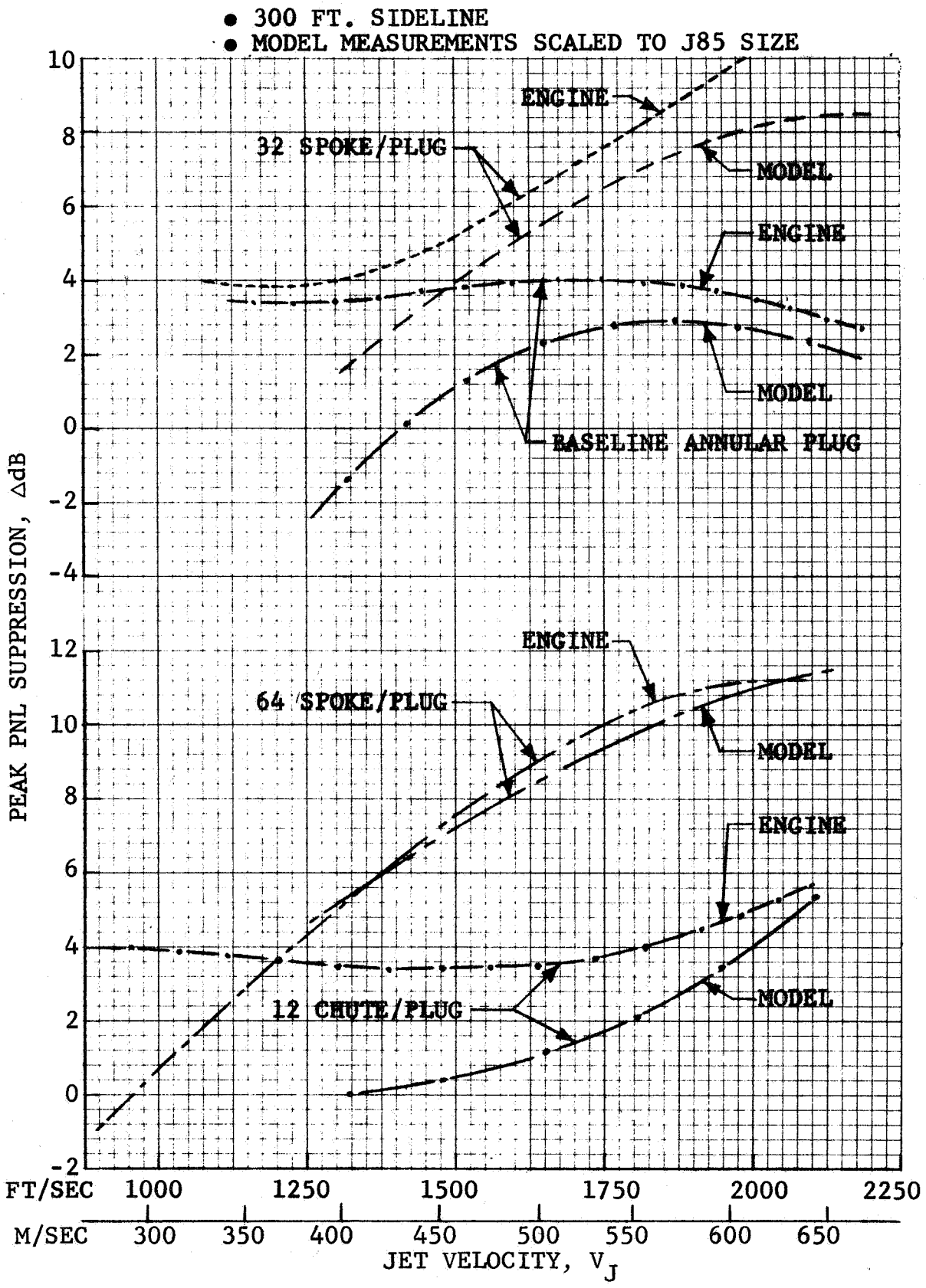

FIGURE 79 COMPARISON OF MEASURED J85 PNL SUPPRESSION TO LEVELS ANTICIPATED FROM MODEL DATA

attained on the engine are seen to be slightly greater in the high velocity region and considerably higher in the low velocity region. For all but the baseline annular plug nozzle the attained suppression levels are continuing to rise with jet velocity, not attaining their maximum suppression range within the J85 max dry velocity range. This is as anticipated from the model measurements which exhibited peak suppression in the 2200 to 2500 ft/sec jet velocity range when spectra were scaled to a larger turbojet engine size. See Figure 5. The higher suppression at low velocity cannot readily be explained unless details of individual spectra are examined between the engine and model measurements.

Conical Ejector - Comparison to SAE Prediction

As one of the study goals was to verify the SAE applicability to prediction of non-suppressed jet peak noise, the ground static peak normalized OASPL and PNL data for the conical-ejector are compared to SAE predictions in Figure 80. The predictions were made using the J85 measured cycle parameters and the SAE prediction procedure and extrapolating to the 300 ft. reference sideline. Peak measured OASPL and PNL values are under the predicted level at high jet velocity and over the predicted level at low jet velocity. The measurements suggest a shallower slope than that prescribed by SAE. The slope of the OASPL curves on the 300 ft. sideline are $V^{8.9}$ for SAE and $V^{7.0}$ for the J85. The PNL curves have $V^{9.7}$ and $V^{7.1}$ slopes, respectively, for SAE and measured.

Comparisons of predicted spectra to measured spectra at the peak OASPL and PNL angles are shown in Figure 81. The upper spectra are for the highest jet velocity attained with conical ejector. They verify that the peak OASPL should be predicted several dB high, due to the lower measured levels at the peak frequencies, and that the peak PNL should only be predicted slightly higher, due to near agreement in the region of high frequency. The spectra in the lower part of Figure 81 are for the lowest jet velocity point with the conical ejector. They show that both peak OASPL and PNL should be under-predicted due to the generally higher measured spectra shape. The shape of the measured spectra at high frequency may indicate that broadband turbomachinery noise could be significant in the low speed measurements of the J85. The turbomachinery

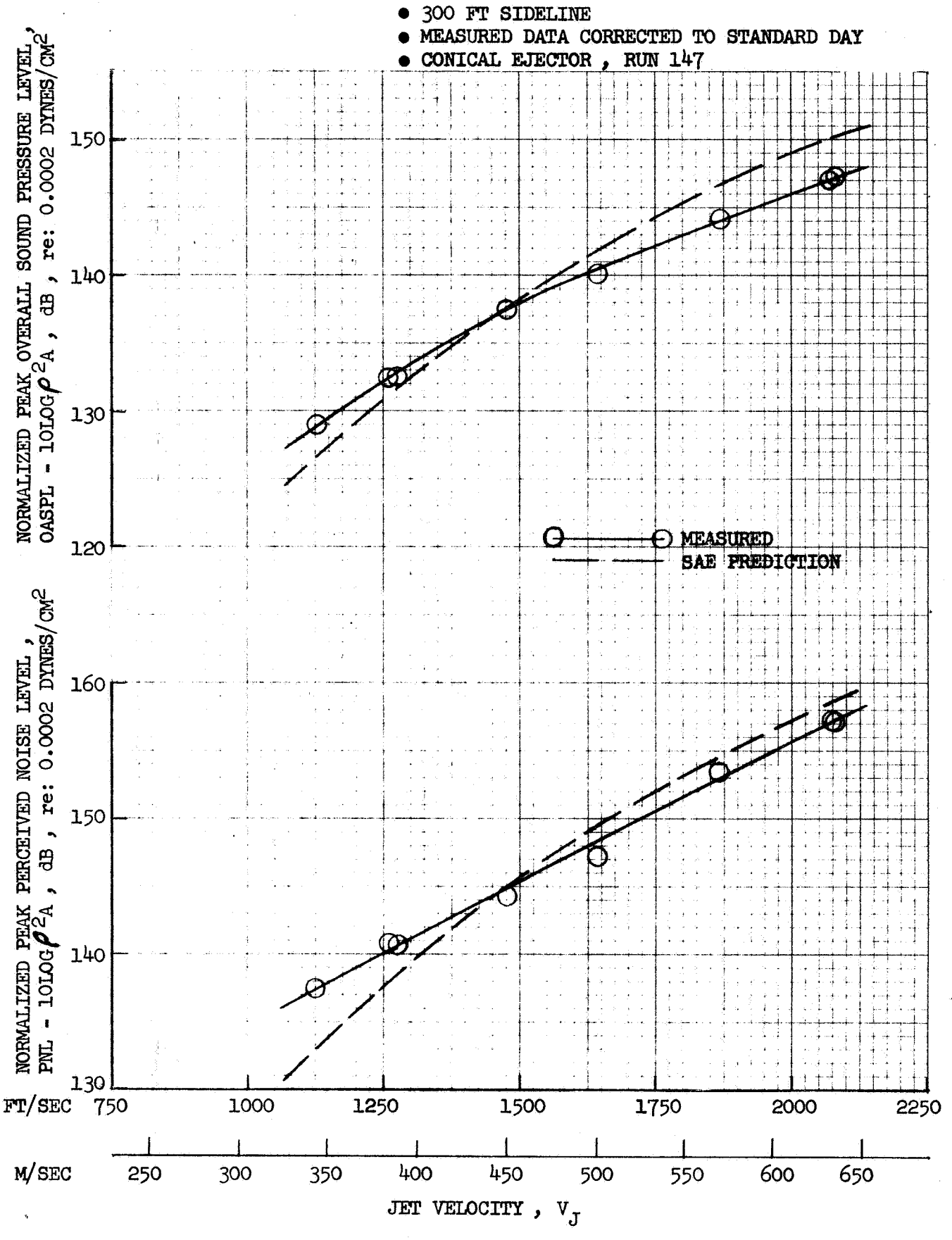

FIGURE 80 COMPARISON OF 300 FT SIDELINE MEASURED PEAK OASPL & PNL TO SAE PREDICTION , CONICAL EJECTOR

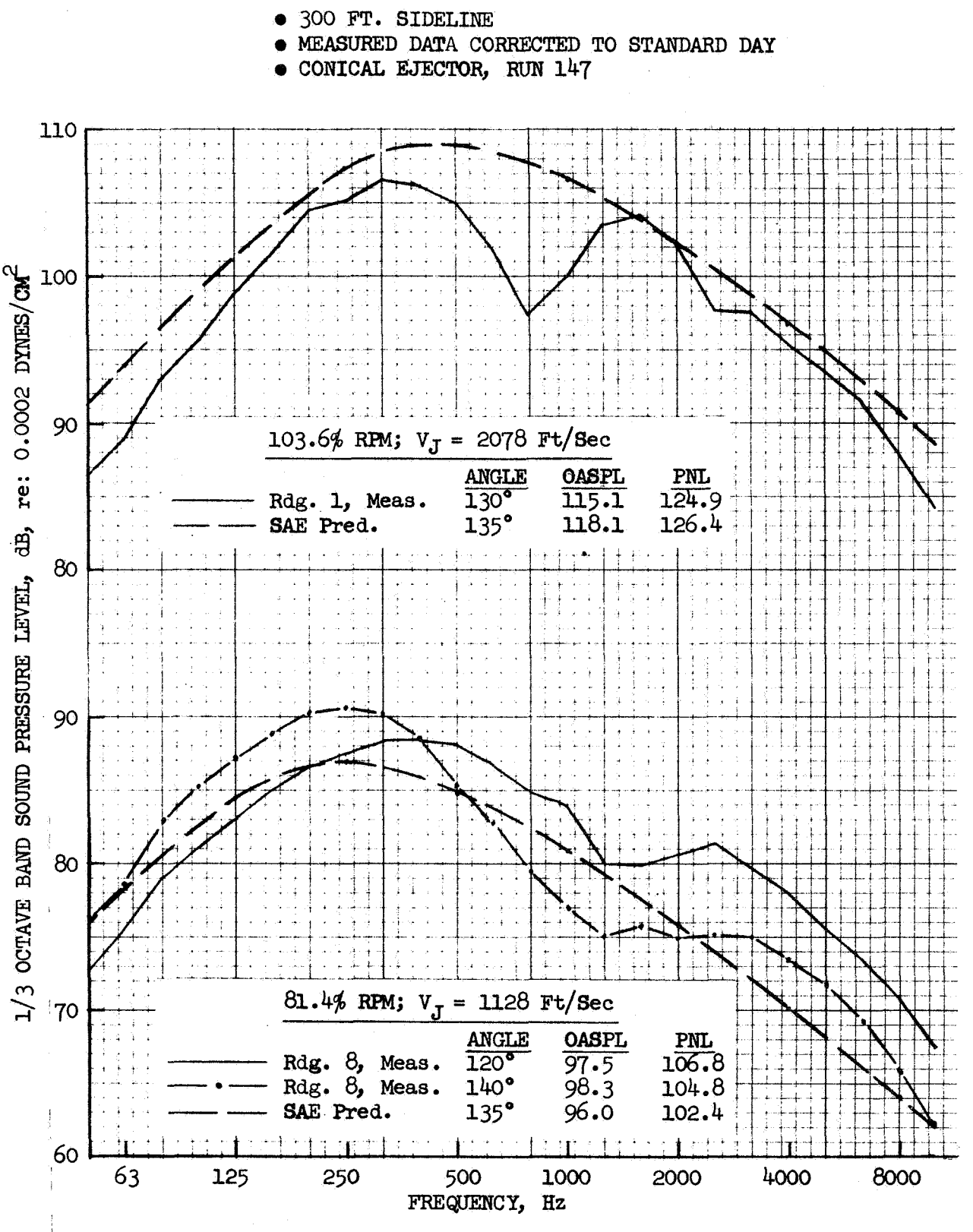

FIGURE 81 COMPARISON OF 300 FT. SIDELINE MEASURED SPECTRA TO SAE PREDICTION, CONICAL EJECTOR

blade passing tones have been corrected for, as discussed under ACOUSTIC DATA REDUCTION - GROUND STATIC RUN-UP; however, broadband turbomachinery noise is less readily identified. Its contribution to the pure jet noise component cannot be easily removed from the total measured noise.

Figure 82 is a check on the magnitude of high frequency divergence from the conventional pure jet spectra. Model measurements from a pure jet hot flow facility test on a convergent primary nozzle are compared to the J85 conical ejector measurements. When plotted on a Strouhal Number basis ((frequency x diameter)/jet velocity), low and high velocity pure jet spectra should agree well. By comparing the model and engine spectra (See Table I, Run 147, Points 1 and 5) it is seen that high frequency noise at low engine speed is considerably above the model data. Initial reaction is to assign the diffferences to engine broadband turbomachinery noise. However, several other factors could have been partially responsible; such as: a) difference in level of initial turbulence within the engine exhaust compared to the model facility, and variance of turbulence with engine speed, or b) varying reflection patterns from the aircraft and wing as the prime jet noise generation region changed with engine speed, compared to a non-installed model configuration.

The presence of greater than anticipated high frequency noise can therefore not totally be assigned to engine rotating machinery. It seems to be a consideration only at low engine speed, and caution should be exercised in applications of the low velocity ground static data. As flight measurements at the same engine speed would have similar turbomachinery noise, conclusions from the study would not be invalidated.

Free Field Correction Effect on Suppression

The question arises as to what effect ground plane interference has on suppression, particularly that of segmented nozzles. If cancellations and reinforcements could significantly interfere with the double humped spectra in the areas of high noy weighting, perhaps PNL suppression would be changed. To investigate the differences, the 100 ft. arc measured data were corrected to free field per the theoretical methods described in references 5 - 8, using the concrete as a hypothetical perfect reflector. The arc data were then again extrapolated to the 300 ft. reference sideline. Peak normalized PNL levels and

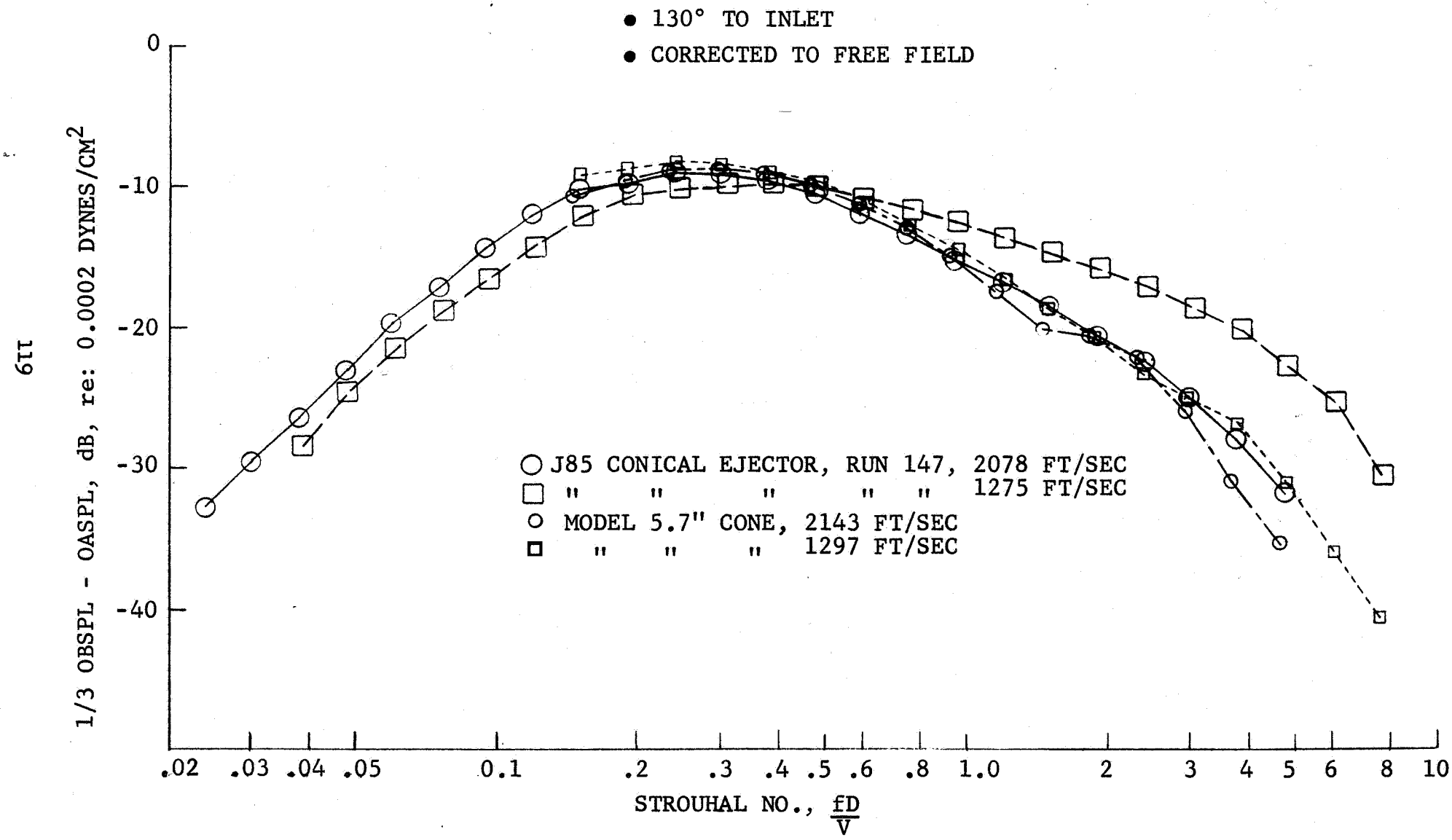

FIGURE 82 300 FT. SIDELINE J85 & MODEL SPECTRA COMPARISON AT LOW & HIGH V_J VS STROUHAL NO.

suppressions from the free field data are presented in Figure 83. When compared to Figure 78, PNL suppression using non-free field data, changes in attained suppression are insignificant. When comparing static spectra to flight data, free field corrections are necessary due to the different measurement geometry.

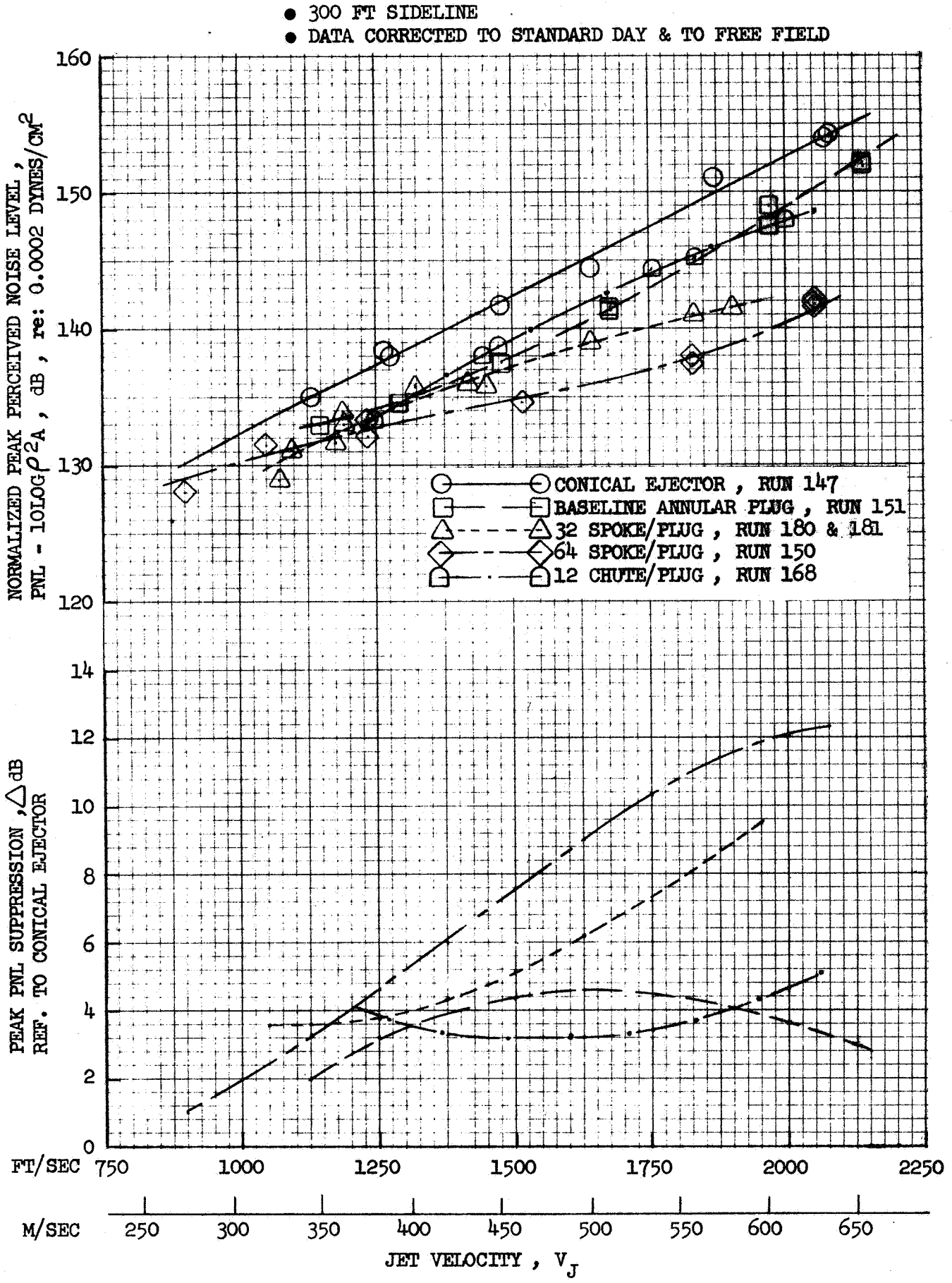

FIGURE 83 GROUND STATIC 300 FT SIDELINE PEAK PNL LEVELS & SUPPRESSIONS , DATA CORRECTED TO FREE FIELD

ACOUSTIC DATA REDUCTION-FLIGHT

The flyby data reduction was performed using a General Radio 1/3 octave band real time analyzer, type 1921, which employed analog filtering and digital detection. In order to have sufficiently detailed data for an analytical study, 1/8 second integration time was chosen, in lieu of the FAR PART 36 prescribed 1/2 second for aircraft type certification. This was necessary due to the short time period of the noise within 10 dB down from peak, resulting from low altitude and high aircraft speed. The integration periods were controlled by an external clock to provide accurate and consistent integration times. The clock also allowed the start of the first integration period at an even 1/8 second real time interval.

Actual integration time was set at .118 second. The analyzer then required a minimum of 2.5 milliseconds dump time to transfer its .118 second of 1/3 octave data sampling into the computer memory. After the data dump, approximately 4.5 milliseconds of dead time passed prior to starting the next data sampling period. Therefore, controlled intervals of exactly .125 seconds between data samples allowed no accumulated time error as the analyzer worked its way through the complete recording of the aircraft's pass.

The data reduction analyzer located the 1/8 second interval of peak OASPL and then stored the peak plus 39 data sets prior to and 40 data sets after the peak. Thus, 80 sets of 1/8 second integrated spectra were available and printed out in 1/3 OBSPL form. Also printed were the measured OASPL and the calculated PNL, PNLT and EPNL levels. This was more than sufficient to define the 10 dB down from peak range and for comparing flight data to matching ground static measurements at the fixed microphone locations. The initial data reduction was "as-measured", corrected only for system response and deemphasis ; not corrected to standard acoustic day. Punched paper tapes of the data were also produced.

Exact clock time for the start of integration was known from the recorded real time code signal and was printed out with the spectra. Since the external clock triggered integration each 1/8 second, cumulative real time was assigned to successive data sets.

By simultaneously reducing the 400 Hz voltage pulse blip and the real time code signal, the overhead aircraft time was established. The acoustic speed of sound, based on the control tower's measurement of T_0, and the aircraft altitude were then used to mate the overhead time to the reduced acoustic data. To assign acoustic angles of noise generation to each integrated data set, the only remaining input was aircraft flight velocity. Angular location was required to compare flight data to ground static noise. Angular assignment, along with correction of the data to standard day, 300 ft. altitude and consistent flight speed, was done through the use of a high speed computer.

Accuracy of Aircraft Overhead Location

To eliminate chance of major error and to average inconsistencies in aircraft overhead positioning due to human judgement, a procedure was introduced to check data repeatability. The as-measured data were reduced versus time and PNL-time histories were plotted for each flyby. For repeat passes (normally three) at the same engine speed, the plots were compared. Location of peak noise plus the rate of decay, or curve shape, gave an excellent check on repetition of overhead blip assignment. Most data sets agreed well, but for several sets an average overhead time was assigned. For the first five passes of Flight 170, where no blip was recorded, the overhead time was assigned directly from repetative flyovers at similar engine speeds. Overall, the data proved to be quite consistent. For the purpose of this study, the aircraft overhead location was felt to be adequately accurate.

"DRAFT" Processing

When comparing data and establishing suppression levels, it is normal practice to correct measurement to a consistent base of reference or standard acoustic day. Several of the flight measuring days varied considerably from the standard meteorological conditions and magnitudes of theoretical atmospheric absorption values were quite above those for standard day. Slight variances in repetitive flight altitudes changed the acoustic path lengths from the noise generation source to the microphone. Flight speed also changed from pass to

pass causing differences in PNLT histories which slightly effect the EPNL calculations. To correct all data to consistent altitude, flight speed and standard day, each pass was processed through the DRAFT (Data Reduction-Acoustic Flight Test) computer program utilizing a high speed computer. The program inputs are the punched digital tape containing the 80 sets of 1/3 octave band data and real time of data reduction, aircraft measured speed and altitude, aircraft overhead time and measuring day meteorological conditions. Referring to Figure 84, the program procedure is as follows:

- Using altitude, aircraft speed, speed of sound, overhead time and integration start time, the aircraft location at the time of noise generation, corresponding to each 1/8 second of received data, is calculated. The position of the aircraft is assigned an acoustic angle of θ at the end of a 1/8 second received interval of data. This acoustic angle is referenced to the engine inlet and is the angle between the straight line from the source to the microphone and the engine centerline. The acoustic path length and offset distance from the overhead location are also calculated. The sight angle, defined as the actual angular location of the aircraft at the time of noise reception at the microphone, is also calculated by the program, however, the acoustic angle is more meaningful and will be used for all data plots.

- Using the SAE procedure for atmospheric absorption correction (ref. 4), the differences between the measured day and standard day (59° F and 70% R.H.) are calculated for the acoustic path length at the assigned angle θ. These are applied to the measured data at the measured altitude.

- Considering the difference between measured altitude and 300 ft. standard altitude, the change in acoustic path length is calculated by projection along the acoustic angle. Because of the change in the acoustic path length, the spectra are also corrected by using the inverse square law and standard day atmospheric absorption. Using the corrected spectra, new values of OASPL, PNL, and EPNL are calculated. (ref. 4 and 9)

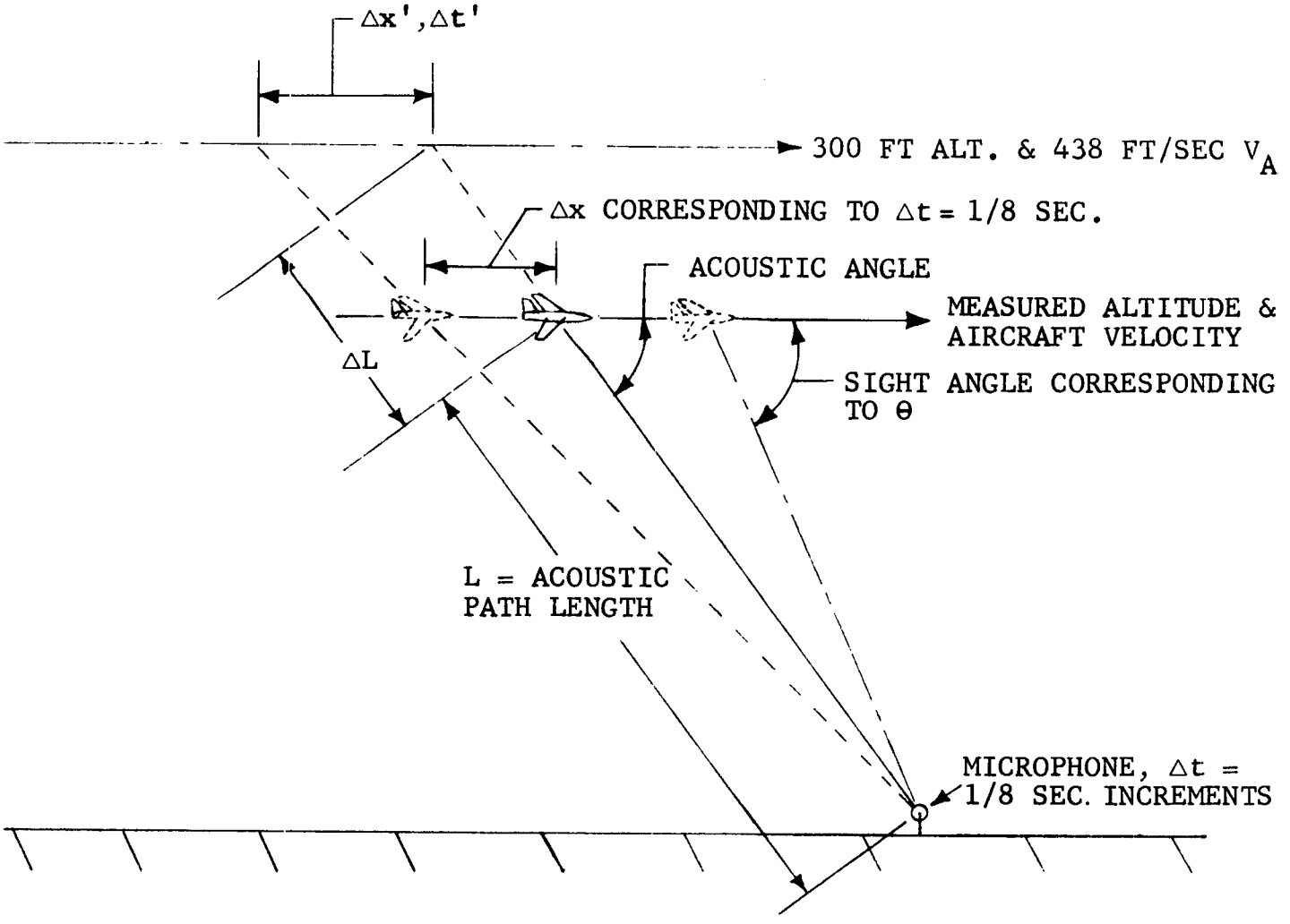

FIGURE 84 SCHEMATIC OF "DRAFT" CORRECTION PROCEDURE

- Using the 300 ft. altitude locations for the progression of acoustic angles, $\Delta x'$ values between acoustic angle intersection points are known. Using the standard aircraft velocity of 438 ft/sec, $\Delta t'$ values are assigned to each $\Delta x'$. By accumulating $\Delta t'$ values from the start of integration, the new time scale is set for the entire aircraft passage. This represents the actual time occurance had the flyover been at 300 ft. altitude and 438 ft/sec. The new time scale with the corrected PNLT values are then used to calculate a corrected EPNL value.
- Sideline microphone data are corrected in the same manner. The computer program incorporates the offset distance and handles the more complex geometry of the sideline microphone.

The acoustic angles set by the DRAFT program are referenced to the aircraft in level flight, without incorporation of the angle of attack to flight path or engine mount angle. Figure 14 shows a resultant 2-1/2° angle between engine centerline and level flight path or horizontal. For comparison to ground static data, this resultant angle must be considered. For example, the ground static fixed location of 150° would be compared to 147.5° in flight. Since this flight angle will probably not occur at the exact end of a 1/8 second data set, the next higher assigned flight angle should be chosen. Thus, if acoustic flight angles of 141° and 149° were assigned to consecutive 1/8 second data sets, the latter set would be chosen for comparison to the static location. Its data were generated from acoustic signals between 141° and 149°.

Influence of Correcting Flight Data to Standard Day

As discussed under ACOUSTIC DATA REDUCTION - GROUND STATIC RUN-UP , it is usually considered that correcting acoustic measurements to a chosen standard day makes the data more consistent for comparison and analysis. The corrections are felt to be fairly accurate for measurement conditions which are not extremely different than standard day and which are applied over relatively short acoustic path lengths. Application to measurements taken over long distances are felt to over-correct the data, particularly when the measuring conditions are quite meteorologically different than the standard acoustic day.

The applied corrections to flight data are of sufficient magnitude to alter final absolute suppression levels (but not conclusions) when compared to as-measured data levels. For measurements under the flight path, where acoustic path lengths are not extremely long, both as-measured and corrected data are presented. At sideline, only as-measured data are presented, as absorption corrections for the longer path lengths proved excessive.

The major influence is not path length in itself, but the wide divergence from standard day under which noise measurements were taken. Table VI is included to show the magnitudes of atmospheric absorption prescribed by SAE ARP 866 (ref. 4). The standard day absorption is 27 dB per 1000 ft in the 10 KHz band. The conical ejector measuring conditions came closest to standard with theoretical absorption of 38 dB. The most extreme case, for the 64 spoke test, is 57.7 dB. The magnitude of correction to apply is the difference between measured and standard, pro-rated over the actual acoustic path length.

Since the corrections are significant only in the high frequency bands, PNL levels from the low frequency dominated spectra of the conical ejector and annular plug are not appreciably changed. The spectra of segmented nozzles, particularly of the 32 and 64 spoke, are high frequency dominated and over-correcting induces error in PNL values.

As indicated, magnitudes of suppression deltas are somewhat changed by correcting to standard day; significant results are not. Therefore, both sets of data are presented for measurements under the flight path. When comparing flight to static, corrected data will be used. The data presented "as-measured" is also not corrected to consistent 300 ft altitude. A check of total correction magnitudes, however, has shown that corrections for altitude variations are very minor when compared to those for atmospheric absorption.

TABLE VI

TOTAL ATMOSPHERIC ABSORPTION VALUES FOR FLIGHT

MEASURED & STANDARD DAY

Nozzle	Conical Ejector	Annular Plug	32 Spoke	64 Spoke	12 Chute	
Flight	146	152	159	155	170	Stand. Day
P_o, in. Hg	30.14	30.27	30.20	30.22	29.41	29.92
T_o, °F	47	32	43	46	61	59
% Rel. Hum.	67	45	39	37	37	70
1/3 Octave Band Center Frequency, Hz	Total Atmospheric Absorption, dB / 1000 ft.*					
1000	1.3	3.0	2.4	2.3	1.7	1.5
1250	1.8	4.2	3.4	3.3	2.3	1.8
1600	2.6	6.0	5.0	4.9	3.3	2.4
2000	3.6	8.3	7.1	7.0	4.6	3.0
2500	5.0	11.4	9.9	9.9	6.5	4.0
3150	7.2	15.7	14.0	14.0	9.5	5.5
4000	10.6	21.6	19.8	19.8	13.9	7.7
5000	12.6	23.8	23.0	23.0	16.5	9.1
6300	18.3	30.1	31.8	31.9	23.8	12.9
8000	26.8	37.8	44.0	44.3	34.6	18.8
10000	38.0	45.5	55.6	57.7	48.7	27.0

* Per SAE ARP 866 (ref. 4)

J75 Flight Idle-Background Noise

The J75 was required to run at idle during flight for operation of the data recorder and to supply fuel pressure to the J85, just as it was for ground static testing. Therefore, flight idle background noise measurements were taken with the J85 off. Figures 85 & 86 present the PNL data for measurements under the flight path; as-measured and corrected respectively. Figures 87 and 88 are as-measured data for the sideline microphone. These data can be compared to individual flyby J85 measurements to detect presence of background interference. No corrections were made to any of the presented J85 data for elimination of J75 idle interference, if and when it occurred.

In general, for under the flight path measurement, there was no interference within the range of 10 dB down from peak noise, therefore, EPNL calculations are valid. Within the range of angles which would compare directly to ground static stations (37.5° to 147.5° to inlet) there was no interference except for the conical ejector test. Due to shifted directivity pattern of this nozzle, low engine speed data had partial interference at the 60° and forward inlet angles.

For the sideline measurements, in general there is no interference in the peak noise or any significant interference within the 10 dB down range which would influence EPNL calculations. At angles toward the inlet, particularly at low speed, the background levels interfere in some of the flybys and each must be checked individually.

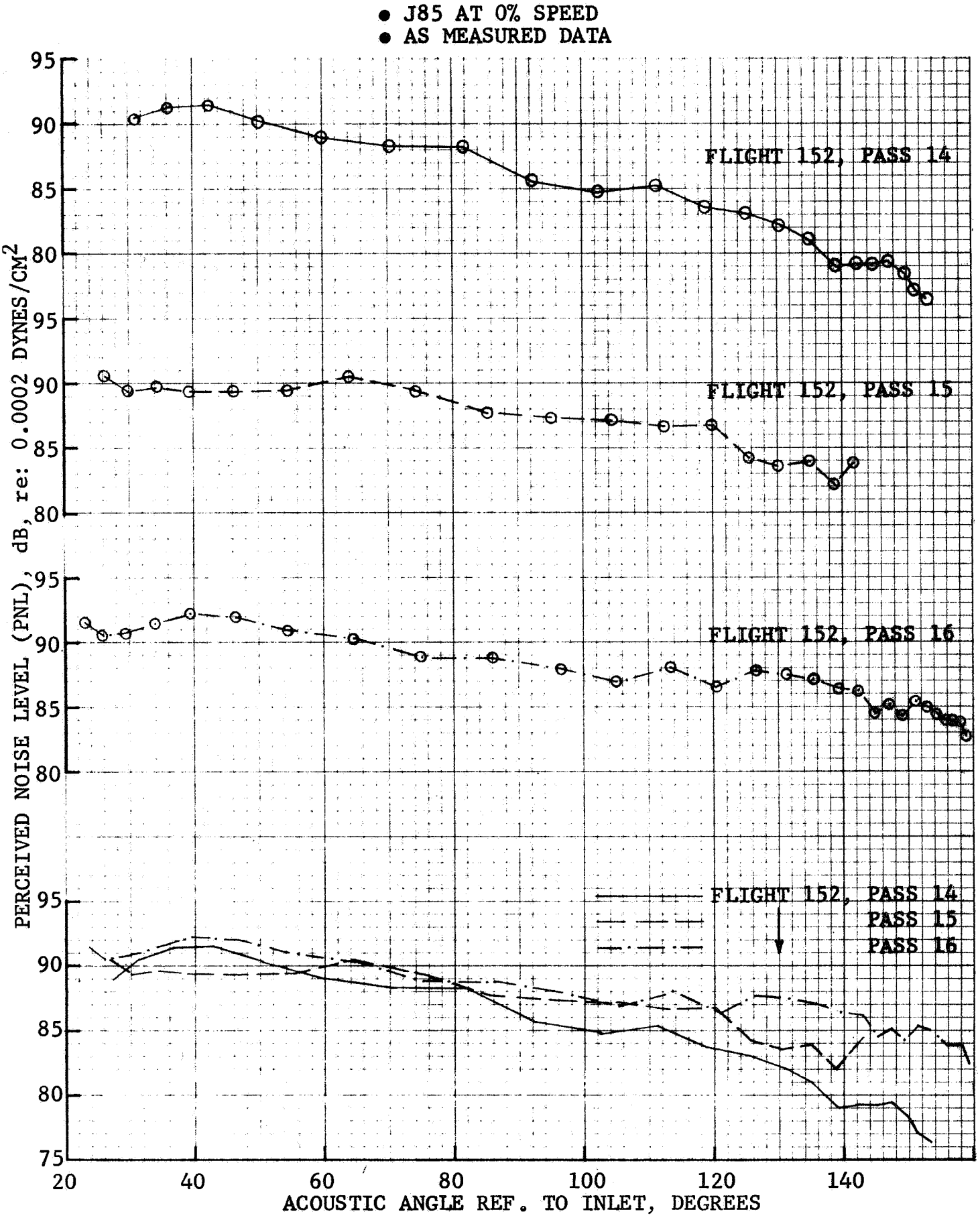

FIGURE 85 J75 FLIGHT-IDLE BACKGROUND NOISE, MIC UNDER FLIGHT PATH

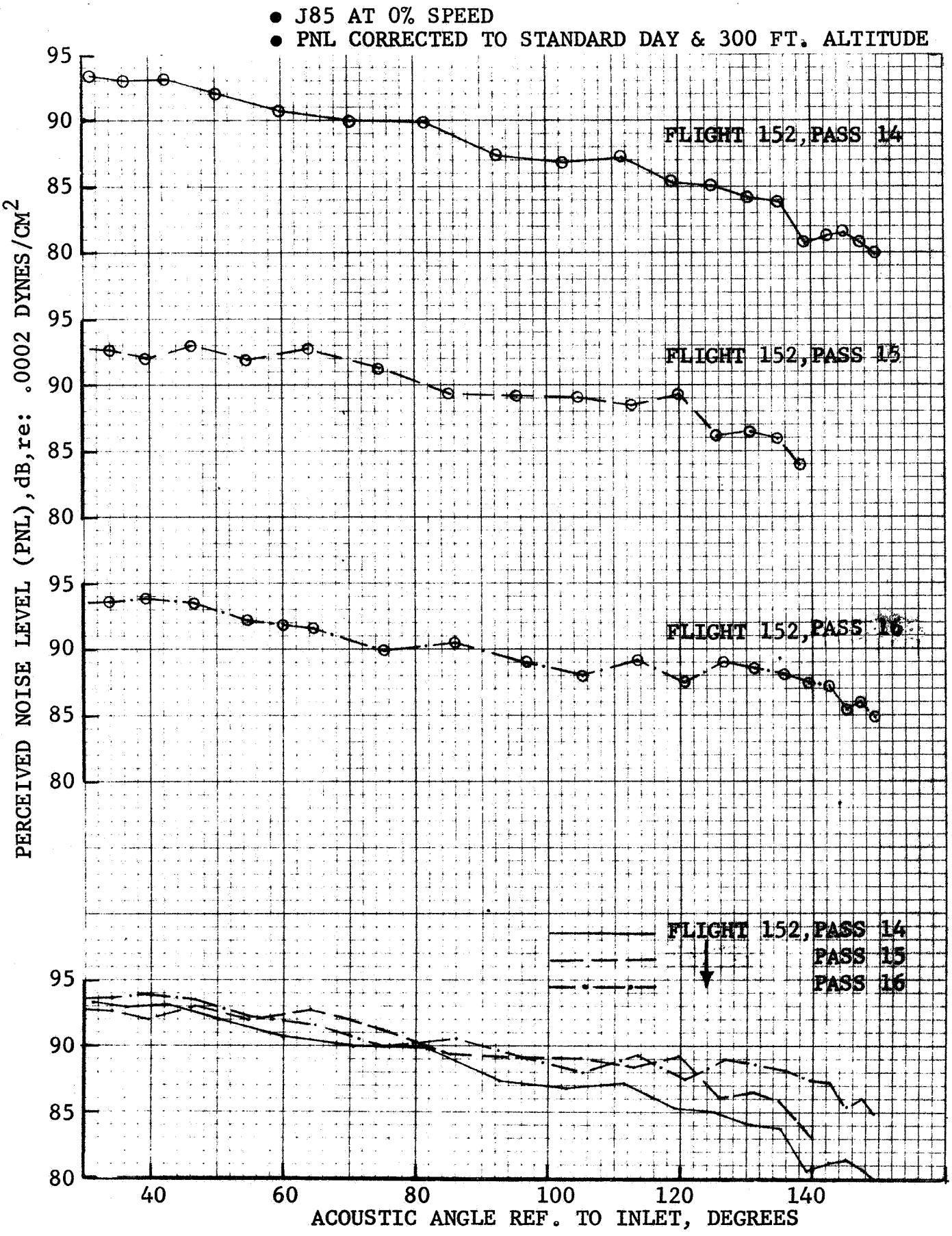

FIGURE 86 J75 FLIGHT-IDLE BACKGROUND NOISE, MIC UNDER FLIGHT PATH

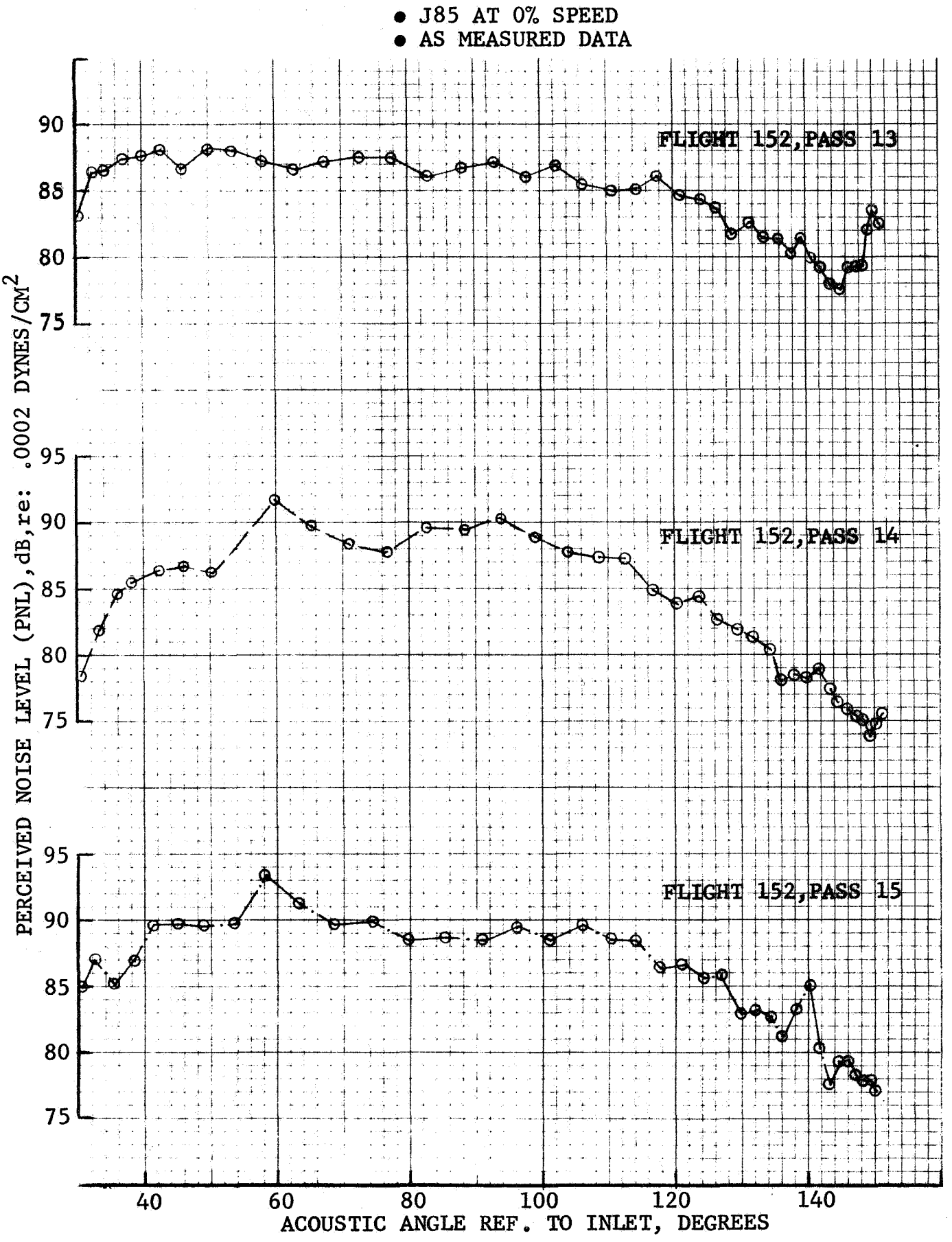

FIGURE 87 J75 FLIGHT-IDLE BACKGROUND NOISE, SIDELINE MIC

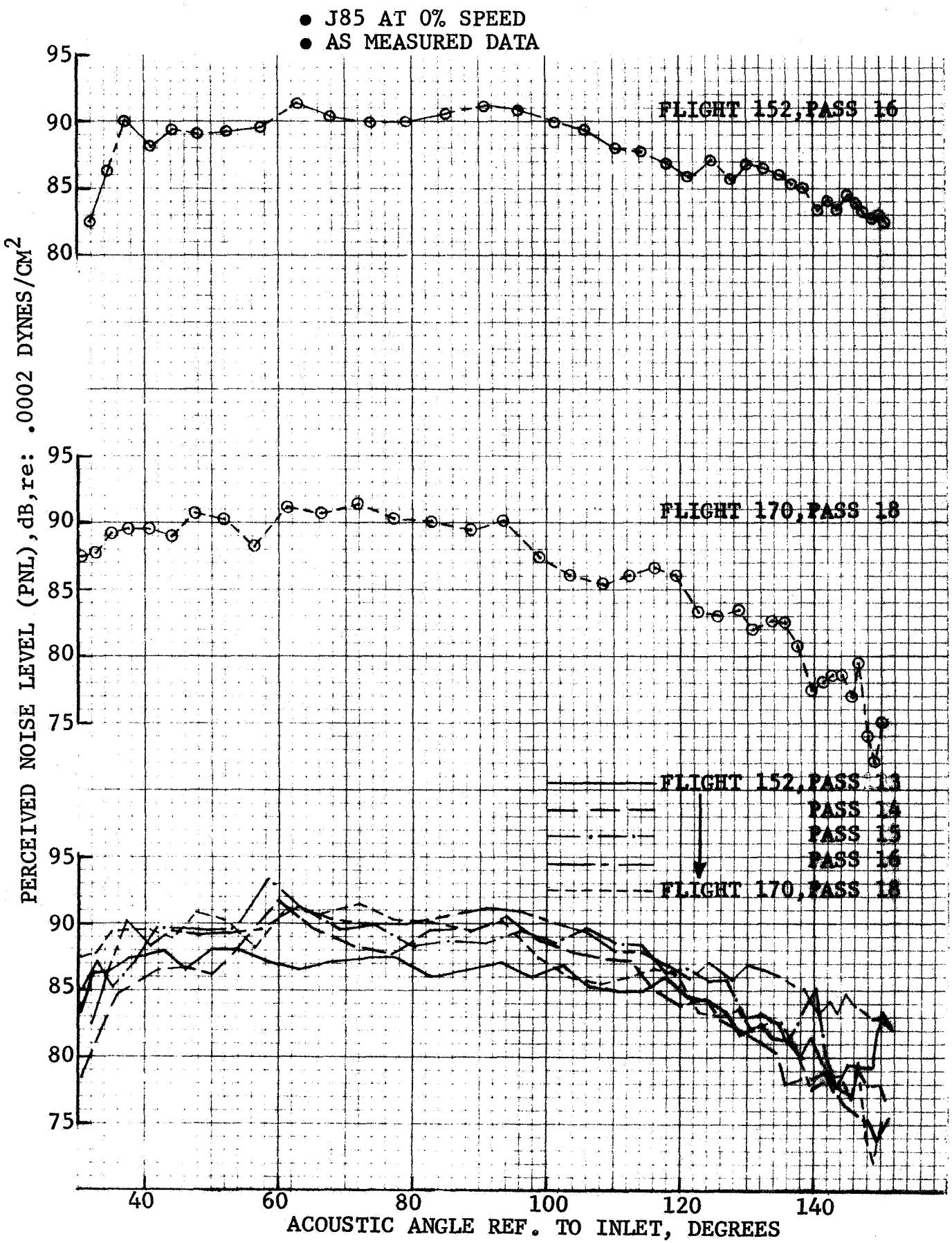

FIGURE 88 J75 FLIGHT-IDLE BACKGROUND NOISE, SIDELINE MIC

PRESENTATION OF FLIGHT DATA

For the purpose of presenting flight data within this report, the subjective rating of PNL and its variance with flight location are considered most important. Although time duration of noise is necessary for EPNL evaluation and would suggest plotting noise against time, the relation to acoustic angle is more meaningful; particularly when interested in directivity or when making comparisons to static measurements. Therefore, the primary data scale is acoustic angle, however, the manner in which the report data are plotted also gives a good indicator of time lapse. Each flight pass is plotted separately using the individual data points. These represent 1/8 second intervals for as-measured data and usually slightly under 1/8 second intervals for corrected data. Thus, by counting data points during any lapsed period, as within the range of 10dB down from peak, a good indicator of time duration is available. The separate PNL plots are then composited for flight passes at similar engine speeds, giving a ready indicator of repeatability.

As the major portion of the measured noise is jet predominant without pure tones, PNLT levels were normally just several dB above the PNL values. Therefore, the PNL plots are a good indicator of PNLT data used for EPNL calculation.

In working with flight data, and particularly with short integration time, volumes of spectra are generated. As all the spectra could not be included in this report, the spectra at peak PNL were chosen as most representative. They are plotted at the acoustic angle of peak corrected PNL. As-measured spectra are also included in these plots at that same angular location, however, in some instances the peak measured and peak corrected PNL's occurred at different acoustic angles.

As previously discussed, as-measured and corrected data for the microphone under the flight path are included. For the sideline microphone, only as-measured PNL data are shown.

Table VII is included as an index to the flight data.

Table VII. INDEX TO FLIGHT DATA CURVES

	Conical Ejector Flt 146	Annular Plug Flt 152	32 Spoke/ Plug Flt 159	64 Spoke/ Plug Flt 155	12 Chute/ Plug Flt 170
	Figure No.				
As Measured PNL Mic Under Flight Path	89-92	101-102	111-114	127-130	143-147
Corrected PNL Mic Under Flight Path	93-96	103-104	115-118	131-134	148-152
Spectra at Peak PNL As-Measured & Corrected Mic Under Flight Path	97-100	105-106	119-122	135-138	153-157
As-Measured PNL Sideline Mic	-	107-110	123-126	139-142	158-163

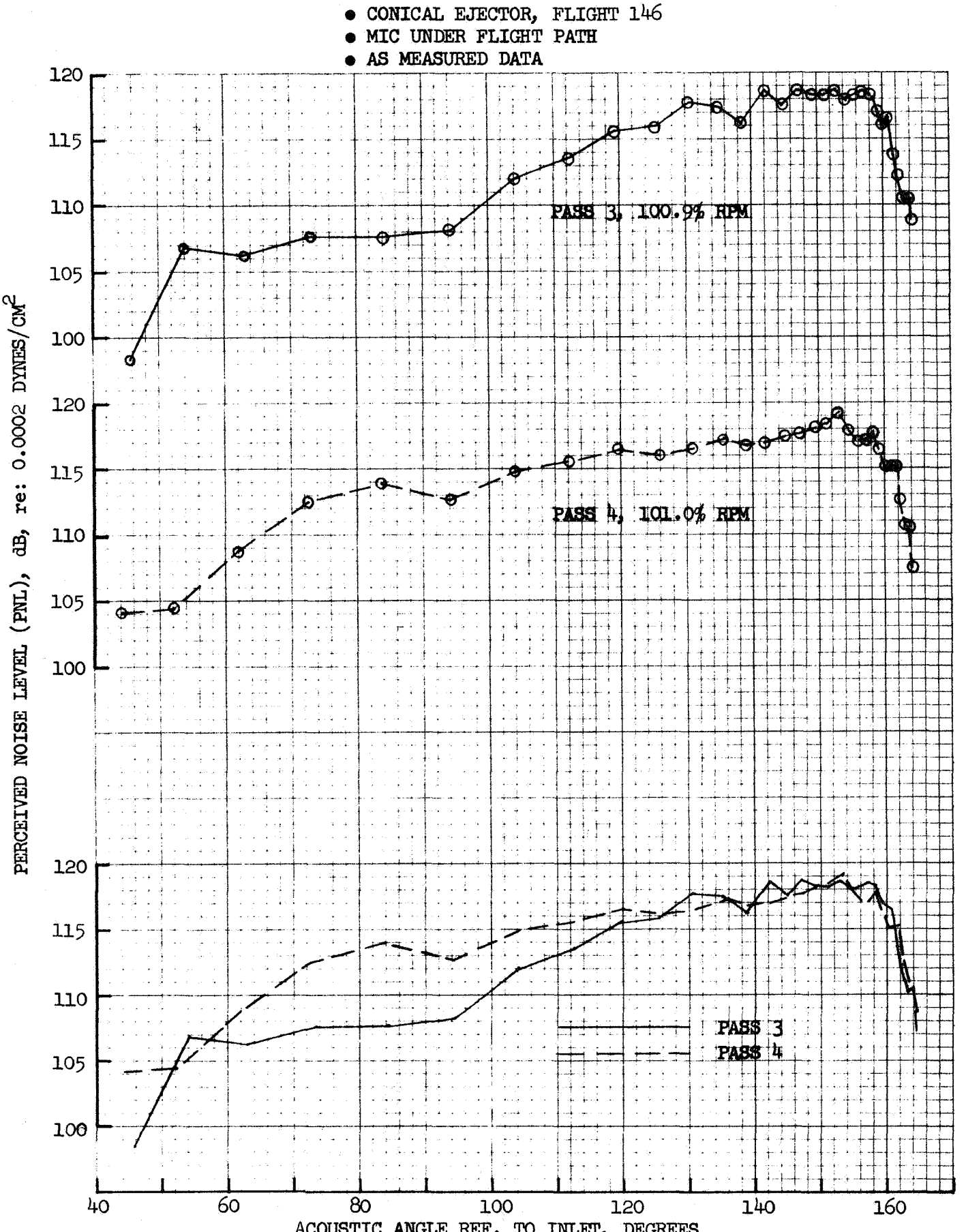

FIGURE 89 FLIGHT PNL, CONICAL EJECTOR, MIC UNDER FLIGHT PATH, AS MEASURED DATA

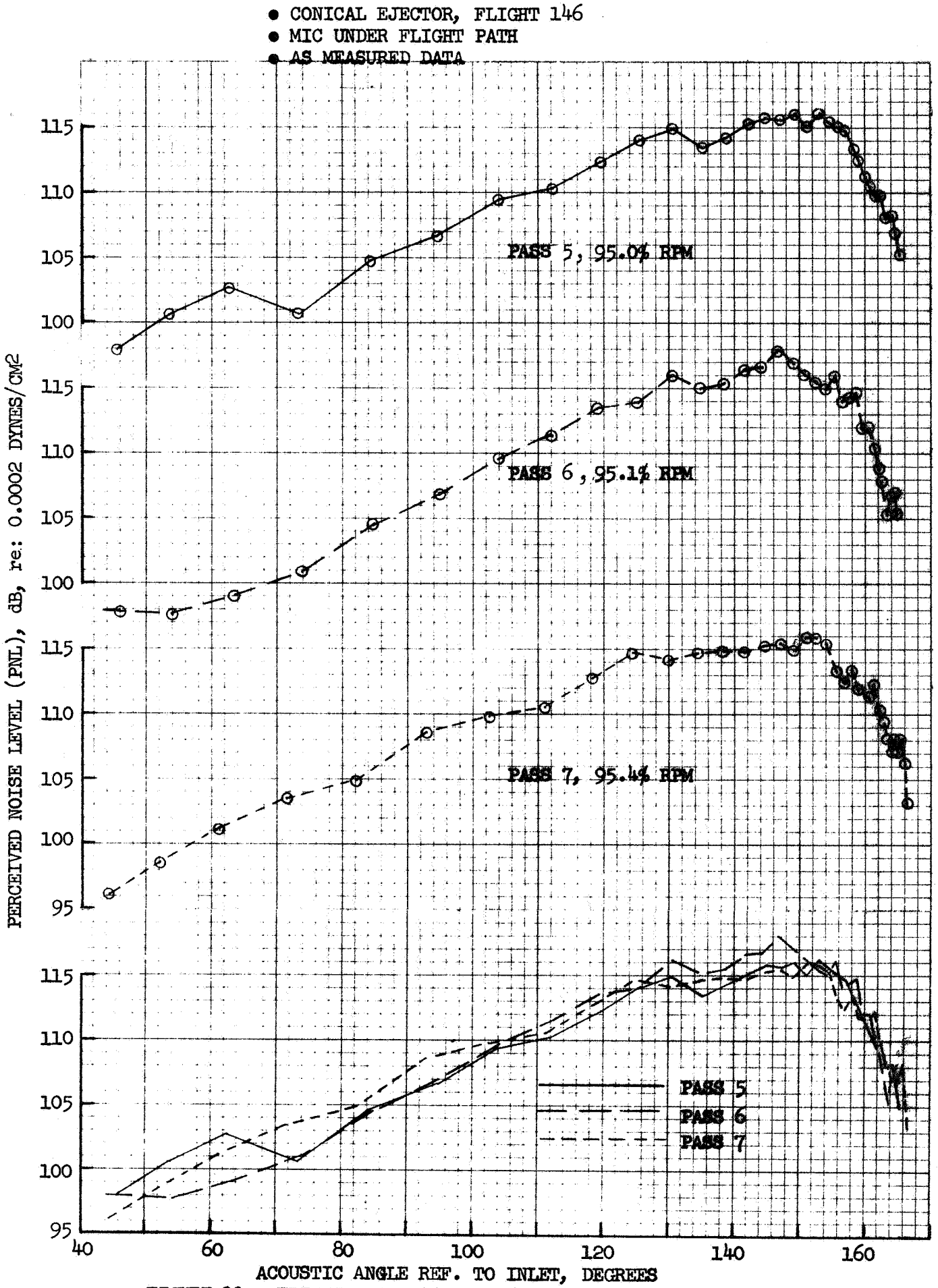

FIGURE 90. FLIGHT PNL, CONICAL EJECTOR, MIC UNDER FLIGHT PATH, AS MEASURED DATA

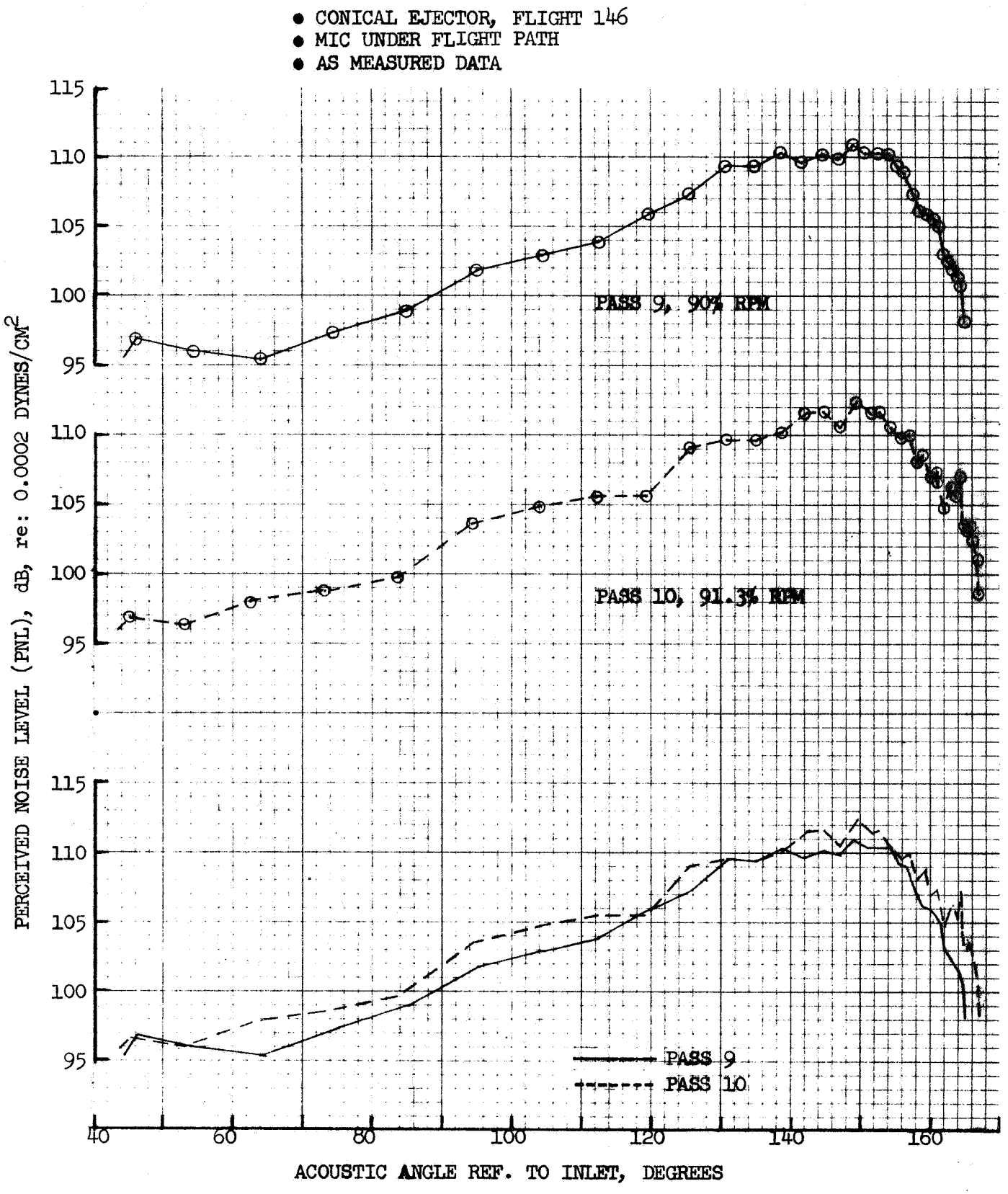

FIGURE 91 FLIGHT PNL, CONICAL EJECTOR, MIC UNDER FLIGHT PATH, AS MEASURED DATA

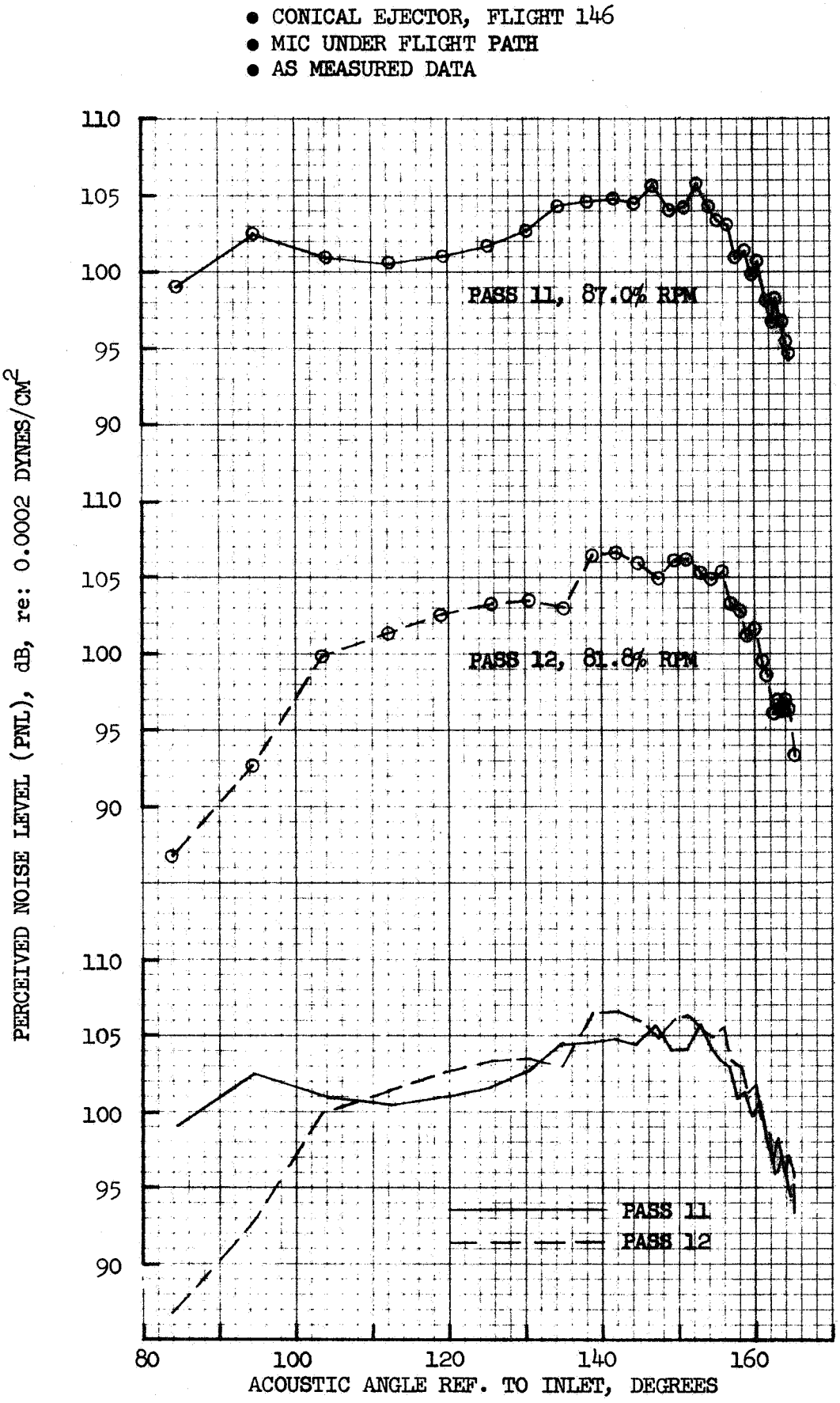

FIGURE 92 FLIGHT PNL, CONICAL EJECTOR, MIC UNDER FLIGHT PATH, AS MEASURED DATA

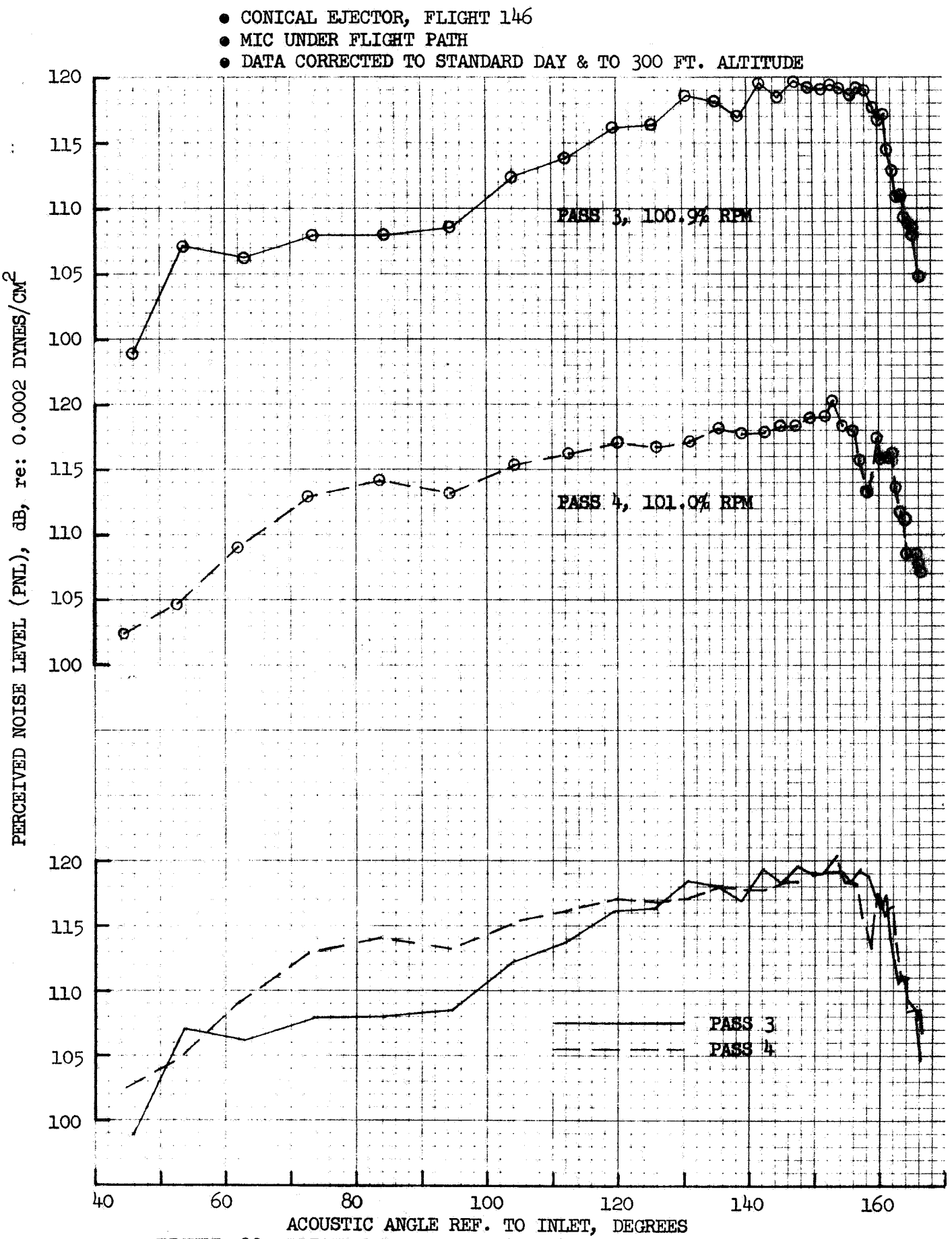

FIGURE 93 FLIGHT PNL, CONICAL EJECTOR, MIC UNDER FLIGHT PATH, CORRECTED DATA

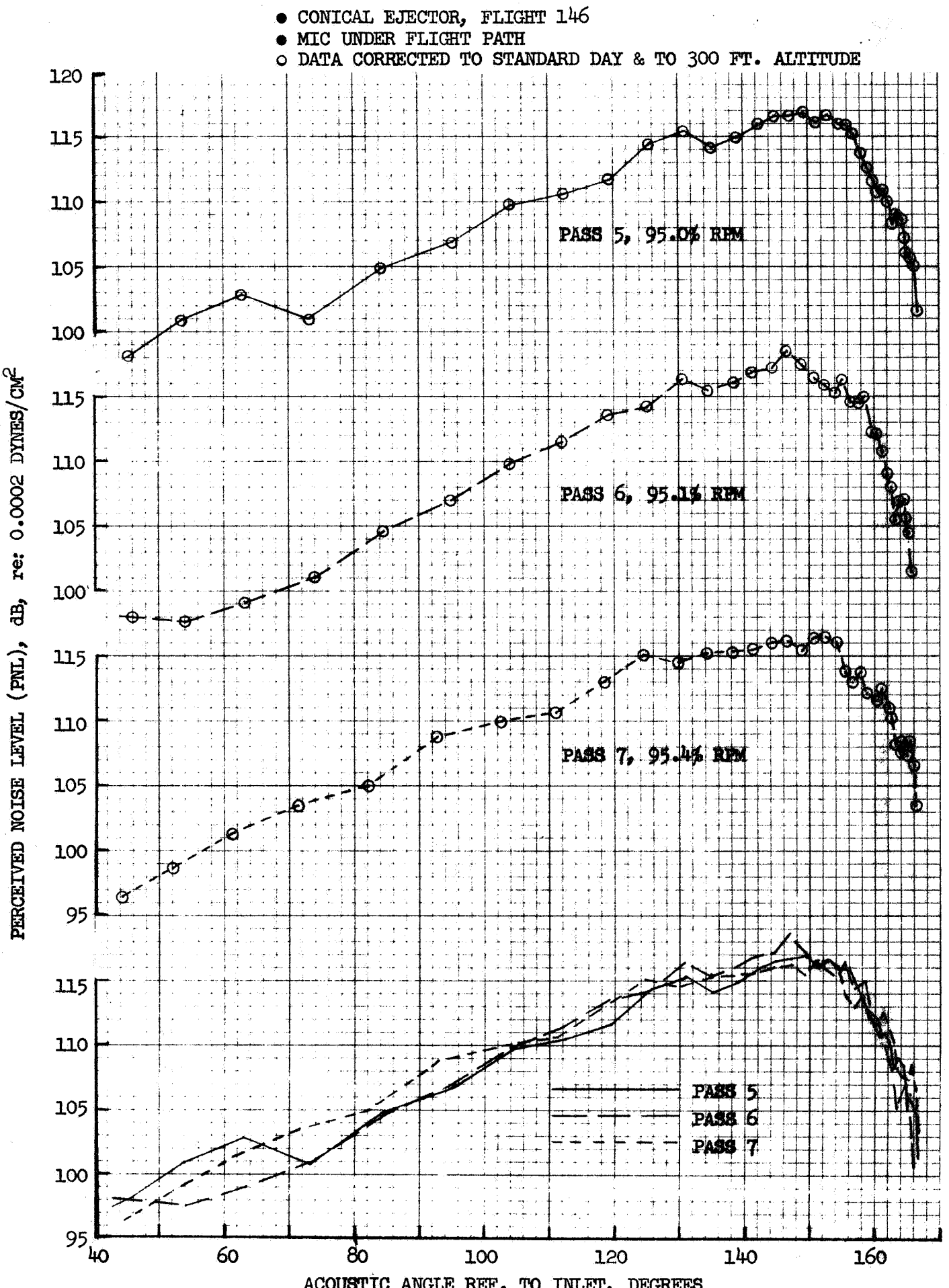

FIGURE 94 FLIGHT PNL, CONICAL EJECTOR, MIC UNDER FLIGHT PATH, CORRECTED DATA

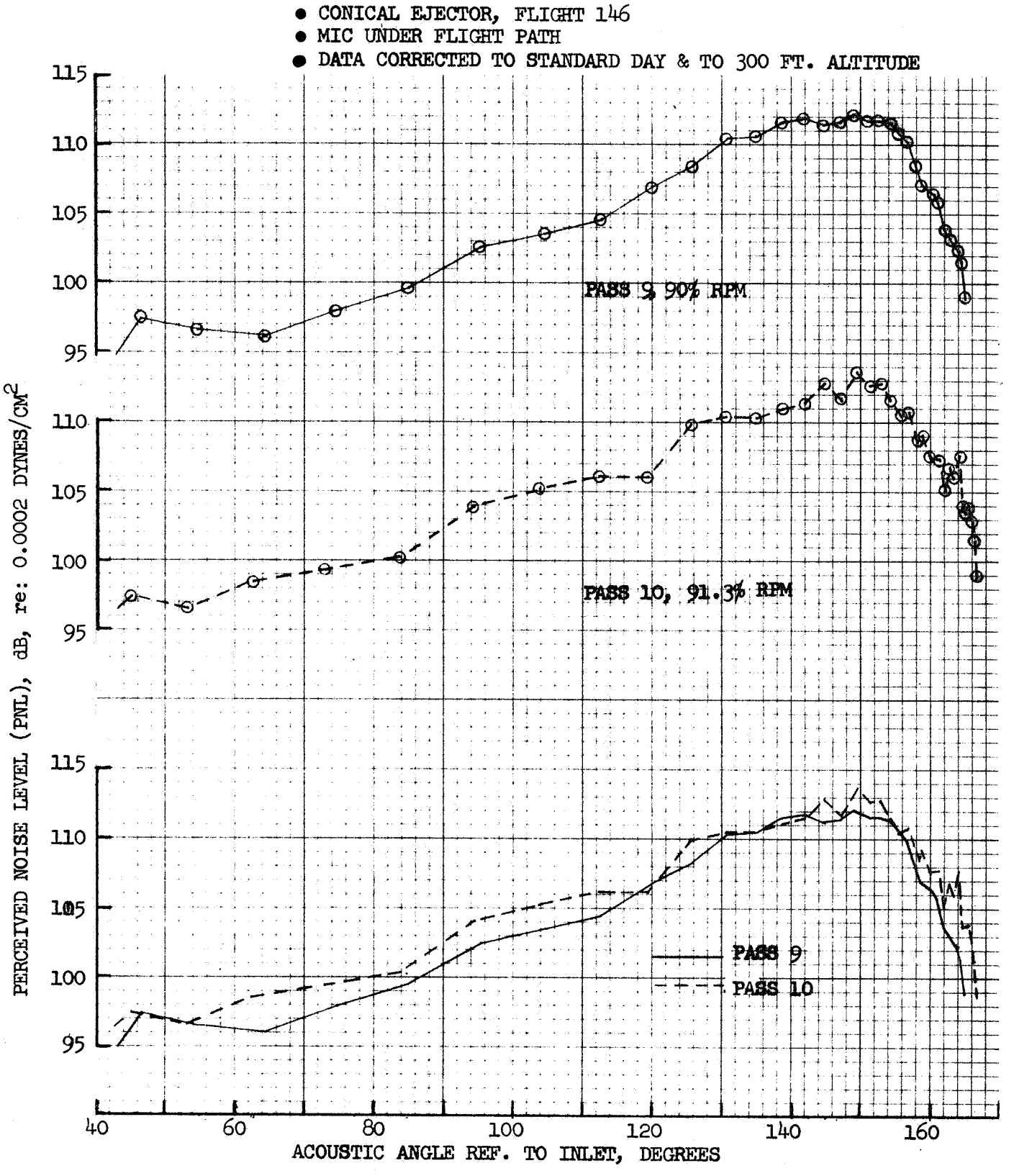

FIGURE 95 FLIGHT PNL, CONICAL EJECTOR, MIC UNDER FLIGHT PATH, CORRECTED DATA

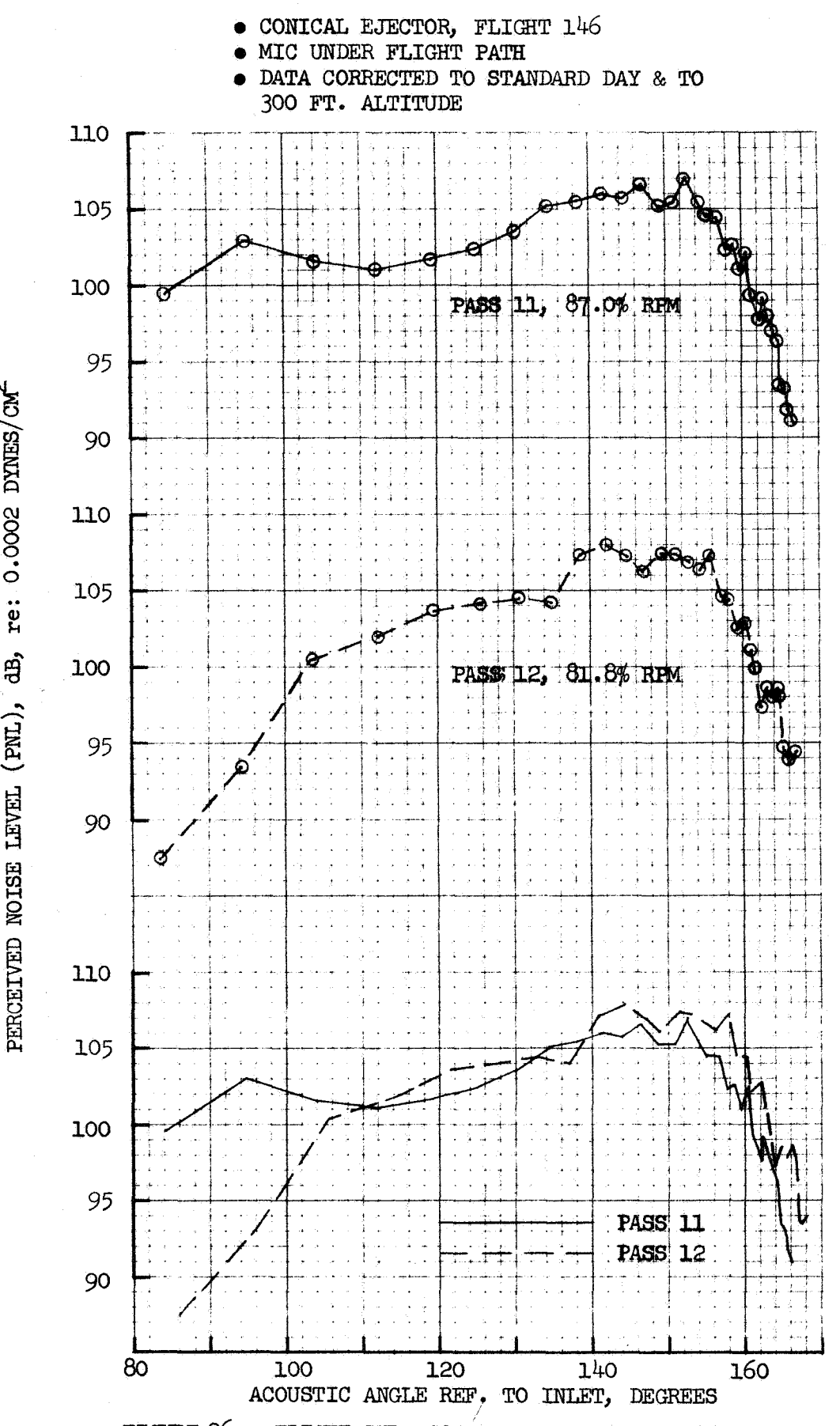

FIGURE 96 FLIGHT PNL, CONICAL EJECTOR, MIC UNDER FLIGHT PATH, CORRECTED DATA

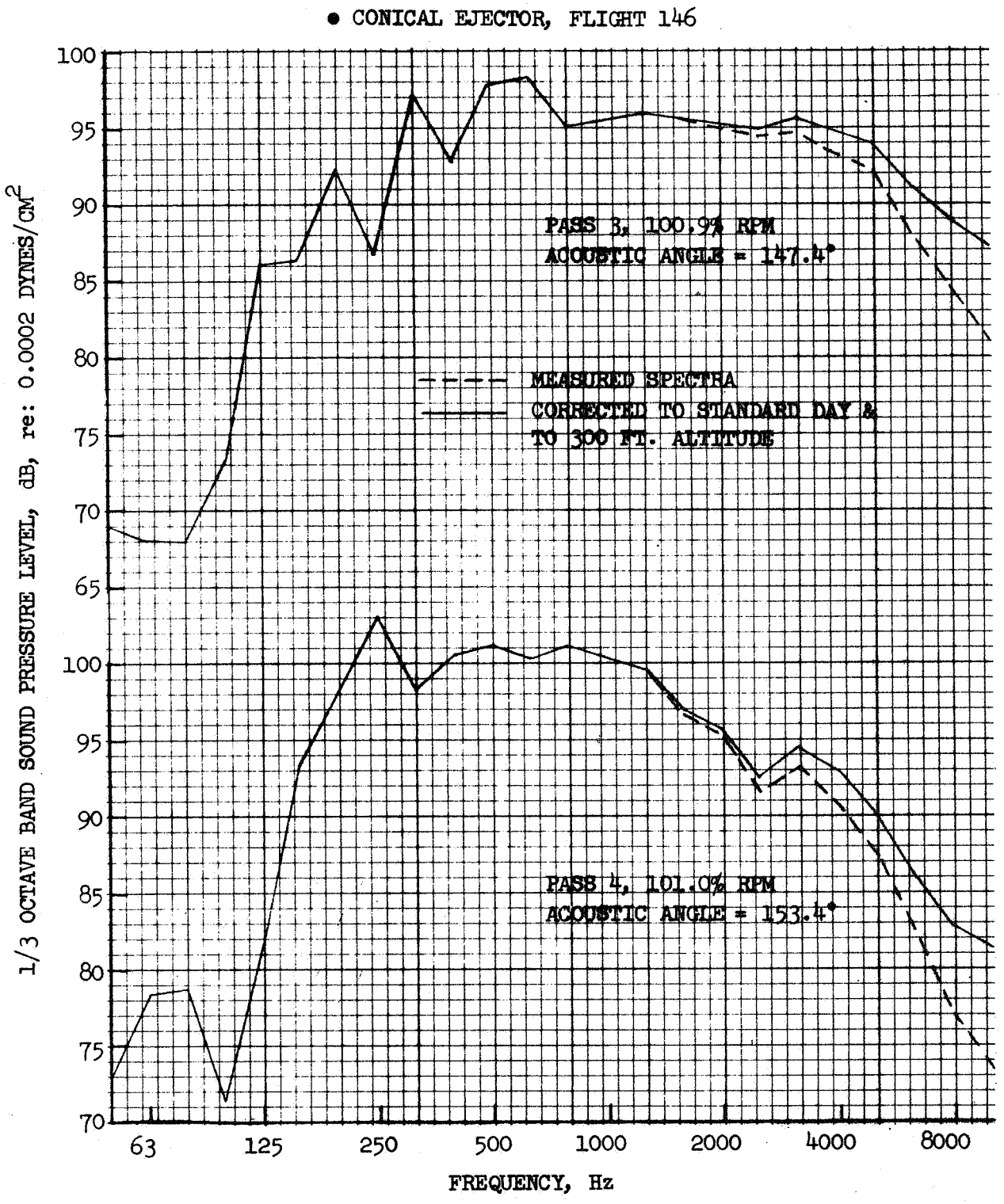

FIGURE 97 FLIGHT SPECTRA AT PEAK PNL, CONICAL EJECTOR, MIC UNDER FLIGHT PATH

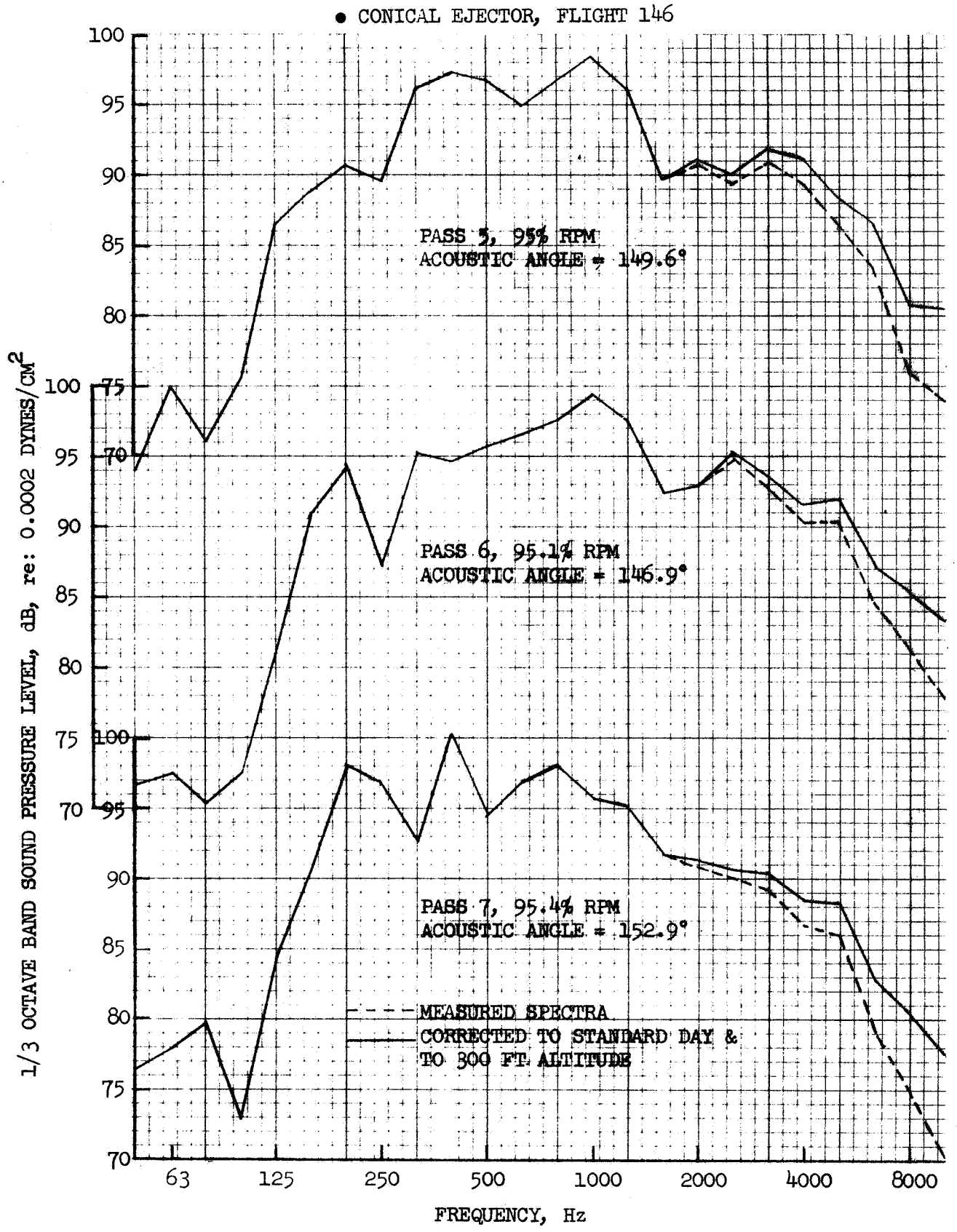

FIGURE 98 FLIGHT SPECTRA AT PEAK PNL, CONICAL EJECTOR, MIC UNDER FLIGHT PATH

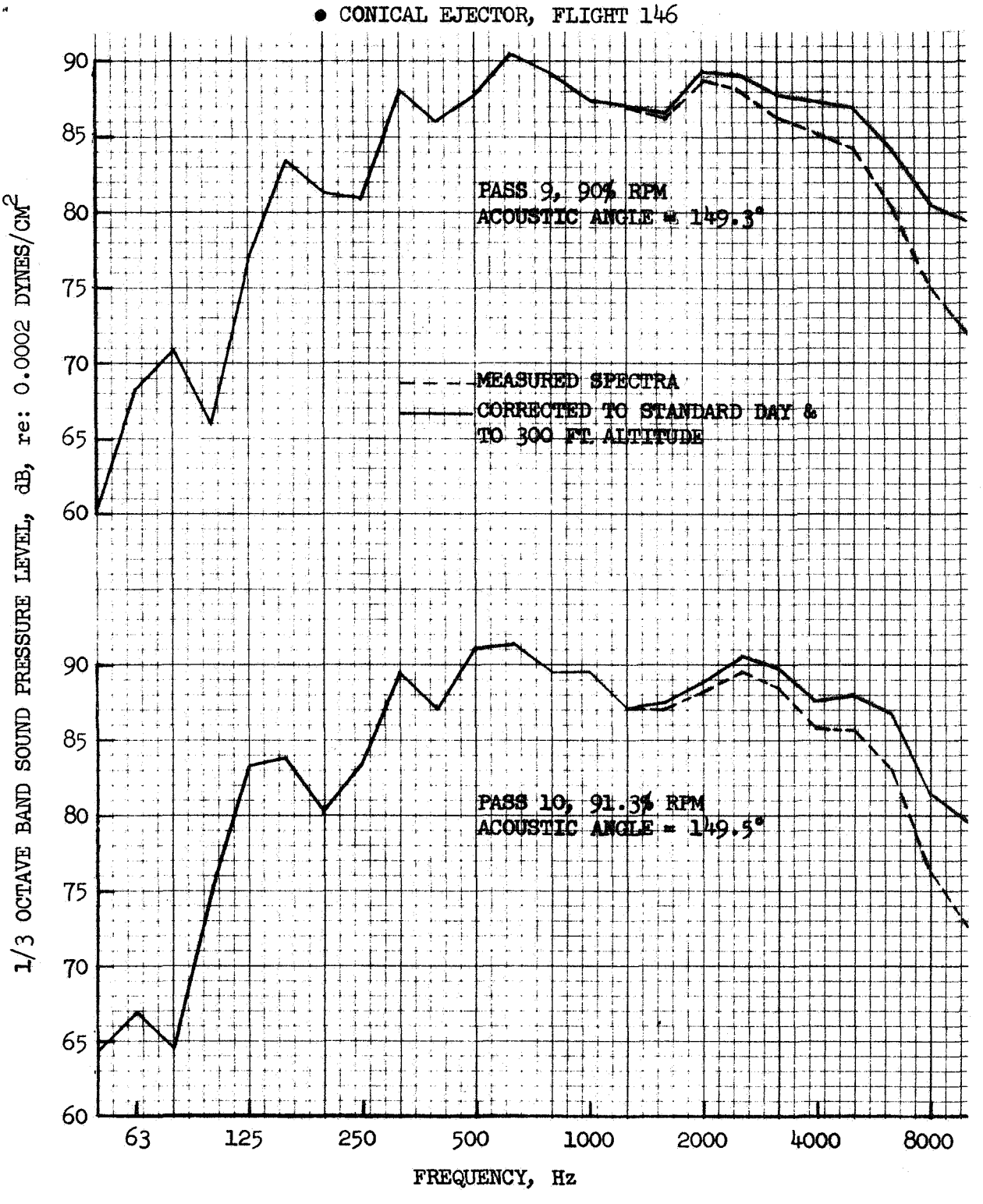

FIGURE 99 FLIGHT SPECTRA AT PEAK PNL, CONICAL EJECTOR, MIC UNDER FLIGHT PATH

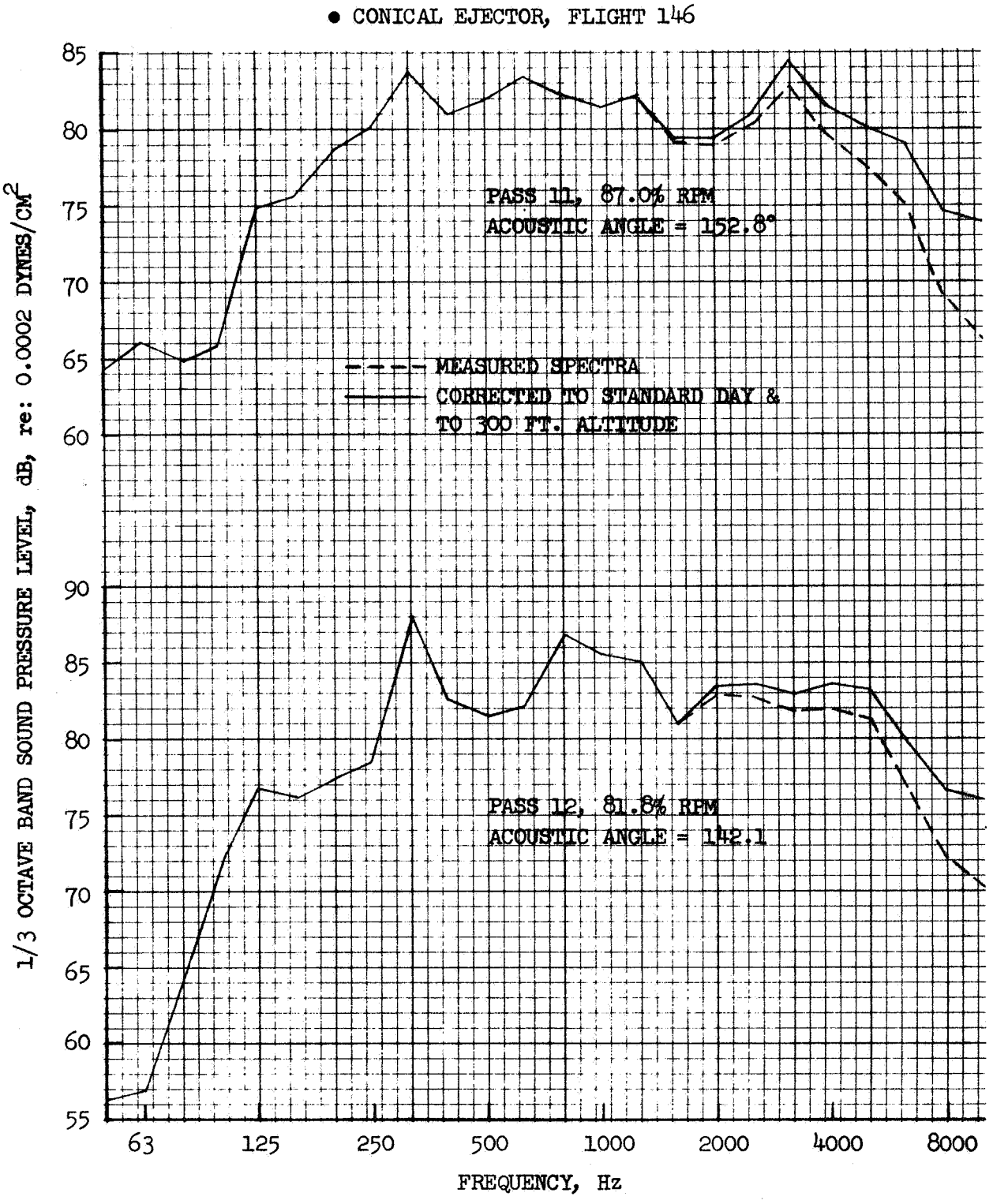

FIGURE 100 FLIGHT SPECTRA AT PEAK PNL, CONICAL EJECTOR, MIC UNDER FLIGHT PATH

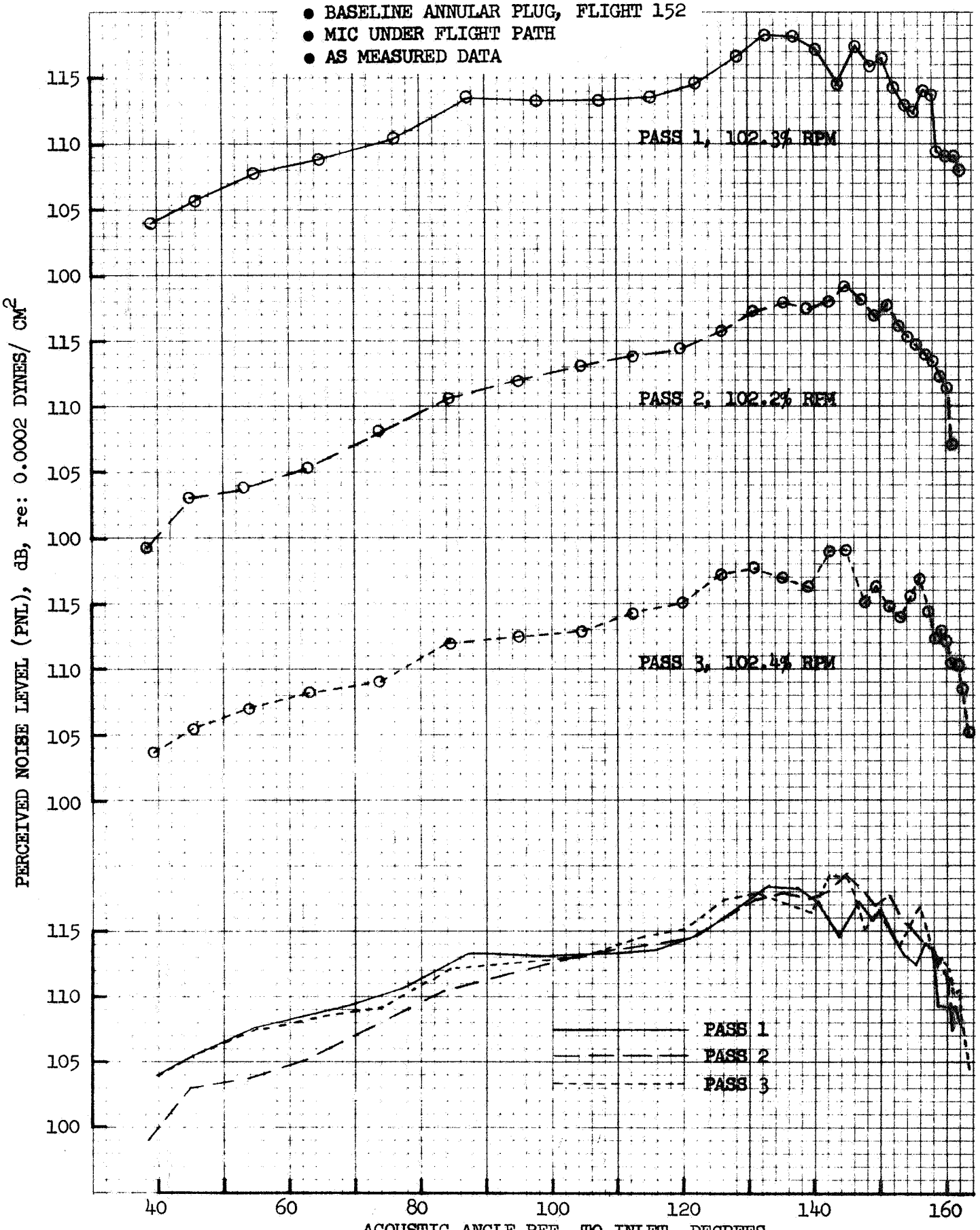

FIGURE 101 FLIGHT PNL, BASELINE ANNULAR PLUG, MIC UNDER FLIGHT PATH, AS MEASURED DATA

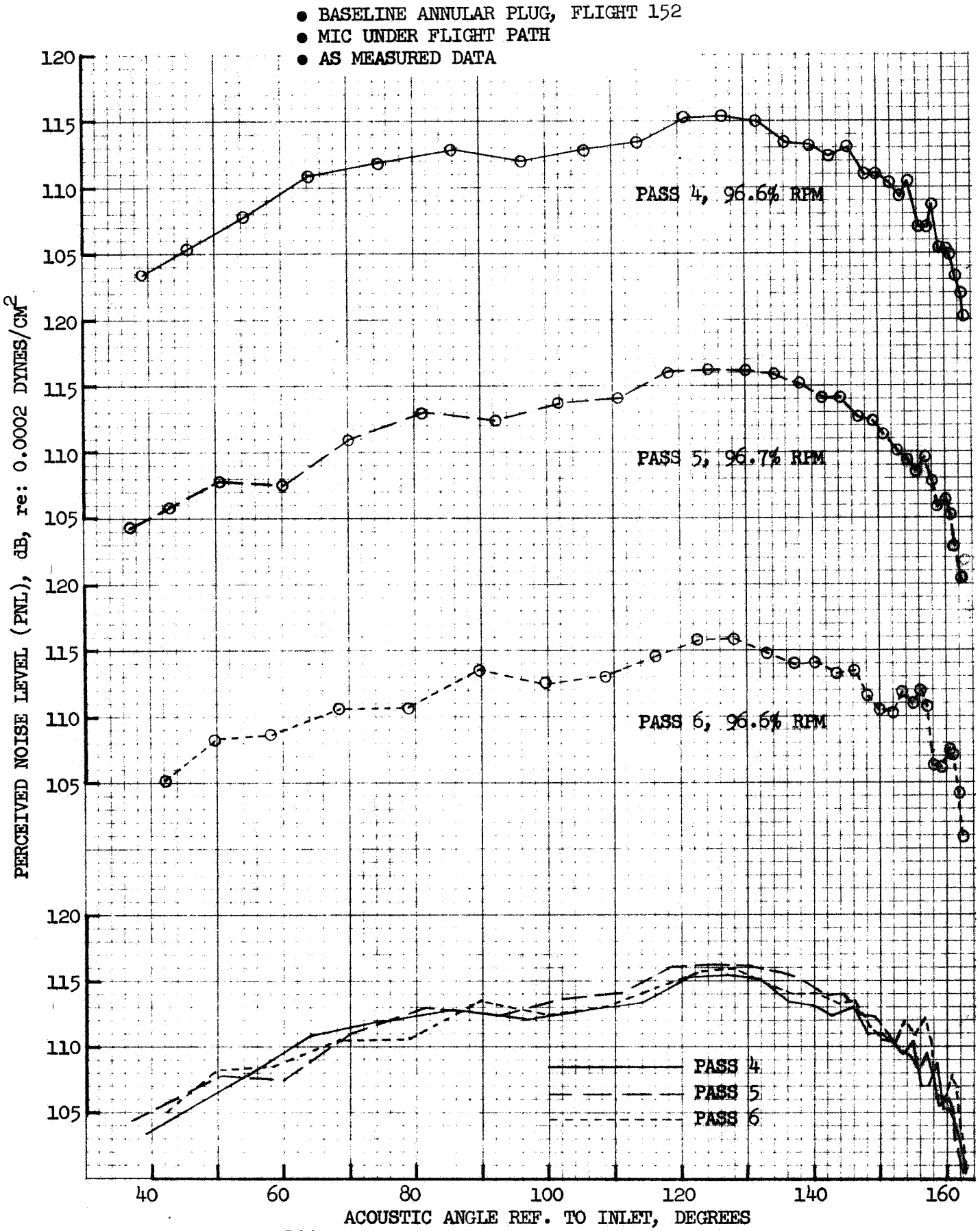

FIGURE 102 FLIGHT PNL, BASELINE ANNULAR PLUG, MIC UNDER FLIGHT PATH, AS MEASURED DATA

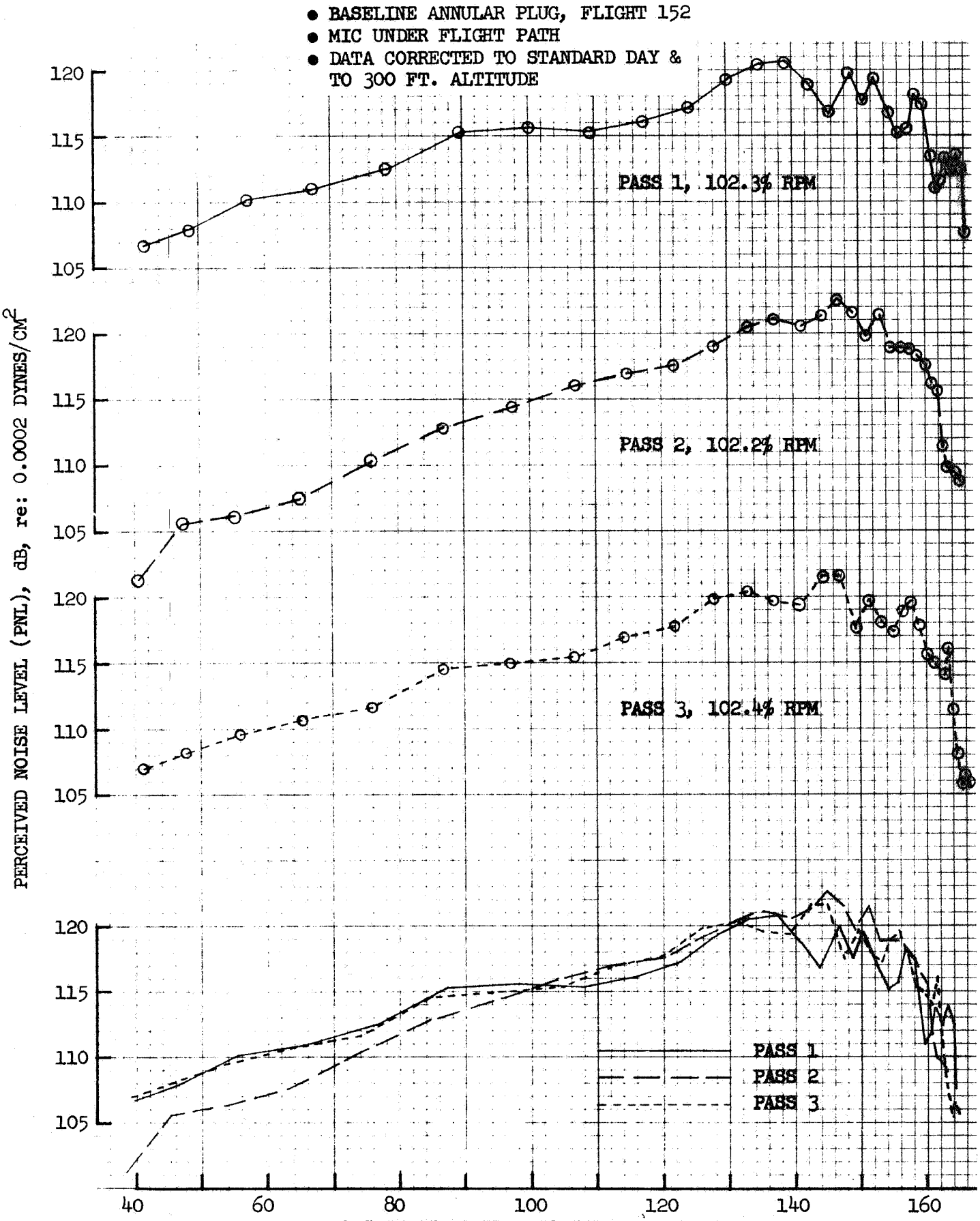

FIGURE 103 FLIGHT PNL, BASELINE ANNULAR PLUG, MIC UNDER FLIGHT PATH, CORRECTED DATA

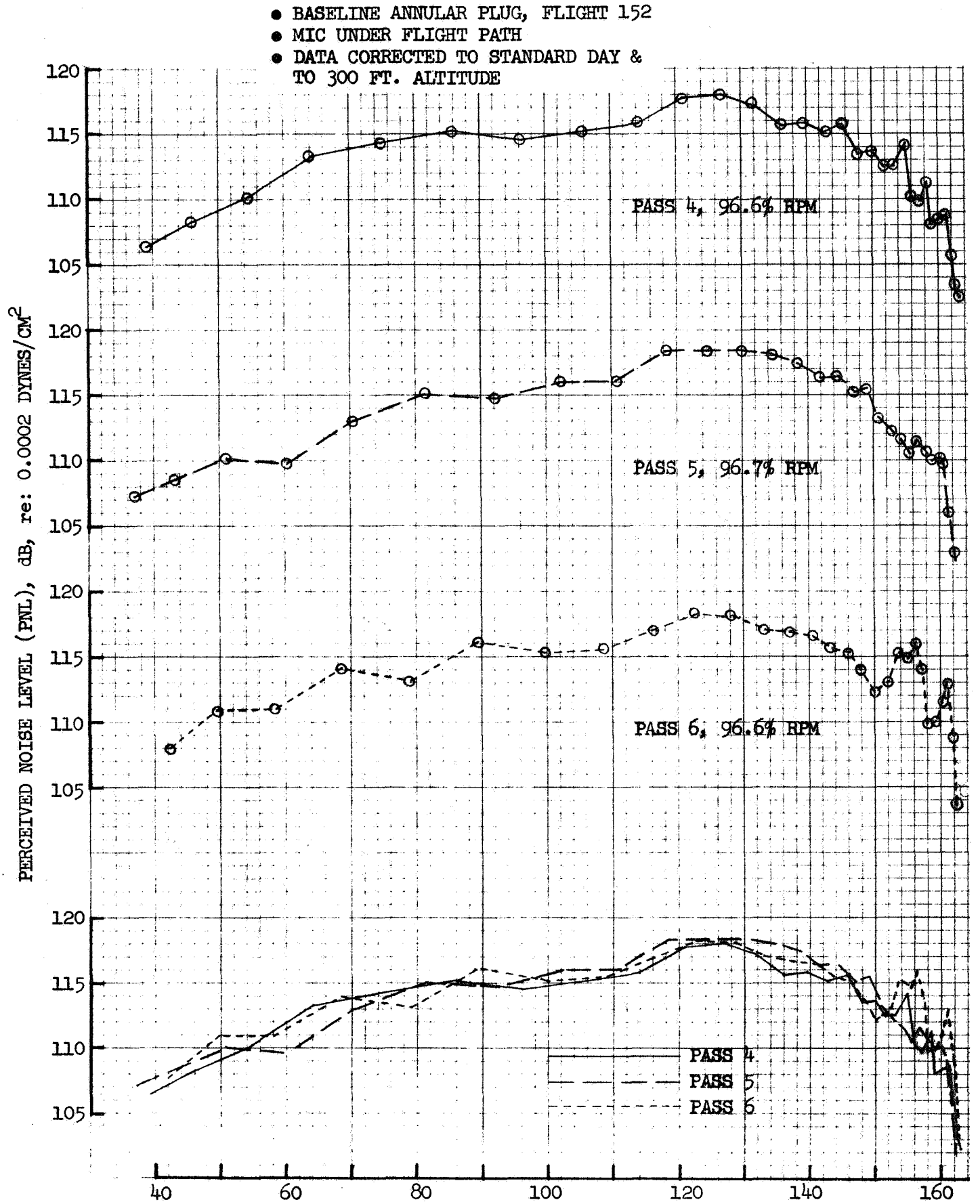

FIGURE 104 FLIGHT PNL, BASELINE ANNULAR PLUG, MIC UNDER FLIGHT PATH, CORRECTED DATA

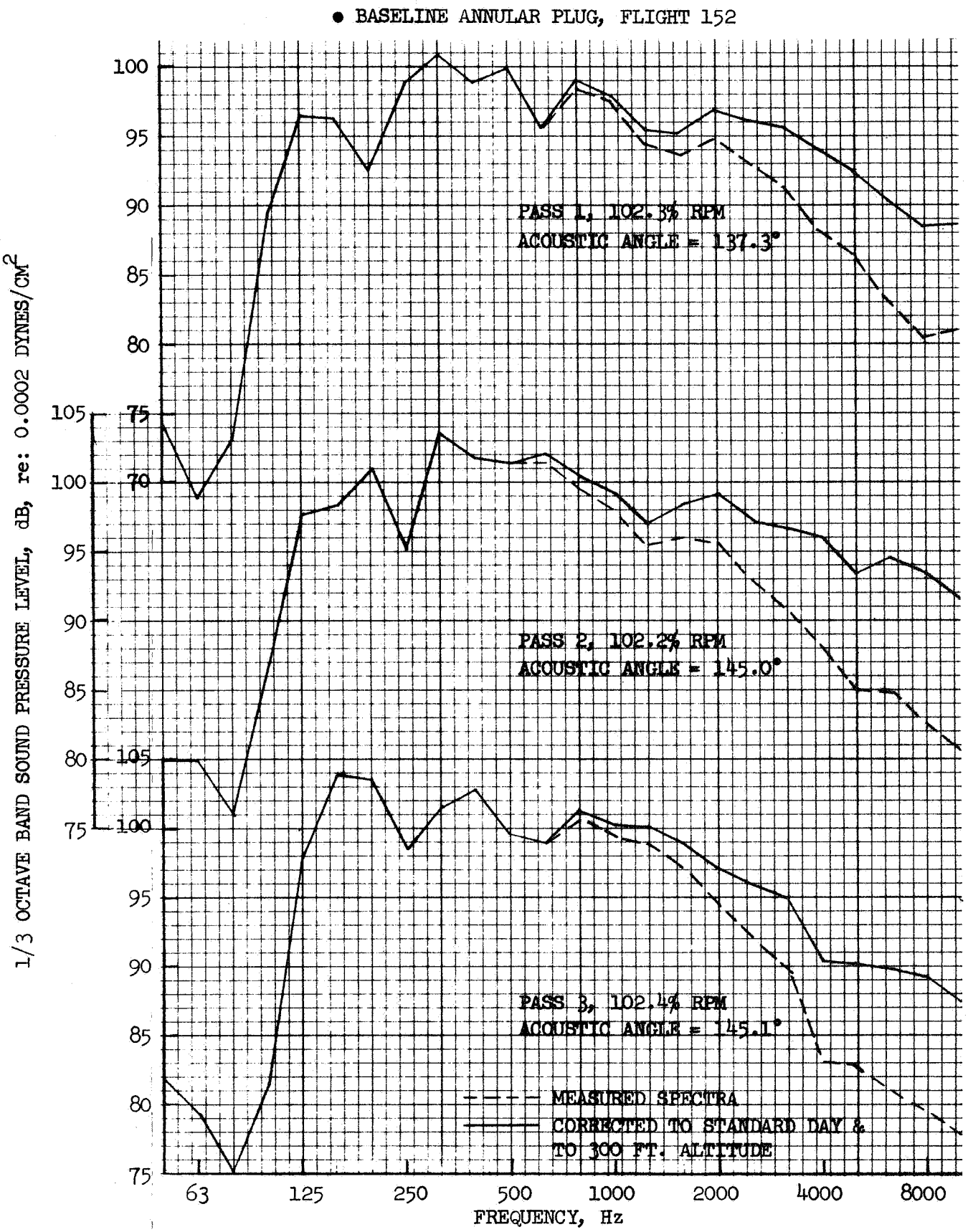

FIGURE 105 FLIGHT SPECTRA AT PEAK PNL, BASELINE ANNULAR PLUG, MIC UNDER FLIGHT PATH

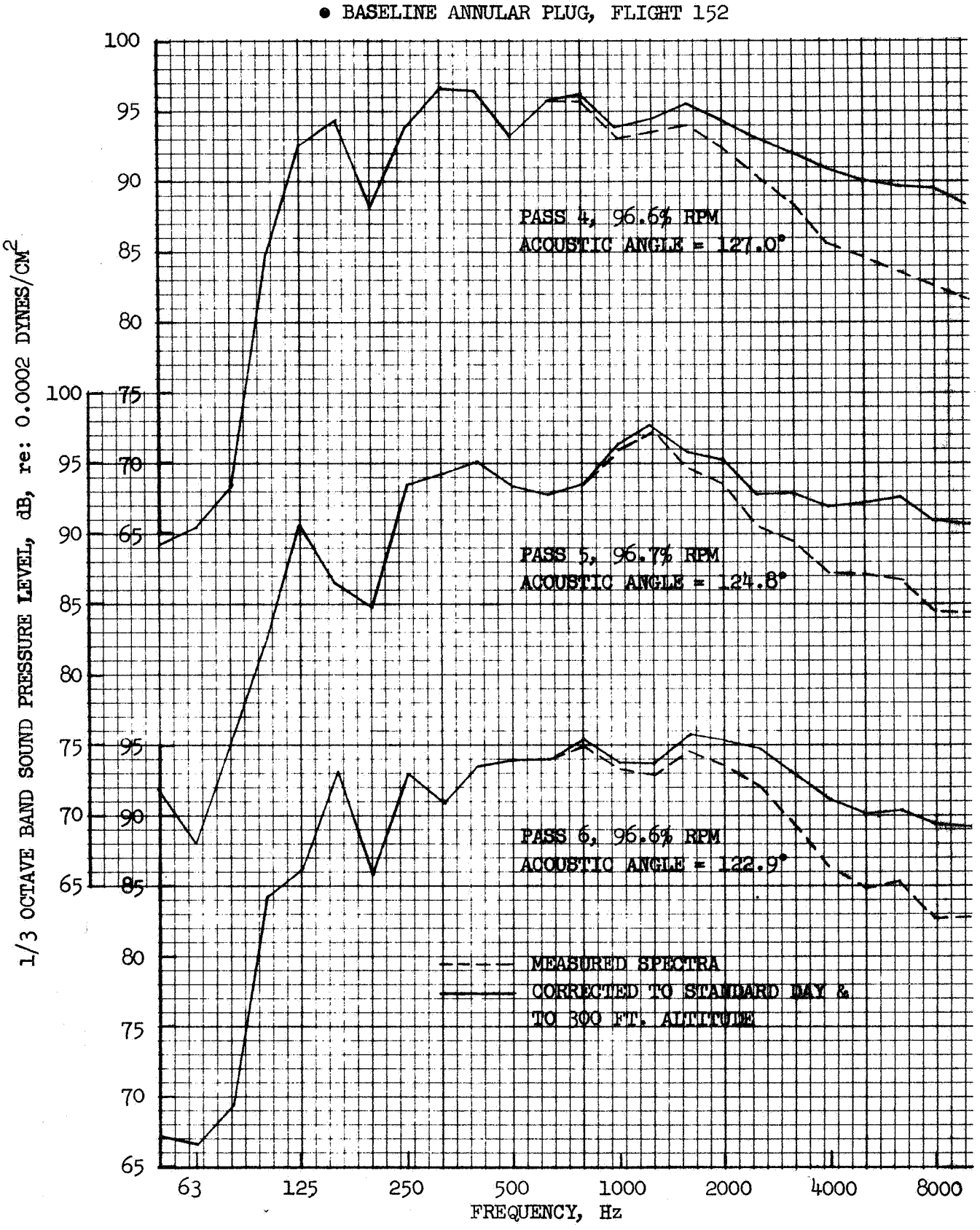

FIGURE 106 FLIGHT SPECTRA AT PEAK PNL, BASELINE ANNULAR PLUG, MIC UNDER FLIGHT PATH

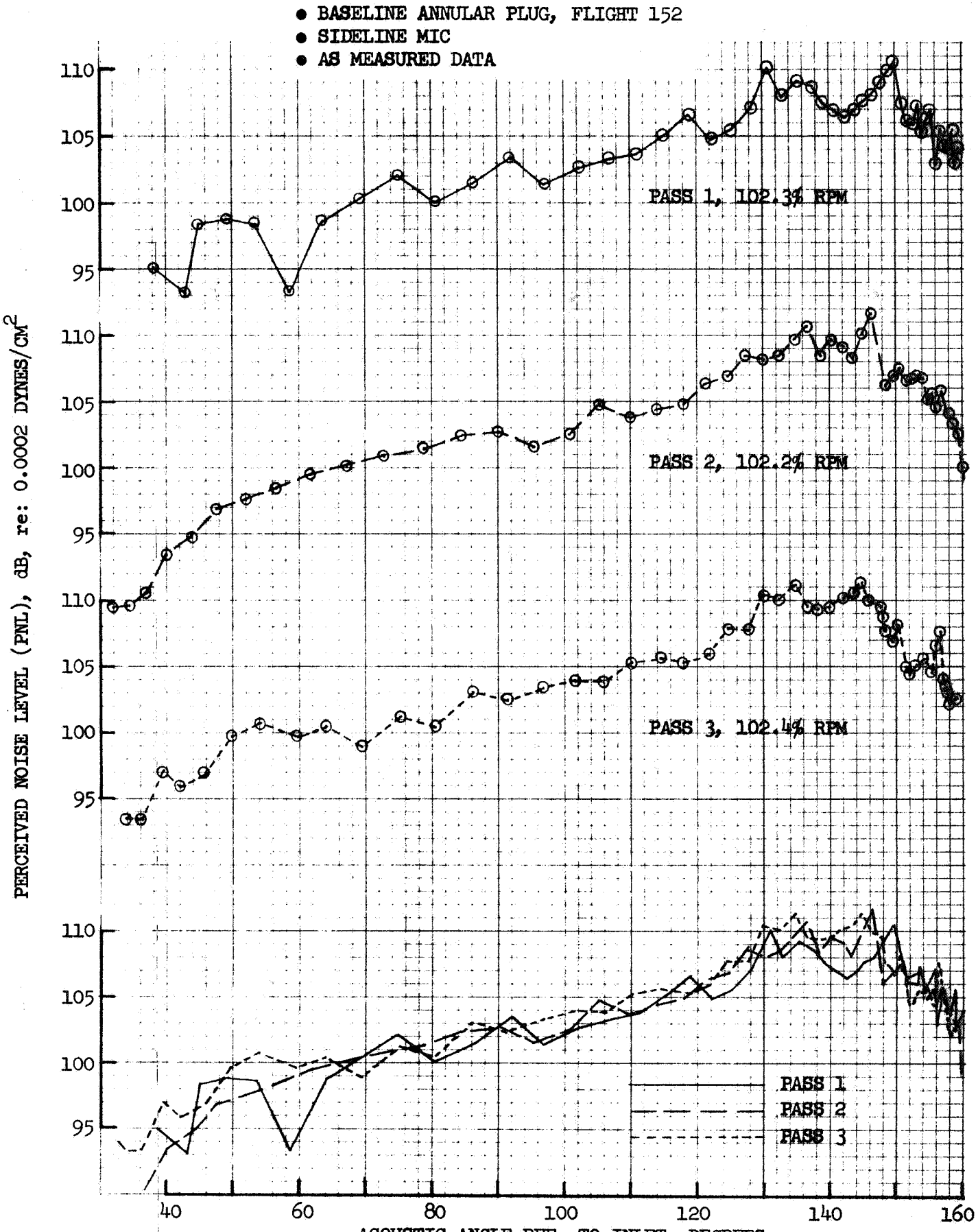

FIGURE 107 FLIGHT PNL, BASELINE ANNULAR PLUG, SIDELINE MIC, AS MEASURED DATA

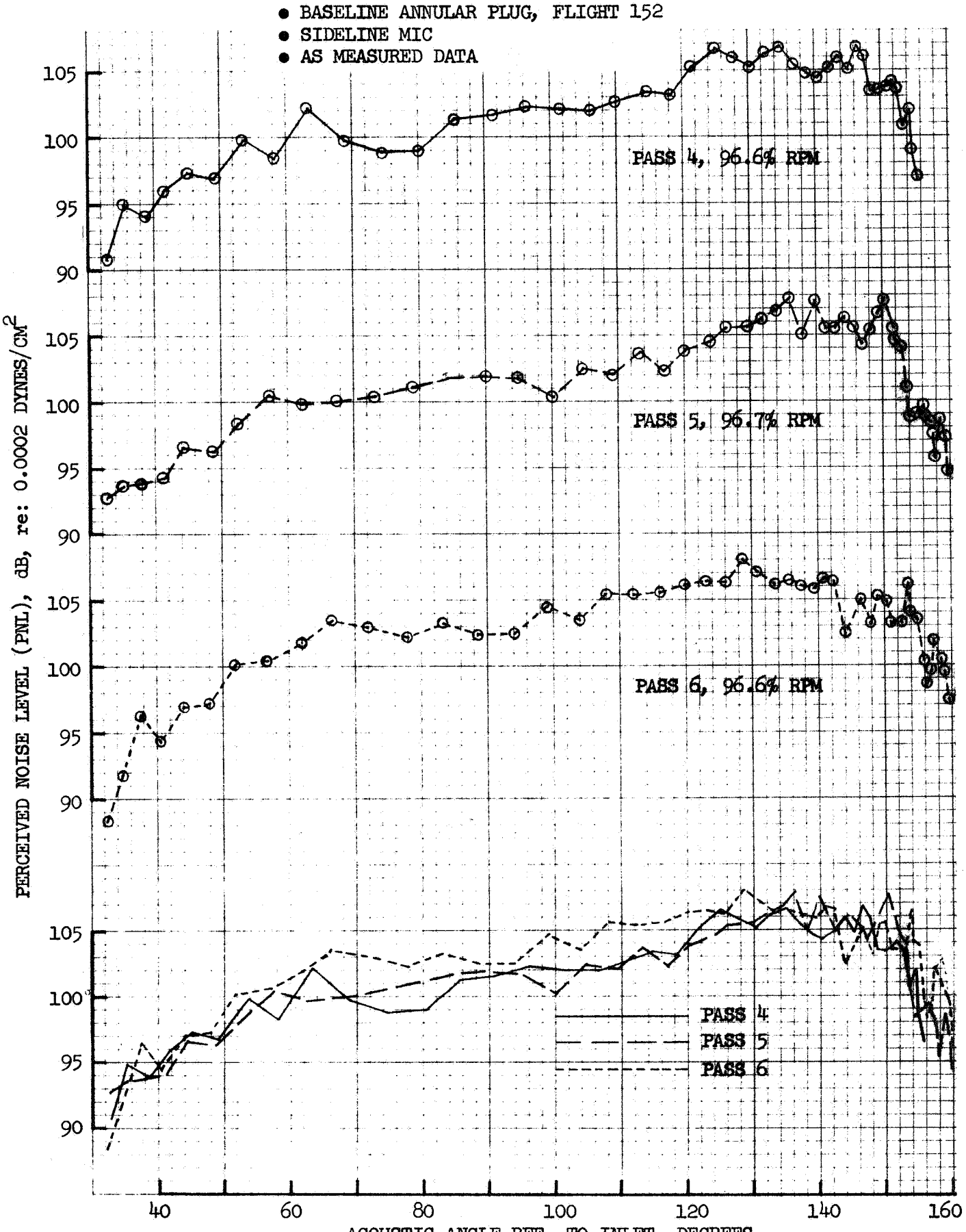

FIGURE 108 FLIGHT PNL, BASELINE ANNULAR PLUG, SIDELINE MIC, AS MEASURED DATA

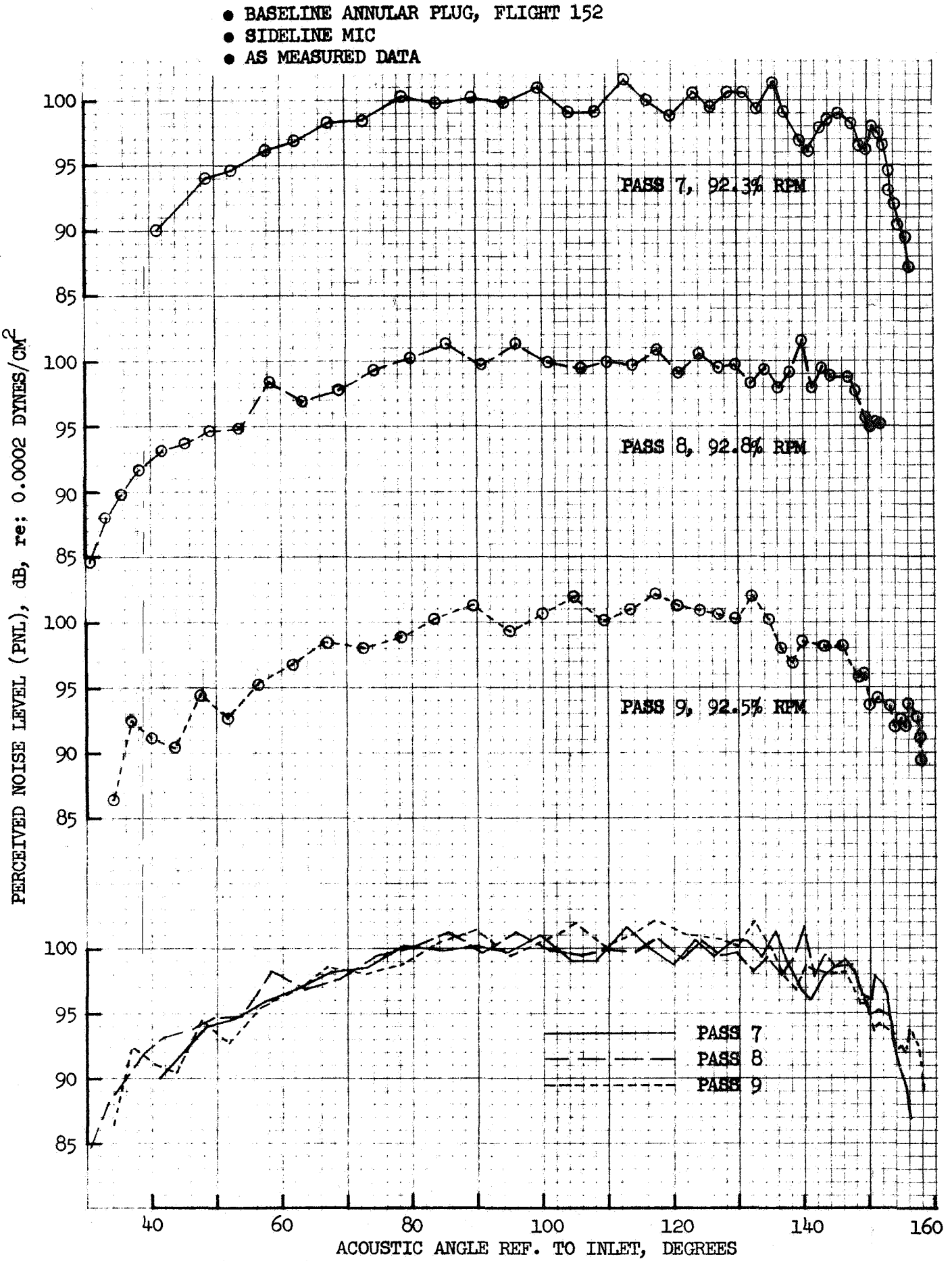

FIGURE 109 FLIGHT PNL, BASELINE ANNULAR PLUG, SIDELINE MIC, AS MEASURED DATA

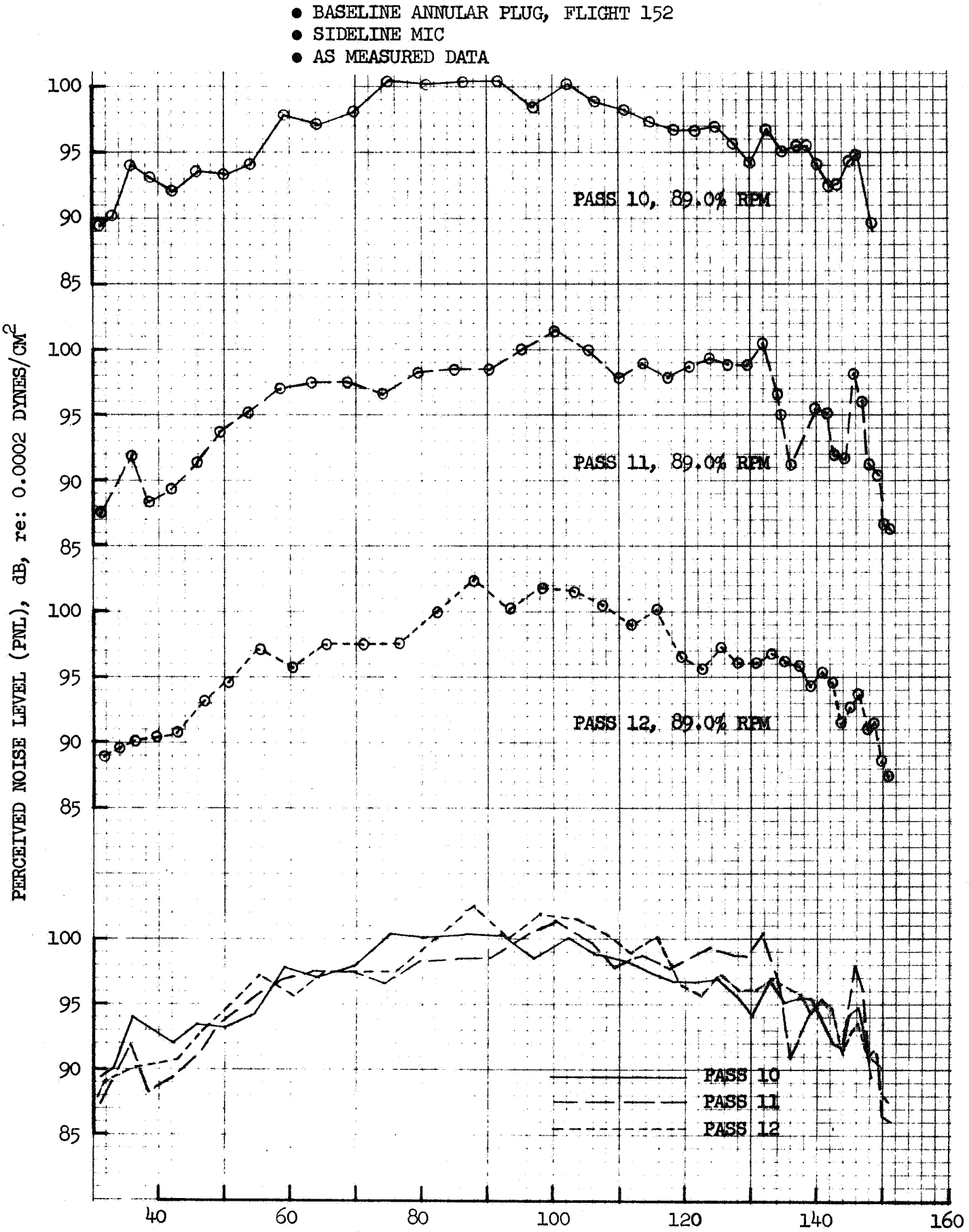

FIGURE 110 FLIGHT PNL, BASELINE ANNULAR PLUG, SIDELINE MIC, AS MEASURED DATA

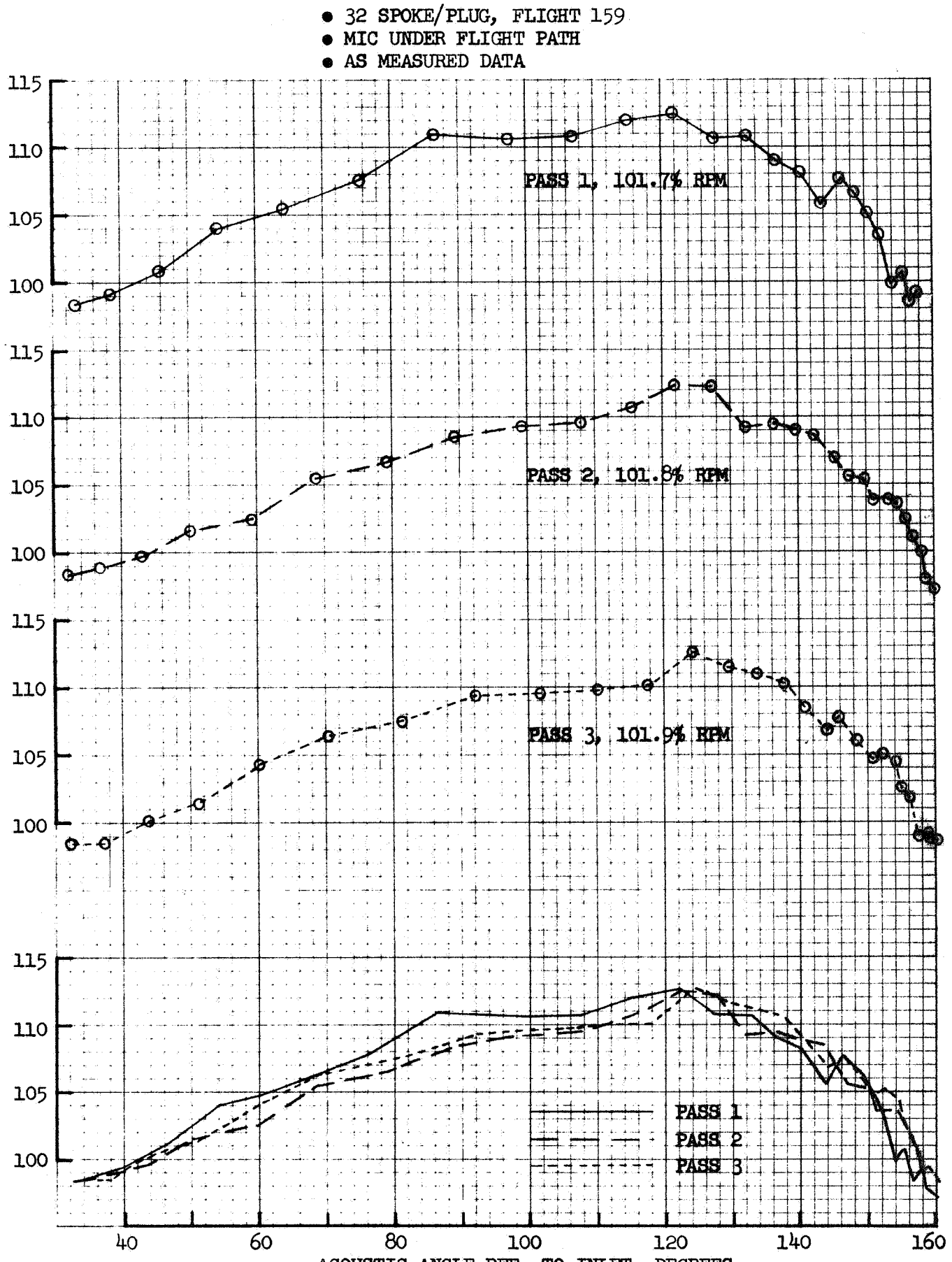

FIGURE 111 FLIGHT PNL, 32 SPOKE/PLUG, MIC UNDER FLIGHT PATH, AS MEASURED DATA

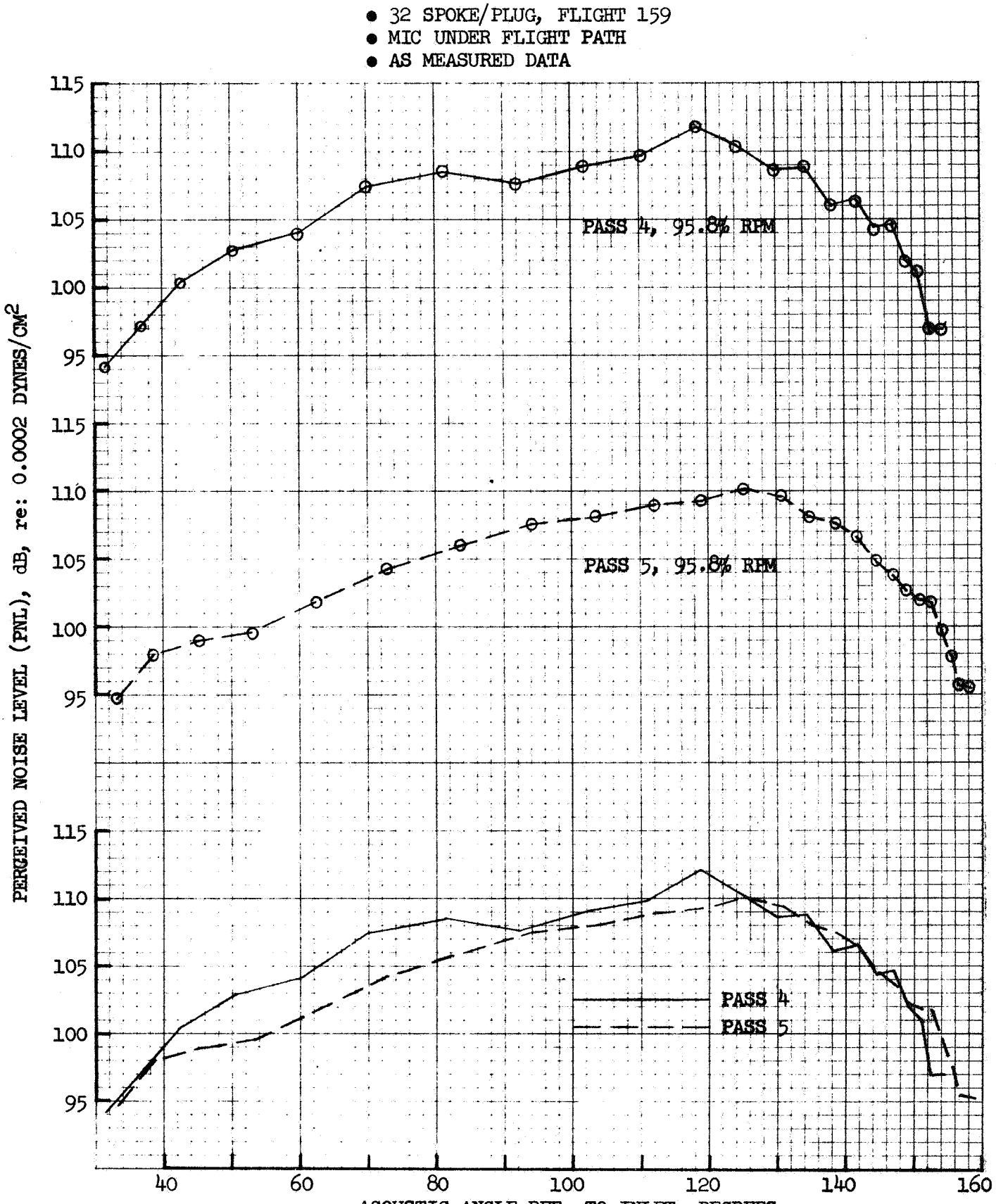

FIGURE 112 FLIGHT PNL, 32 SPOKE/PLUG, MIC UNDER FLIGHT PATH AS MEASURED DATA

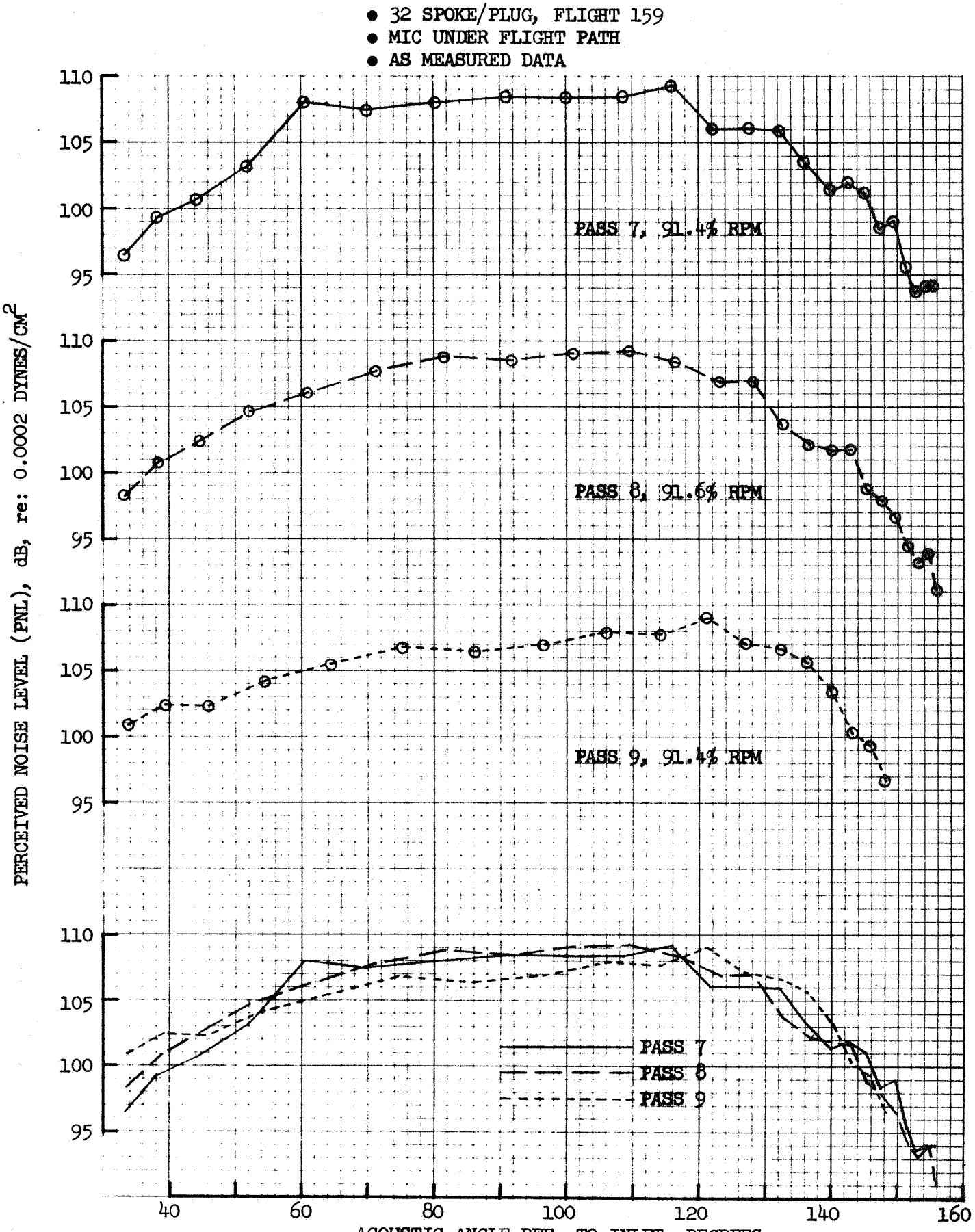

FIGURE 113 FLIGHT PNL, 32 SPOKE/PLUG, MIC UNDER FLIGHT PATH, AS MEASURED DATA

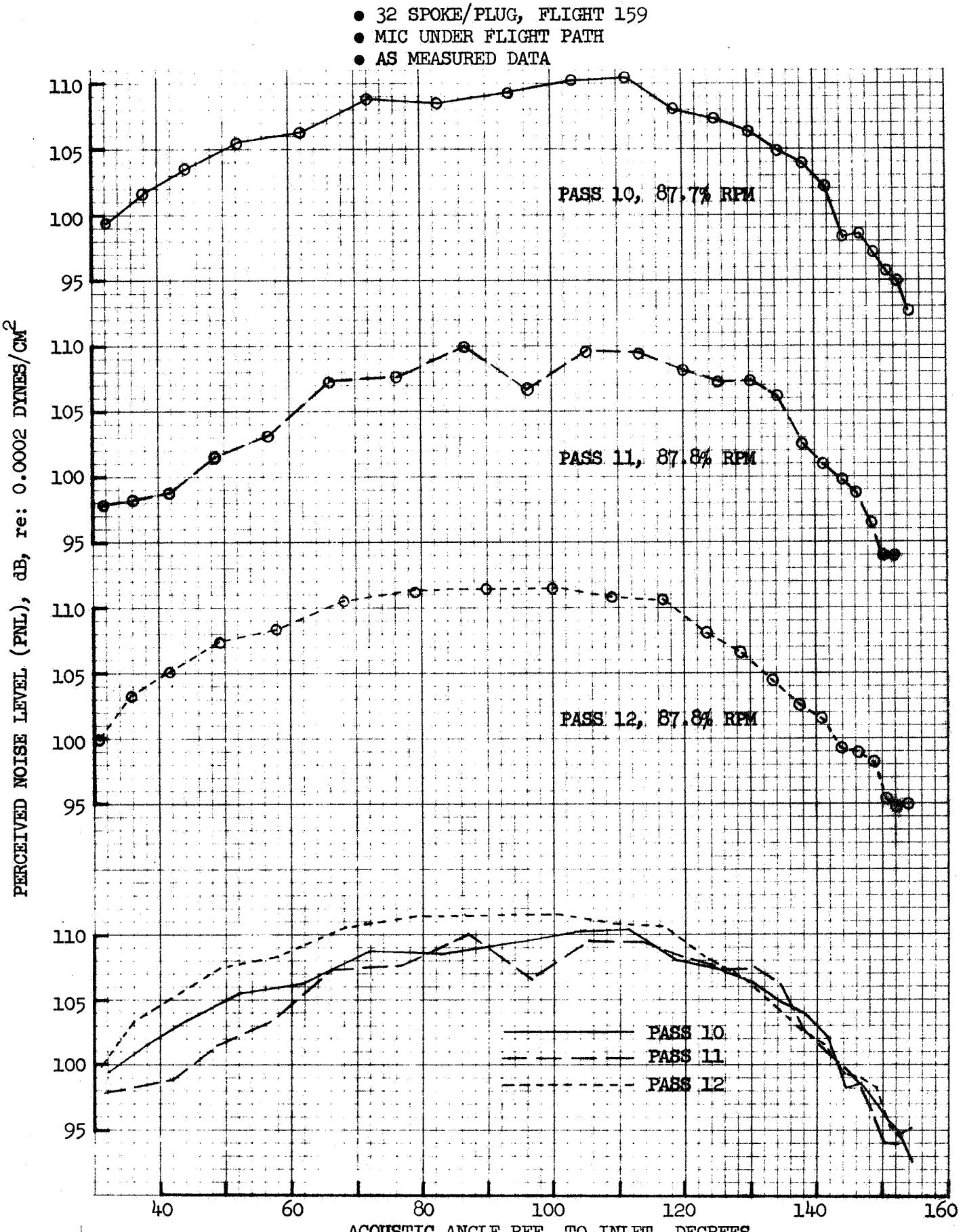

FIGURE 114 FLIGHT PNL, 32 SPOKE/PLUG, MIC UNDER FLIGHT PATH, AS MEASURED DATA

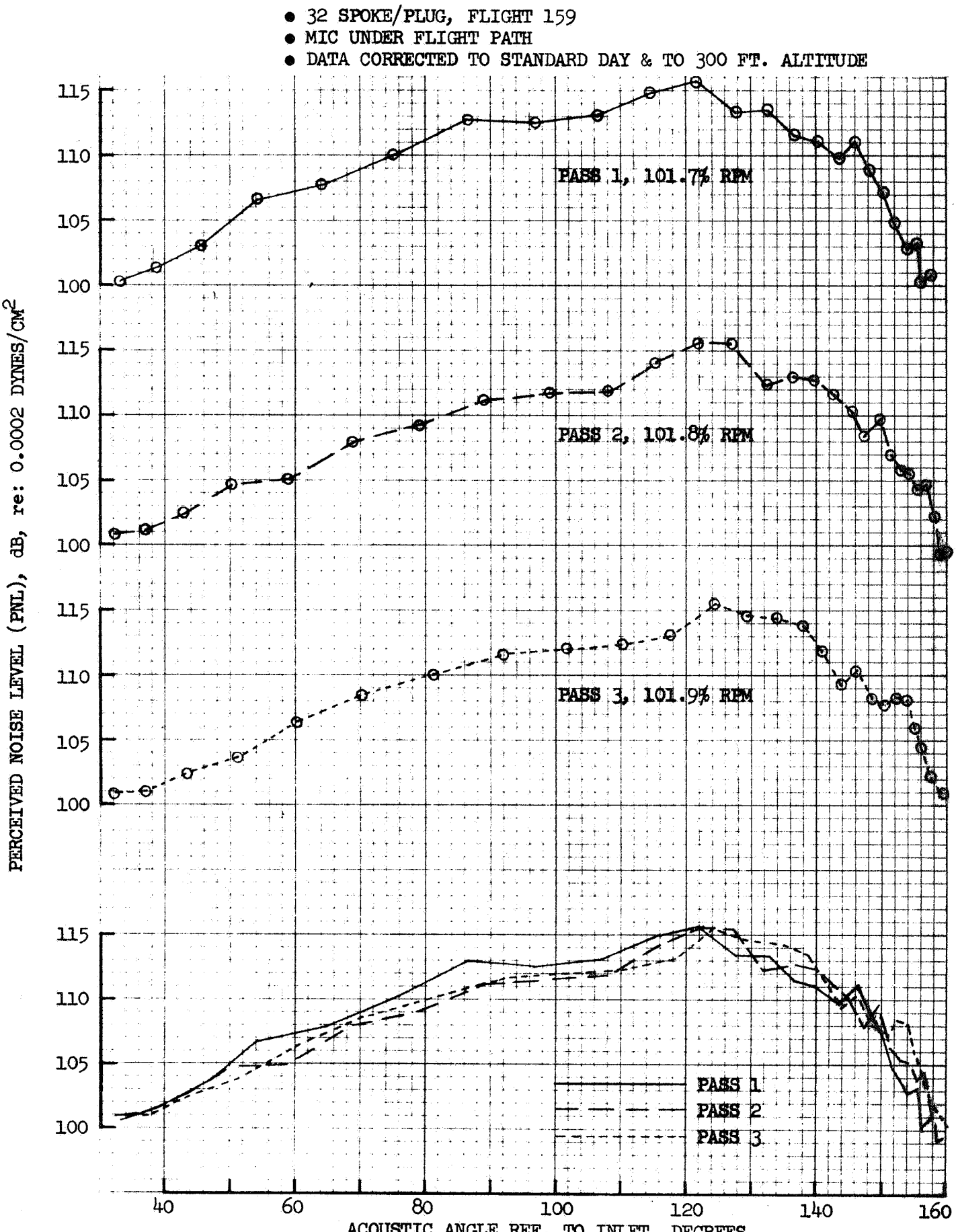

FIGURE 115 FLIGHT PNL, 32 SPOKE/PLUG, MIC UNDER FLIGHT PATH, CORRECTED DATA

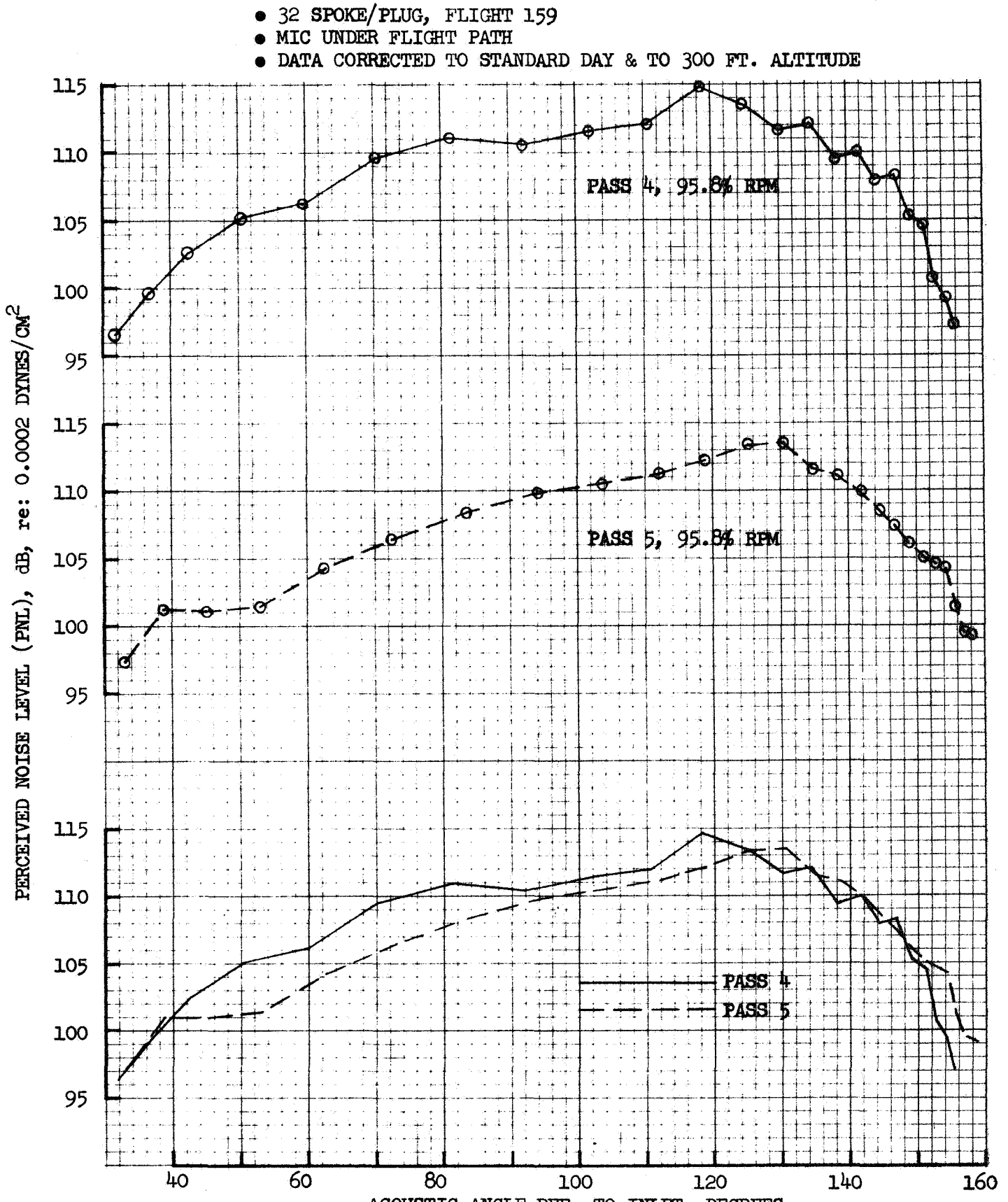

FIGURE 116 FLIGHT PNL, 32 SPOKE/PLUG, MIC UNDER FLIGHT PATH CORRECTED DATA

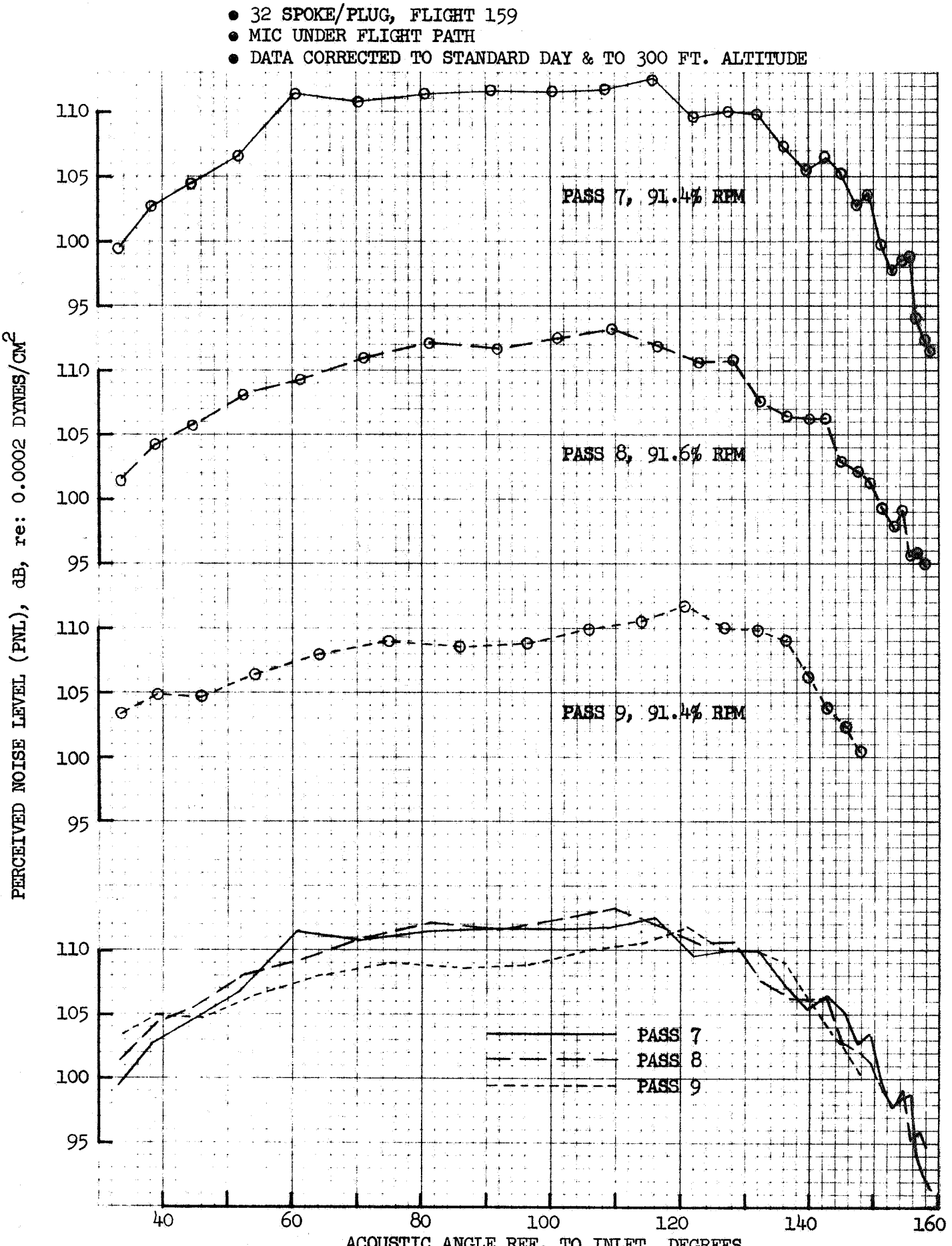

FIGURE 117 FLIGHT PNL, 32 SPOKE/PLUG, MIC UNDER FLIGHT PATH, CORRECTED DATA

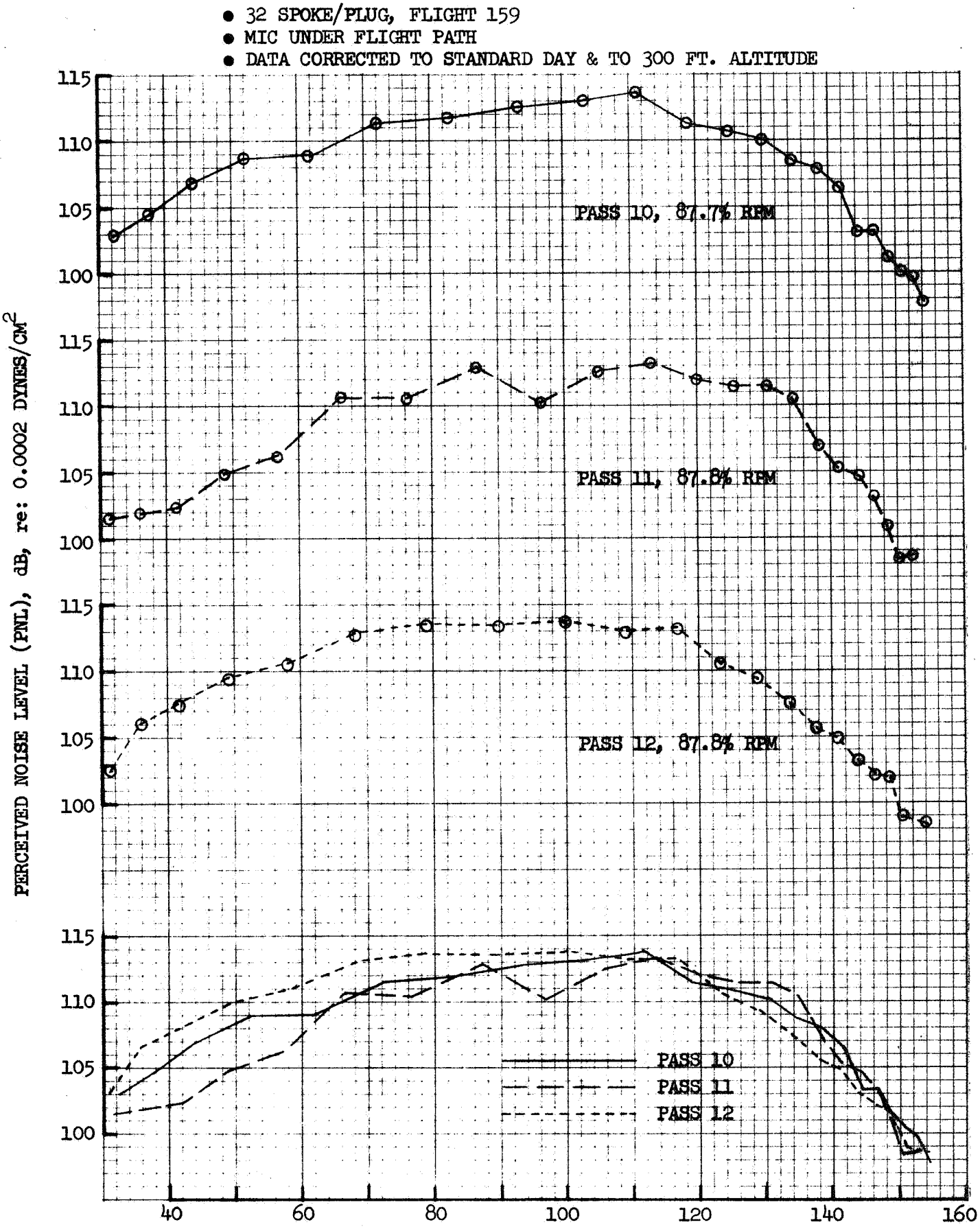

FIGURE 118 FLIGHT PNL, 32 SPOKE/PLUG, MIC UNDER FLIGHT PATH, CORRECTED DATA

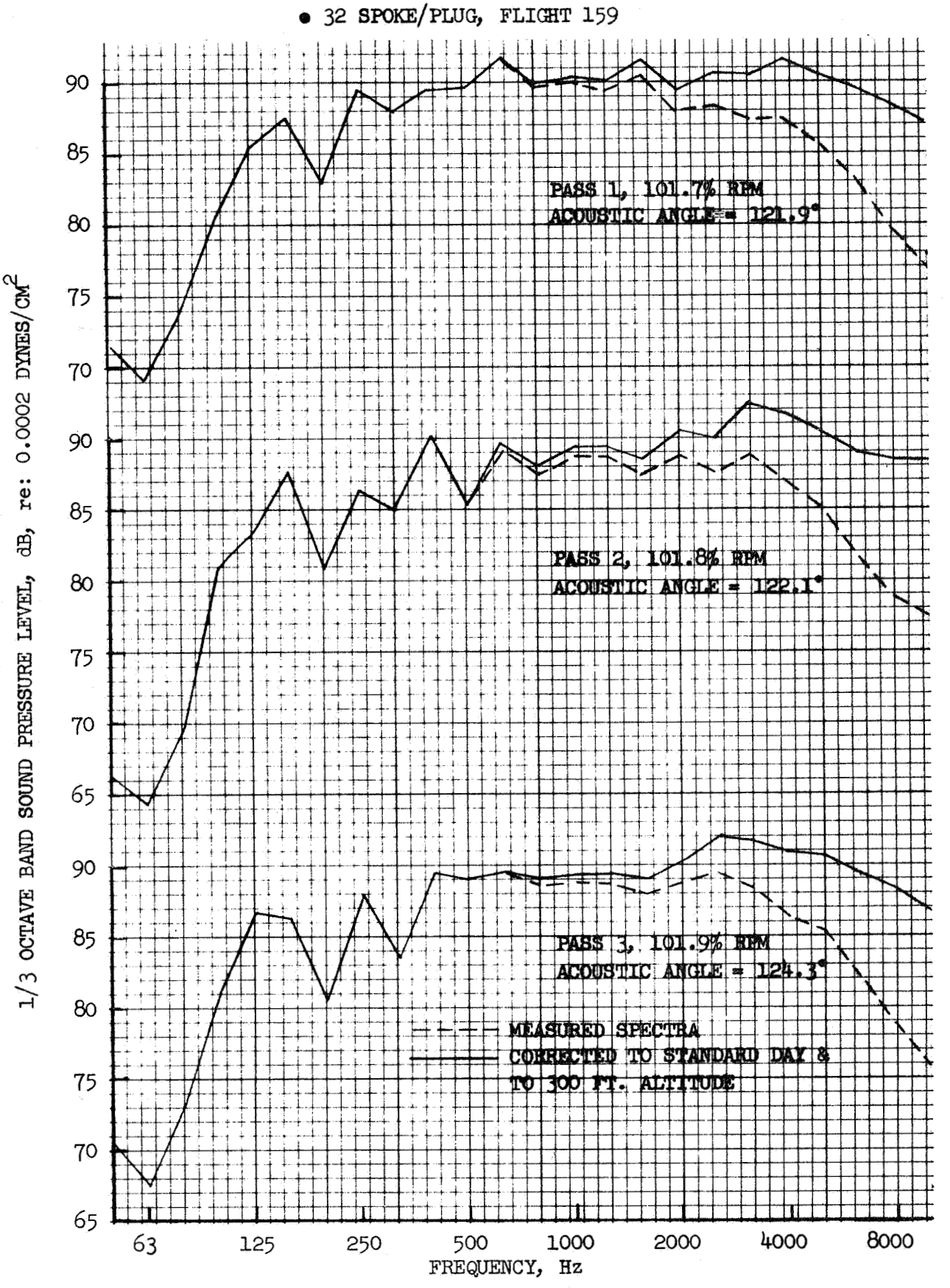

FIGURE 119 FLIGHT SPECTRA AT PEAK PNL, 32 SPOKE/PLUG, MIC UNDER FLIGHT PATH

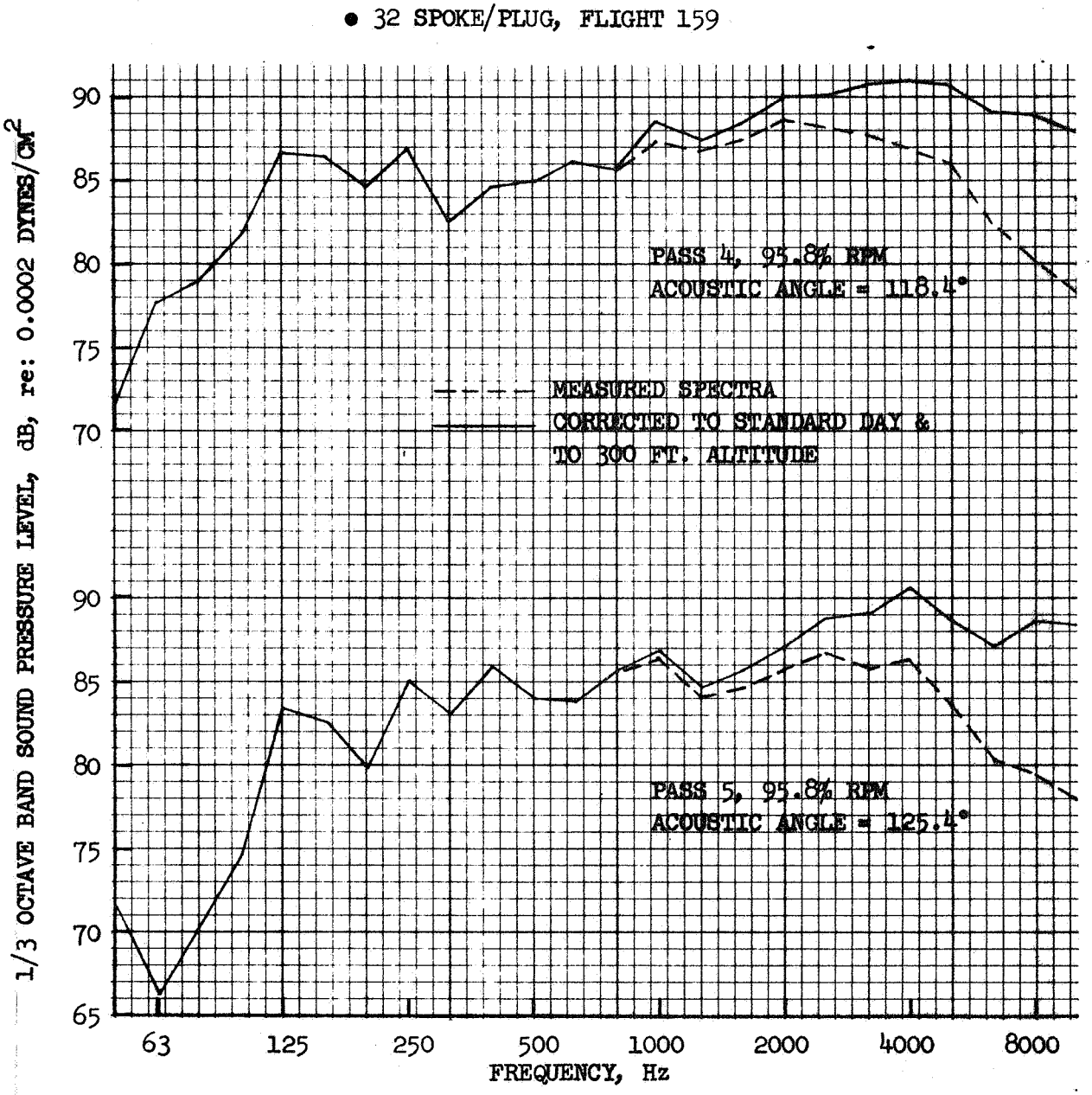

FIGURE 120 FLIGHT SPECTRA AT PEAK PNL, 32 SPOKE/PLUG, MIC UNDER FLIGHT PATH

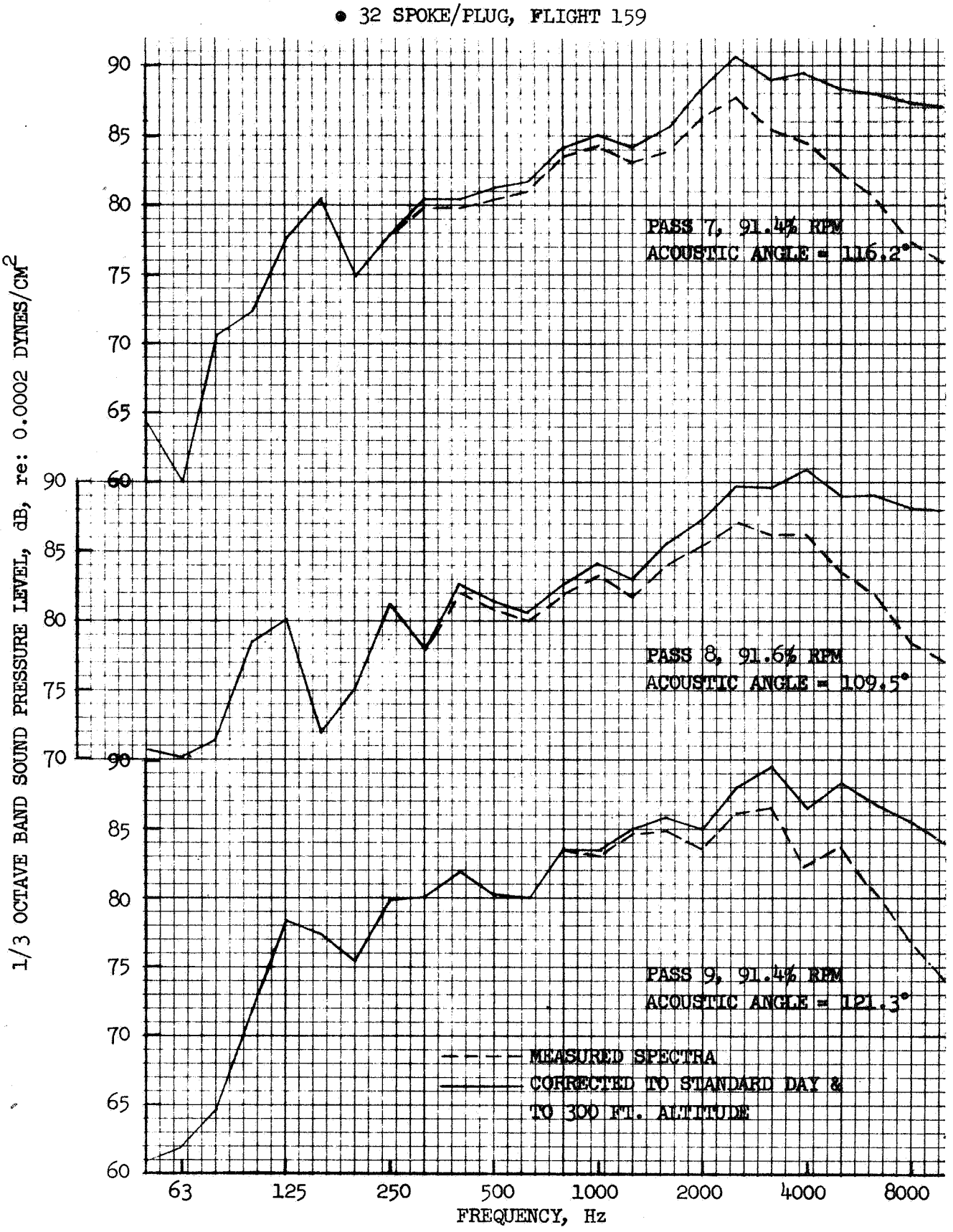

FIGURE 121 FLIGHT SPECTRA AT PEAK PNL, 32 SPOKE/PLUG, MIC UNDER FLIGHT PATH

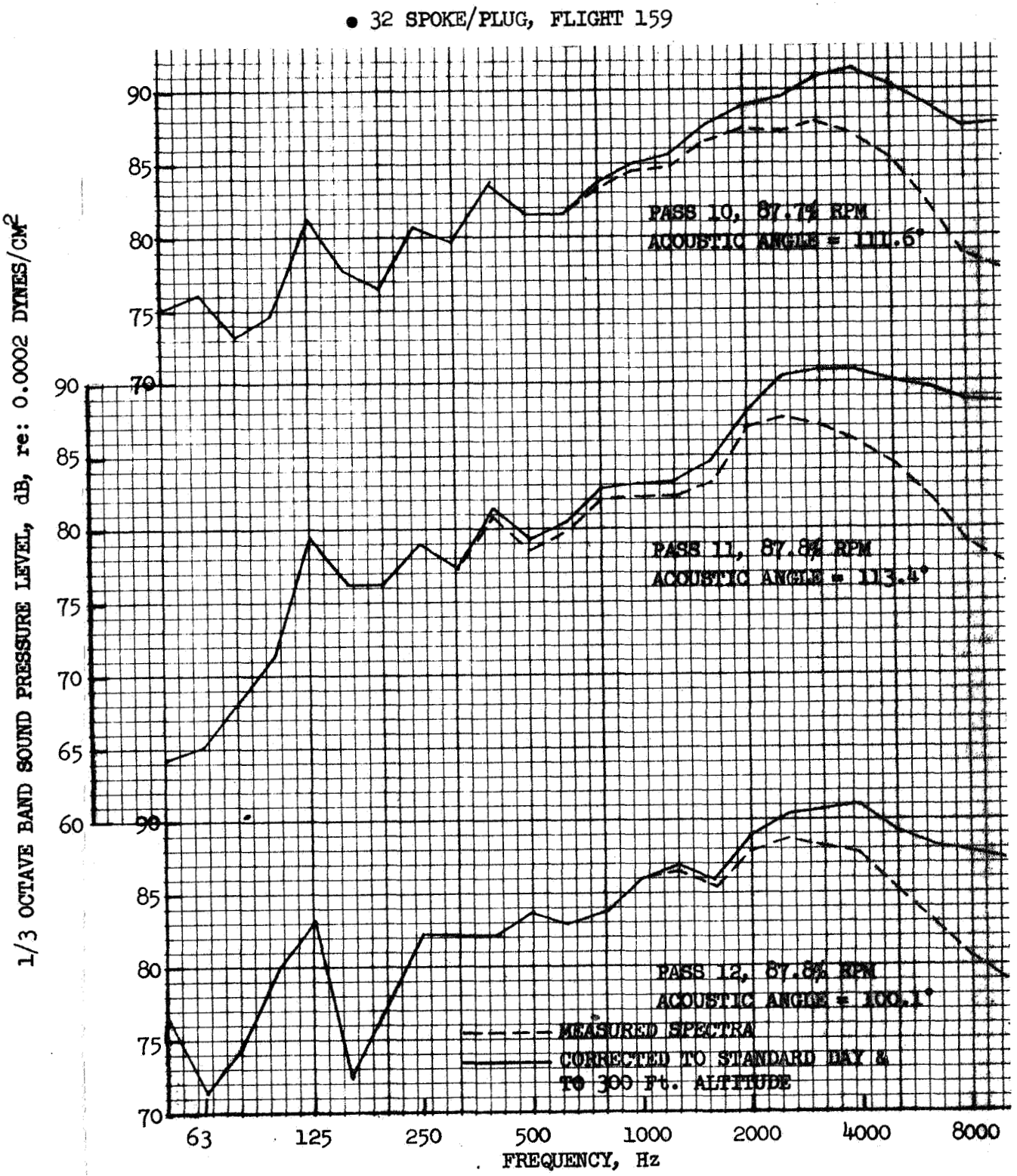

FIGURE 122 FLIGHT SPECTRA AT PEAK PNL, 32 SPOKE/PLUG, MIC UNDER FLIGHT PATH

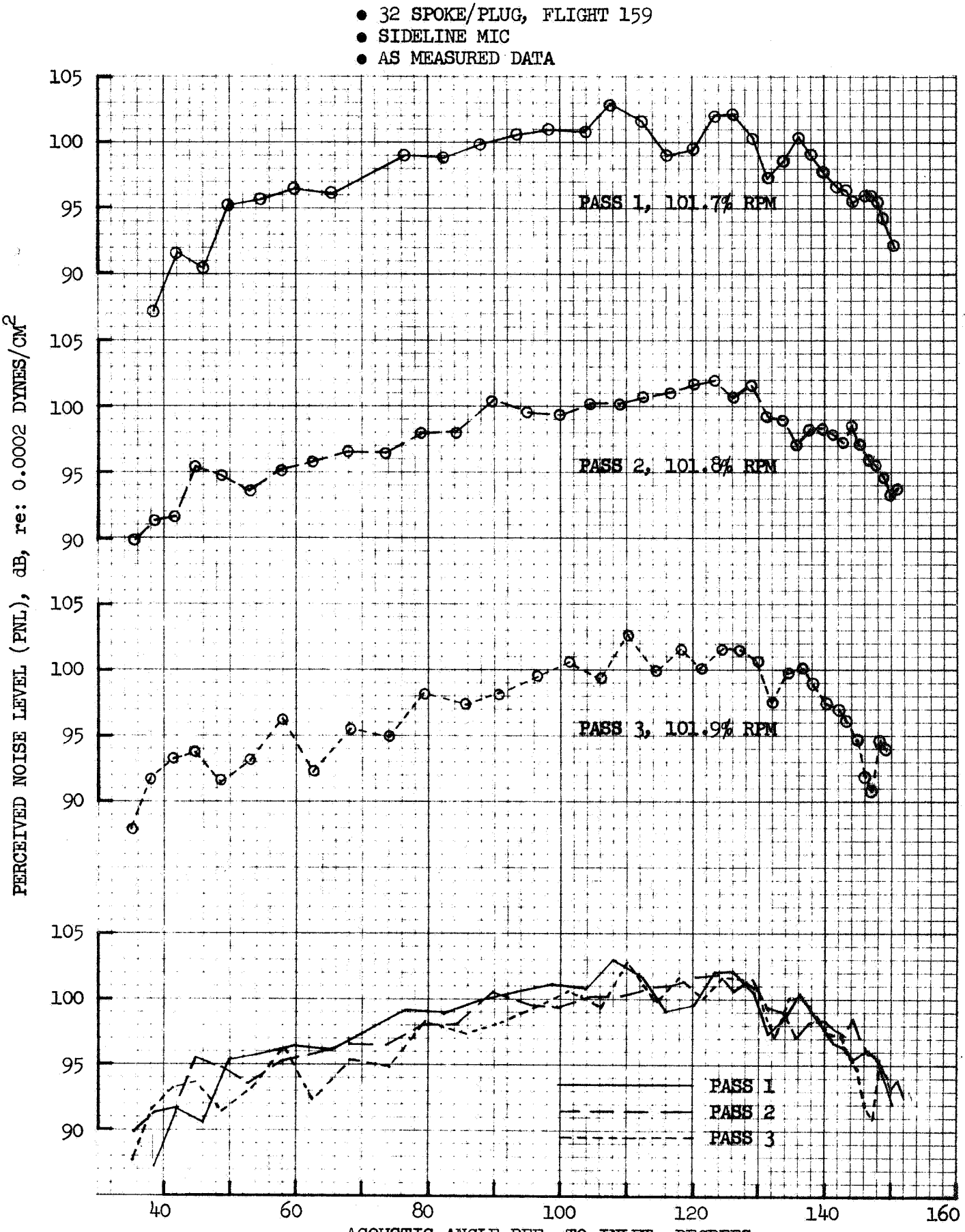

FIGURE 123 FLIGHT PNL, 32 SPOKE/PLUG, SIDELINE MIC, AS MEASURED DATA

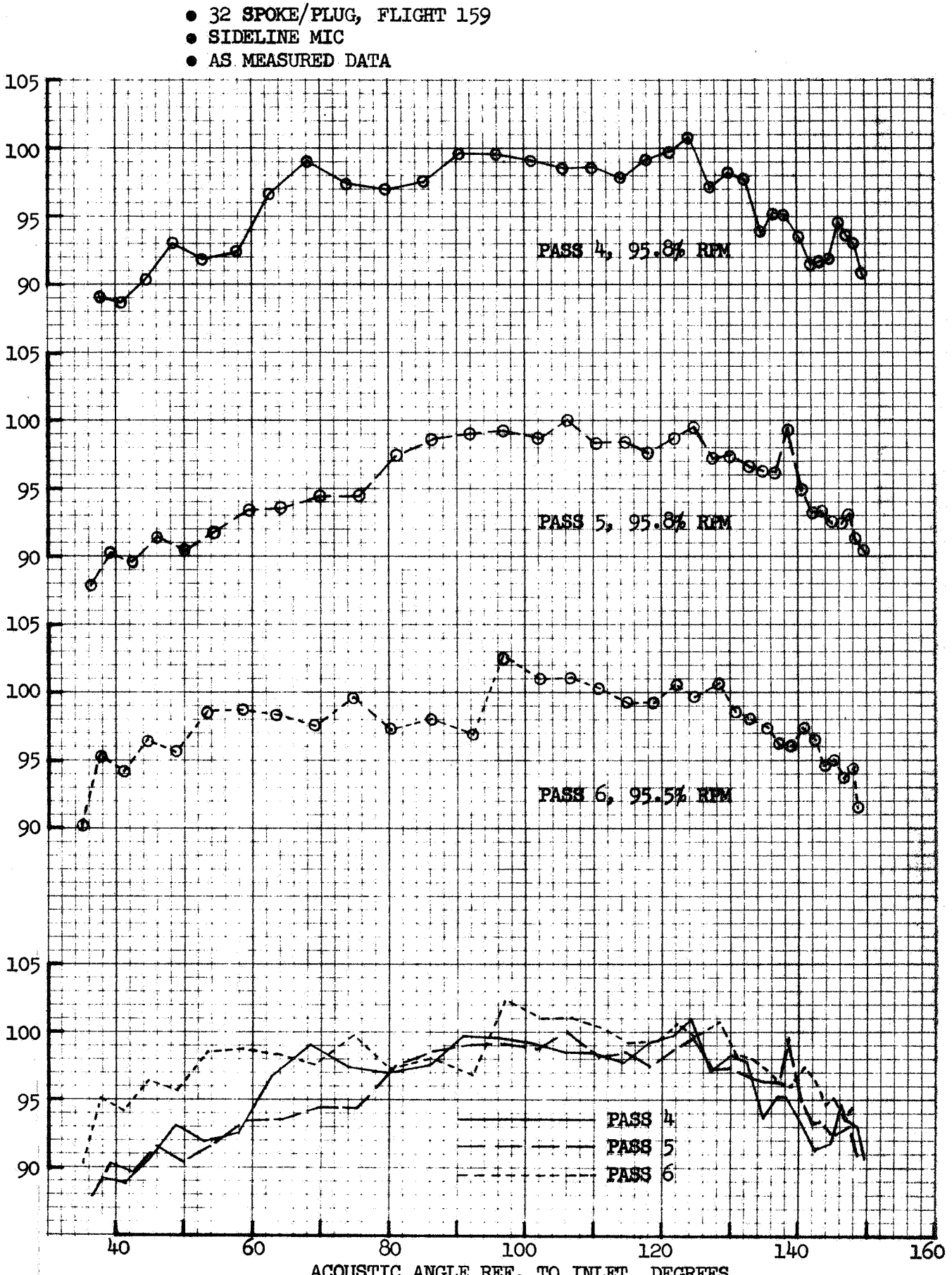

FIGURE 124 FLIGHT PNL, 32 SPOKE/PLUG, SIDELINE MIC, AS MEASURED DATA

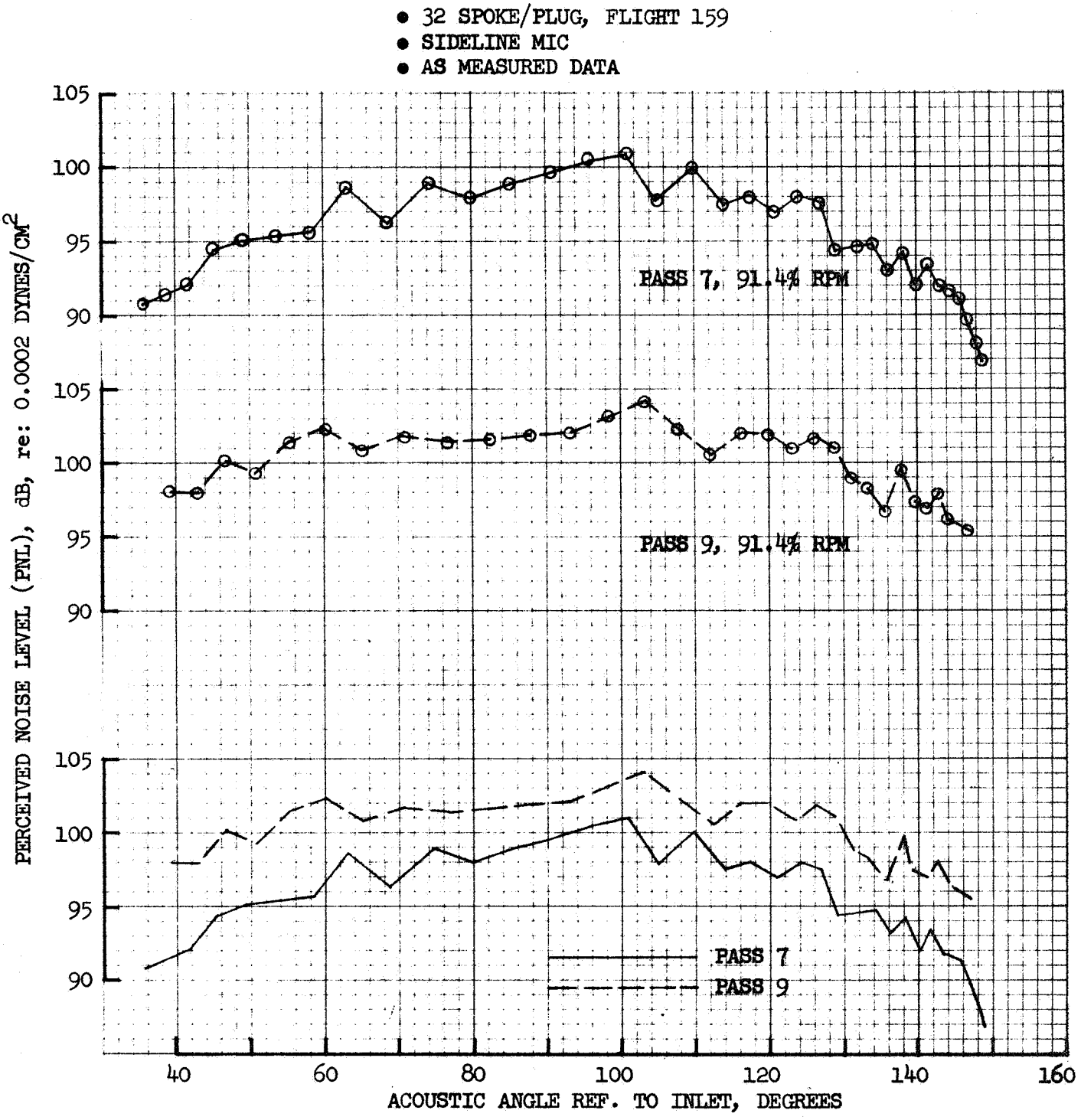

FIGURE 125 FLIGHT PNL, 32 SPOKE/PLUG, SIDELINE MIC, AS MEASURED DATA

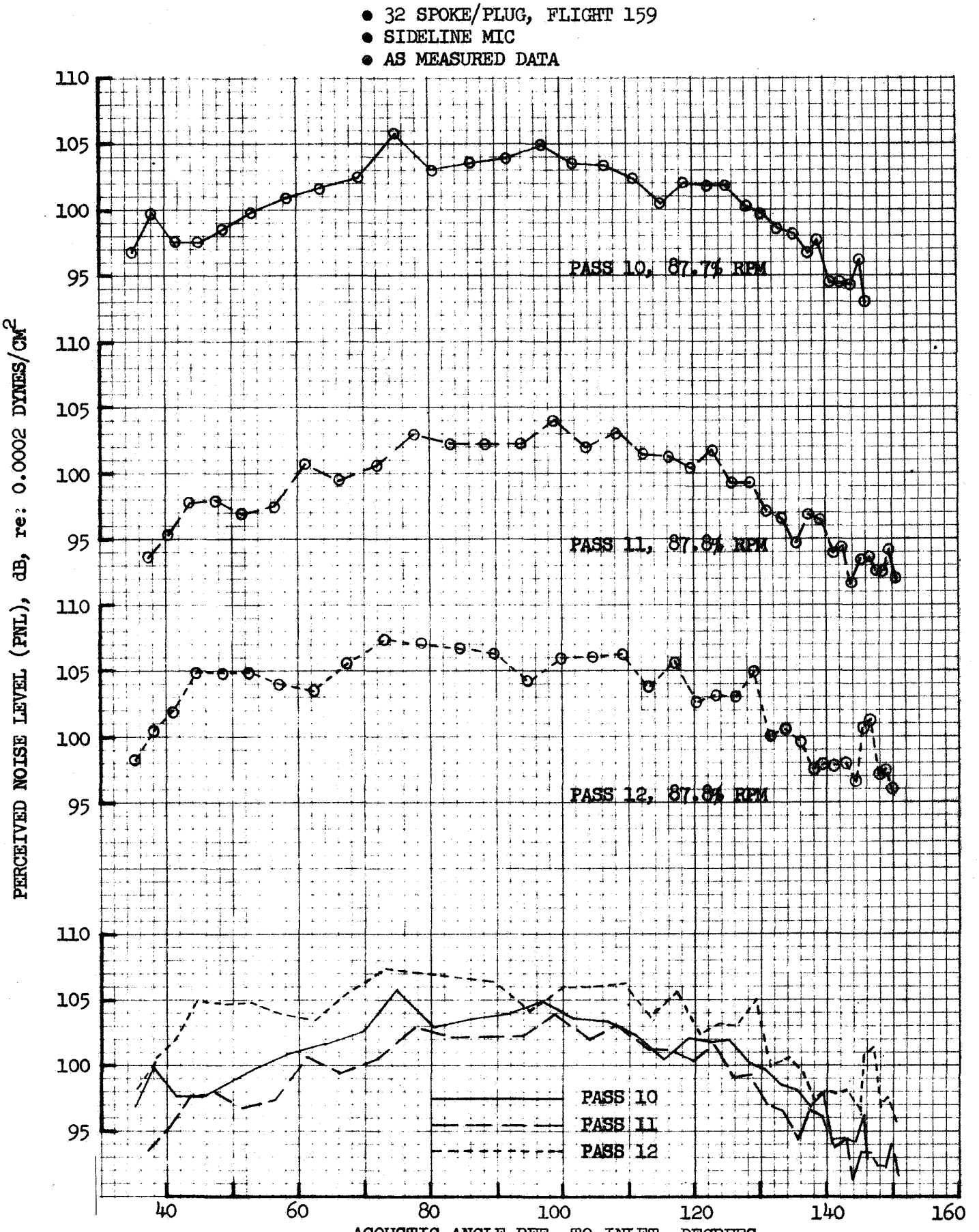

FIGURE 126 FLIGHT PNL, 32 SPOKE/PLUG, SIDELINE MIC, AS MEASURED DATA

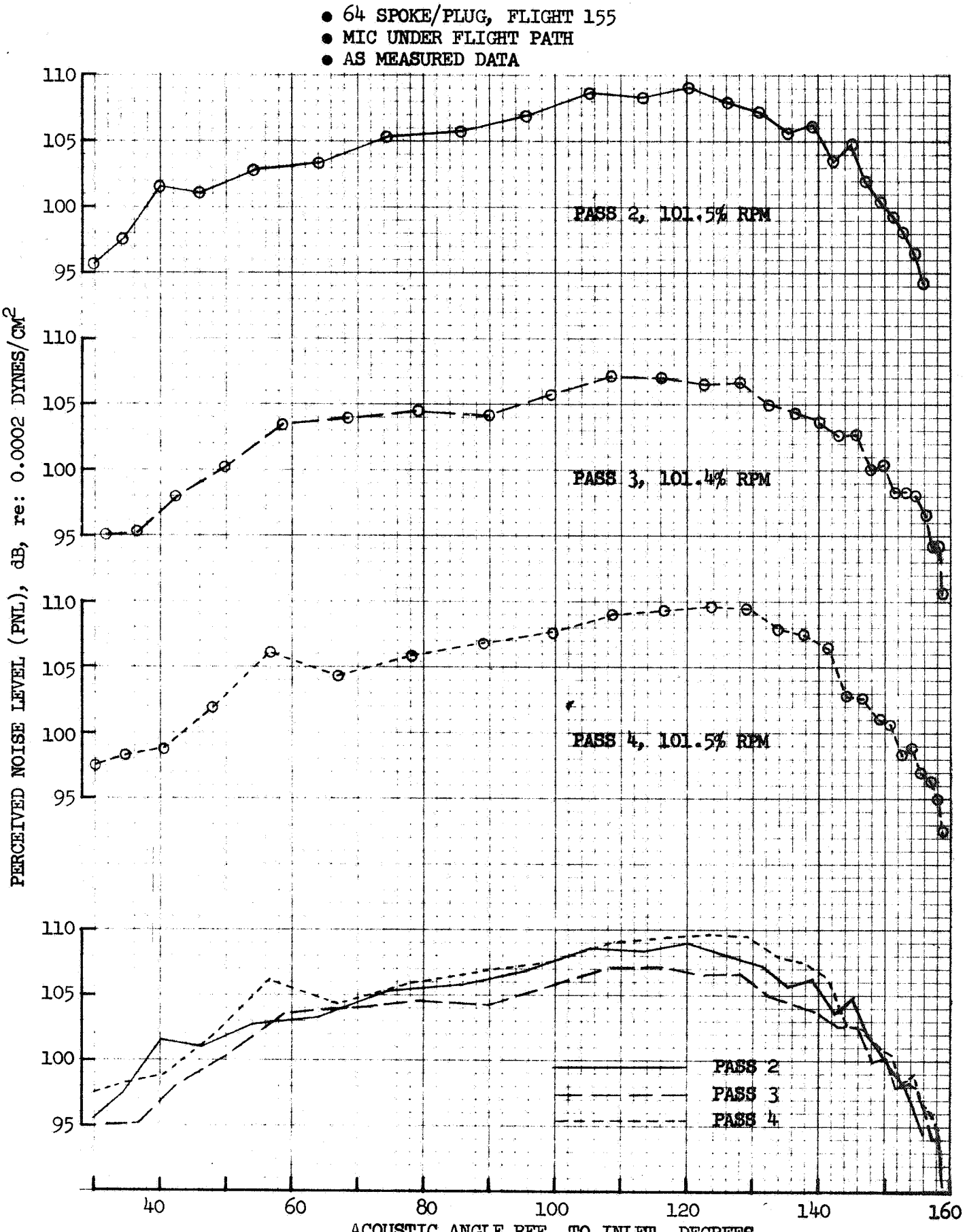

FIGURE 127 FLIGHT PNL, 64 SPOKE/PLUG, MIC UNDER FLIGHT PATH, AS MEASURED DATA

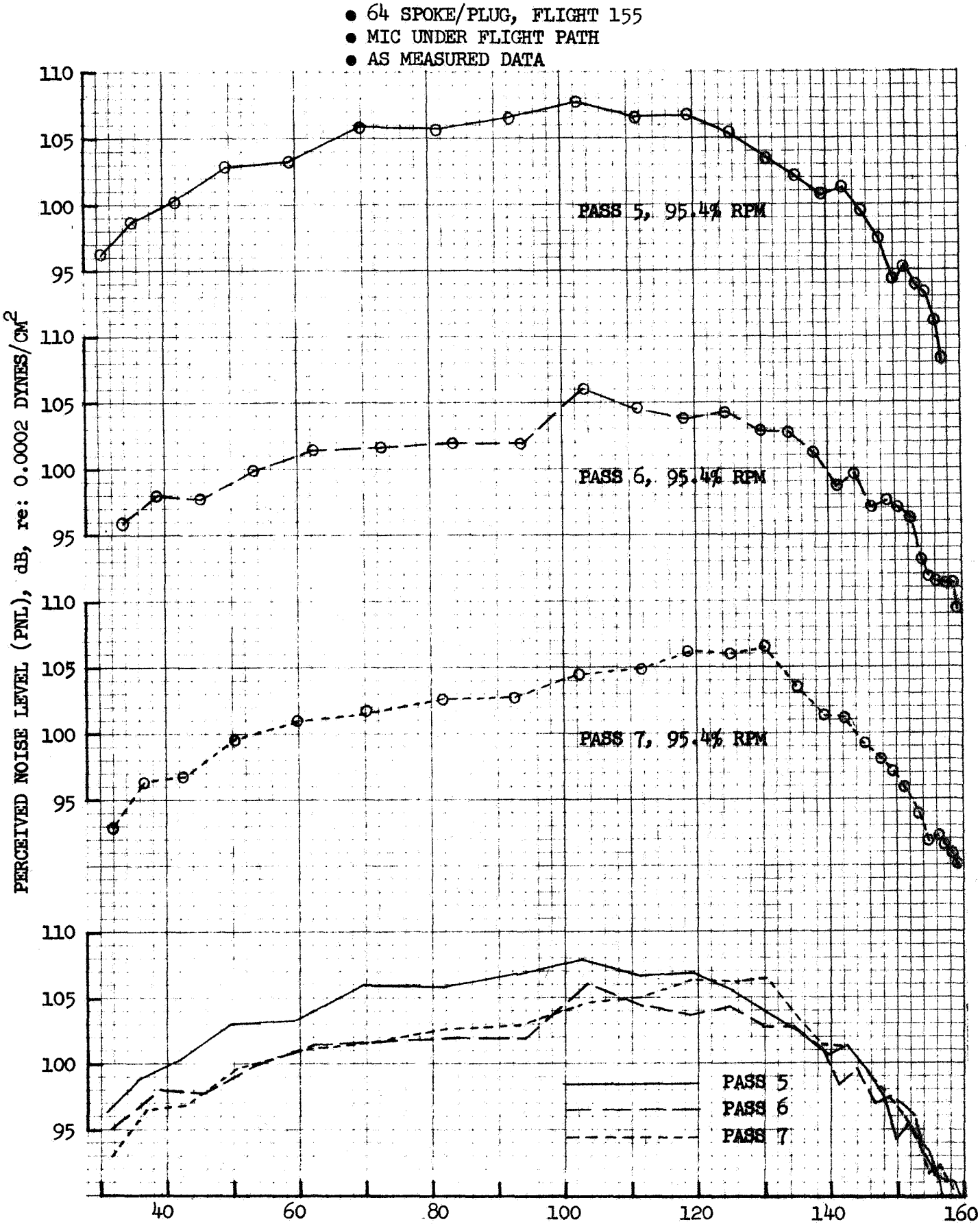

FIGURE 128 FLIGHT PNL, 64 SPOKE/PLUG, MIC UNDER FLIGHT PATH, AS MEASURED DATA

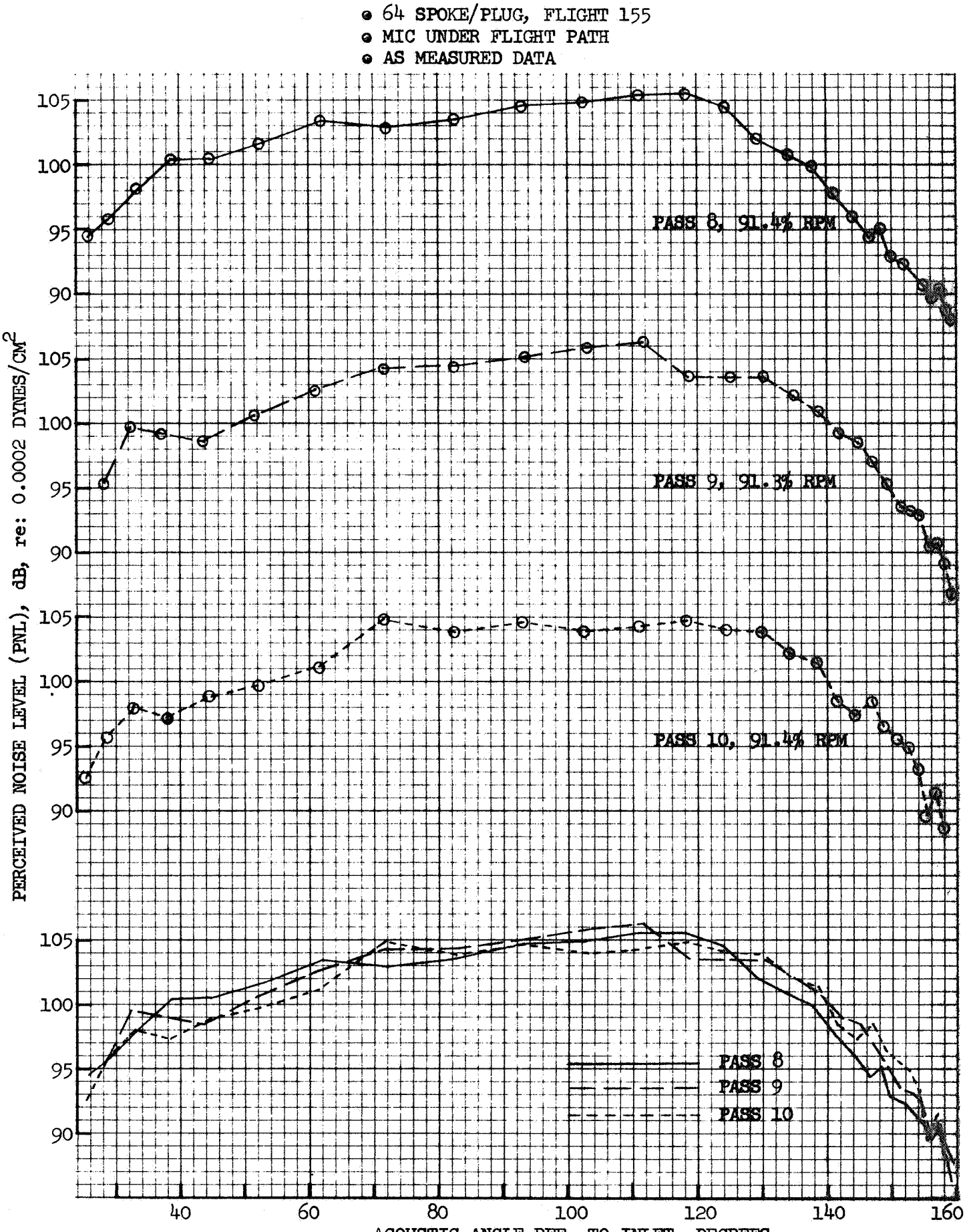

FIGURE 129 FLIGHT PNL, 64 SPOKE/PLUG, MIC UNDER FLIGHT PATH, AS MEASURED DATA

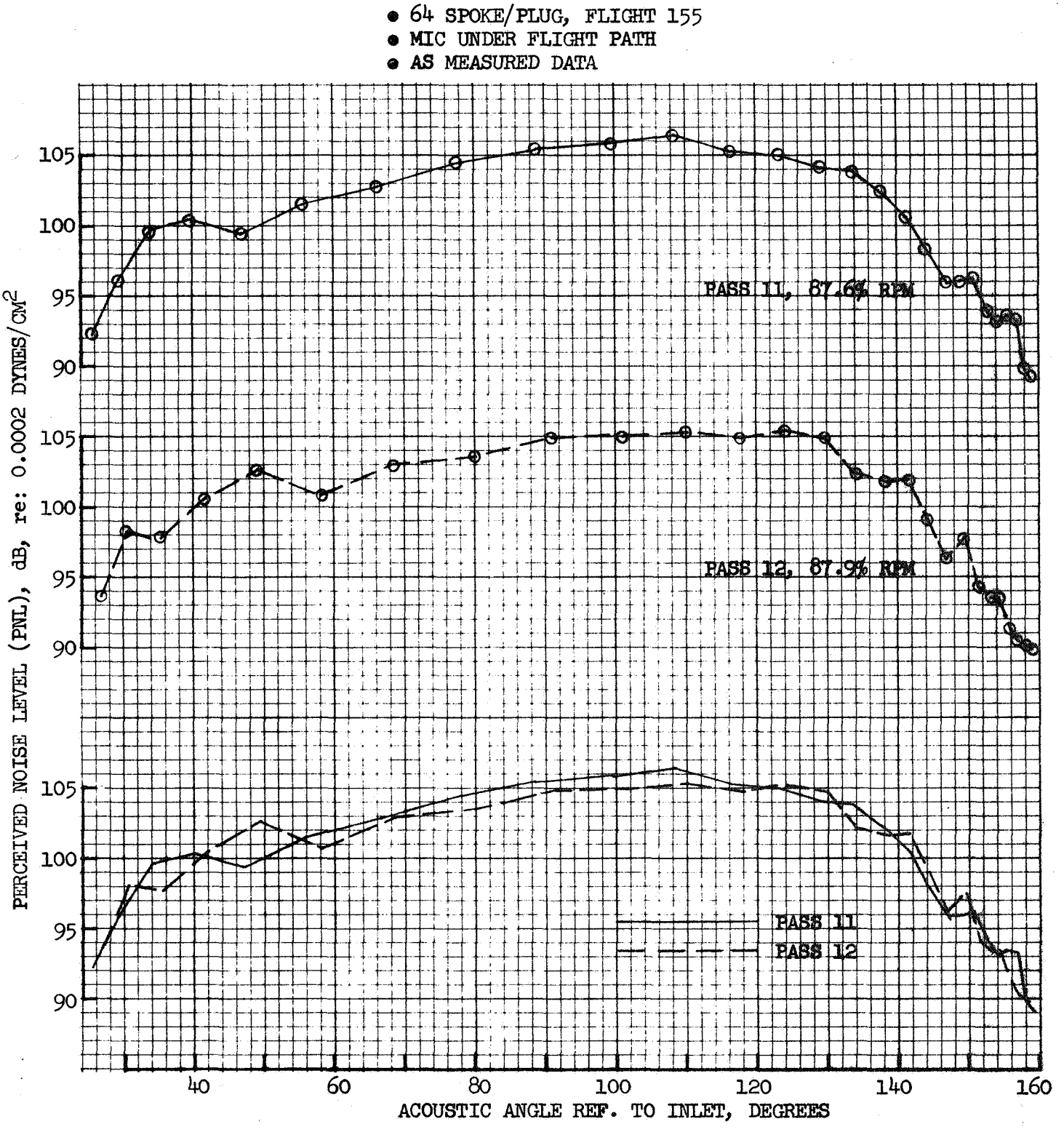

FIGURE 130 FLIGHT PNL, 64 SPOKE/PLUG, MIC UNDER FLIGHT PATH, AS MEASURED DATA

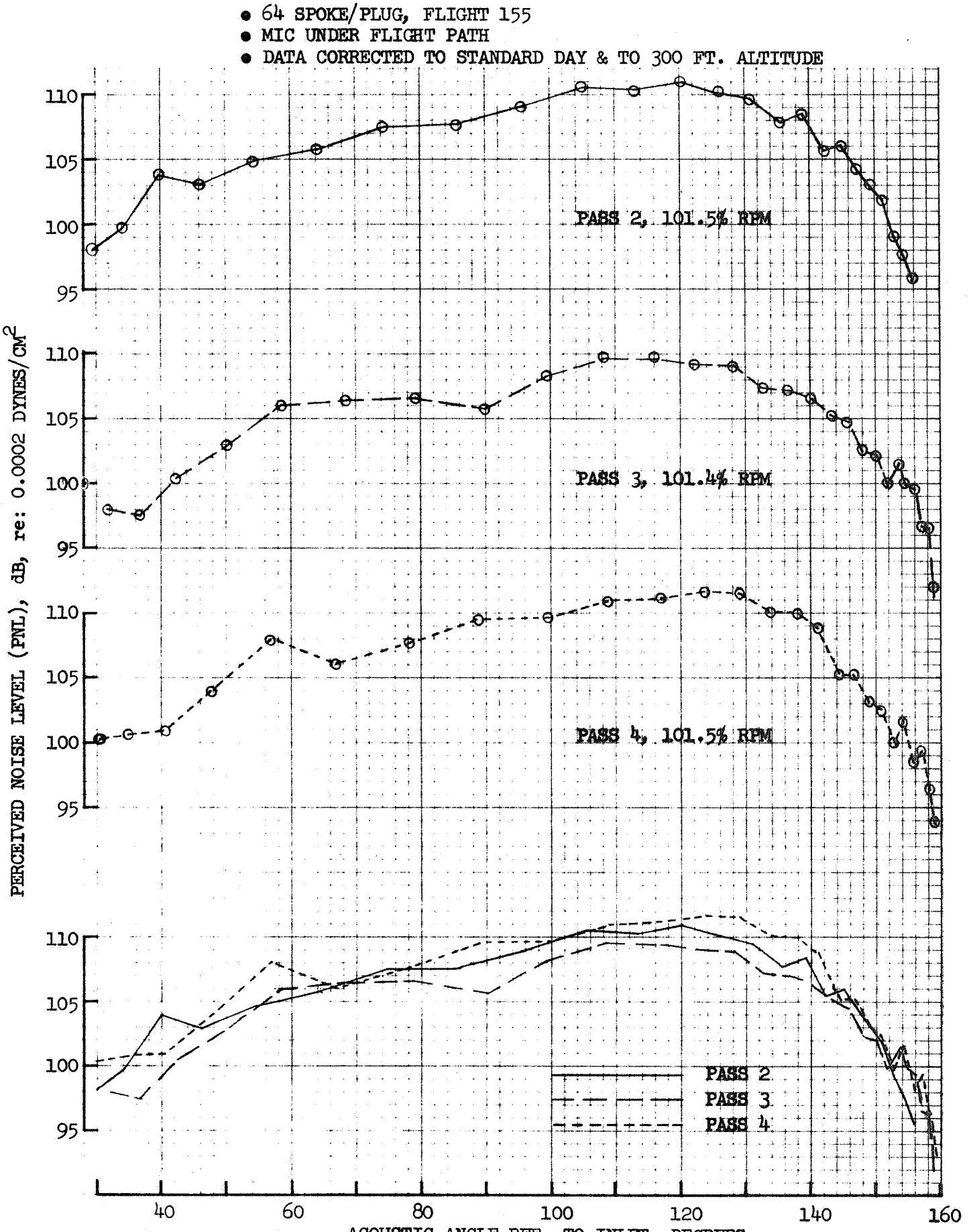

FIGURE 131 FLIGHT PNL, 64 SPOKE/PLUG, MIC UNDER FLIGHT PATH, CORRECTED DATA

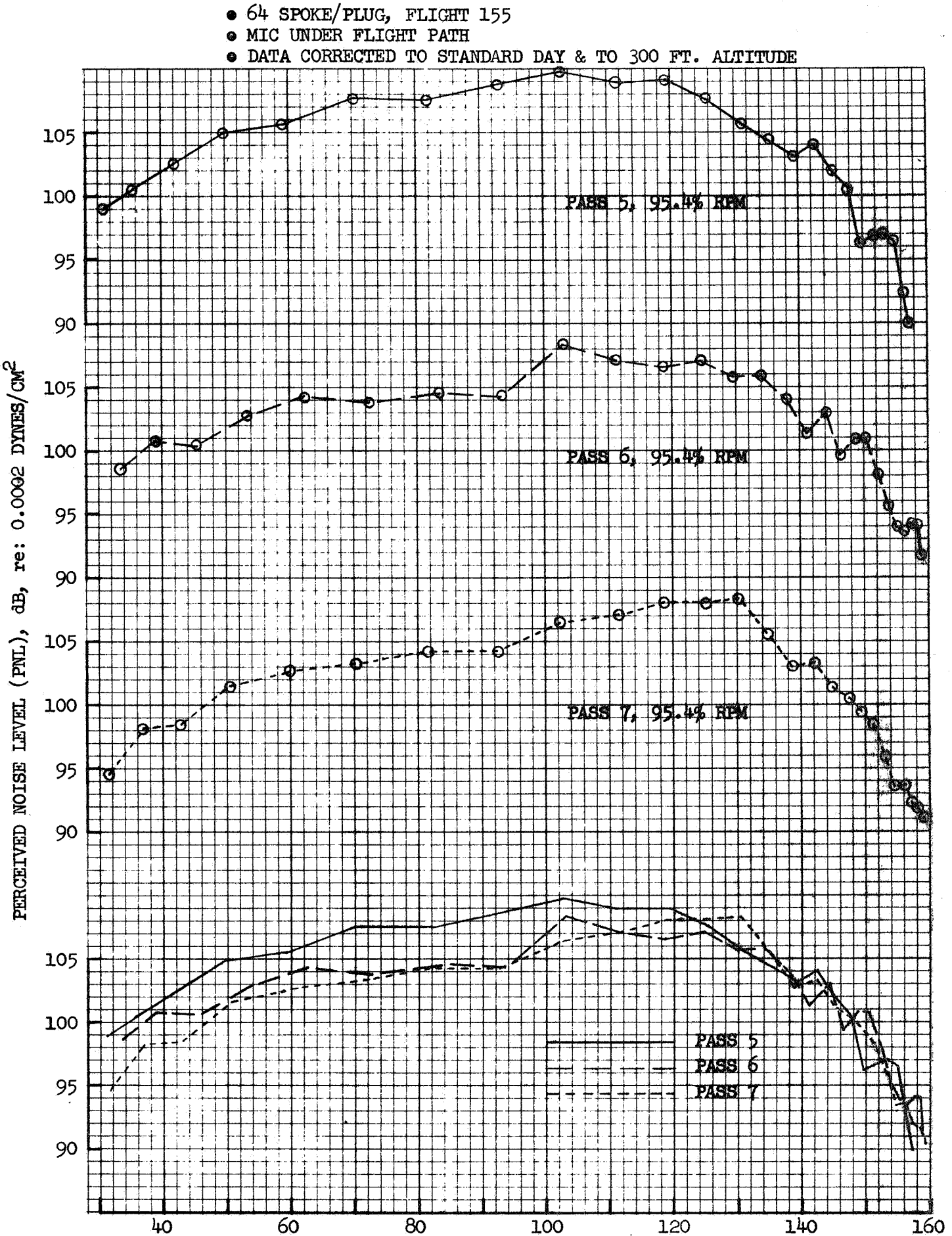

FIGURE 132 FLIGHT PNL, 64 SPOKE/PLUG, MIC UNDER FLIGHT PATH, CORRECTED DATA

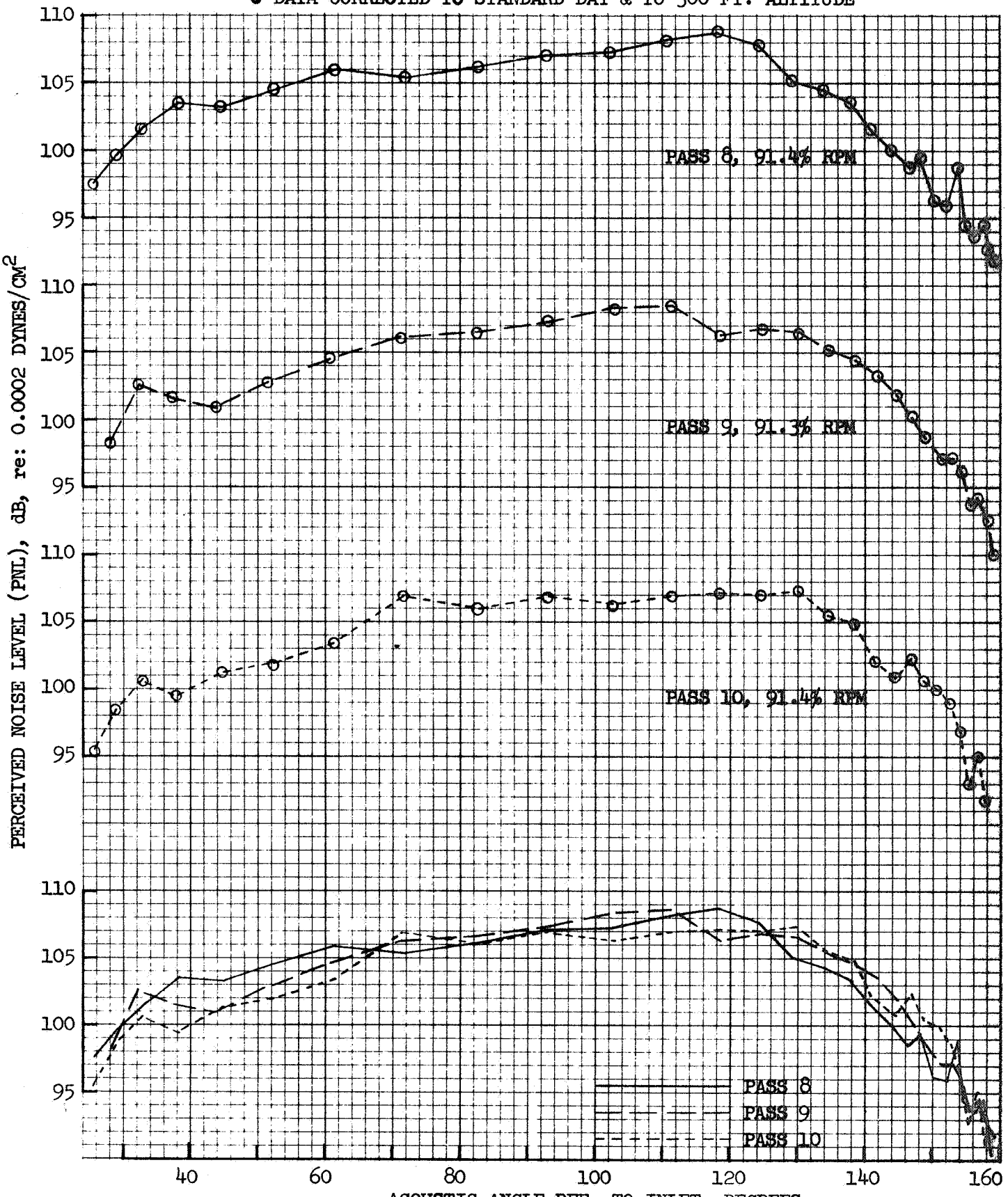

FIGURE 133 FLIGHT PNL, 64 SPOKE/PLUG, MIC UNDER FLIGHT PATH, CORRECTED DATA

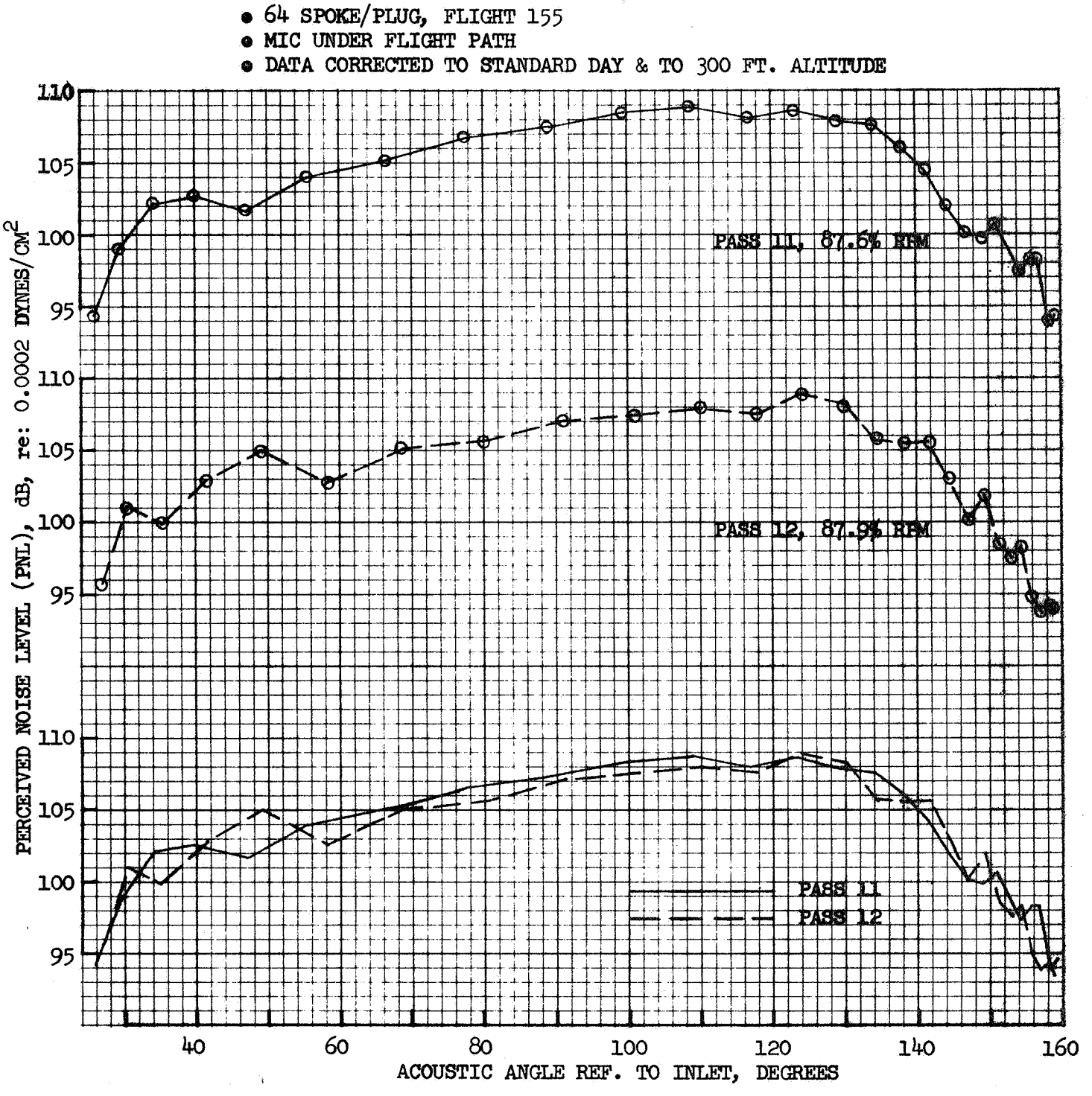

FIGURE 134 FLIGHT PNL, 64 SPOKE/PLUG, MIC UNDER FLIGHT PATH, CORRECTED DATA

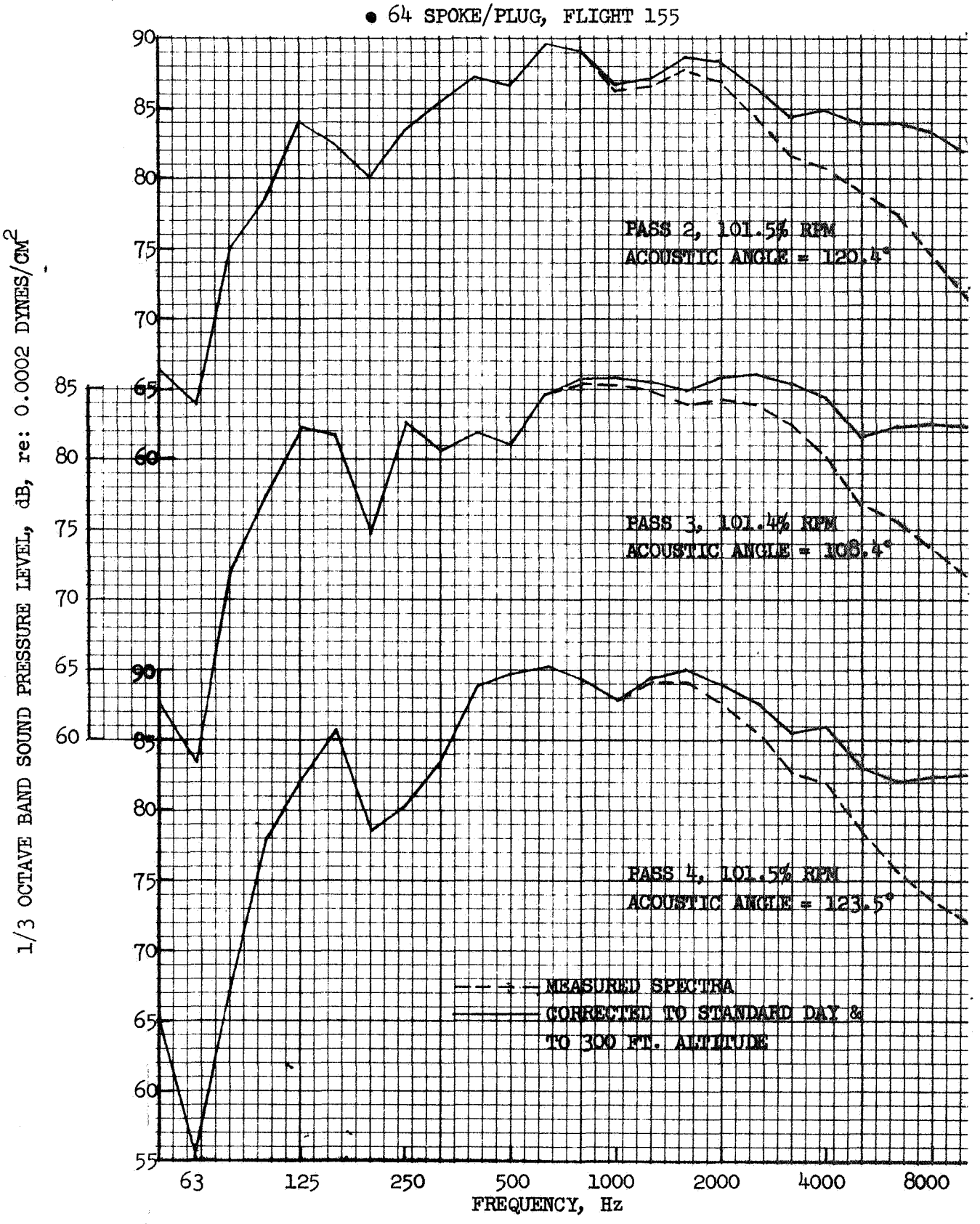

FIGURE 135 FLIGHT SPECTRA AT PEAK PNL, 64 SPOKE/PLUG, MIC UNDER FLIGHT PATH

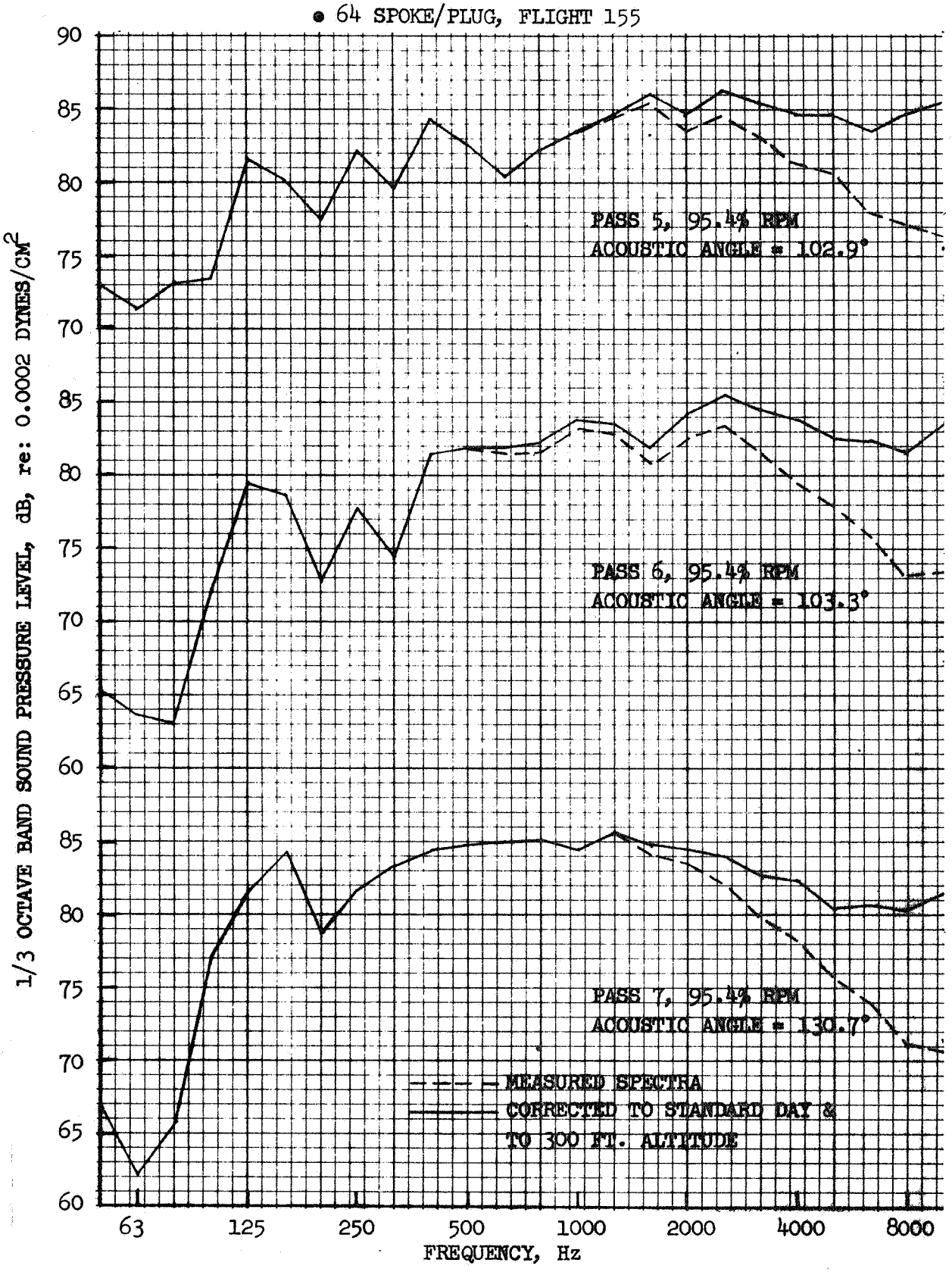

FIGURE 136 FLIGHT SPECTRA AT PEAK PNL, 64 SPOKE/PLUG, MIC UNDER FLIGHT PATH

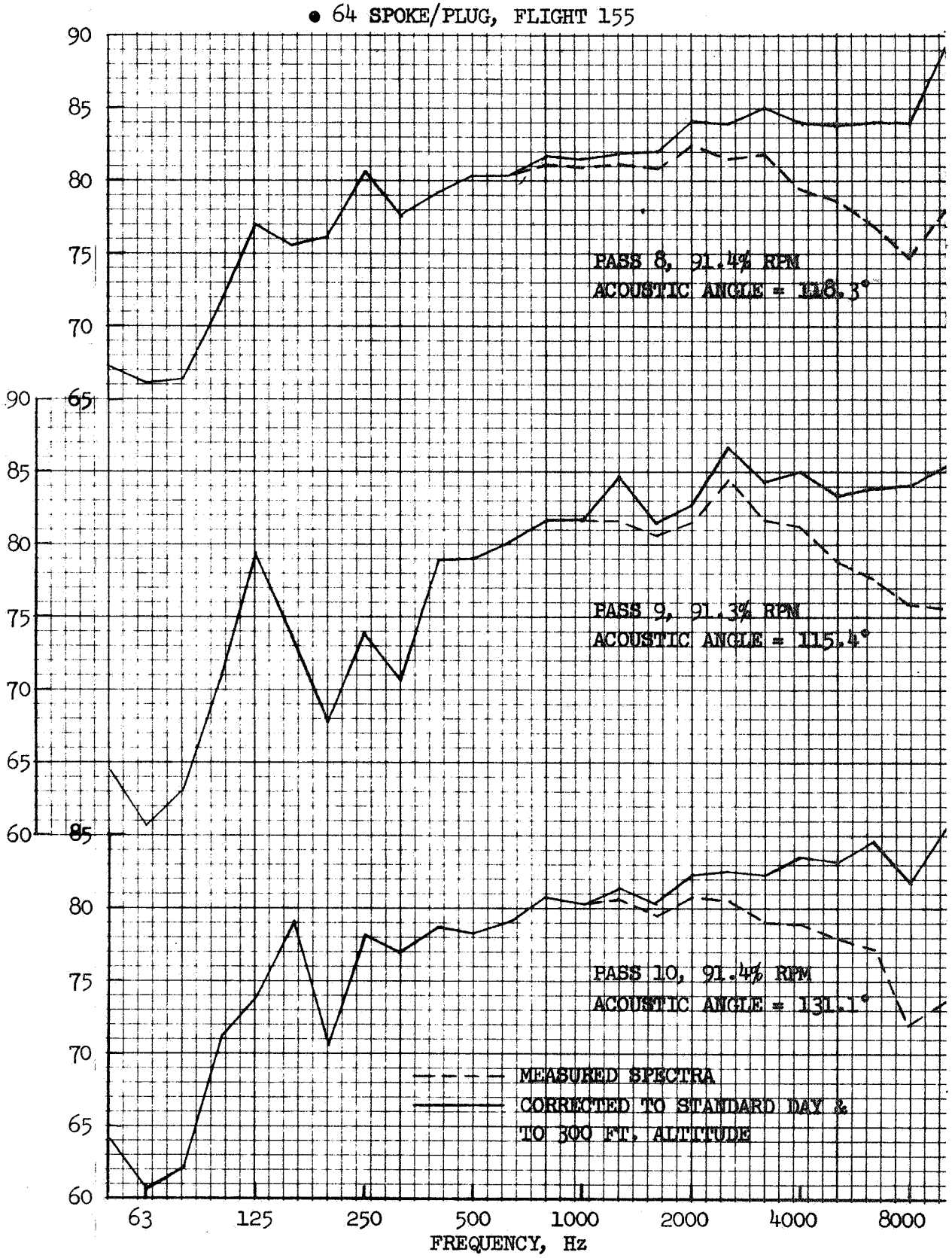

FIGURE 137 FLIGHT SPECTRA AT PEAK PNL, 64 SPOKE/PLUG, MIC UNDER FLIGHT PATH

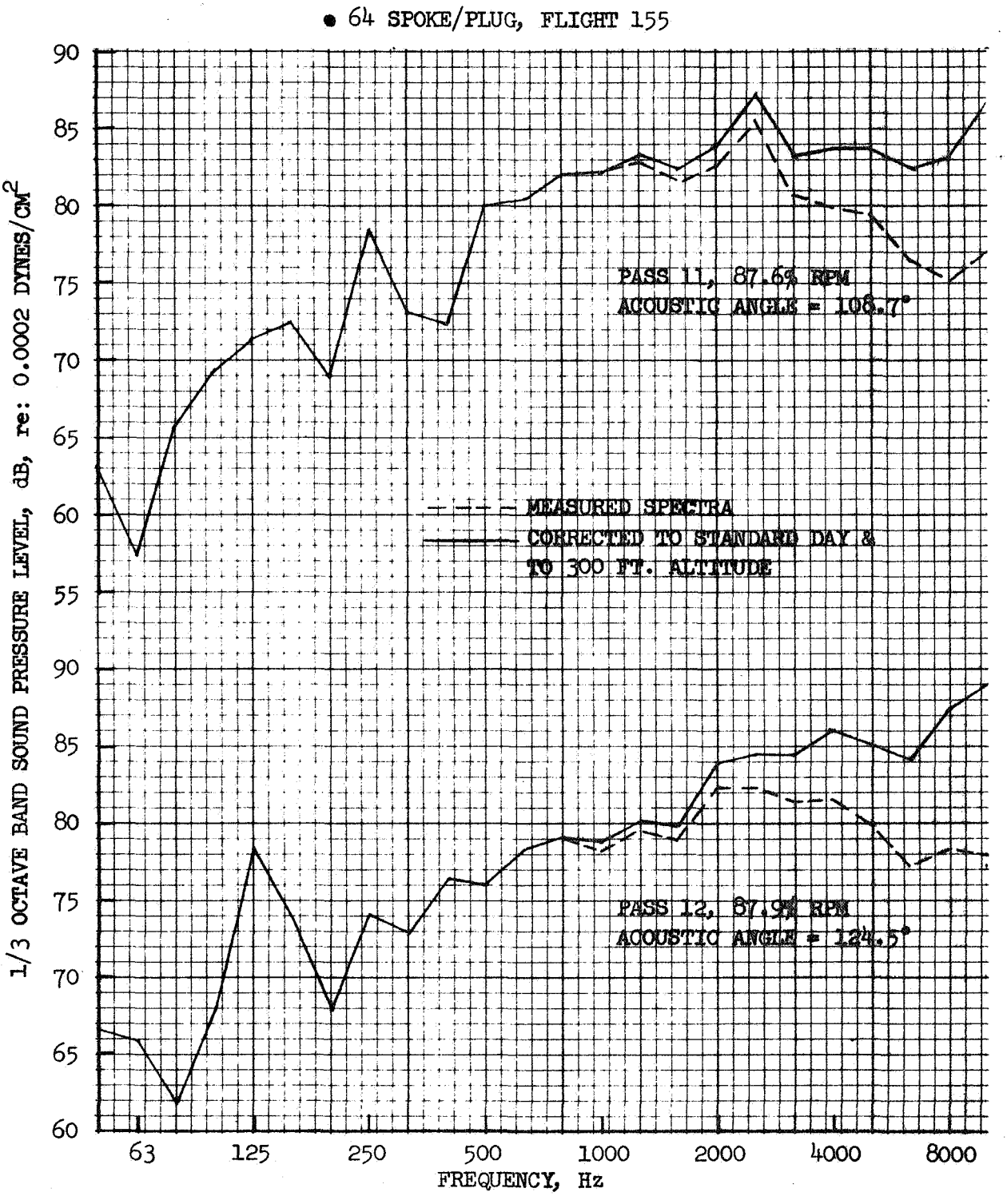

FIGURE 138 FLIGHT SPECTRA AT PEAK PNL, 64 SPOKE/PLUG, MIC UNDER FLIGHT PATH

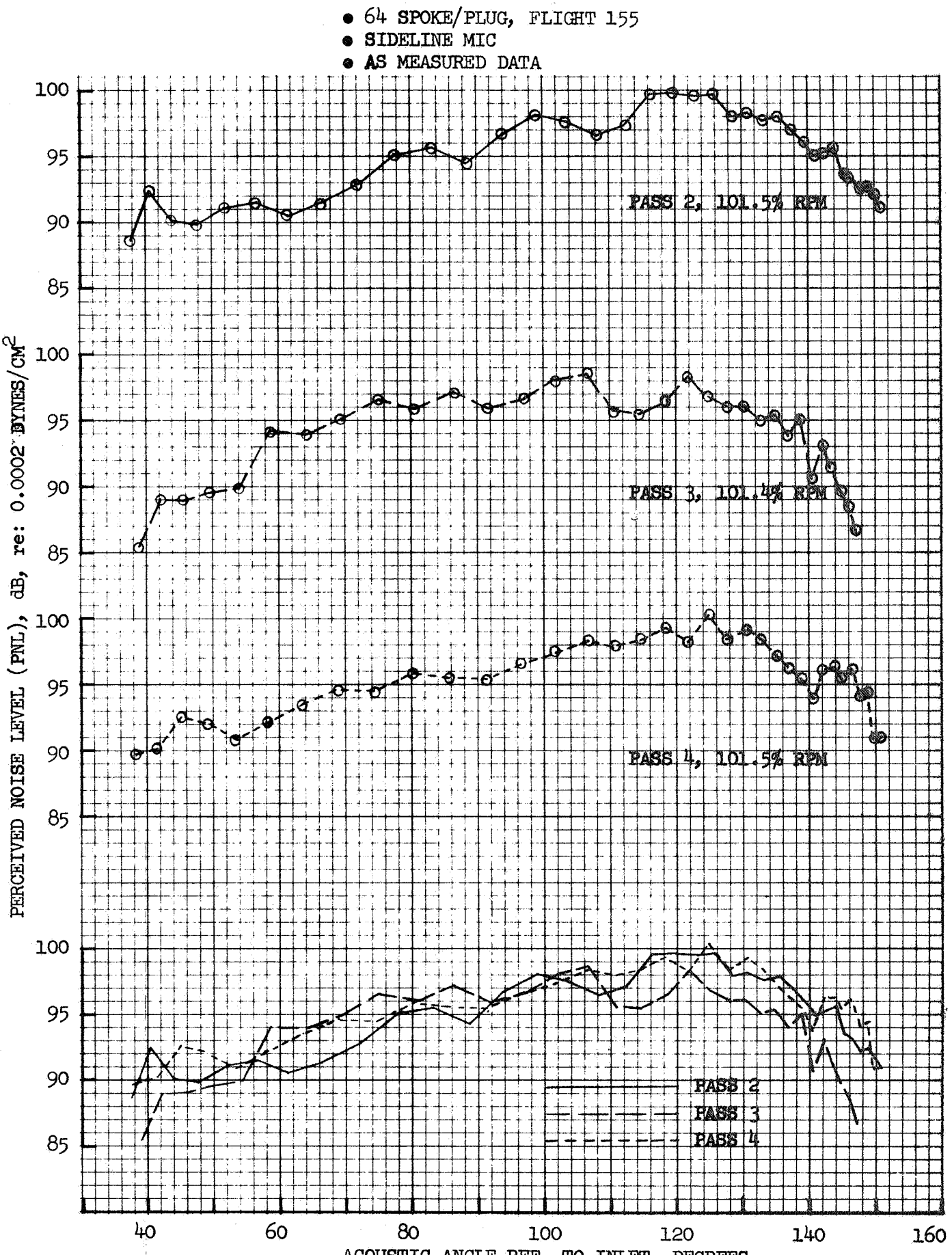

FIGURE 139 FLIGHT PNL, 64 SPOKE/PLUG, SIDELINE MIC, AS MEASURED DATA

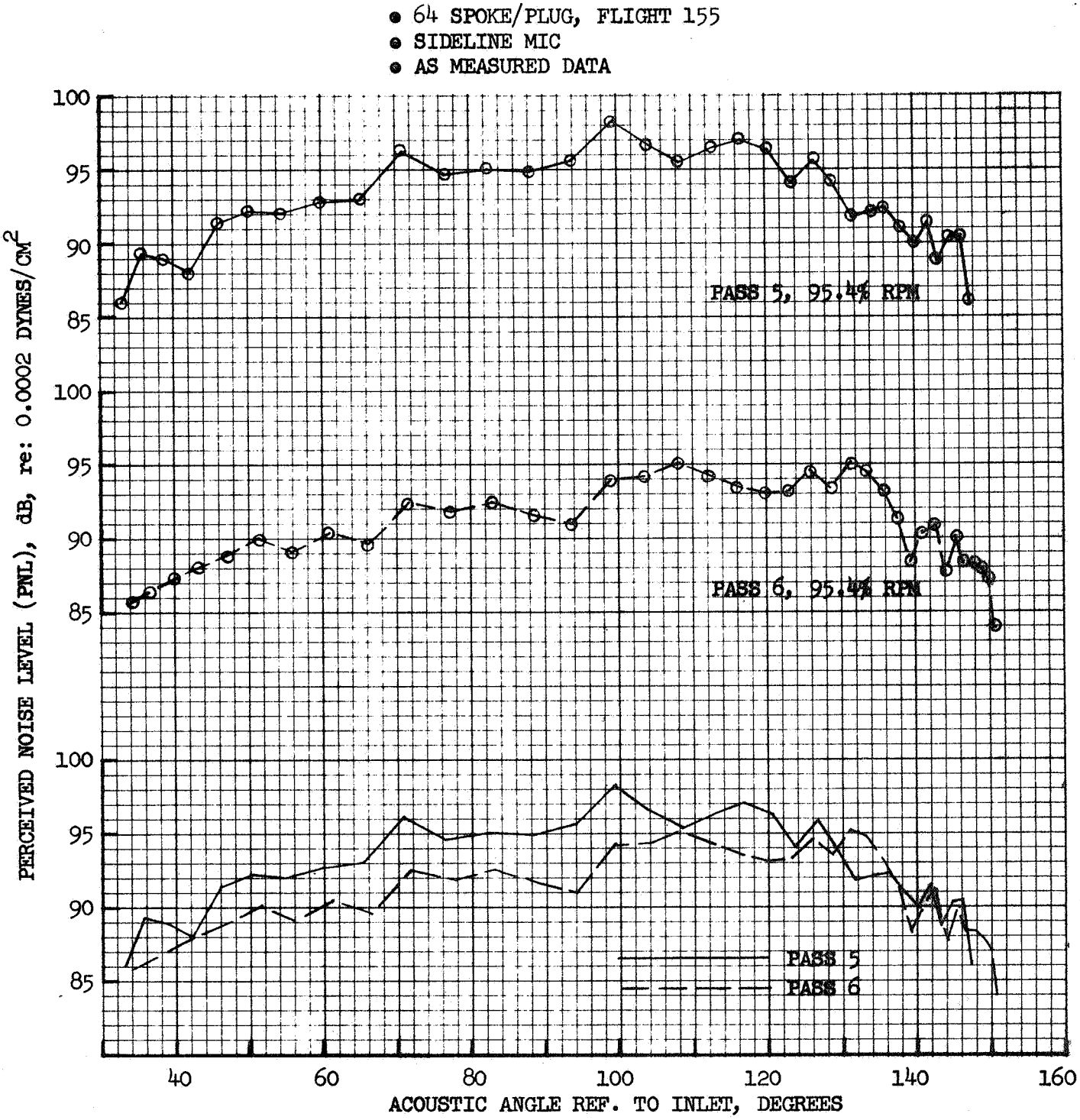

FIGURE 140 FLIGHT PNL, 64 SPOKE/PLUG, SIDELINE MIC, AS MEASURED DATA

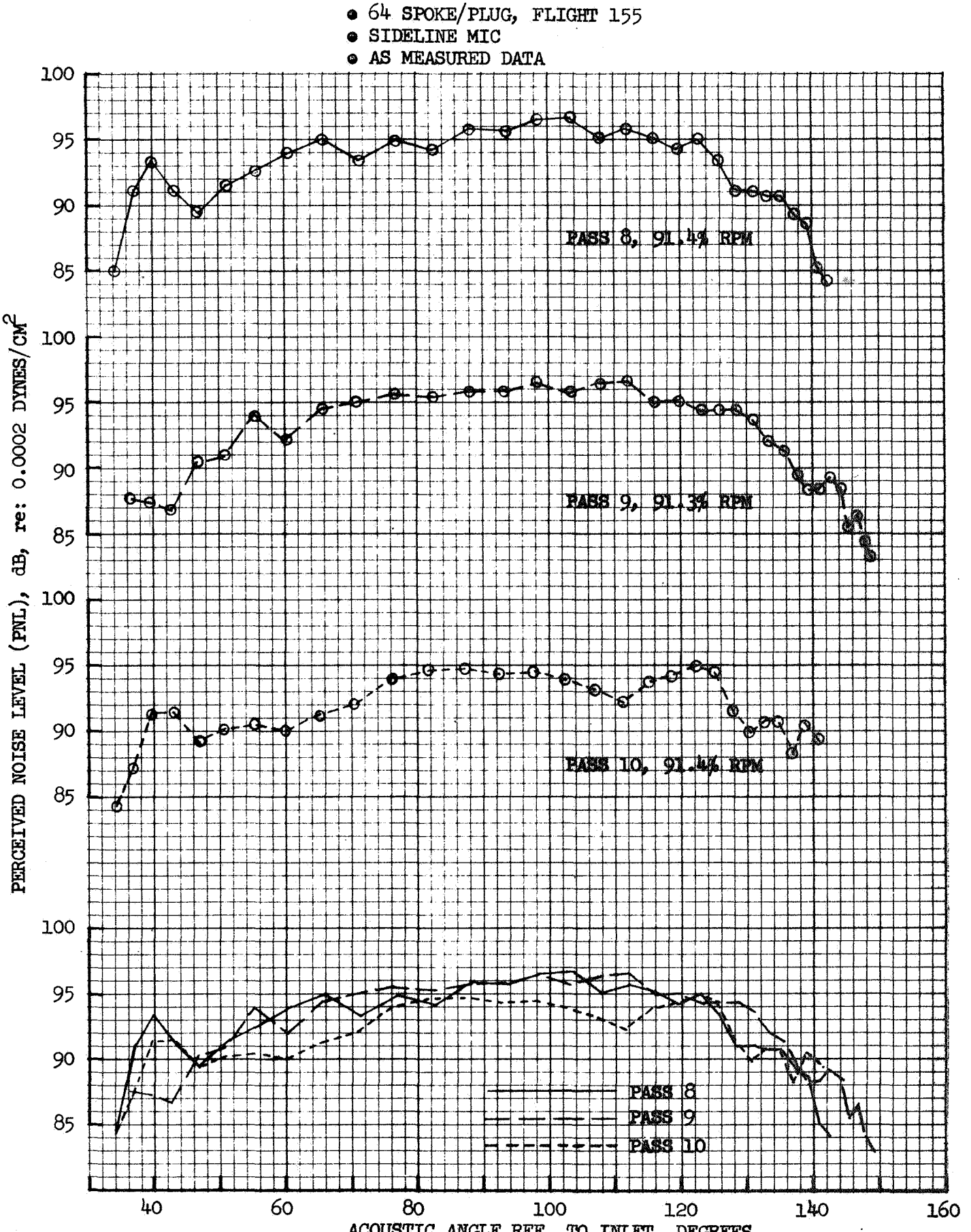

FIGURE 141 FLIGHT PNL, 64 SPOKE/PLUG, SIDELINE MIC, AS MEASURED DATA

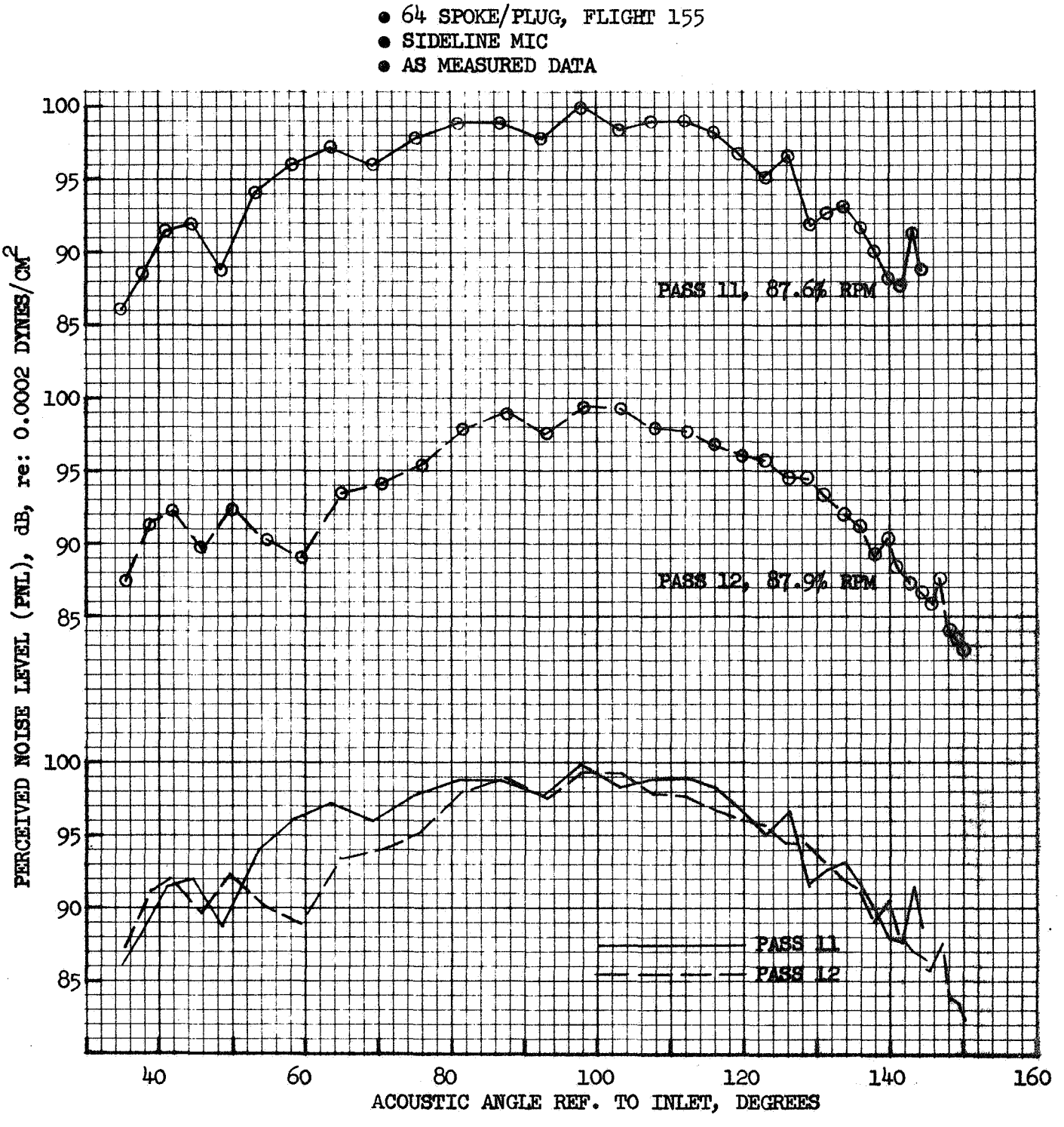

FIGURE 142 FLIGHT PNL, 64 SPOKE/PLUG, SIDELINE MIC, AS MEASURED DATA

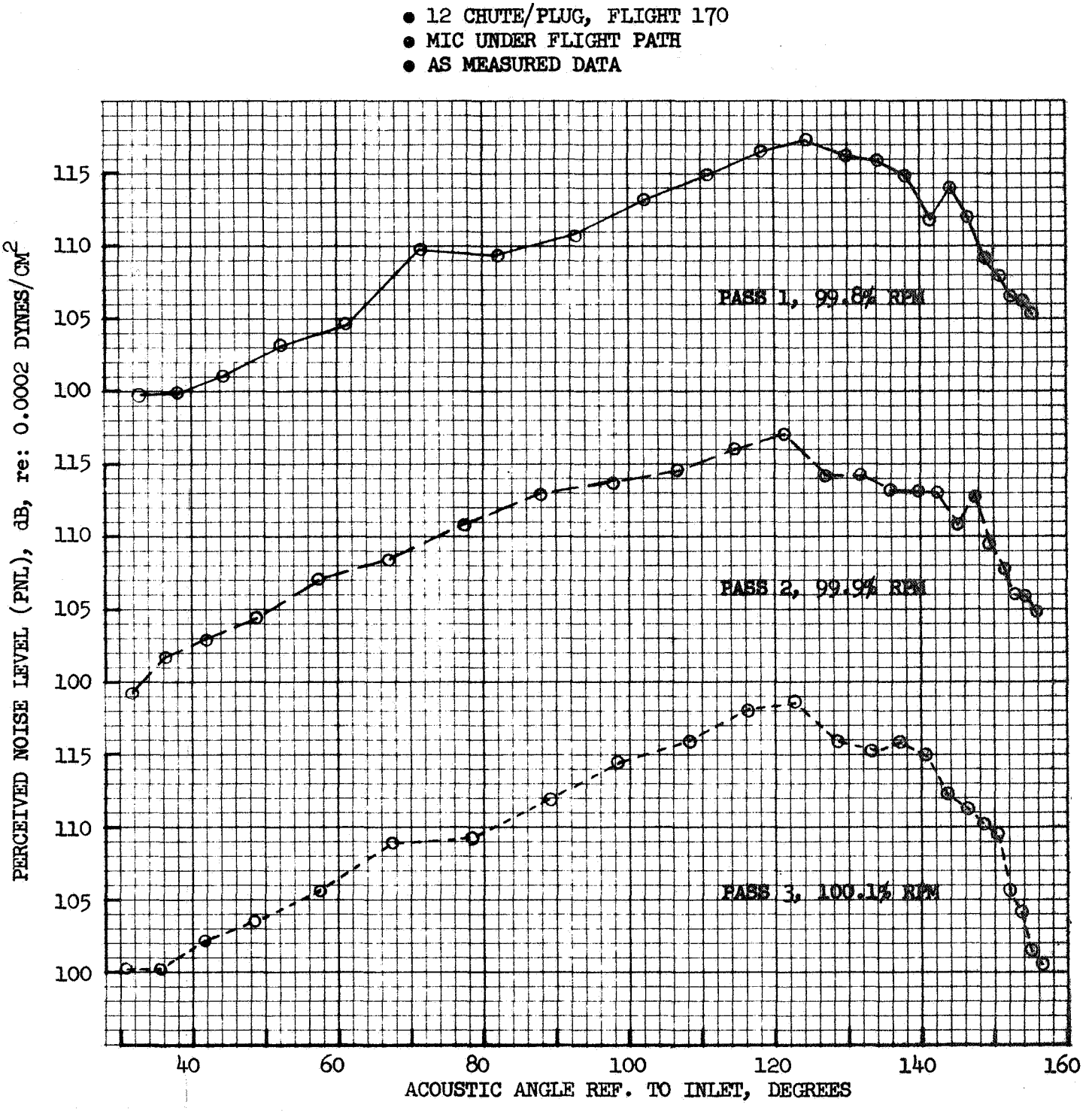

FIGURE 143 FLIGHT PNL, 12 CHUTE/PLUG, MIC UNDER FLIGHT PATH, AS MEASURED DATA

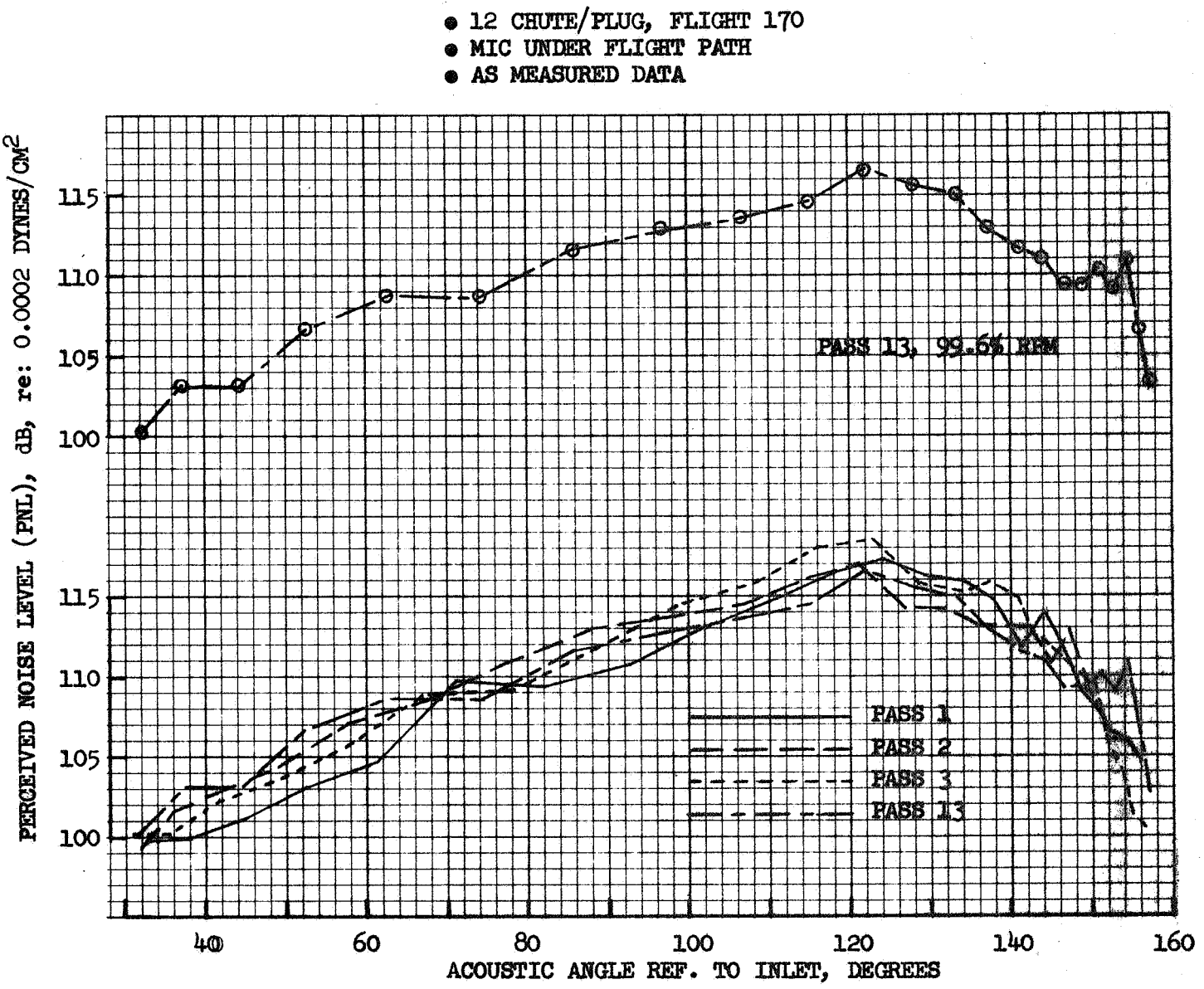

FIGURE 144 FLIGHT PNL, 12 CHUTE/PLUG, MIC UNDER FLIGHT PATH, AS MEASURED DATA

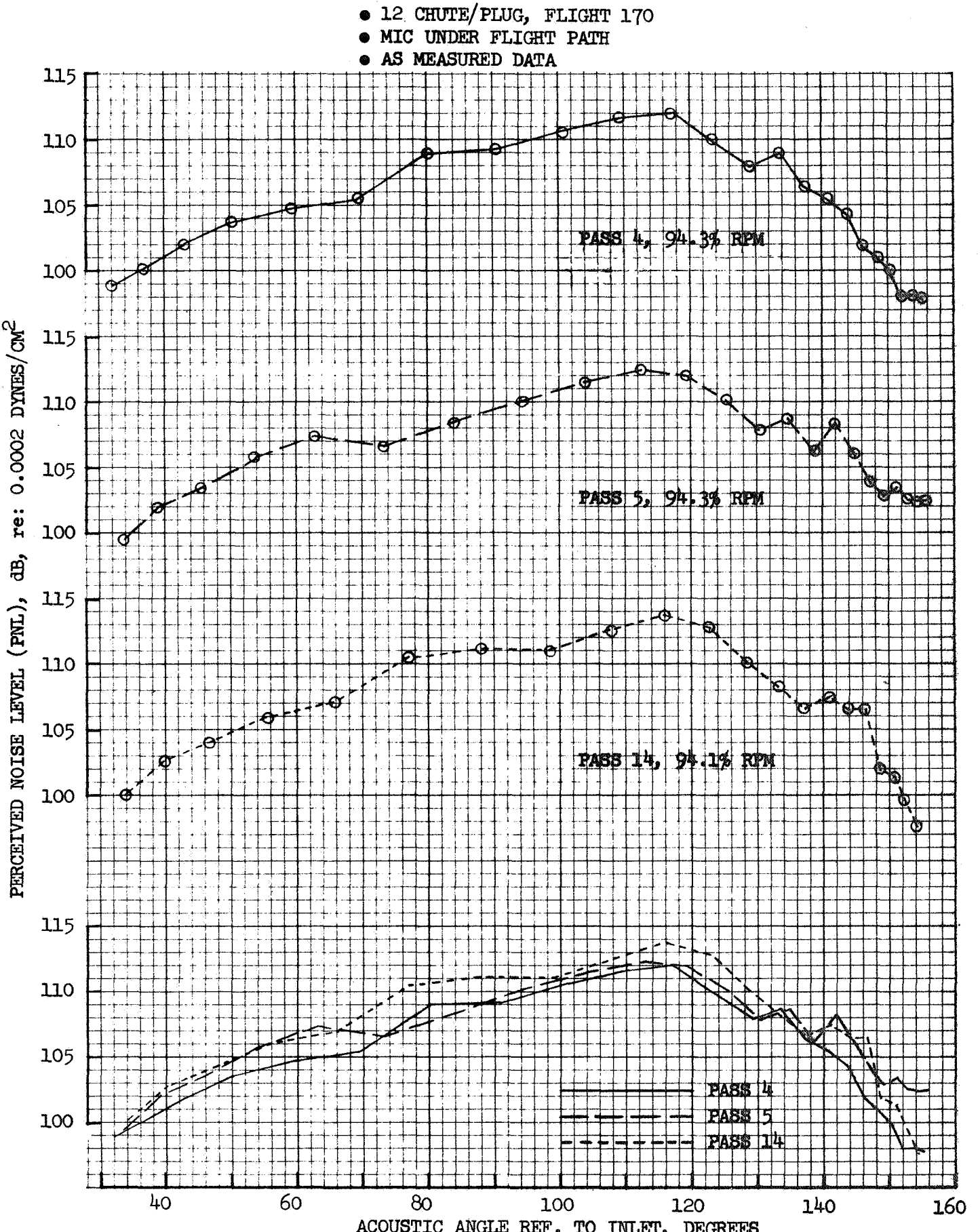

FIGURE 145 FLIGHT PNL, 12 CHUTE/PLUG, MIC UNDER FLIGHT PATH, AS MEASURED DATA

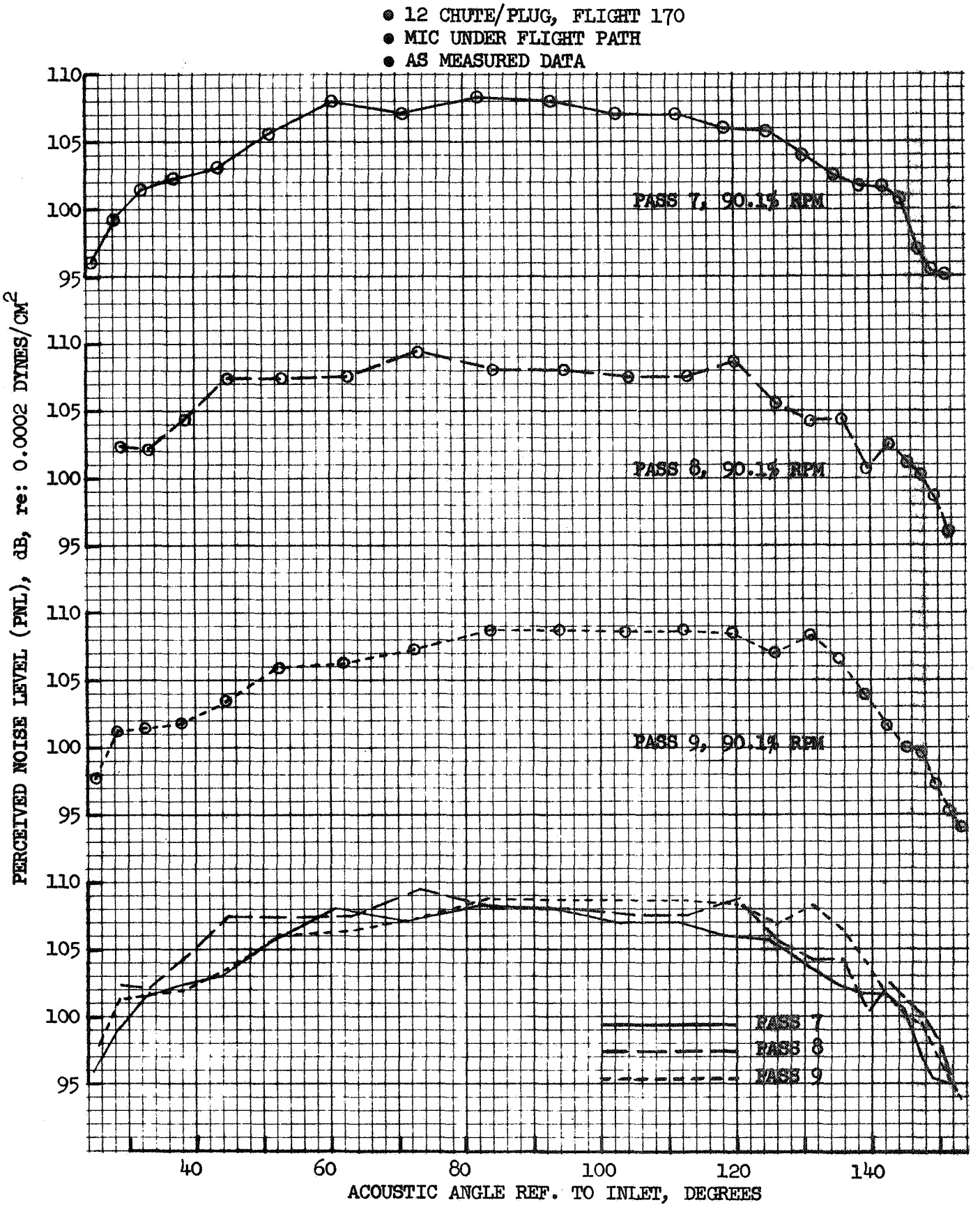

FIGURE 146 FLIGHT PNL, 12 CHUTE/PLUG, MIC UNDER FLIGHT PATH, AS MEASURED DATA

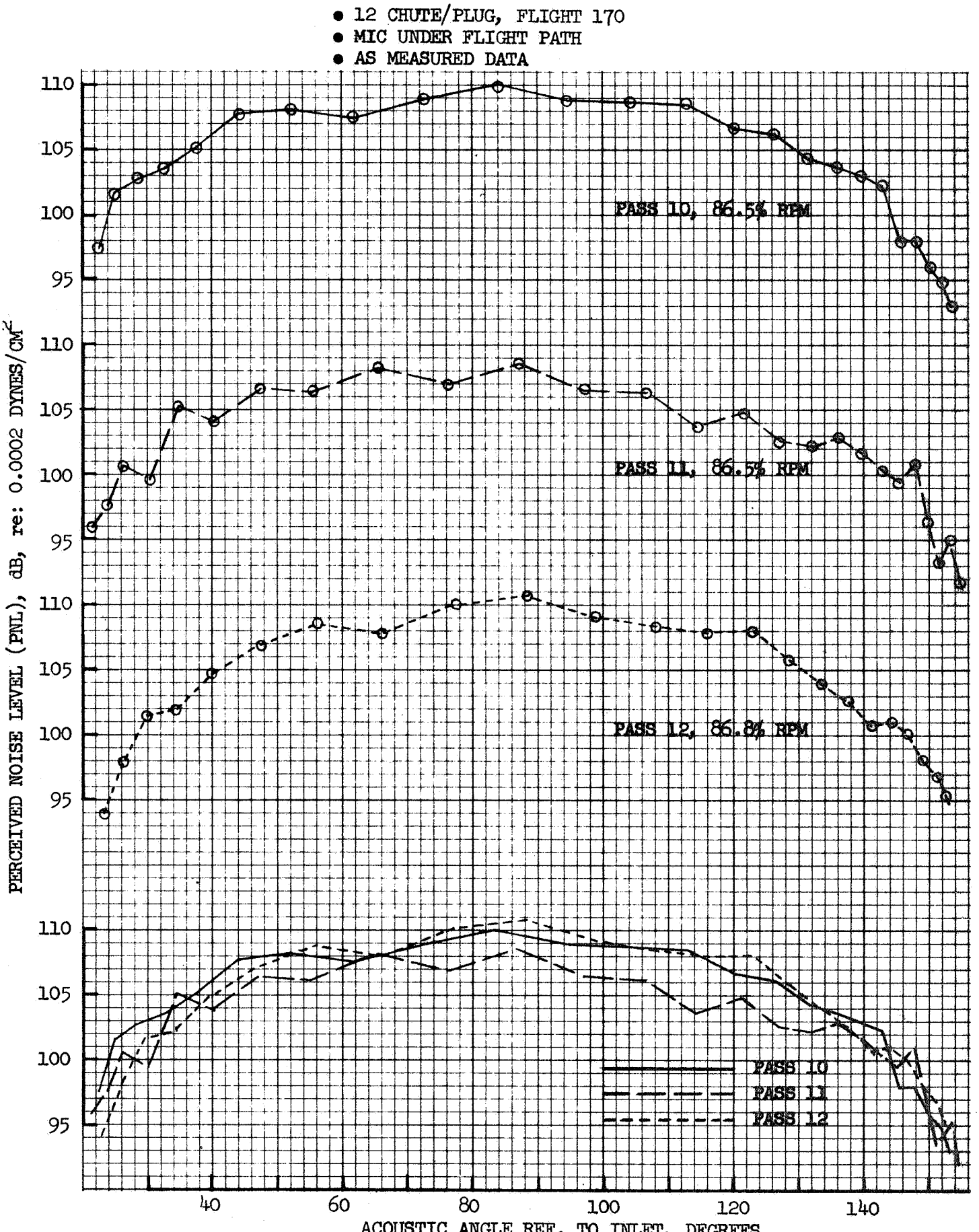

FIGURE 147 FLIGHT PNL, 12 CHUTE/PLUG, MIC UNDER FLIGHT PATH, AS MEASURED DATA

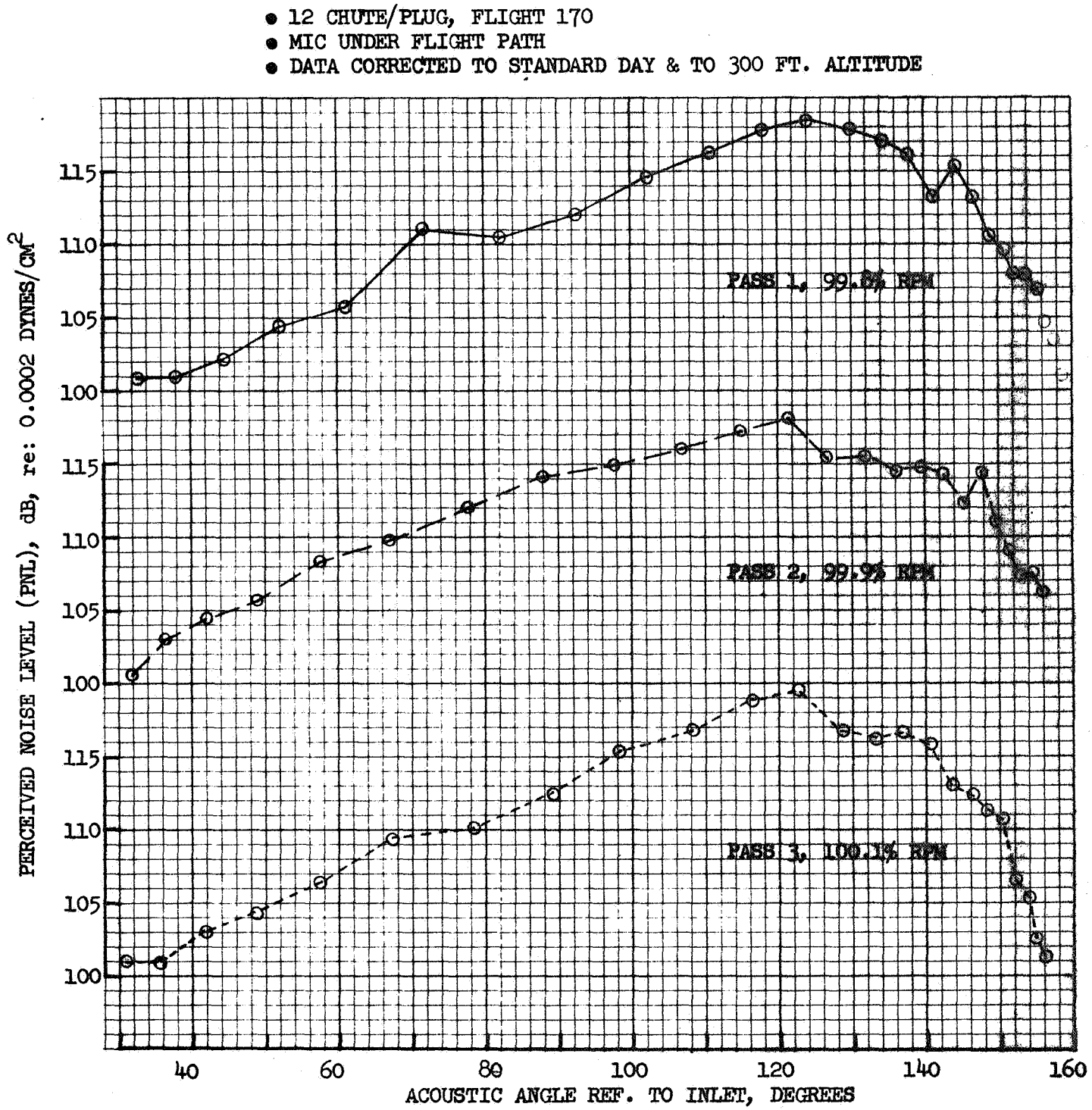

FIGURE 148 FLIGHT PNL, 12 CHUTE/PLUG, MIC UNDER FLIGHT PATH, CORRECTED DATA

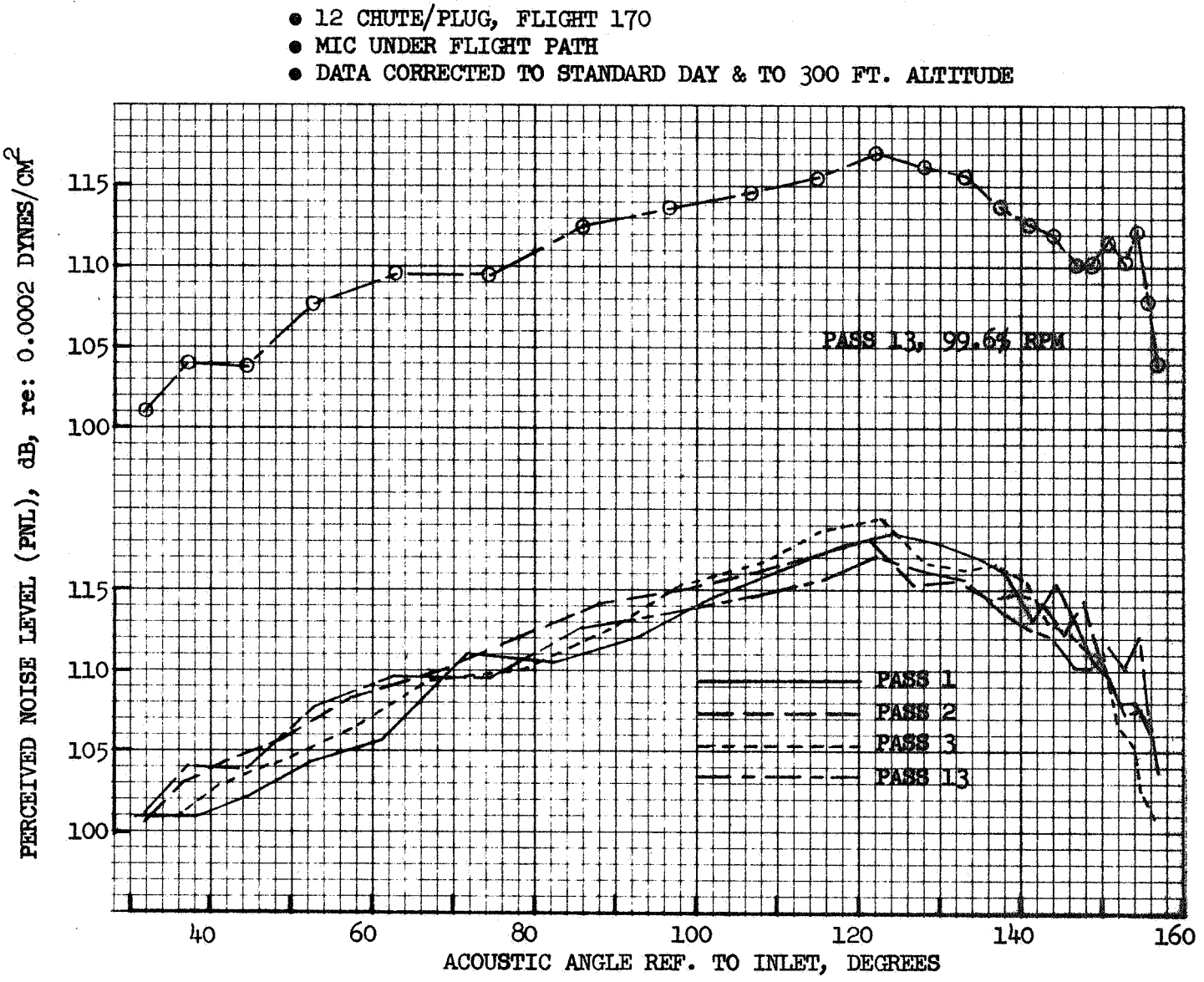

FIGURE 149 FLIGHT PNL, 12 CHUTE/PLUG, MIC UNDER FLIGHT PATH, CORRECTED DATA

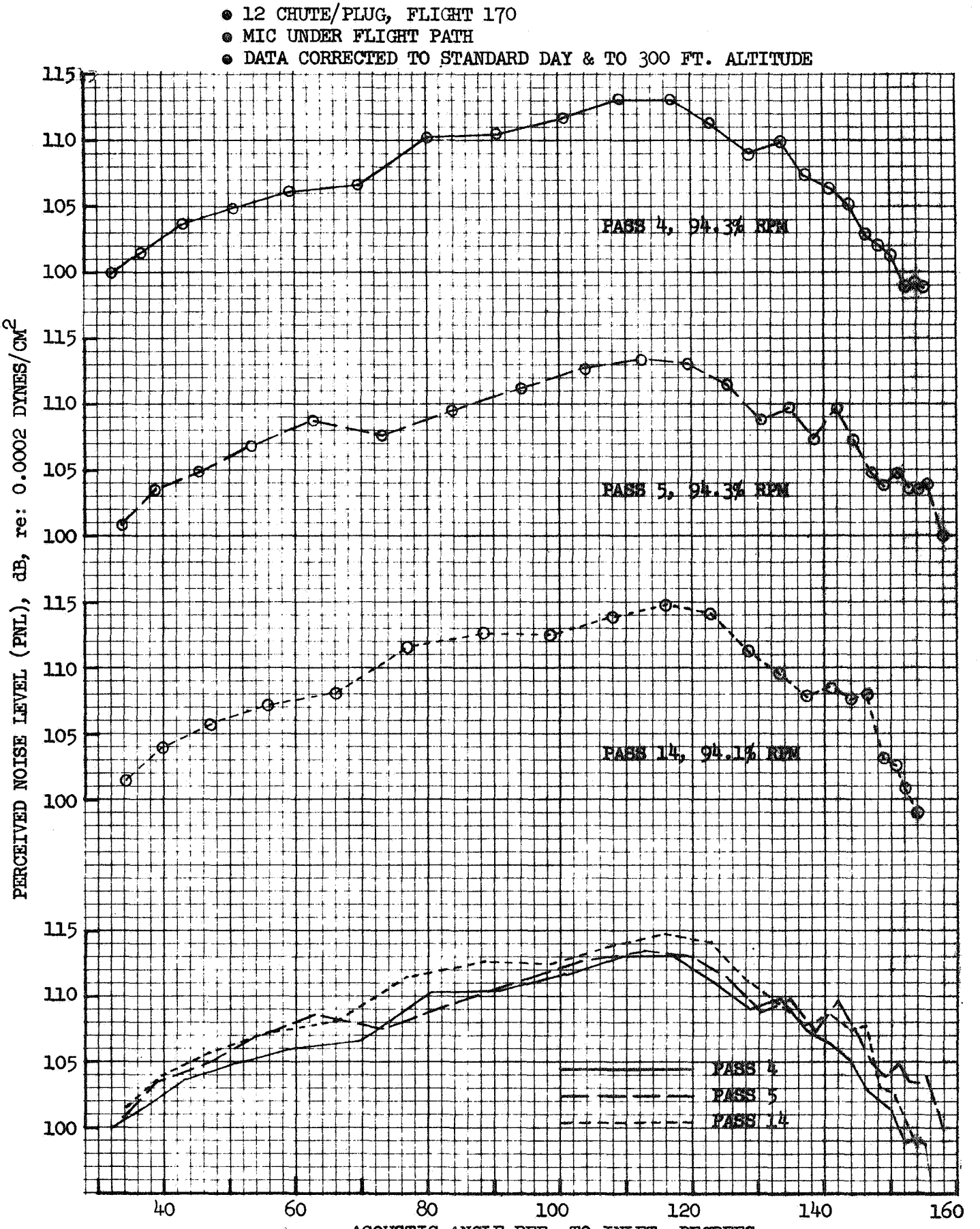

FIGURE 150 FLIGHT PNL, 12 CHUTE/PLUG, MIC UNDER FLIGHT PATH, CORRECTED DATA

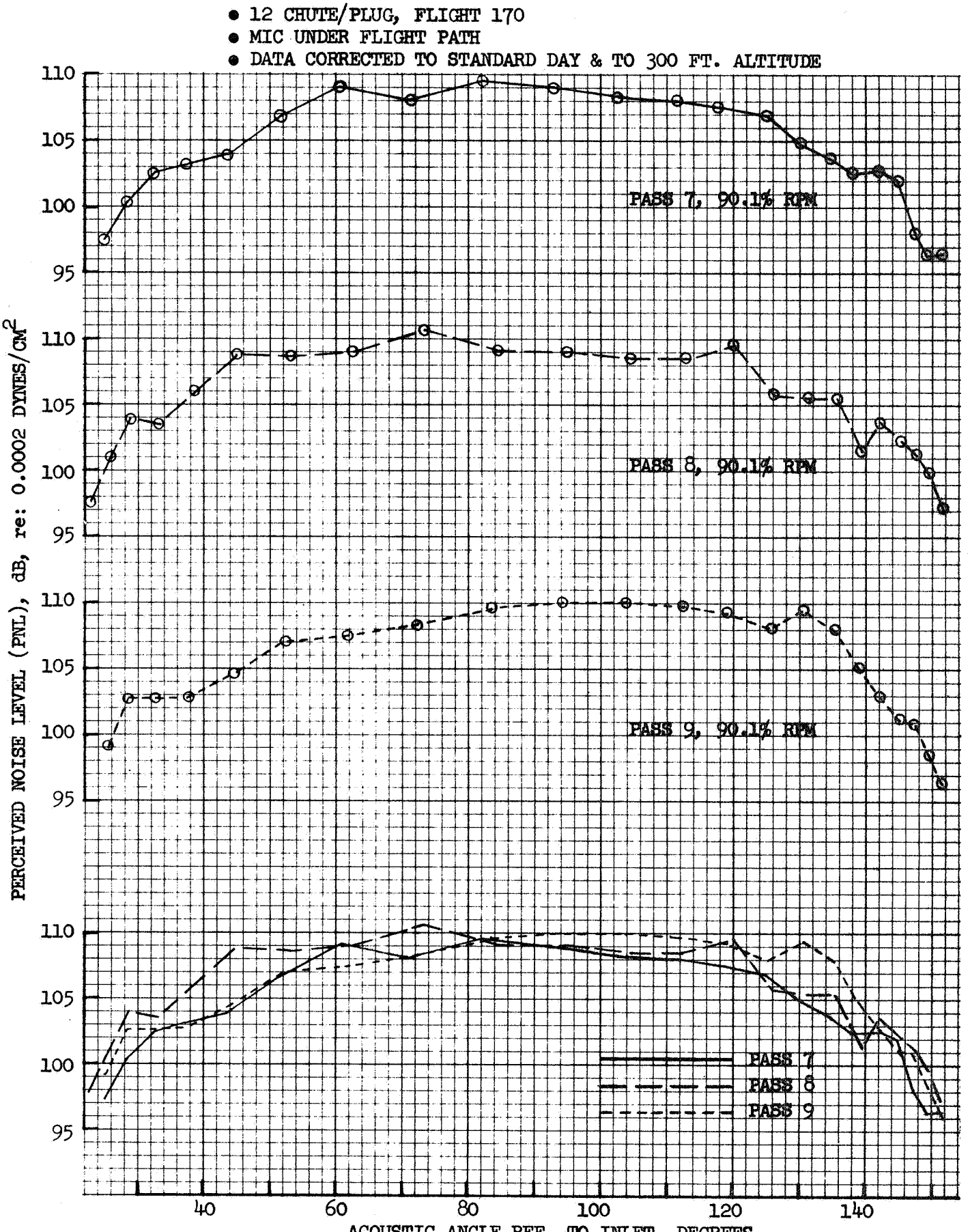

FIGURE 151 FLIGHT PNL, 12 CHUTE/PLUG, MIC UNDER FLIGHT PATH, CORRECTED DATA

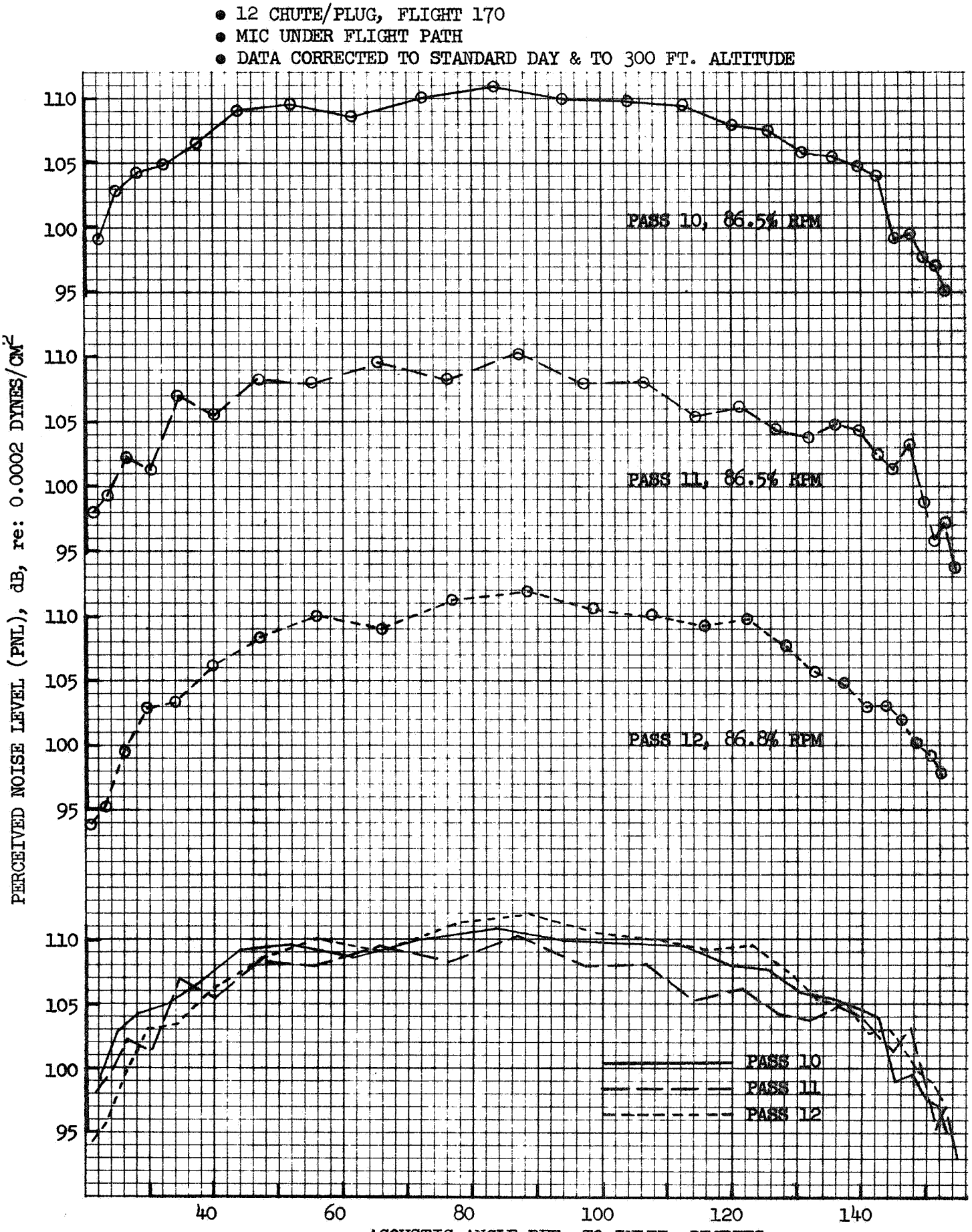

FIGURE 152 FLIGHT PNL, 12 CHUTE/PLUG, MIC UNDER FLIGHT PATH, CORRECTED DATA

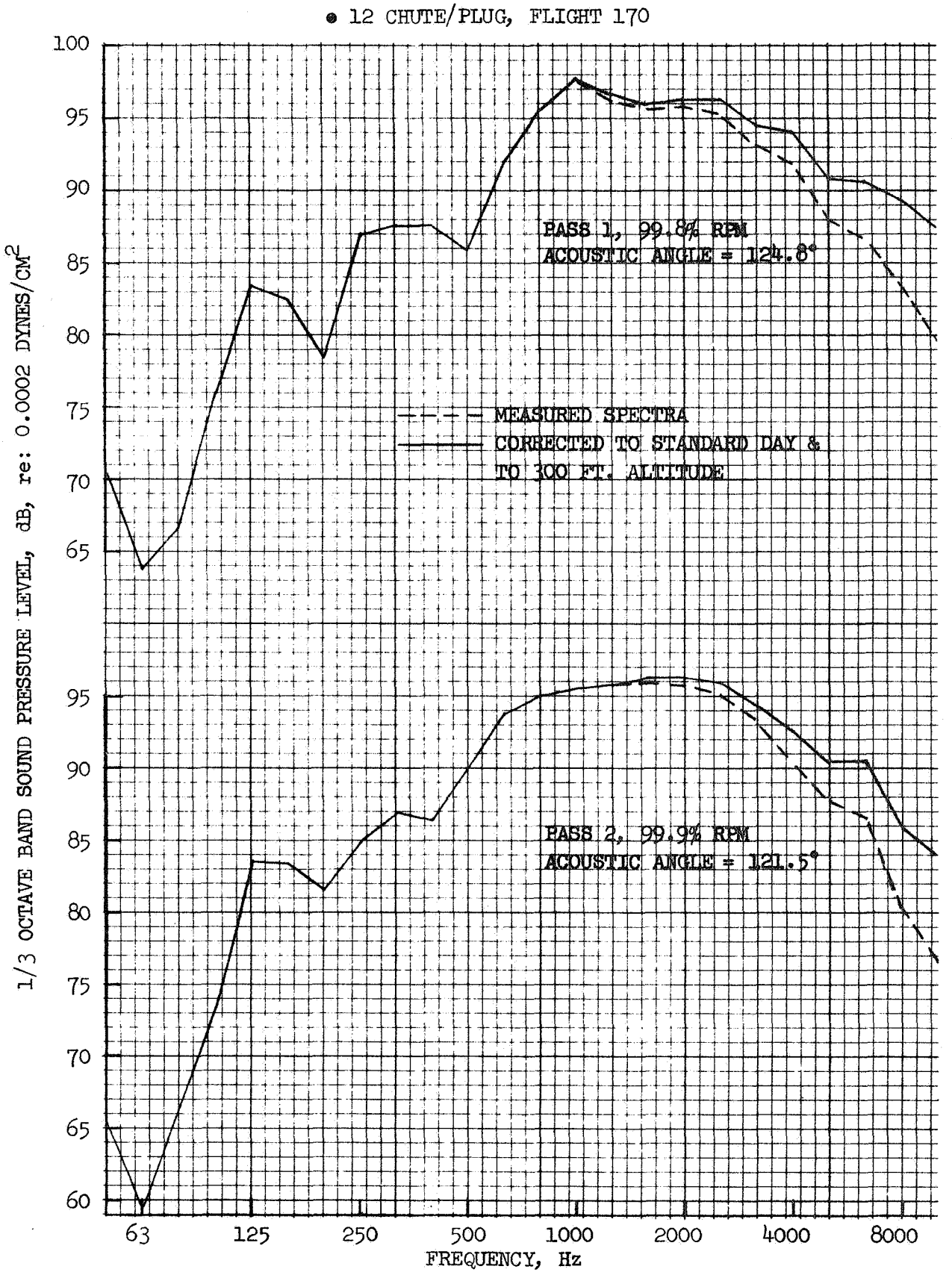

FIGURE 153 FLIGHT SPECTRA AT PEAK PNL, 12 CHUTE/PLUG, MIC UNDER FLIGHT PATH

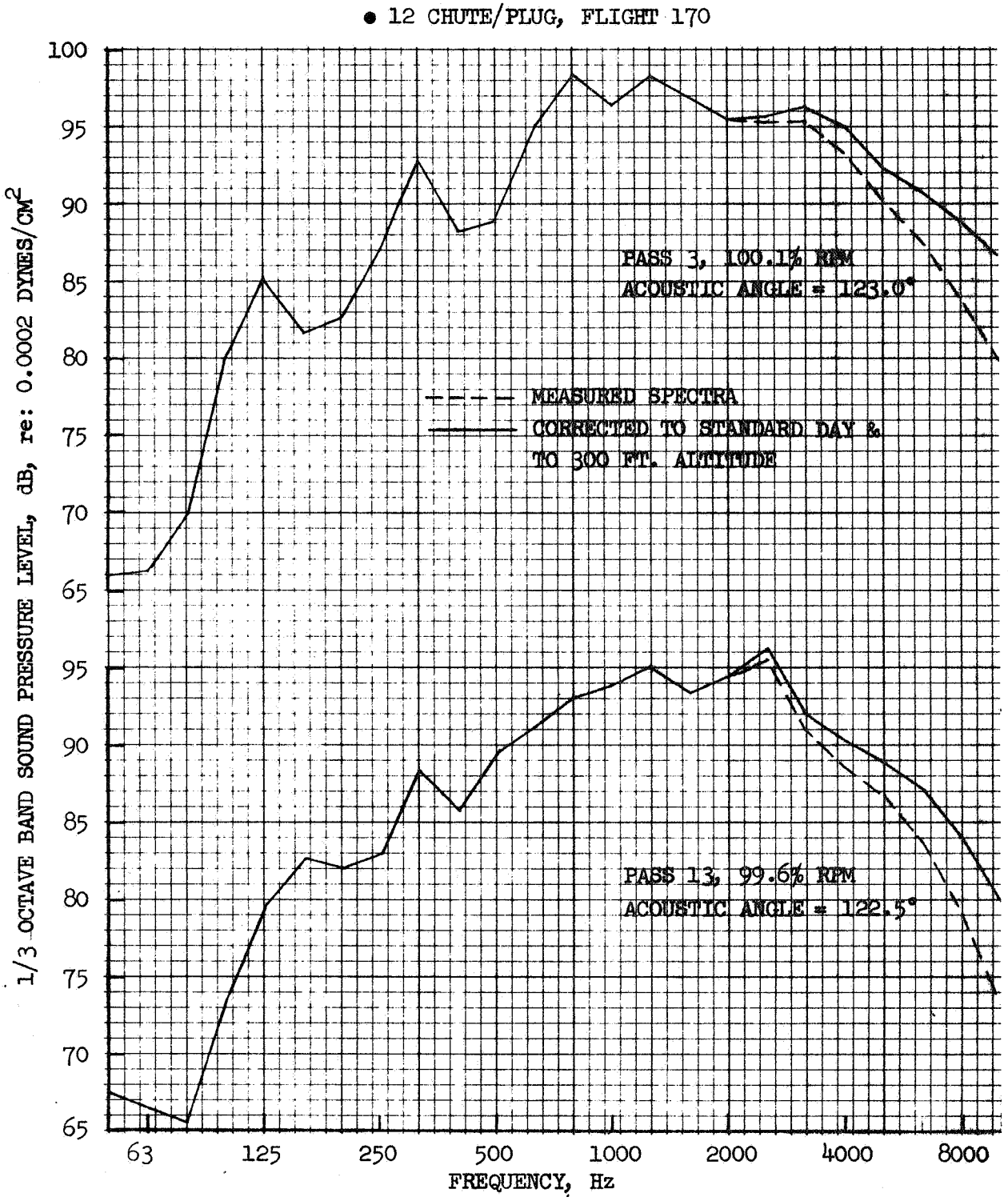

FIGURE 154 FLIGHT SPECTRA AT PEAK PNL, 12 CHUTE/PLUG, MIC UNDER FLIGHT PATH

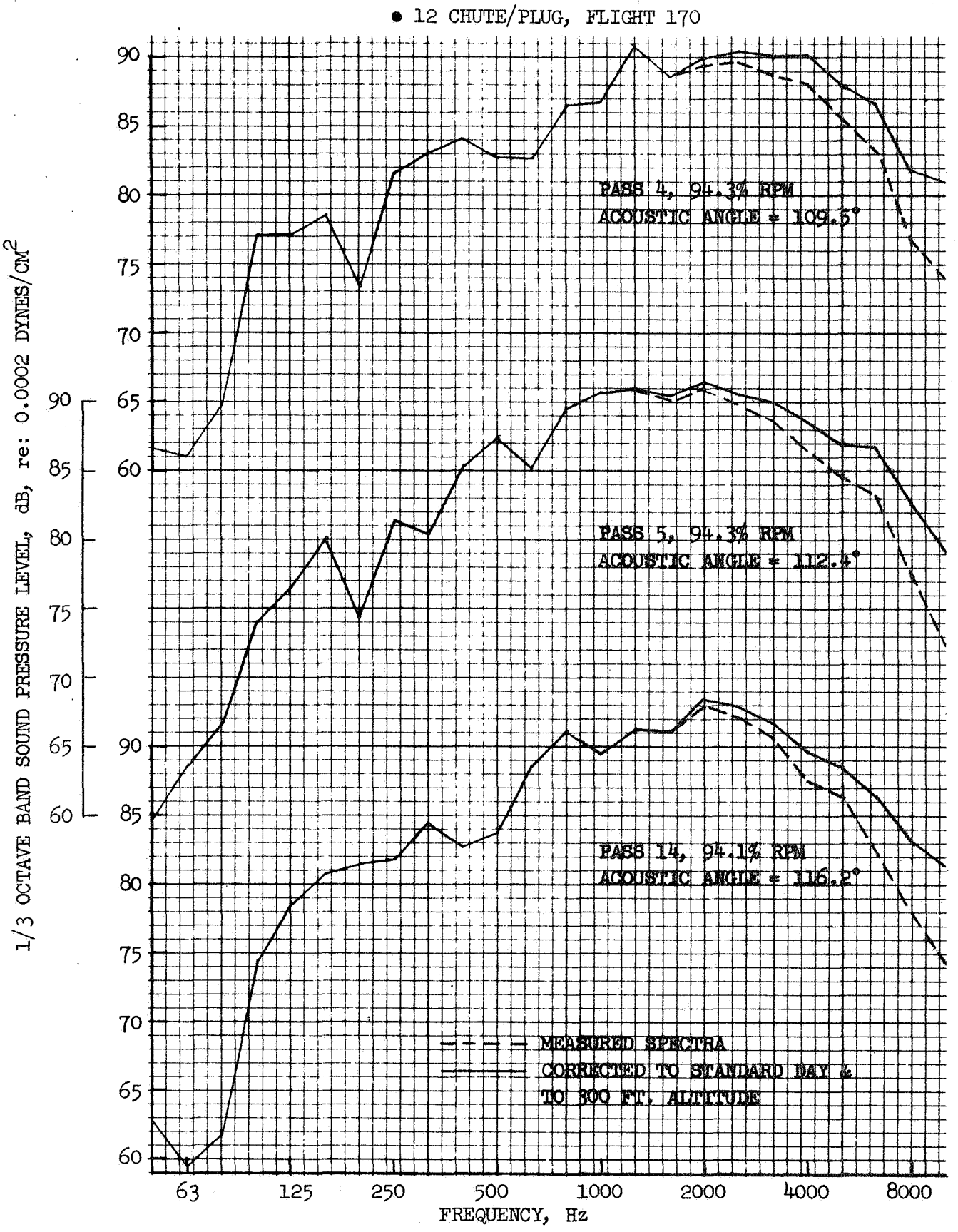

FIGURE 155 FLIGHT SPECTRA AT PEAK PNL, 12 CHUTE/PLUG, MIC UNDER FLIGHT PATH

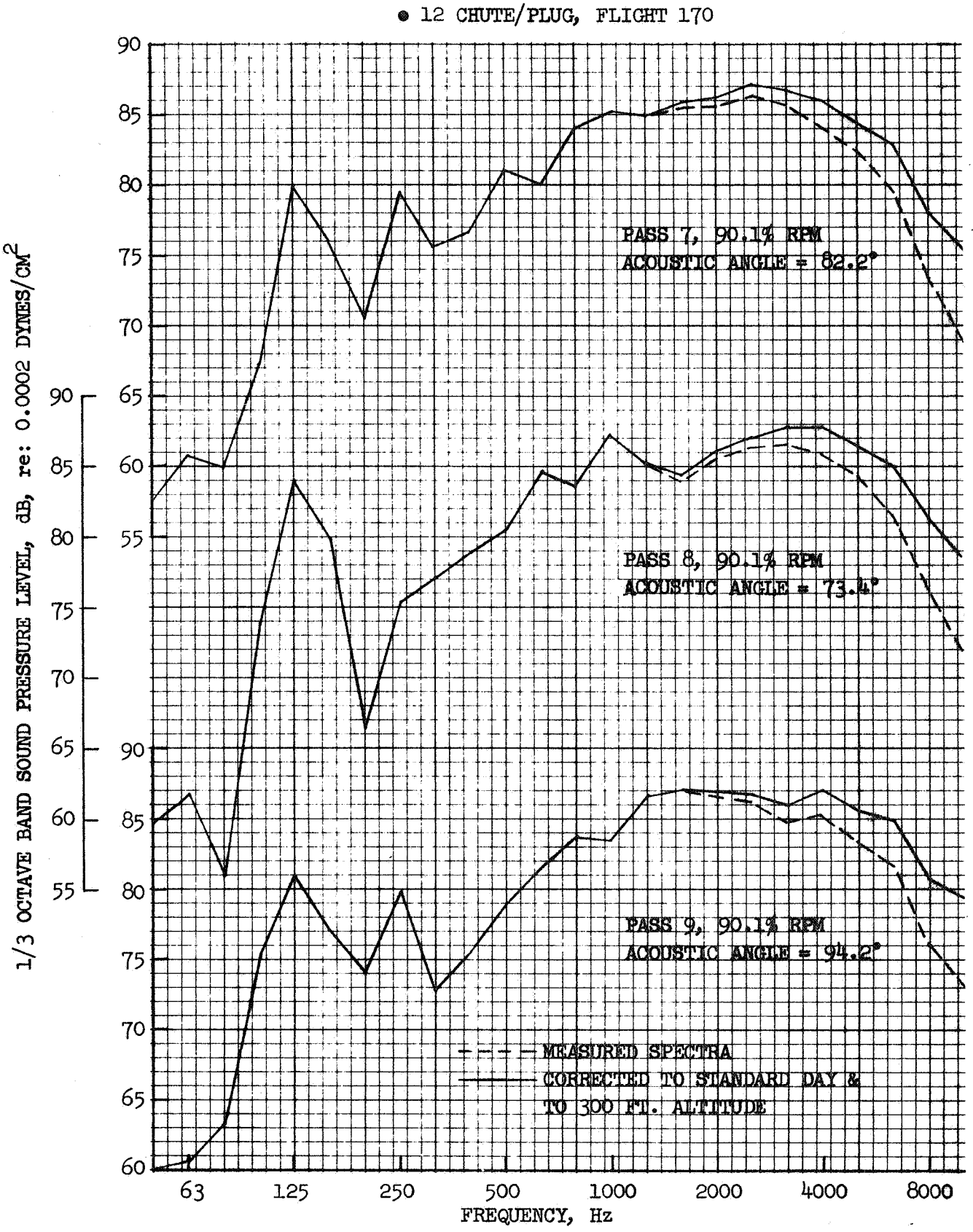

FIGURE 156 FLIGHT SPECTRA AT PEAK PNL, 12 CHUTE/PLUG, MIC UNDER FLIGHT PATH

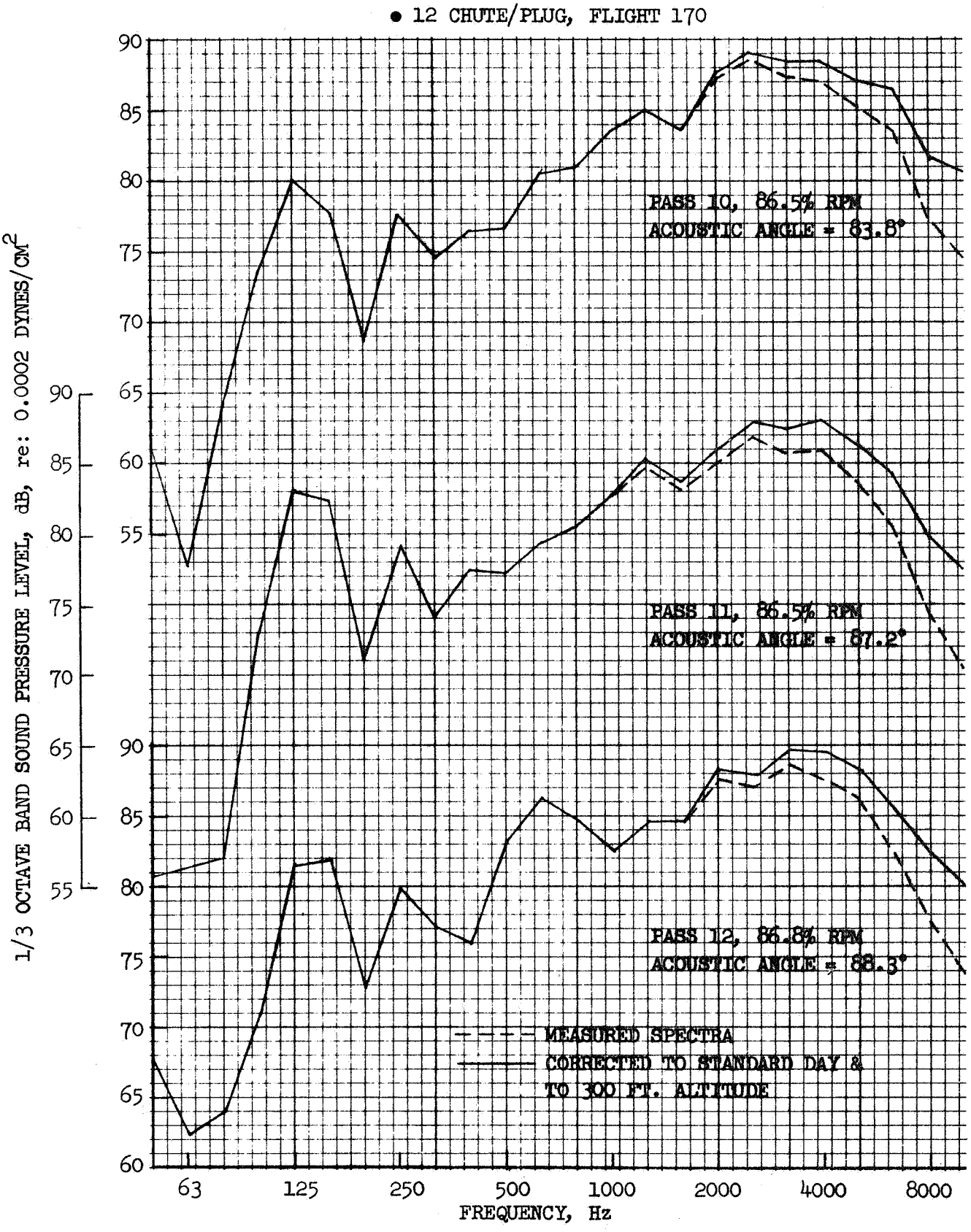

FIGURE 157 FLIGHT SPECTRA AT PEAK PNL, 12 CHUTE/PLUG, MIC UNDER FLIGHT PATH

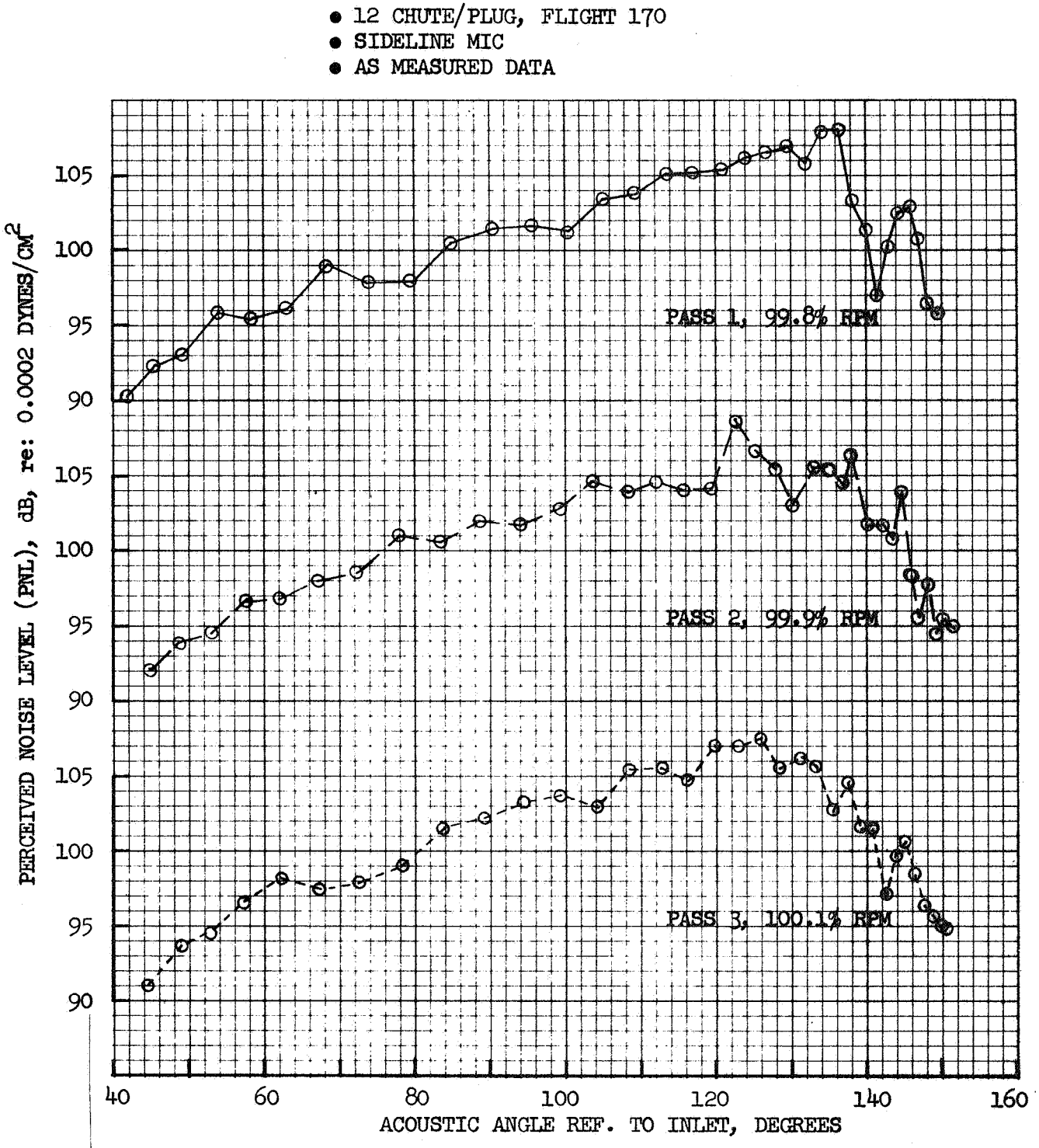

FIGURE 158 FLIGHT PNL, 12 CHUTE/PLUG, SIDELINE MIC, AS MEASURED DATA

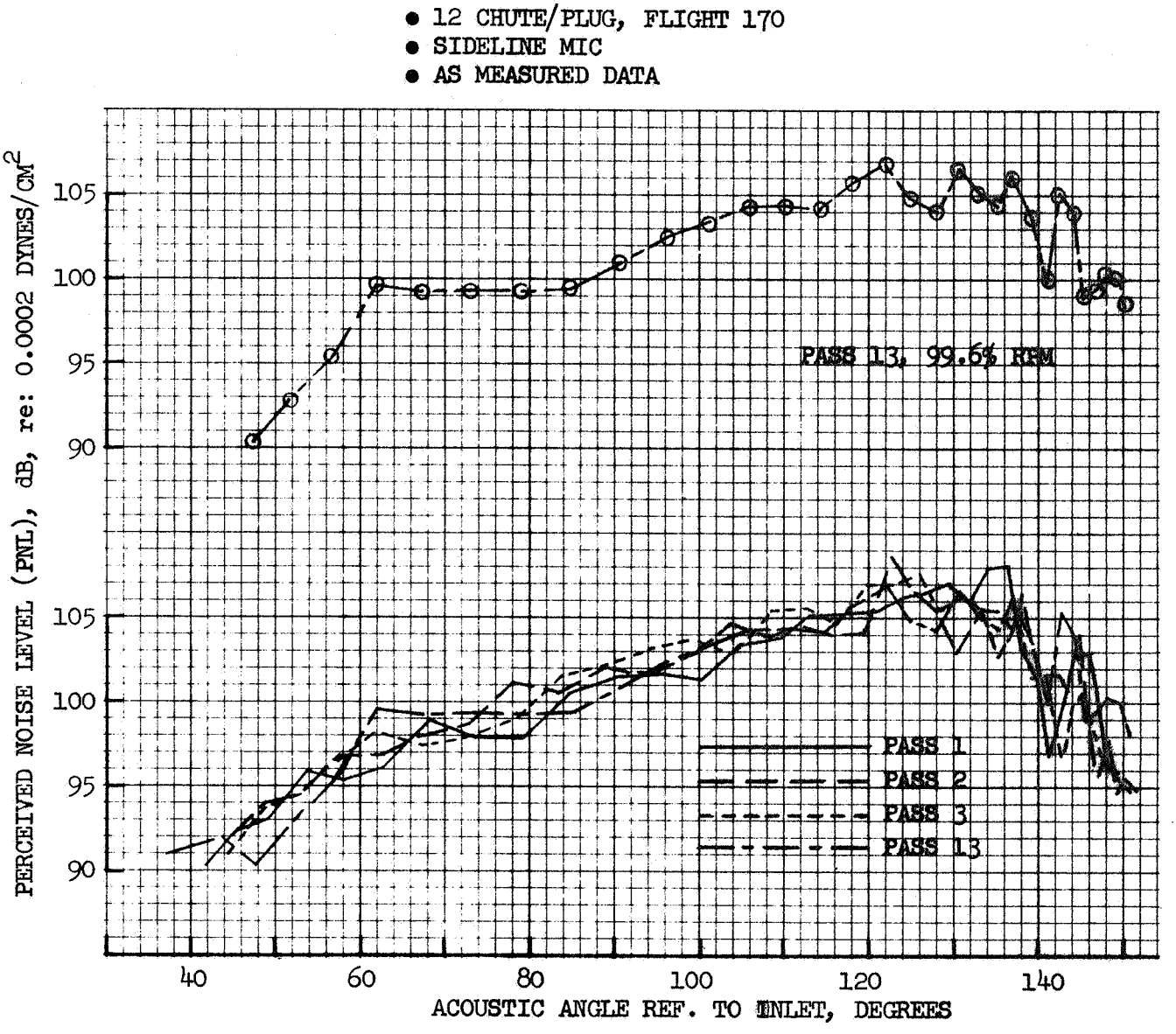

FIGURE 159 FLIGHT PNL, 12 CHUTE/PLUG, SIDELINE MIC, AS MEASURED DATA

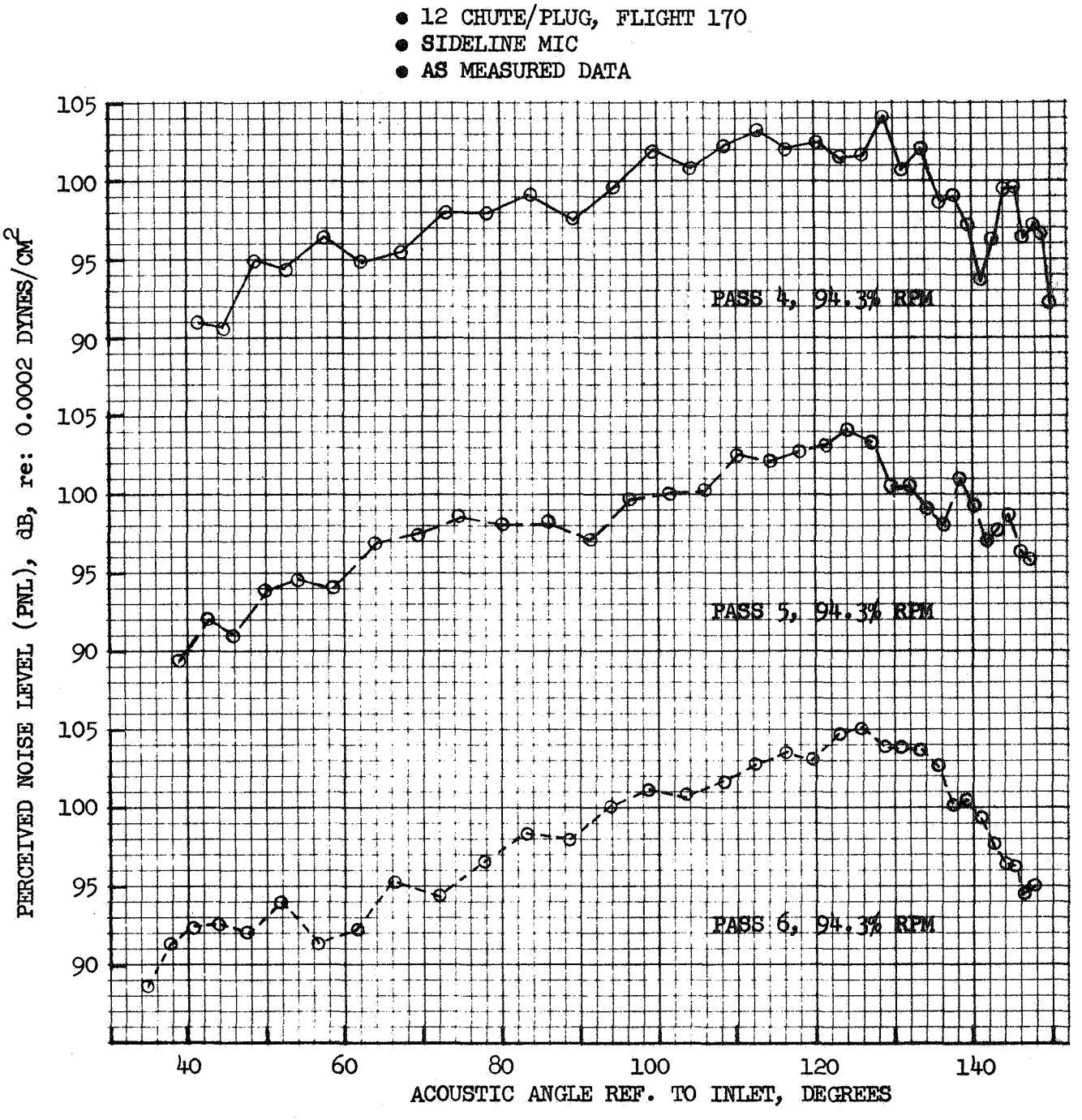

FIGURE 160 FLIGHT PNL, 12 CHUTE/PLUG, SIDELINE MIC, AS MEASURED DATA

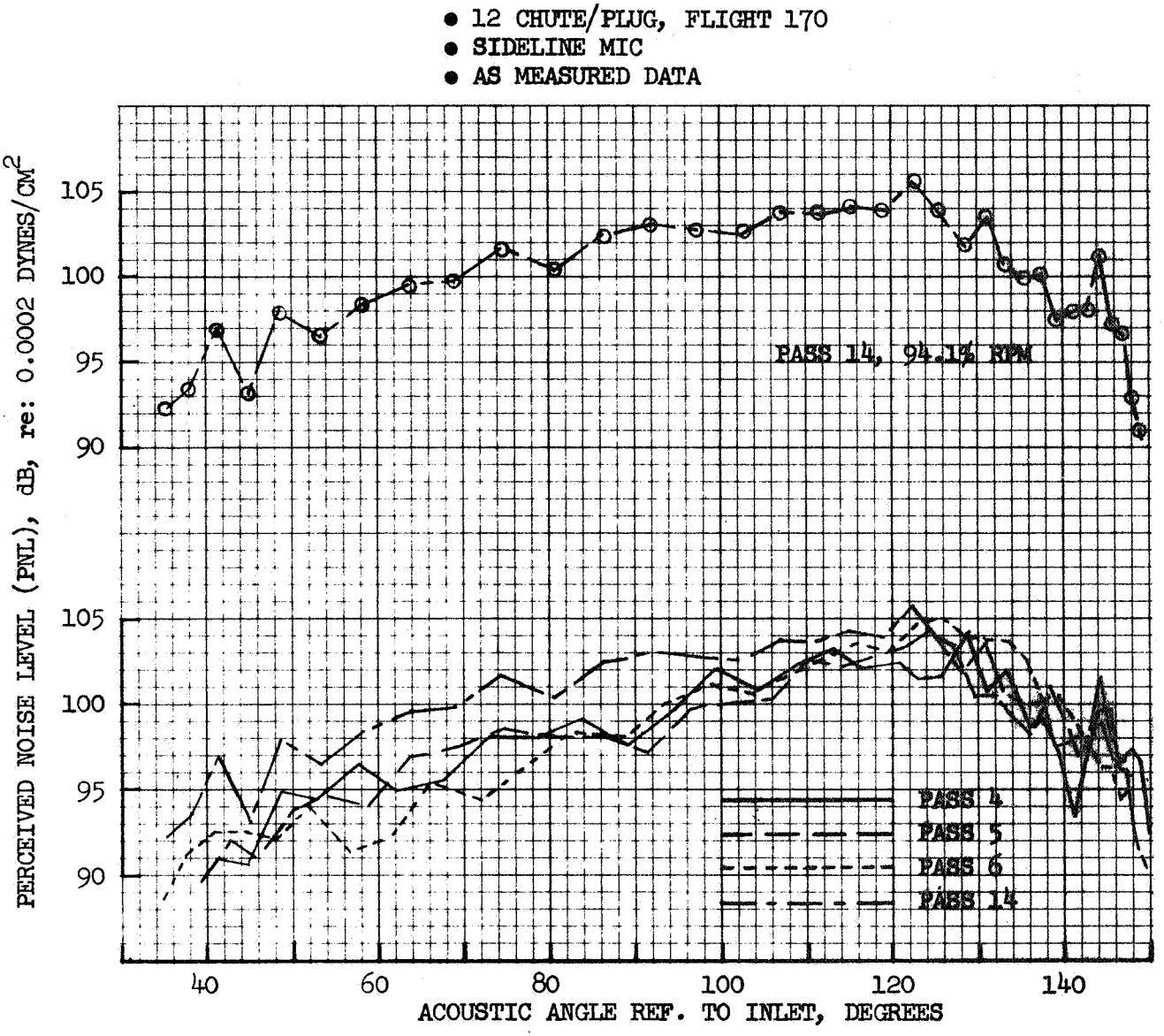

FIGURE 161 FLIGHT PNL, 12 CHUTE/PLUG, SIDELINE MIC, AS MEASURED DATA

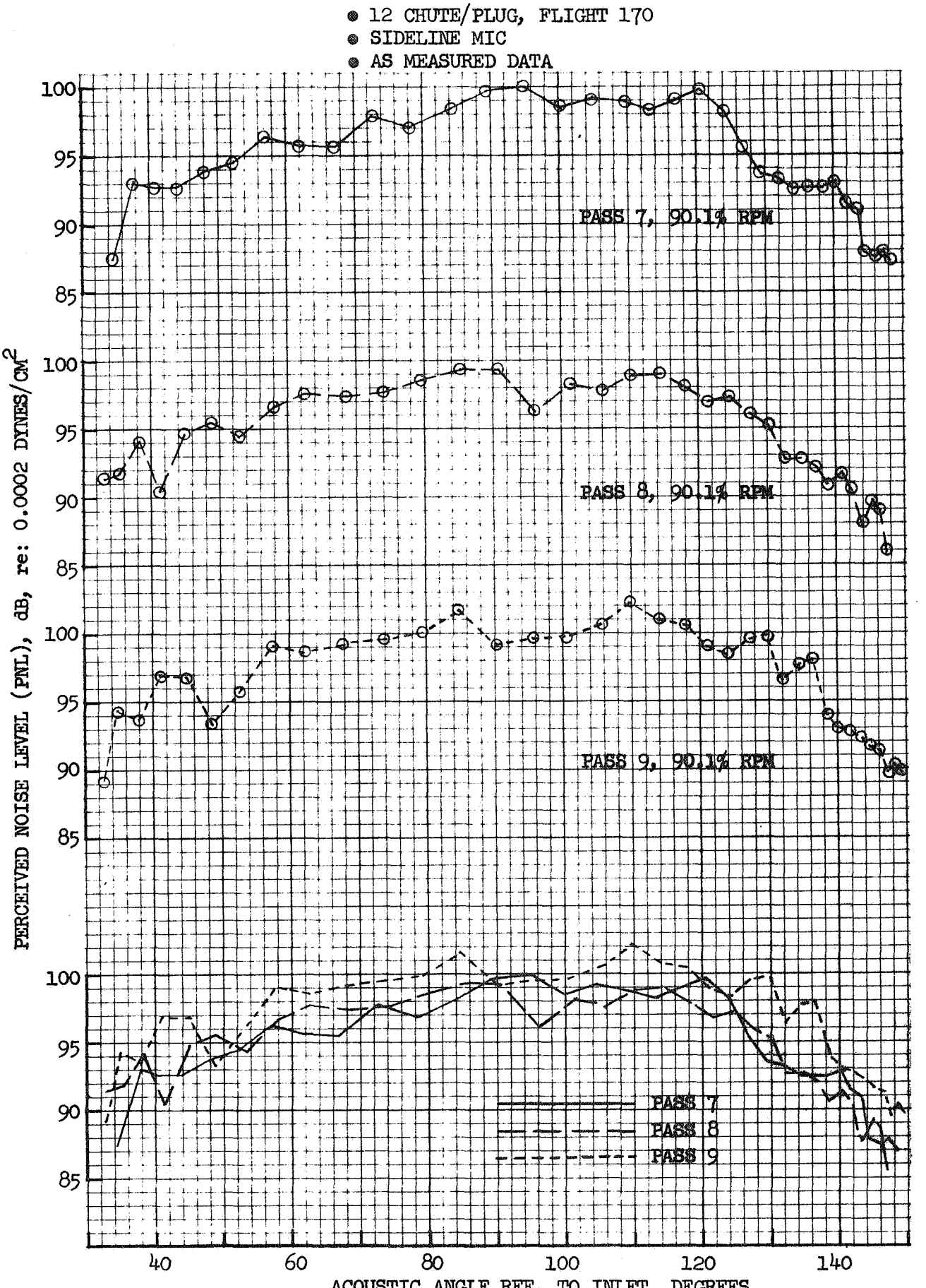

FIGURE 162 FLIGHT PNL, 12 CHUTE/PLUG, SIDELINE MIC, AS MEASURED DATA

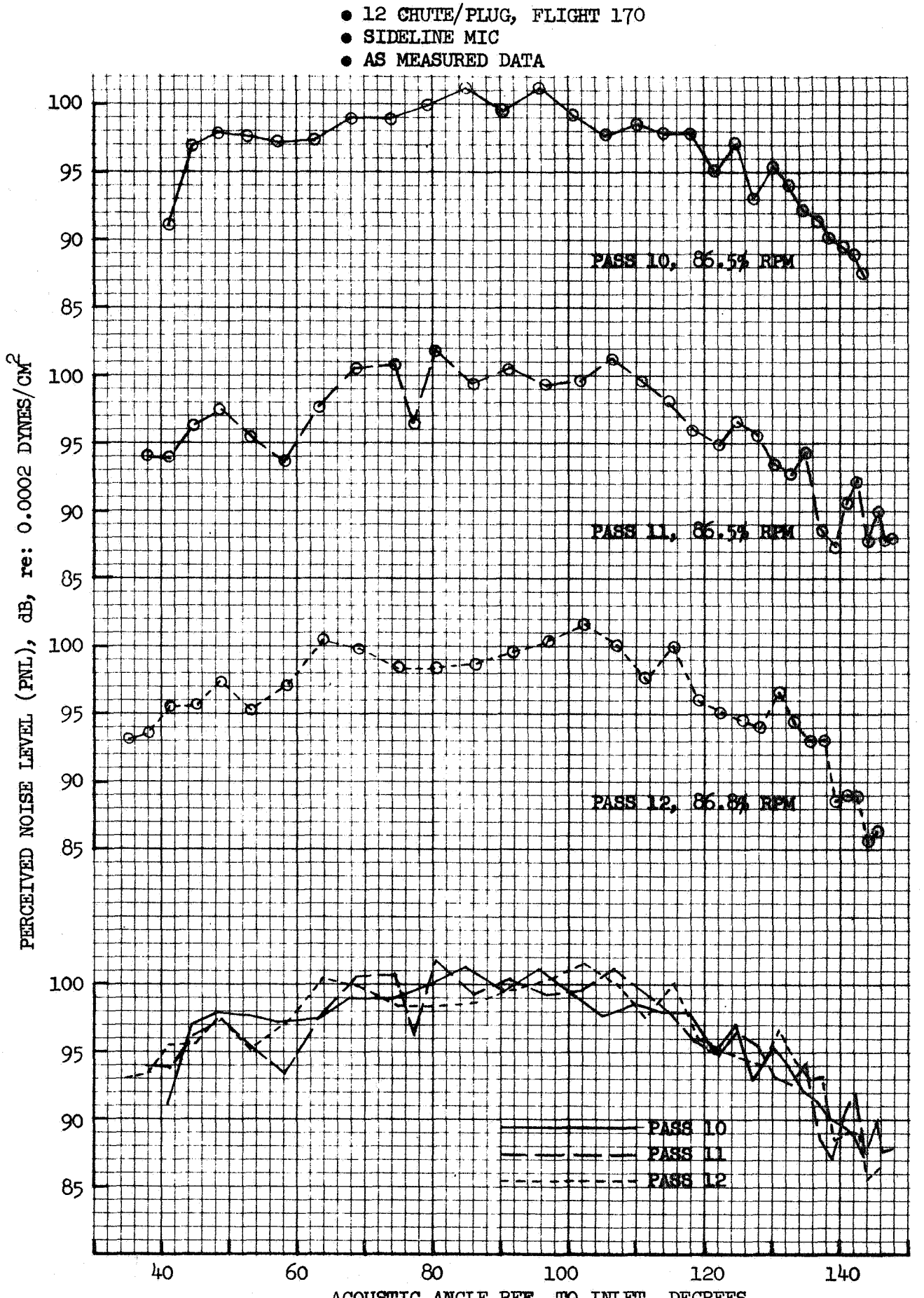

FIGURE 163 FLIGHT PNL, 12 CHUTE/PLUG, SIDELINE MIC, AS MEASURED DATA

DISCUSSION OF FLIGHT DATA

General observations from the flight data curves presented in Figures 89 through 163 are as follows:

- Repeatability of PNL histories, for multiple passes at the same engine speed, is normally very consistent; a good indicator of data reliability.
- The reference conical ejector has peak noise in the 150° to inlet area, closer to the jet exhaust than the peak of the static data. The suppressor nozzles have flatter directivity than the conical ejector with peak noise occurring at angles closer to the overhead location.
- Spectra are not as distinctly individualistic for each nozzle as ground static data were, however, characteristics such as double hump spectra or predominance of high or low frequencies are still discernable.
- The magnitude of correction to standard day and 300 ft. altitude are seen on the peak spectra plots, particularly the large corrections to high frequencies applied to the 32 and 64 spoke nozzles. On a PNL basis, comparison of as-measured to corrected data shows little change for the conical ejector nozzle and up to 3 and 4 dB change on the 32 and 64 spoke nozzles.

Peak OASPL, Peak PNL & EPNL

As was done for the ground static data, plots of flight peak OASPL, peak PNL and EPNL, all normalized, are presented in Figures 164 through 172. Figures 164, 165 and 166 are for as-measured under the flight path data. Figures 167, 168 and 169 are corrected data for the same mic. Figures 170, 171 and 172 are as-measured data for the sideline mic. All plots are done against relative velocity where $V_R = V_{jet} - V_{aircraft}$. To assess the data on a jet velocity basis, 438 feet/second should be added to the presented scale. Suppression levels, referenced to the conical ejector nozzle, are on the lower half of

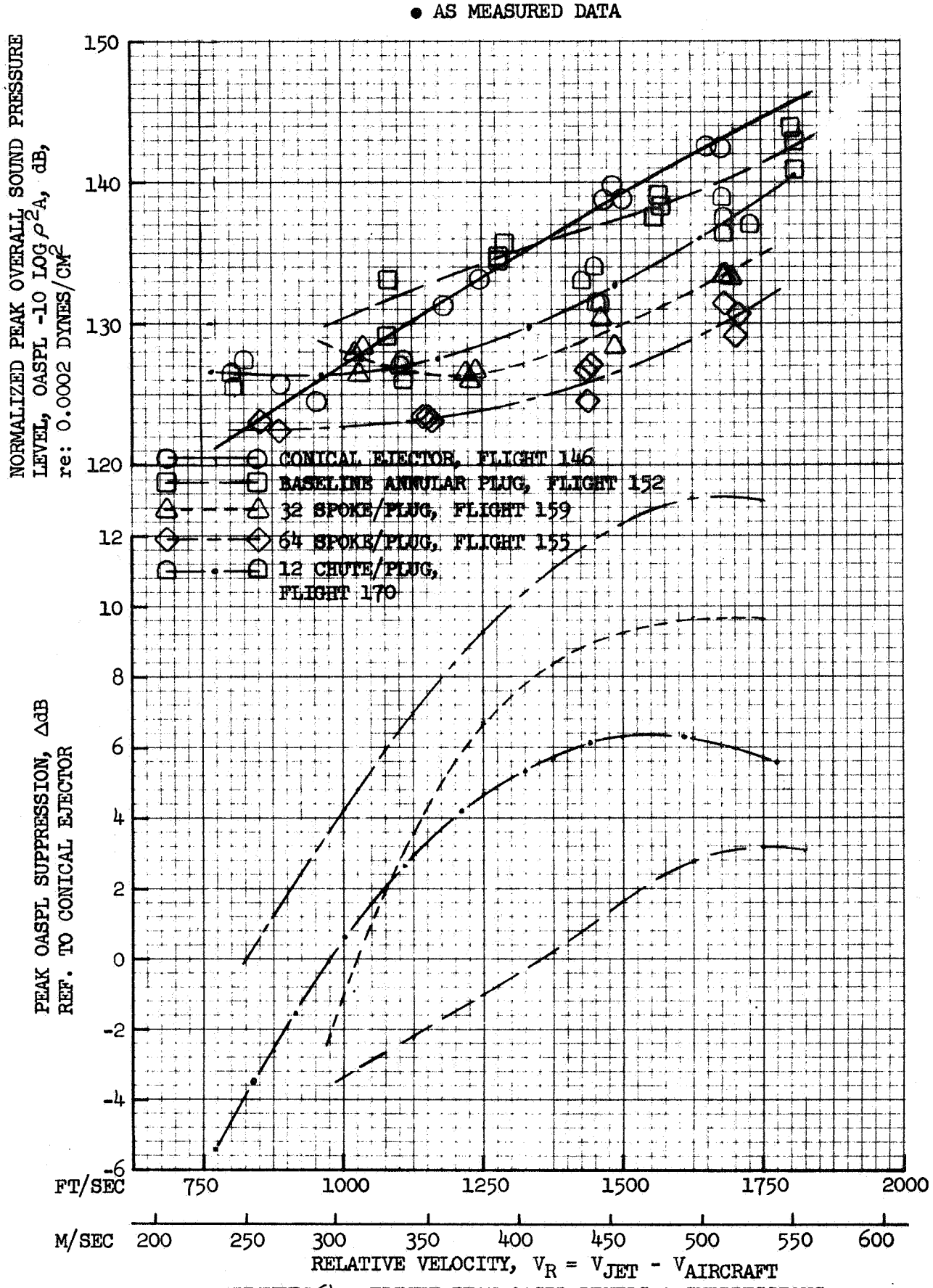

FIGURE 164 FLIGHT PEAK OASPL LEVELS & SUPPRESSIONS, MIC UNDER FLIGHT PATH

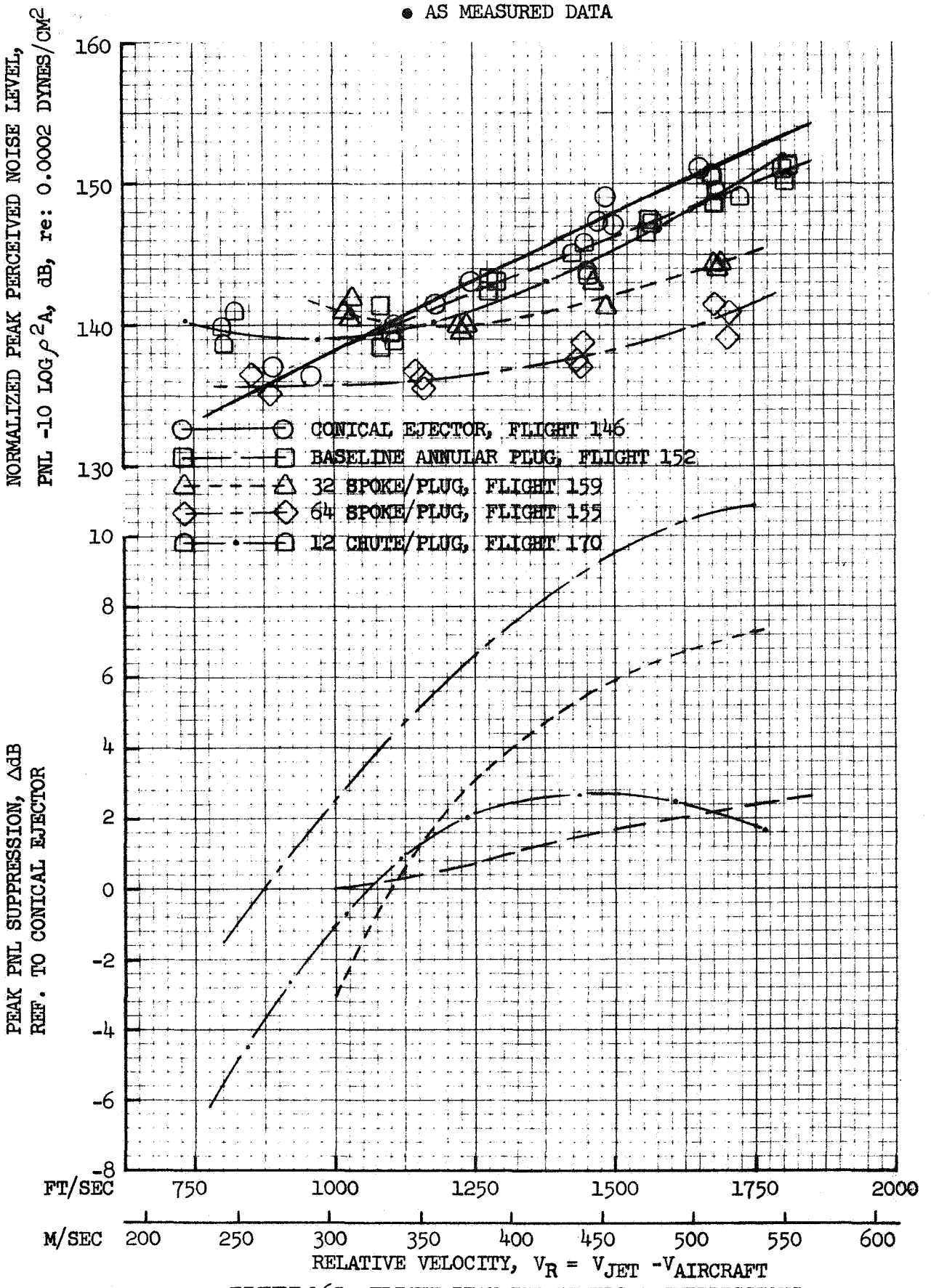

FIGURE 165 FLIGHT PEAK PNL LEVELS & SUPPRESSIONS, MIC UNDER FLIGHT PATH

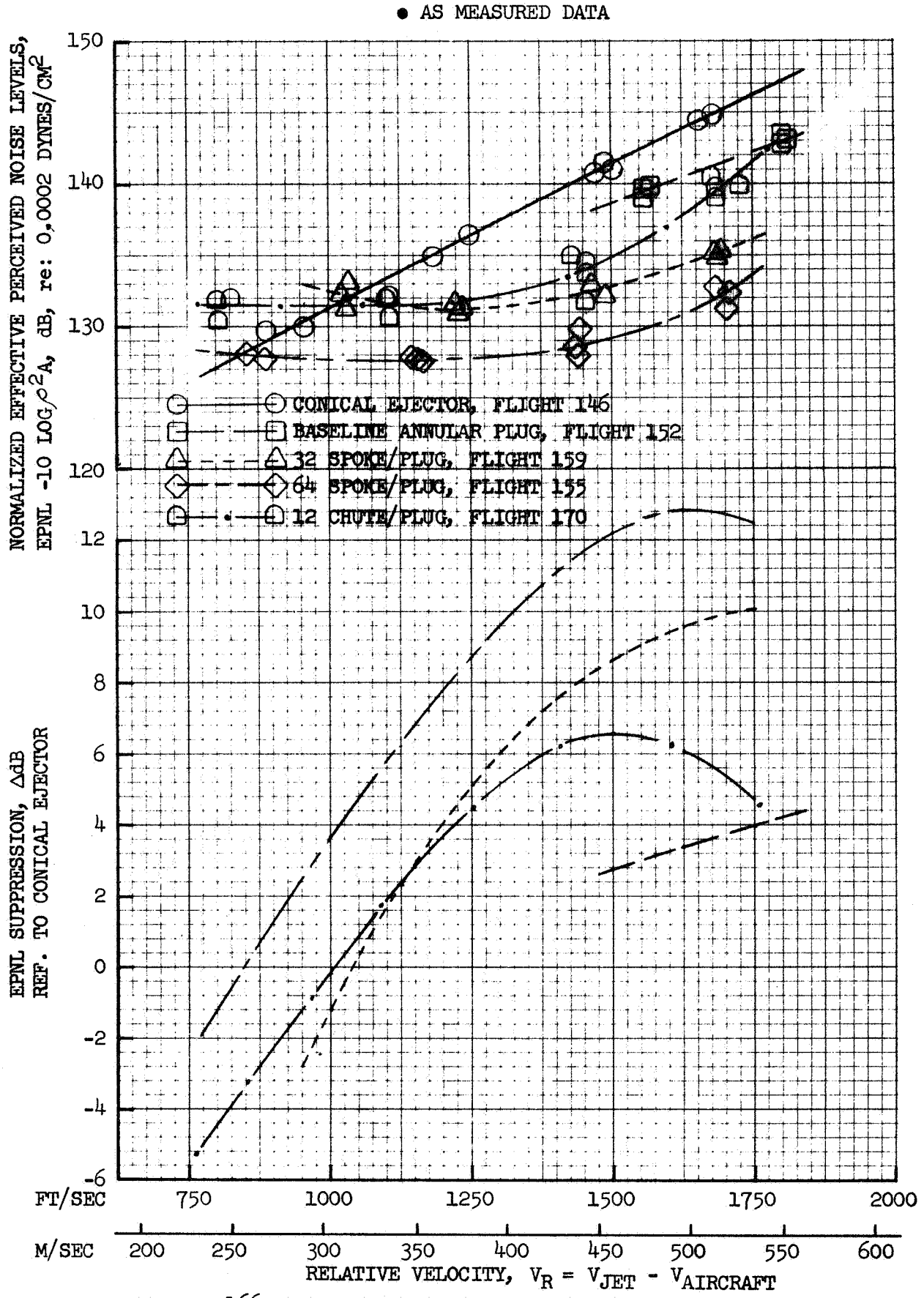

FIGURE 166 FLIGHT EPNL LEVELS & SUPPRESSIONS, MIC UNDER FLIGHT PATH

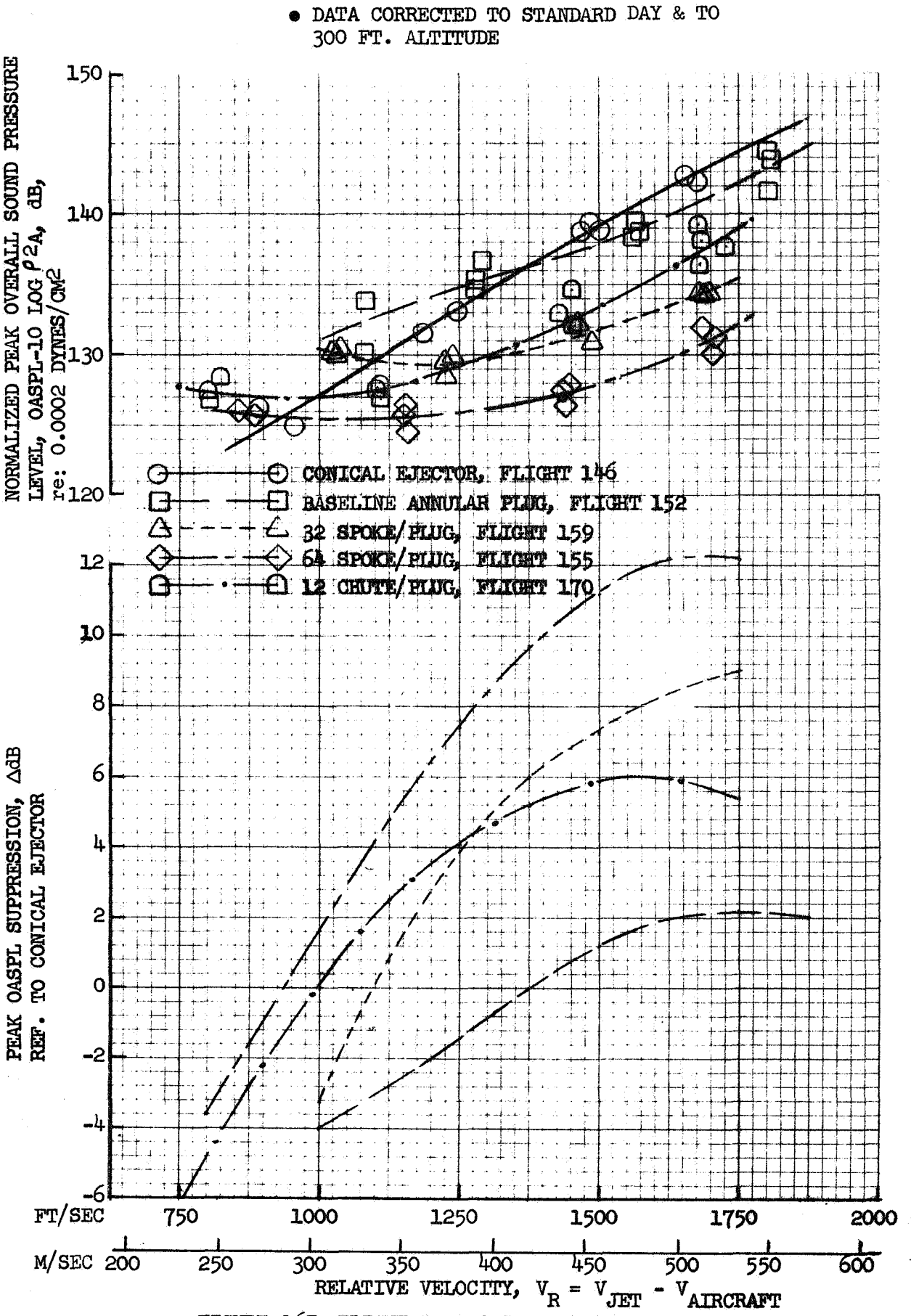

FIGURE 167 FLIGHT PEAK OASPL LEVELS & SUPPRESSIONS, MIC UNDER FLIGHT PATH

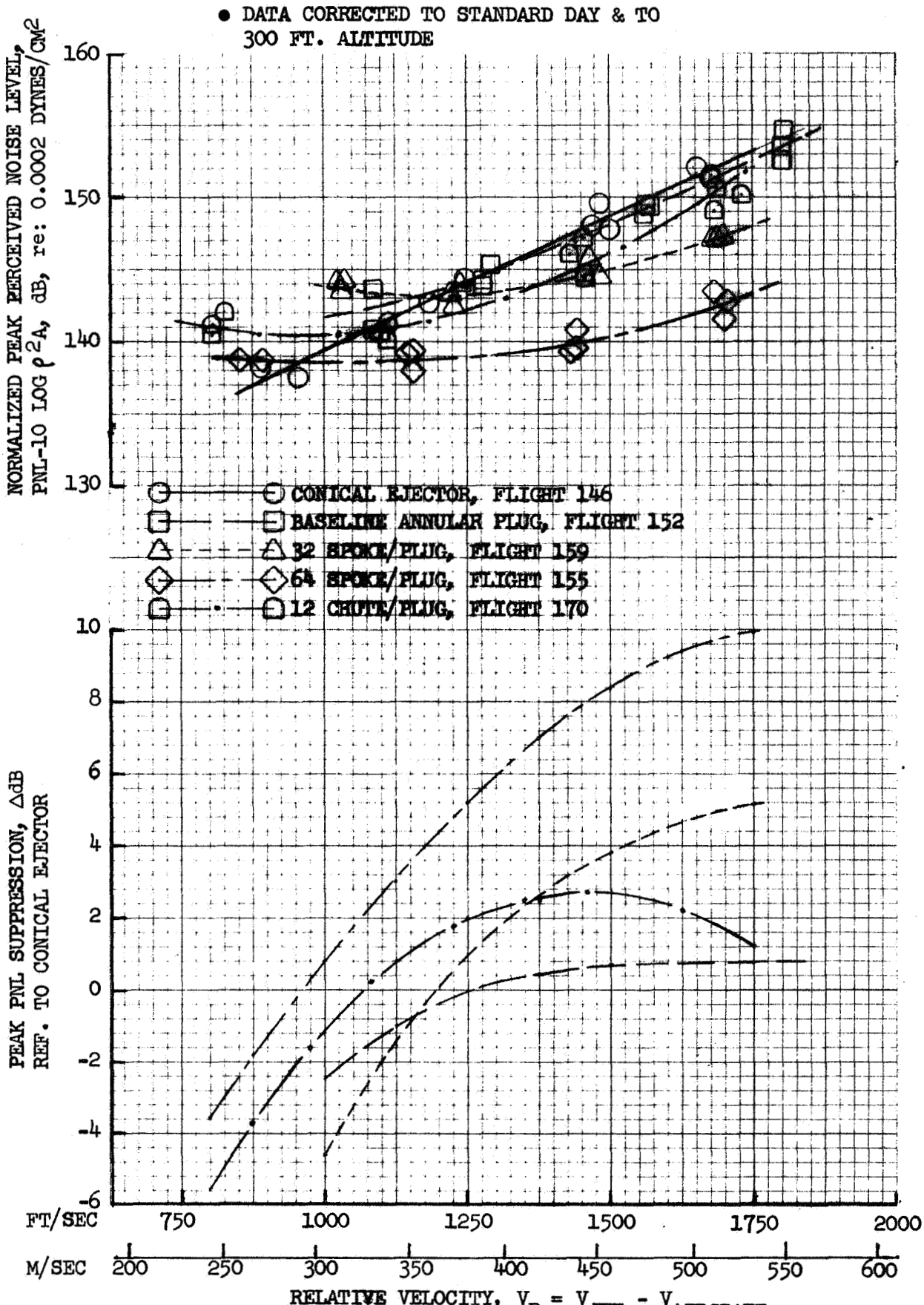

FIGURE 168 FLIGHT PEAK PNL LEVELS & SUPPRESSIONS, MIC UNDER FLIGHT PATH

● DATA CORRECTED TO STANDARD DAY, TO 300 FT. ALTITUDE & TO CONSISTENT FLIGHT SPEED

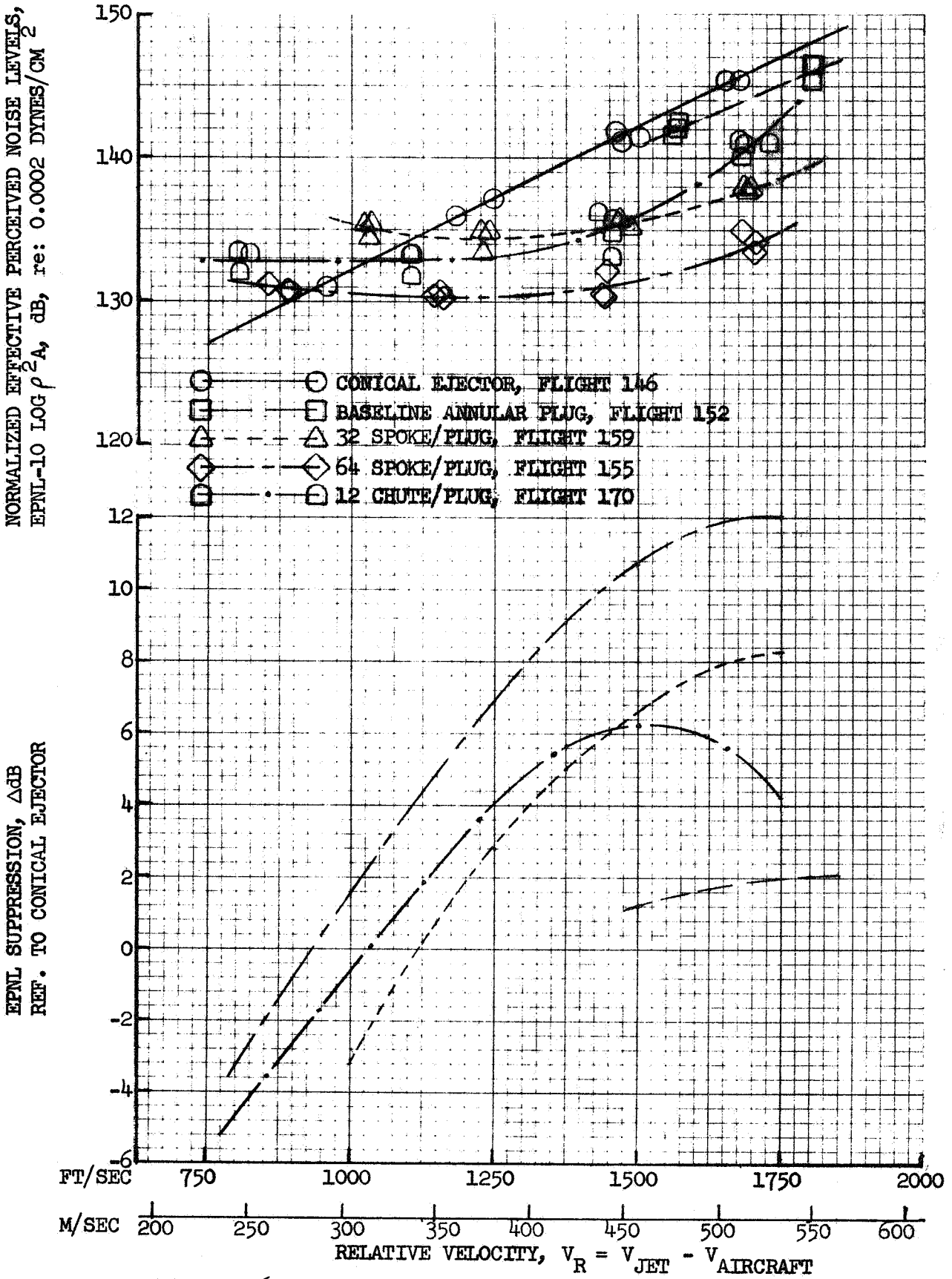

FIGURE 169 FLIGHT EPNL LEVELS & SUPPRESSIONS, MIC UNDER FLIGHT PATH

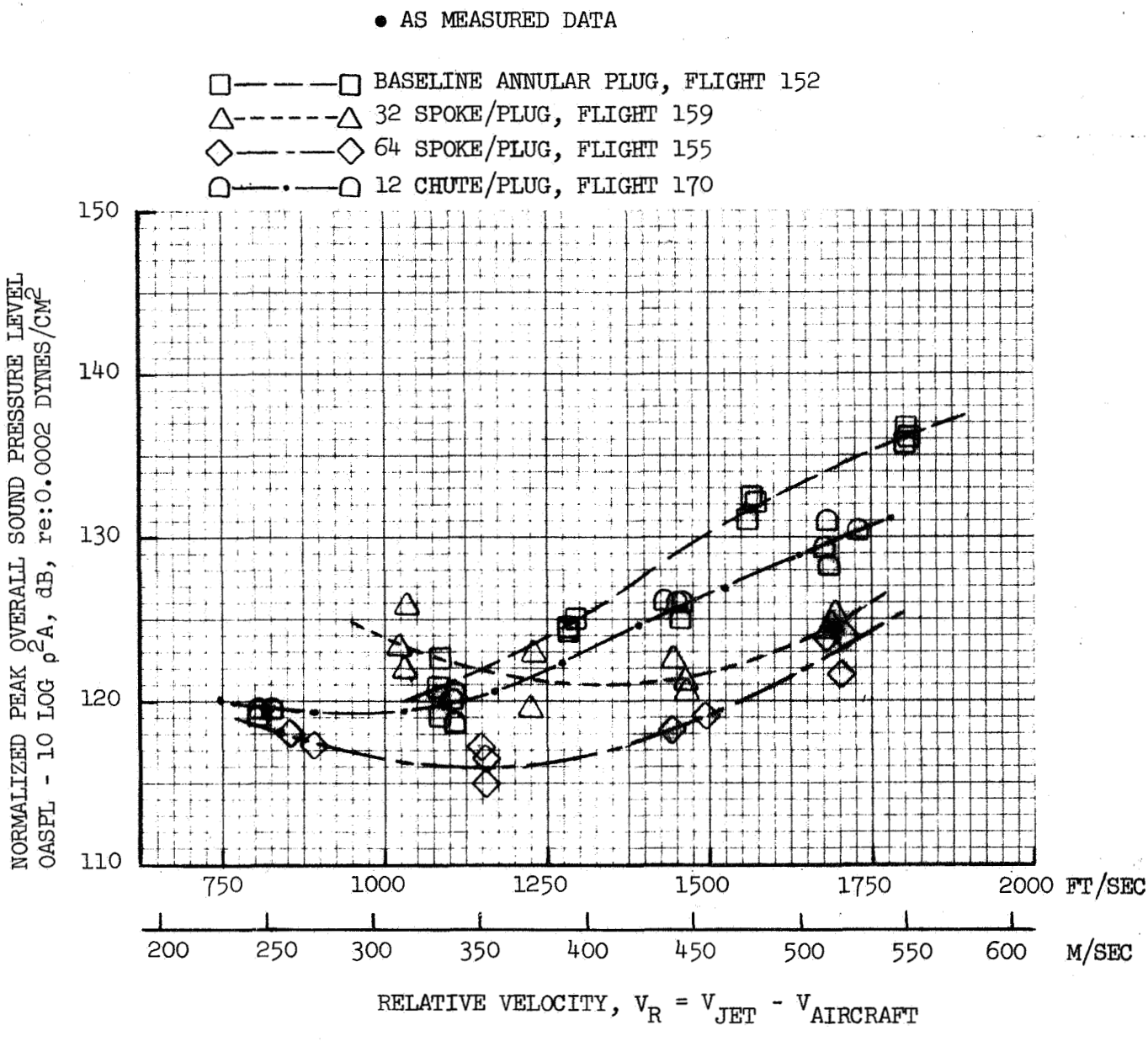

FIGURE 170 SUPPRESSED NOZZLES PEAK FLIGHT OVERALL SOUND PRESSURE LEVELS, SIDELINE MIC

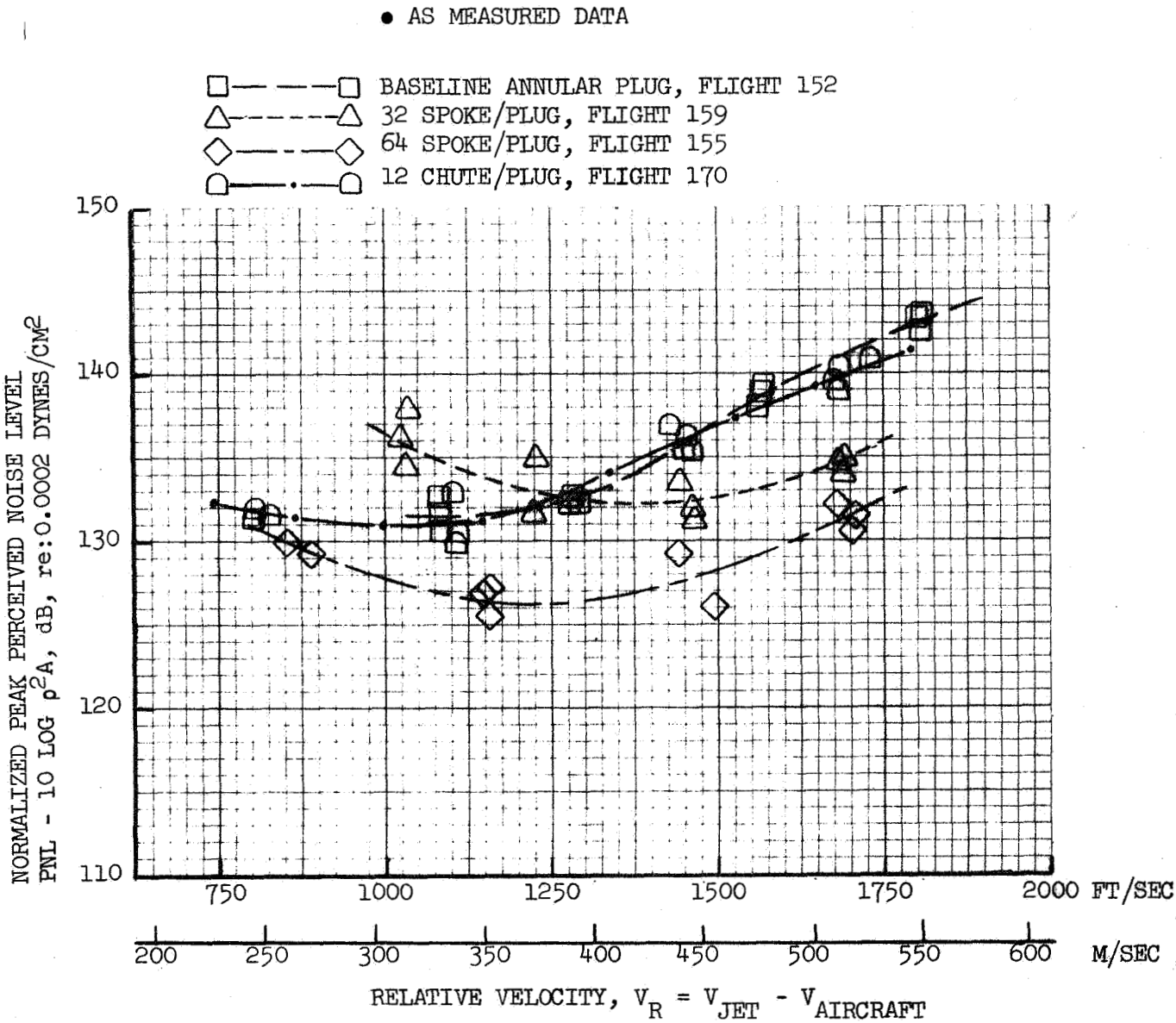

FIGURE 171 SUPPRESSED NOZZLES PEAK FLIGHT PERCEIVED NOISE LEVELS, SIDELINE MIC

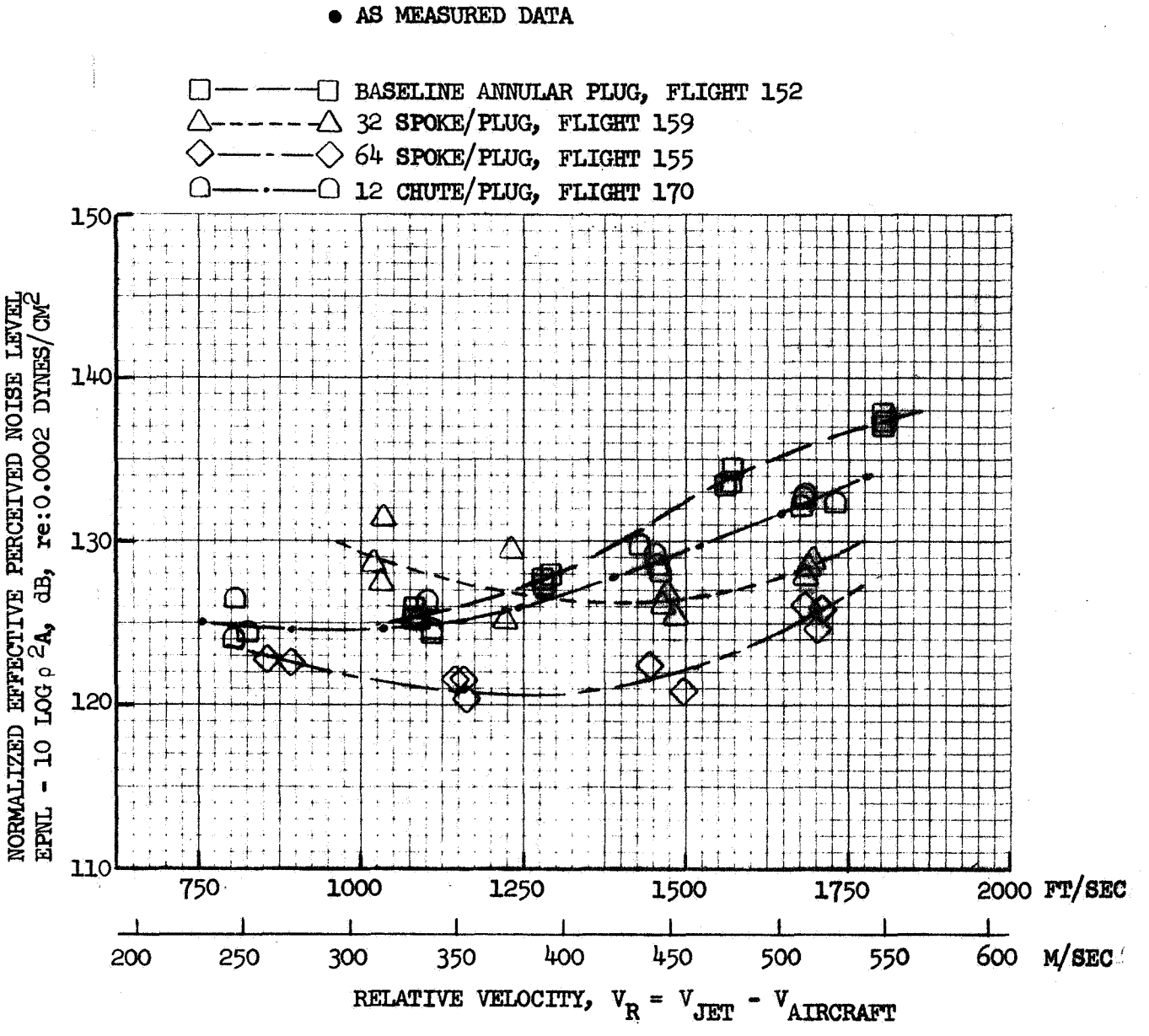

FIGURE 172 SUPPRESSED NOZZLES FLIGHT EFFECTIVE PERCEIVED NOISE LEVELS, SIDELINE MIC

each figure for flight line data. As no sideline data were available for the conical ejector in flight, the normalized levels are presented without suppression deltas in Figures 170 through 172.

Inspecting the curves supports the following remarks:

- Magnitude of attained suppression is a function of the parameter in question and the jet or relative velocity. At a given velocity the OASPL, PNL and EPNL suppressions were not the same for any selected nozzle.
- At maximum dry engine setting, high suppression levels are seen for the 32 and 64 spoke nozzles, 7 to 13 ΔdB, depending on the parameter. The 12 chute/plug shows medium suppression, 3 to 6 Δdb, and the baseline plug has about 2 ΔdB suppression.
- As engine speed is decreased, suppression drops off rapidly, the suppressor nozzles becoming noisier than the reference nozzle at lowest speeds.
- Within the range of jet velocity of the J85 cycle to max. dry, the 32 and 64 spoke suppressors may not have attained their peak suppression. This is suggested by the slope of the curves in Figures 165 and 168. The baseline plug nozzle suppression is fairly flat (Figure 168) and probably has reached its peak level. The 12 chute/plug nozzle has attained its peak PNL and EPNL suppression level and is decreasing at max. dry velocity.
- Comparing the as-measured data to corrected data shows attained suppressions to be lower for the corrected data, exact amount varying with each nozzle and with velocity. This delta is due primarily to the lesser magnitude of correction applied to the conical ejector data than to the suppressor nozzles to bring it to standard day. PNL suppression is changed more than OASPL suppression since the corrections are applied to the high frequency region which more heavily influences PNL due to annoyance weighting.

- Comparing the peak PNL and EPNL suppressions (Figure 168 versus 169) shows that all the nozzles experienced greater EPNL suppression than peak PNL suppresssion when referenced to the conical ejector. Each nozzle also had a larger gain at high velocity than at low velocity. The 64 spoke gained 2 ΔdB at high V_R but none at low V_R. The 32 spoke gained 3 ΔdB at high and 1 ΔdB at low V_R. The 12 chute gained 3 ΔdB at high and .5 ΔdB at low V_R. The baseline plug gained about 1 ΔdB at high V_R.

The influence allowing the additional EPNL suppression is the more favorable PNL (or PNLT) directivity patterns of the suppressed nozzles. The conical ejector nozzle has a PNL directivity pattern which peaks near the exhaust axis (about 150° to the inlet) and has a long duration time for the range of 10 dB down from the peak noise. The suppressor nozzles have a much flatter PNL directivity pattern with peak jet noise occurring much closer to the overhead position and with fast drop off of jet noise at angles nearer the jet exhaust axis. These are shown in Figure 173 for the conical ejector, 32 and 64 spoke nozzles at 101 and 91% corrected speed settings for the upper and lower curve sets, respectively. The time duration of noise within the range of 10 dB down from peak is longer for the conical ejector nozzle than for the suppressors. Duration correction is therefore less favorable for the conical ejector and a smaller delta from peak PNL(PNLT) to EPNL is applied. Thus a favorable EPNL suppressor should have peak noise near the overhead position and quick drop off characteristics of jet noise, leading to short time duration of noise within the 10 dB down range.

- MIC UNDER FLIGHT PATH
- DATA CORRECTED TO STANDARD DAY & TO 300 FT. ALTITUDE

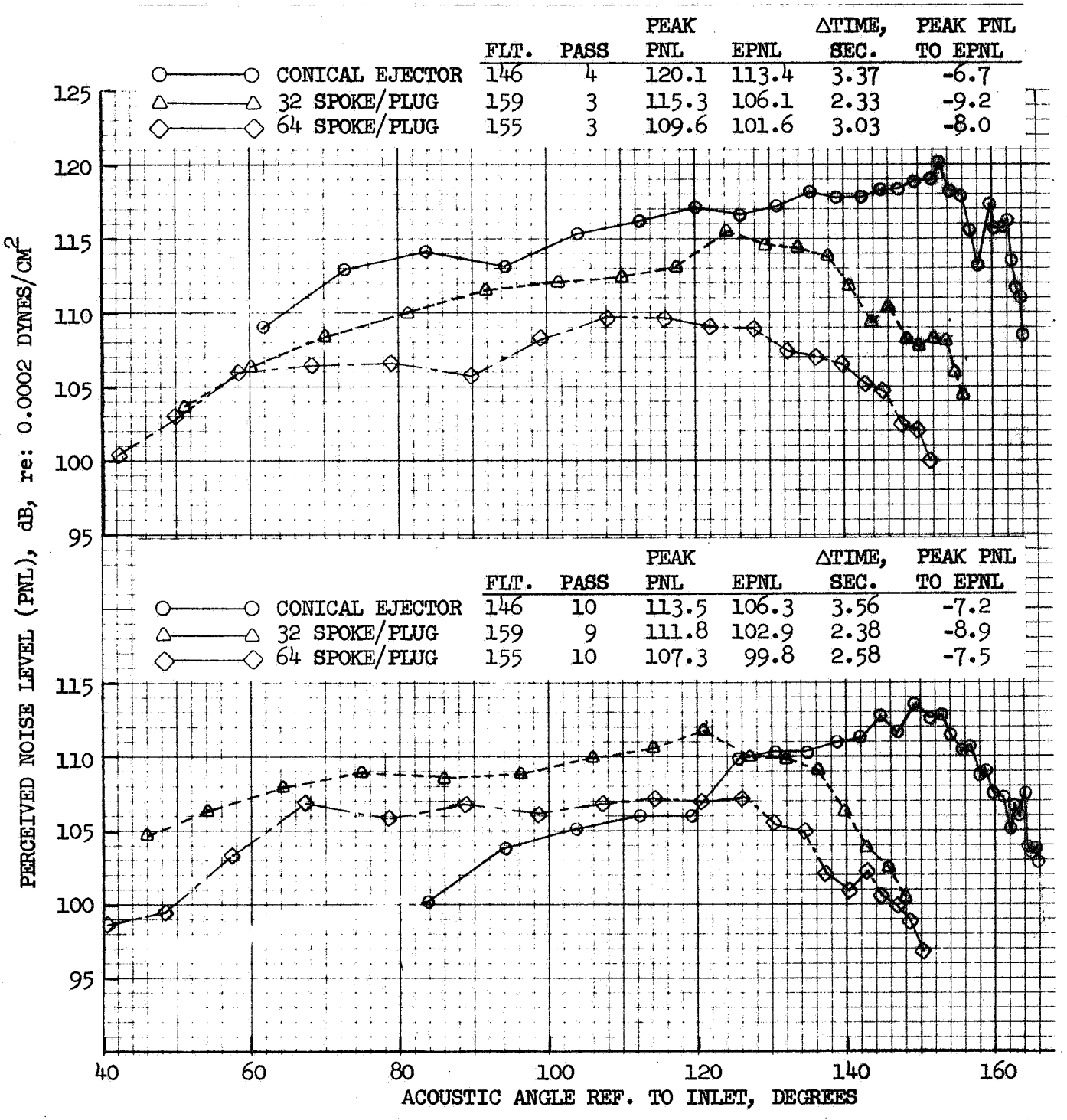

FIGURE 173 COMPARISON OF PNL HISTORIES TO EXEMPLIFY EFFECT ON EPNL

THRUST MEASUREMENTS AND RESULTS

Thrust and thrust minus drag measurements were taken for static and flight tests on all the nozzles. The results are presented in Figures 174 and 175 for static and flight respectively, in the form of installed gross thrust coefficient, defined as measured thrust or thrust minus drag divided by ideal thrust. The thrust data were supplied directly by NASA as reduced from their aircraft recorder measurements and corrected as necessary for secondary flow. For static measurements, several readings were taken during each acoustic test point and individual data points are shown. Those data points flagged in Figure 174 were measured while using the external cooling air from the air start cart. They are identified, as no calculated correction was possible for effects of the cooling air. The flight measurements are presented as curves derived from cross plots of measurements with variable secondary weight flow. The data have been corrected to a common 6% corrected secondary weight flow.

In general the spoke nozzle aerodynamic performance was low, as anticipated, since they were chosen only as characteristic nozzles for generating typical acoustic data. No refinement was done to these nozzles to obtain optimum performance. Other configurations within the model parametric study performed with much lower thrust losses. In addition, means have been identified to substantially improve aerodynamic performance while maintaining high suppression levels. The 32 spoke performance is within $\pm$ 1% of anticipated results from model static and wind tunnel tests.

The conical ejector performance was quite low due to the presence of the ejector. The thrust loss for segmented suppressors is normally higher in flight than for static tests due to lower base pressure on the suppressor elements. The abrupt turn angles required of the flow over the outer shroud and down the back side of the spoke are more difficult to maneuver with external flow and base pressures become lower contributing to higher total loss. Chutes entrain air more efficiently and substantially reduce base drag as seen with the 12 chute/plug suppressor.

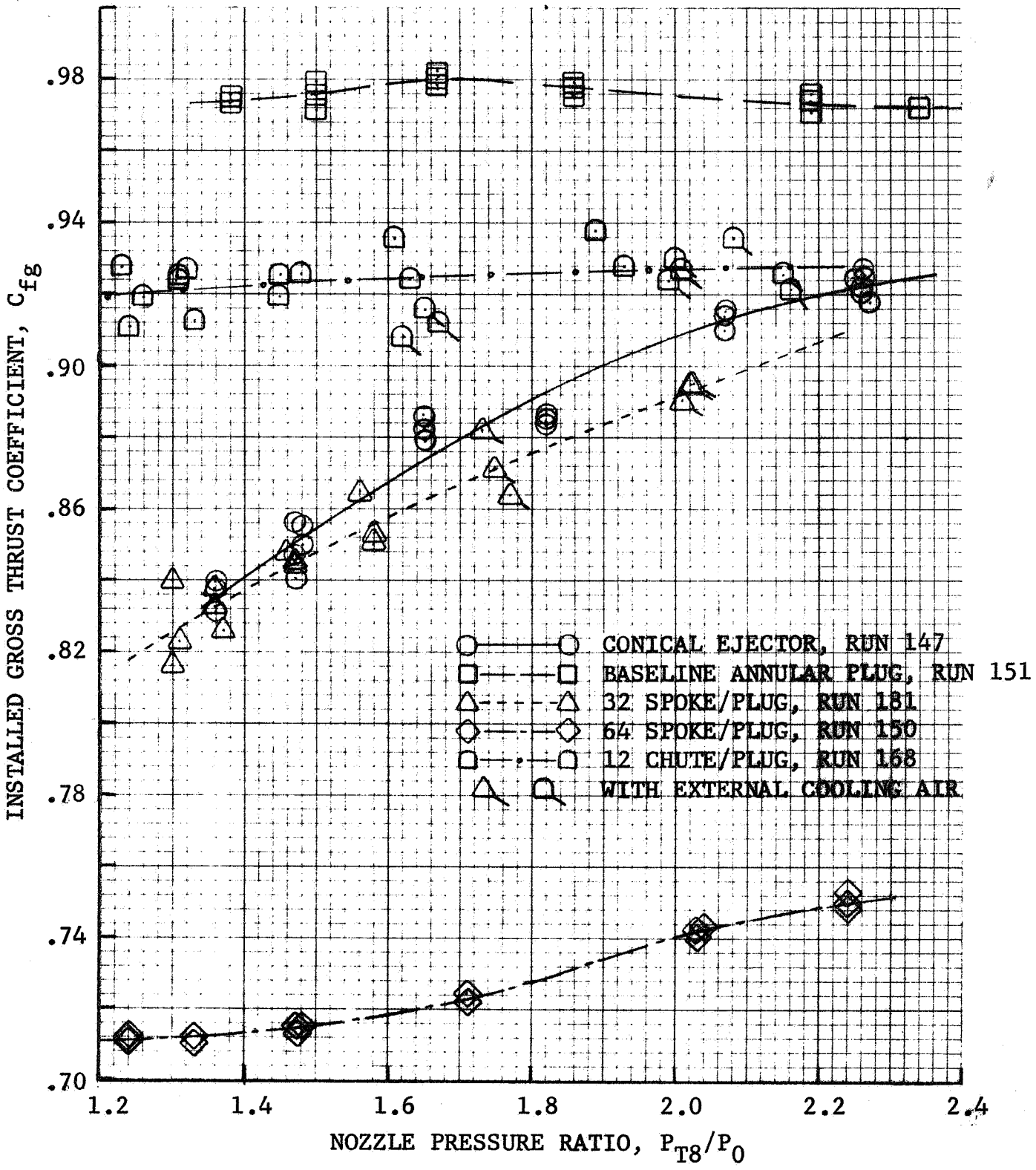

FIGURE 174 F106/J85 NOZZLE STATIC AERODYNAMIC PERFORMANCE

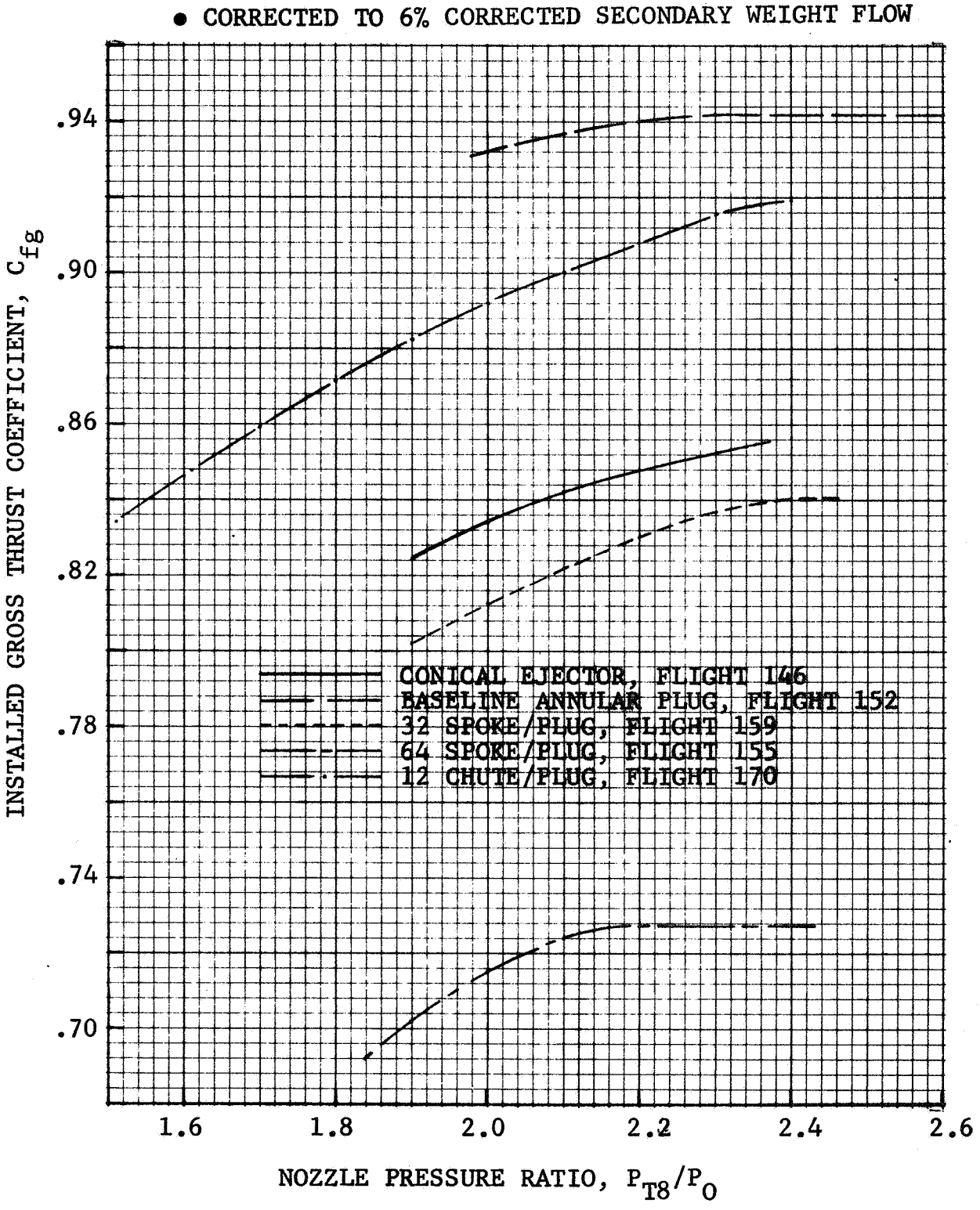

FIGURE 175 F106/J85 NOZZLE FLIGHT AERODYNAMIC PERFORMANCE

DISCUSSION OF FLIGHT VELOCITY EFFECTS

Conical Ejector - Comparison to SAE Prediction

As was done for the static data, to check the SAE prediction procedure's (ref. 2) applicability to non-suppressed conical ejector peak jet noise, the flight peak normalized OASPL and PNL data are compared to SAE predictions in Figure 176. The predictions were made using the J85 measured cycle parameters plus flight velocity, altitude, angle of attack to flight path and engine mount angle within the SAE prediction procedure, then extrapolating to the 300 ft. flyover altitude. Both peak OASPL and peak PNL agree fairly well with predictions at max. dry and 96% speeds, but are highly underpredicted at low velocity, particularly on PNL. The measurements are consistent in forming a uniform curve, decreasing noise with velocity, but again suggest much shallower slopes than those of the SAE technique. The OASPL varies on a slope of $V^{8.4}$ for SAE and $V^{6.4}$ for measured data. The PNL curves have $V^{9.4}$ and $V^{5.4}$ slopes respectively for SAE and measured.

The SAE procedure is based on two parts, a curve of normalized peak OASPL versus relative velocity and an assignment of spectra shape using the peak OASPL and a curve of OBSPL - OASPL versus Strouhal Number (fD/V). The fairly close match of predicted and measured OASPL in Figure 176 suggest that for the conical ejector at peak noise angle the full relative velocity effect is present at all but the lowest speed setting. For this particular nozzle geometry, since it is a primary nozzle - ejector system and not a true conical convergent primary alone, the data do suggest that possibly a shallower slope of $V^{6.4}$ instead of $V^{8.4}$ should be used for the prediction.

Check of compatibility of predicted and measured spectra is done in Figure 177. The upper curve set is at the highest velocity setting (V_J = 2107 ft/sec, V_R = 1677 ft/sec) and the lower curve set is at the lowest velocity setting (V_J = 1328 ft/sec, V_R = 889 ft/sec). At the high velocity setting the spectra shapes agree fairly well, being of magnitude just under the predicted levels and suggesting a lower measured PNL than what was predicted. Peak PNL and peak OASPL were not at the same flight angle so spectra at both angles are plotted.

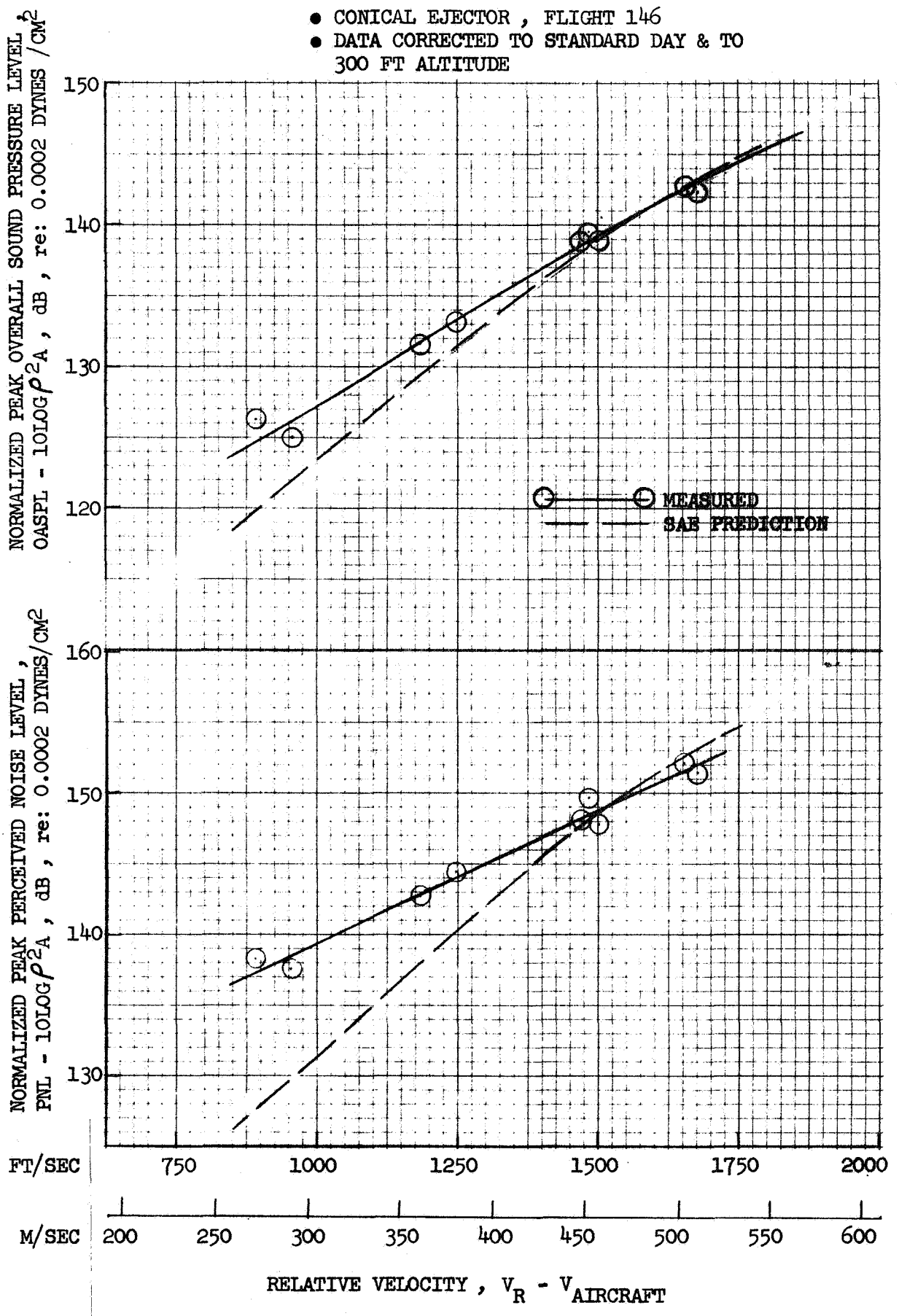

FIGURE 176 COMPARISON OF FLIGHT MEASURED PEAK OASPL & PNL TO SAE PREDICTION , CONICAL EJECTOR , MIC UNDER FLIGHT PATH

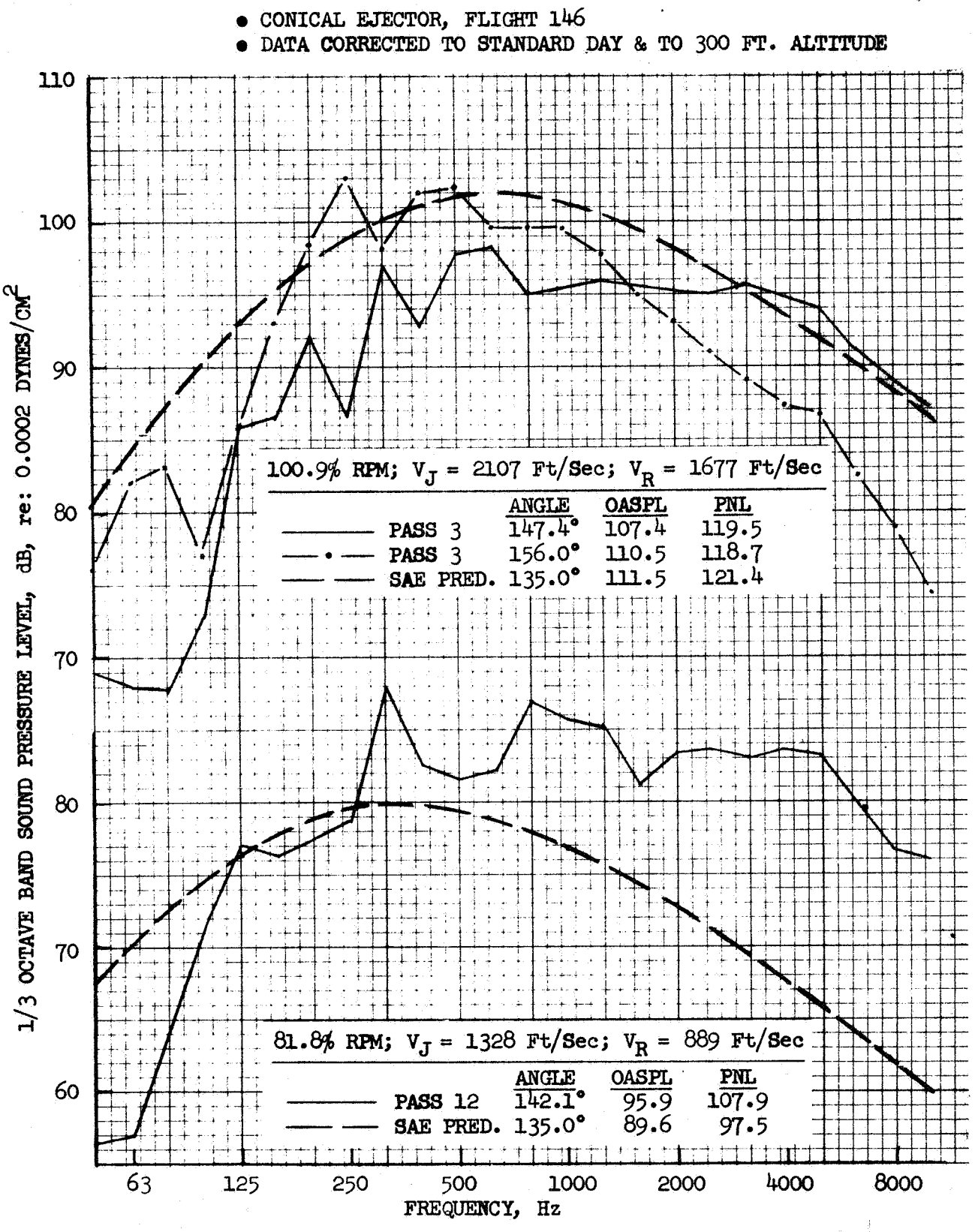

FIGURE 177 COMPARISON OF FLIGHT MEASURED SPECTRA TO SAE PREDICTION, CONICAL EJECTOR, MIC UNDER FLIGHT PATH

At the low speed setting the measured spectra high frequencies are considerably above the predicted levels, contributing to the gross mismatch of predicted and measured PNL levels. This suggests either a large flight velocity influence on high frequency jet noise at low power settings or a contribution of high frequency noise from sources other than the pure jet.

Comparison of Static and Flight Suppressions

To illustrate the effect of flight velocity on final subjective noise suppression, composite curves of static and flight data are shown in Figure 178 and 179. Figure 178 is for the baseline annular plug and the 32 spoke nozzles. Figure 179 is for the 64 spoke and the 12 chute nozzles. Each figure contains a) flight peak PNL suppression from Figure 168, b) flight EPNL suppression from Figure 169, c) ground static J85 peak PNL suppresssion from Figure 78, and d) ground static peak PNL suppression for model data scaled to the J85 size from Figure 6. The flight data are from the flight path microphone; the ground static data are at the 300 ft sideline. All data are corrected to standard day and plotted against jet velocity for a direct comparison of noise at the same noise generation velocity conditions so that flight velocity influence can be observed. Inspecting the curves supports the following comments:

- As mentioned in DISCUSSION OF STATIC DATA, for all nozzles at all jet velocities, engine static PNL suppression was somewhat higher than anticipated from model measurements scaled to J85 size; the only exception in magnitude being the 64 spoke nozzle which nearly paralleled the model data. Largest divergence is at low jet velocity where the measured engine suppression is considerably higher than the model expectations.
- The general trend was for loss of PNL suppression in flight when compared at similar jet velocities, particularly at low jet velocity.
- If the flight PNL suppression curves are shifted by the aircraft speed of 438 ft/sec to compare suppression on a relative velocity basis (static $V_J = V_R$), somewhat more consistent results are observed. The 64 spoke suppression levels are then nearly identical for static and flight suggesting only minor suppression loss in flight. The

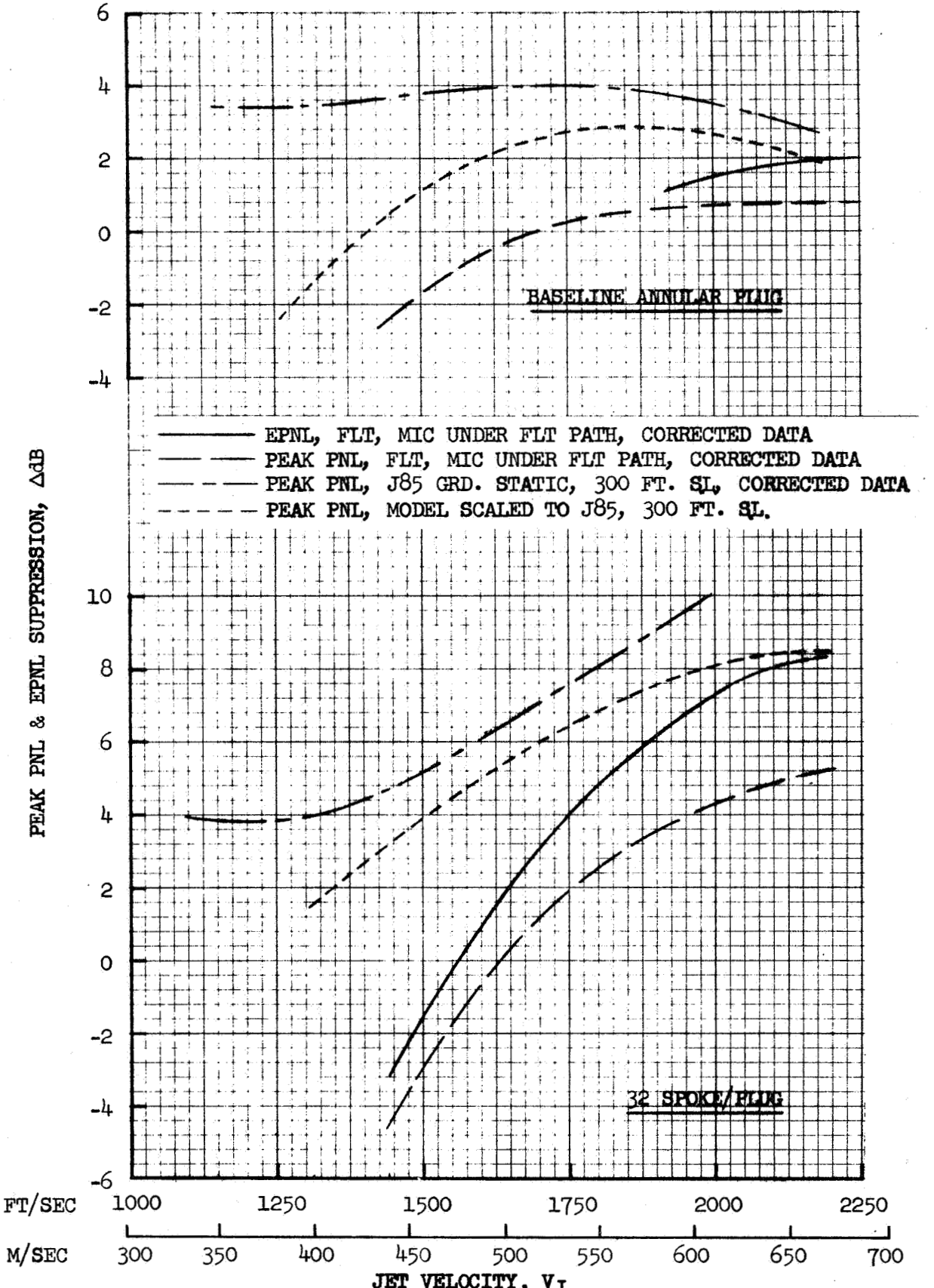

FIGURE 178 COMPARISON OF STATIC & FLIGHT SUPPRESSION LEVELS, PEAK PNL & EPNL

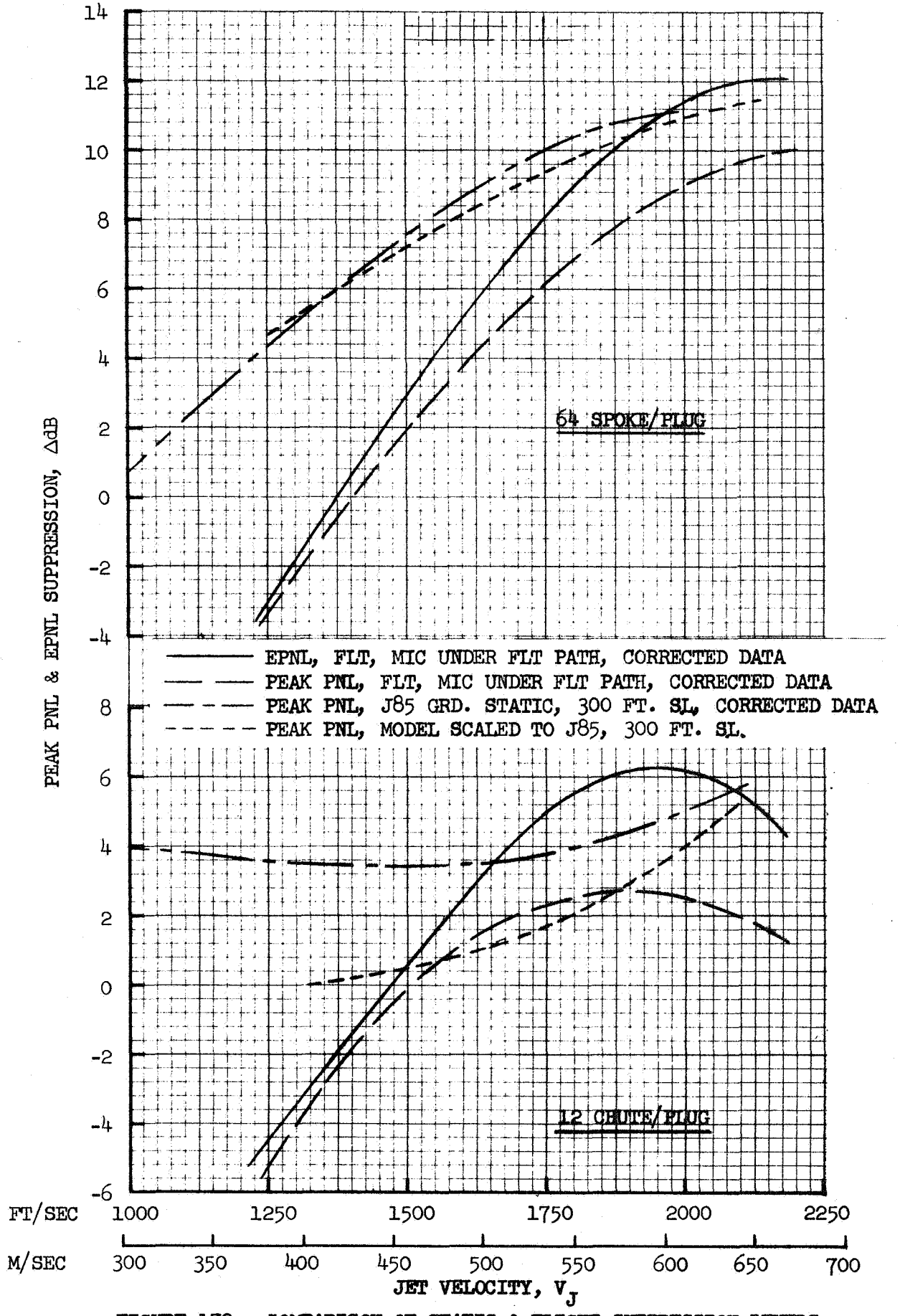

FIGURE 179 COMPARISON OF STATIC & FLIGHT SUPPRESSION LEVELS, PEAK PNL & EPNL

32 spoke nozzle shows nearly the same suppression levels in the 1250 to 1750 ft/sec V_R region but diverge at lower V_R. The 12 chute and annular plug nozzles have flatter peak PNL suppression curves and by shifting, only slightly better agreement is seen but with no substantial change.

Observation on a peak PNL suppression basis, therefore, produces no absolute general trends to prove or disprove influence of external flow. Flight velocity effects must first be established for each individual nozzle. On a suppression basis the analysis is complicated by the flight velocity influencing both nozzles simultaneously. The data must be analyzed on a finer basis of absolute PNL levels and their basic spectra.

Presentation of the comparison curves of Figures 178 and 179, however, are quite useful since they show the real life suppression levels attainable in flight.

- As mentioned in DISCUSSION OF FLIGHT DATA, comparison of the flight peak PNL and EPNL suppressions show that all nozzles experienced higher EPNL suppression. Magnitudes of change are seen in Figures 178 and 179.

PNL Directivity and Level Comparisons - Static to Flight

To determine the effect of flight velocity on PNL directivity, the ground static 300 ft sideline PNL data from Figures 30, 41, 52, 63 and 74 should be compared to the flight composite PNL histories in Figures 93 - 96, 103 - 104, 115 - 118, 131 - 134, and 148 - 152. Selected samples are presented in Figures 180 through 184 for the conical ejector, annular plug, 32 spoke, 64 spoke and 12 chute in that order. Flight PNL are plotted, as previously done, against acoustic angle referenced to the inlet. The ground static data, shown as symbols, were chosen as the data points with the closest jet velocity to the flight measurements. By comparing at the same jet velocity, the jet stream generating the noise should be similar for static and flight (assuming no stream change due to external flow) and any changes in the noise levels could then be assigned to the general category of flight velocity effects. For most comparisons the static data points were not at the exact same jet velocity as the flight data. To compensate for the differences and make the data more compatible, the change in peak PNL for the difference in V_J was obtained from the static peak PNL plots in Figure 78 for each nozzle. This delta was applied to the measured PNL at each angle to bring it to the level anticipated at the value of flight V_J. The magnitude of correction is indicated on each curve. This procedure is not exact for angles other than peak, however, by estimating true PNL change with V_J at each angle, from Figures 30, 41, 52, 63 and 74, the correction is seen to be adequately accurate for the purpose of comparison.

The static data are plotted at angles 2-1/2° off the actual static measuring location to compensate for the angle of attack to flight path and engine mount angle. Thus, by comparing the absolute levels and directivity shapes the magnitudes of difference are those experienced due to flight effects. These deltas must then be analyzed as to their origin of change to explain the constituent pieces which comprise the total flight velocity effect.

Comparing only the ground static data, shown as symbols, to the average of the flight data in Figures 180 through 184 leads to the following comments:

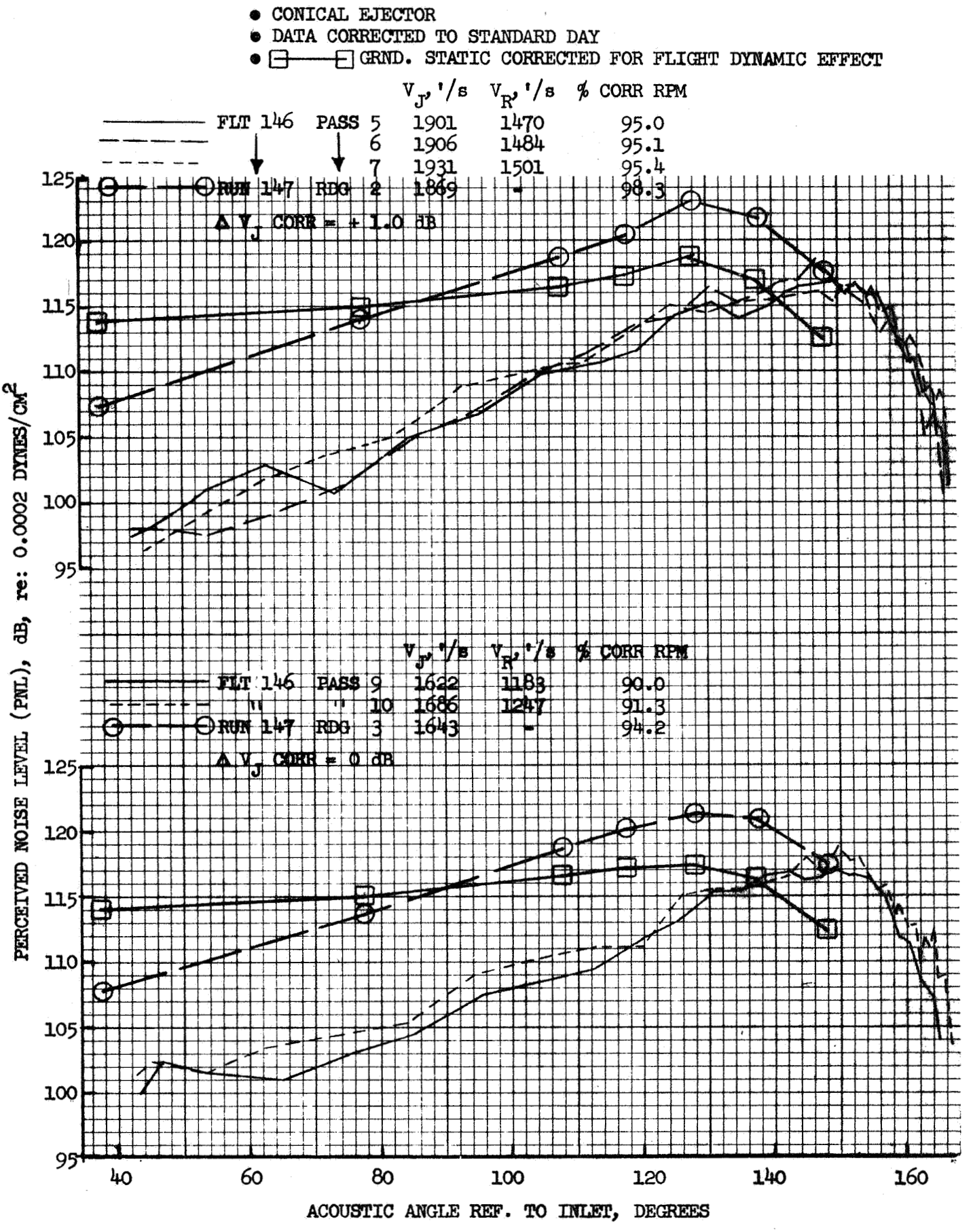

FIGURE 180 COMPARISON OF STATIC AND FLIGHT PNL DIRECTIVITY

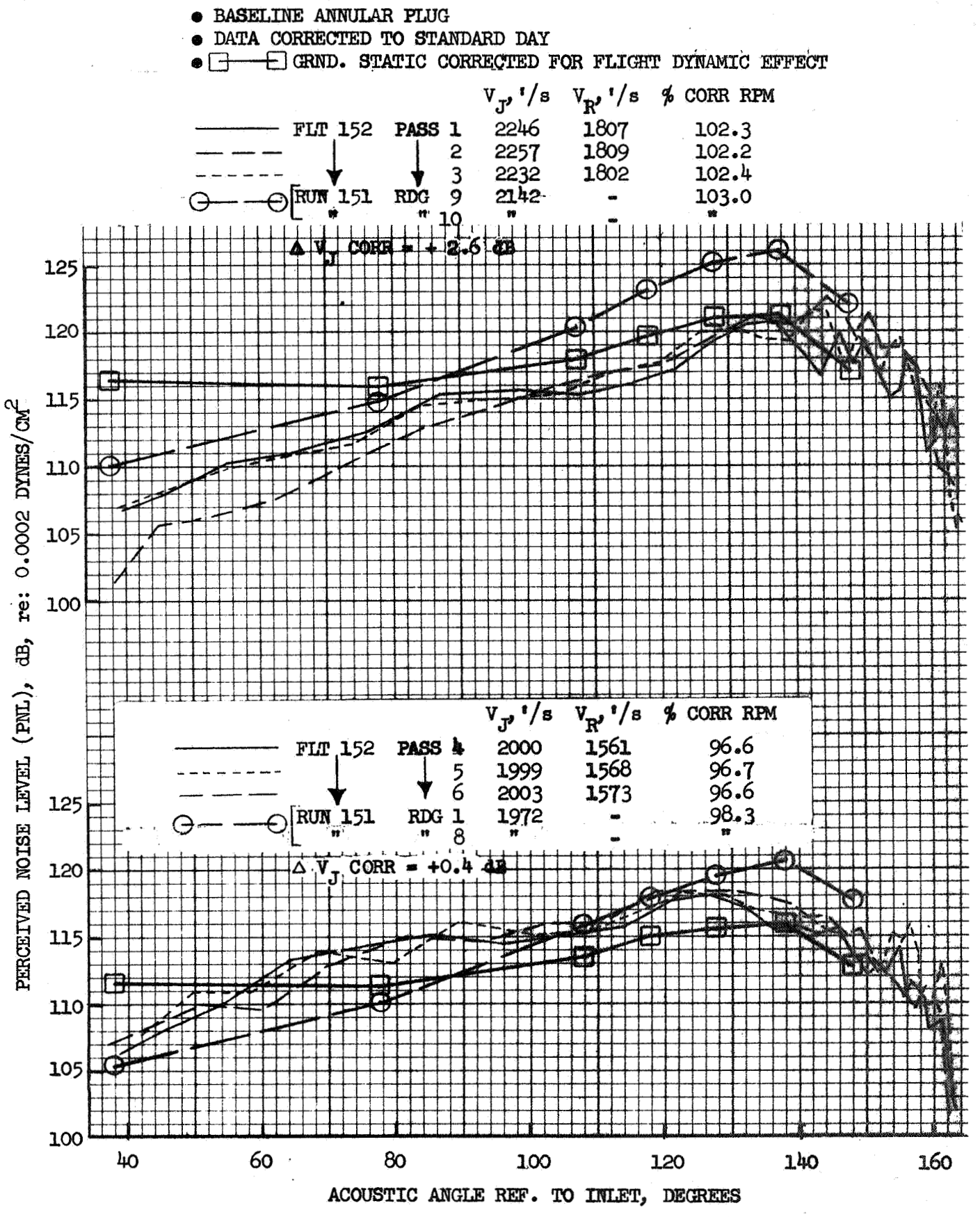

FIGURE 181 COMPARISON OF STATIC AND FLIGHT PNL DIRECTIVITY

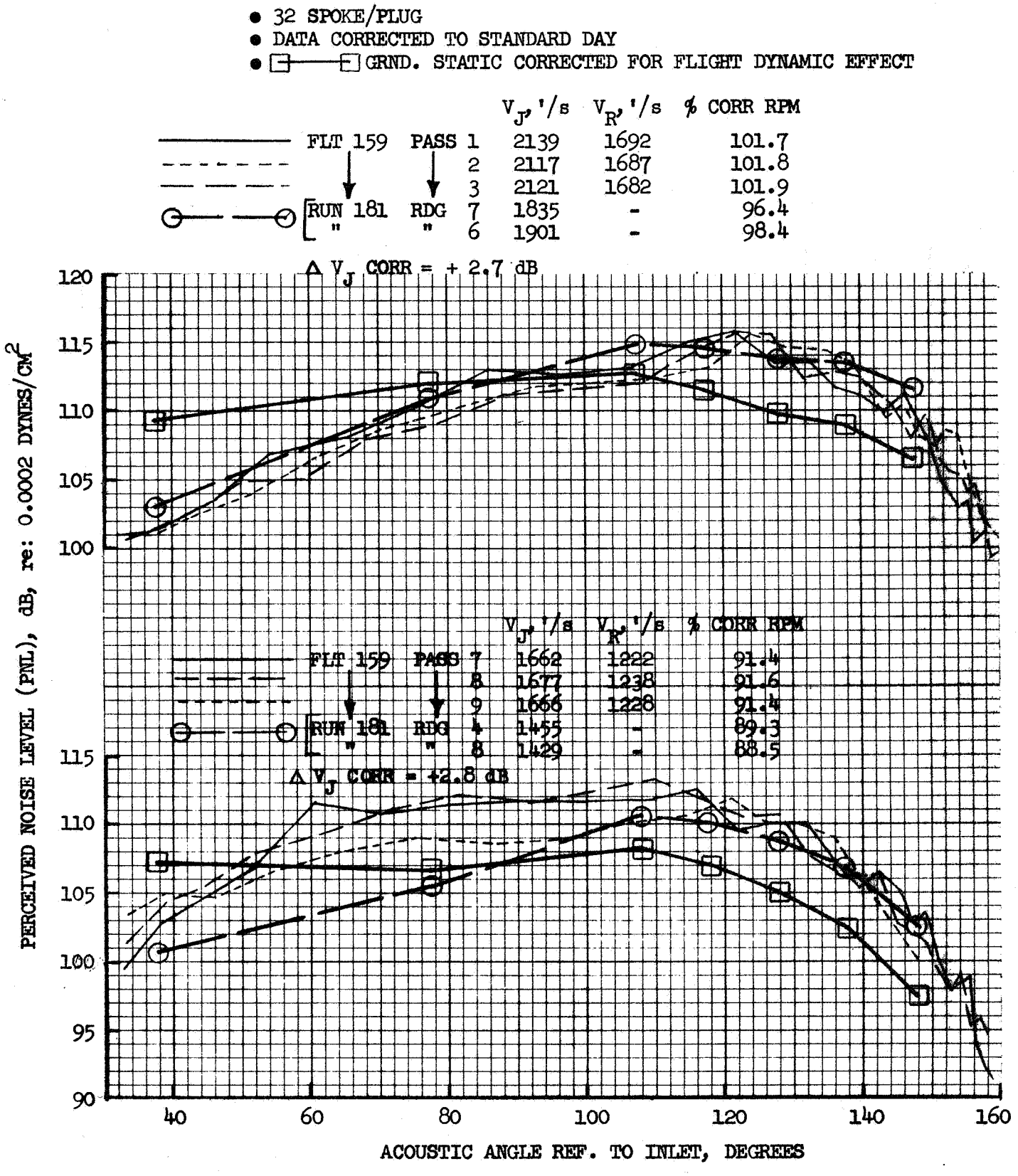

FIGURE 182 COMPARISON OF STATIC AND FLIGHT PNL DIRECTIVITY

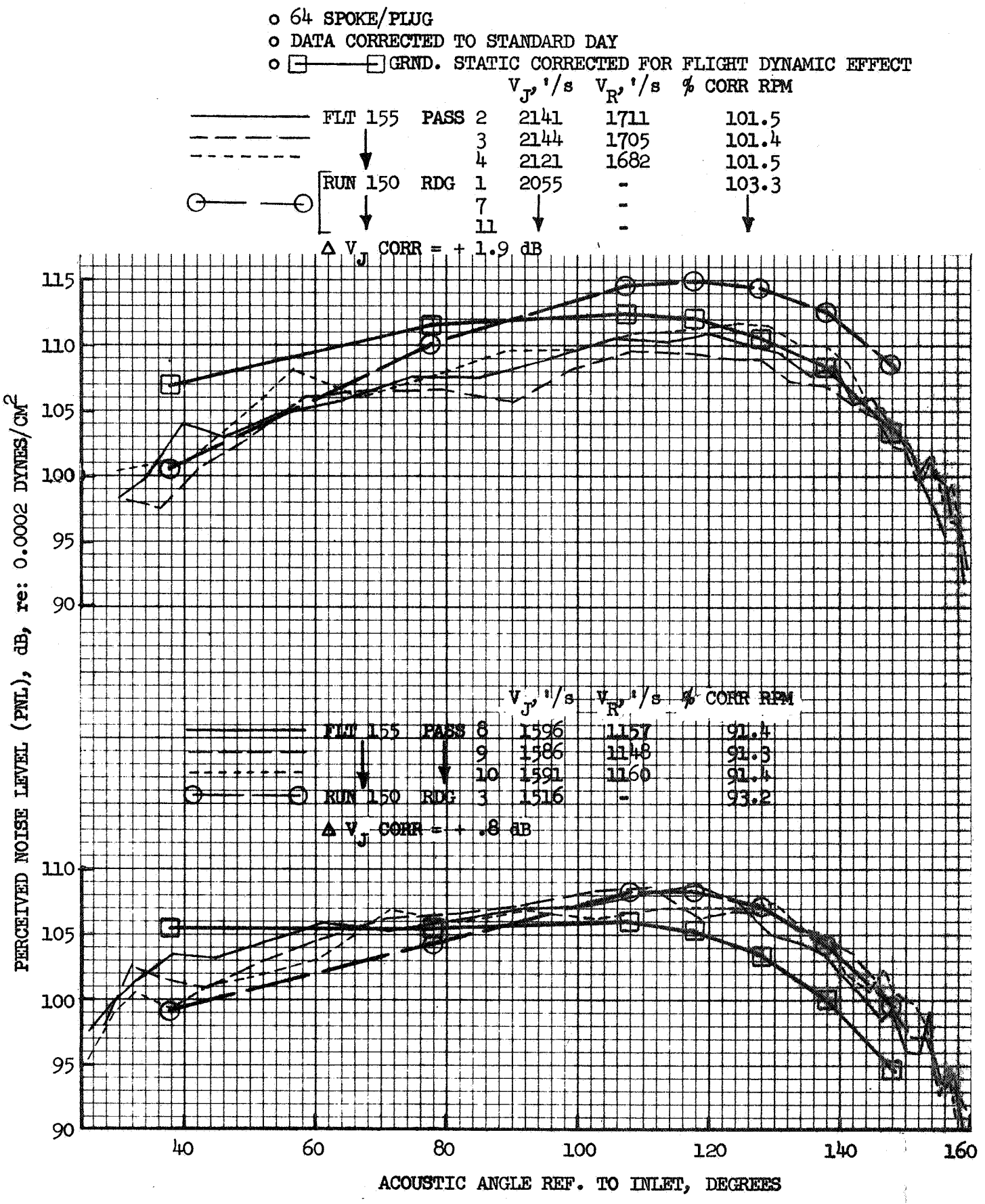

FIGURE 183 COMPARISON OF STATIC AND FLIGHT PNL DIRECTIVITY

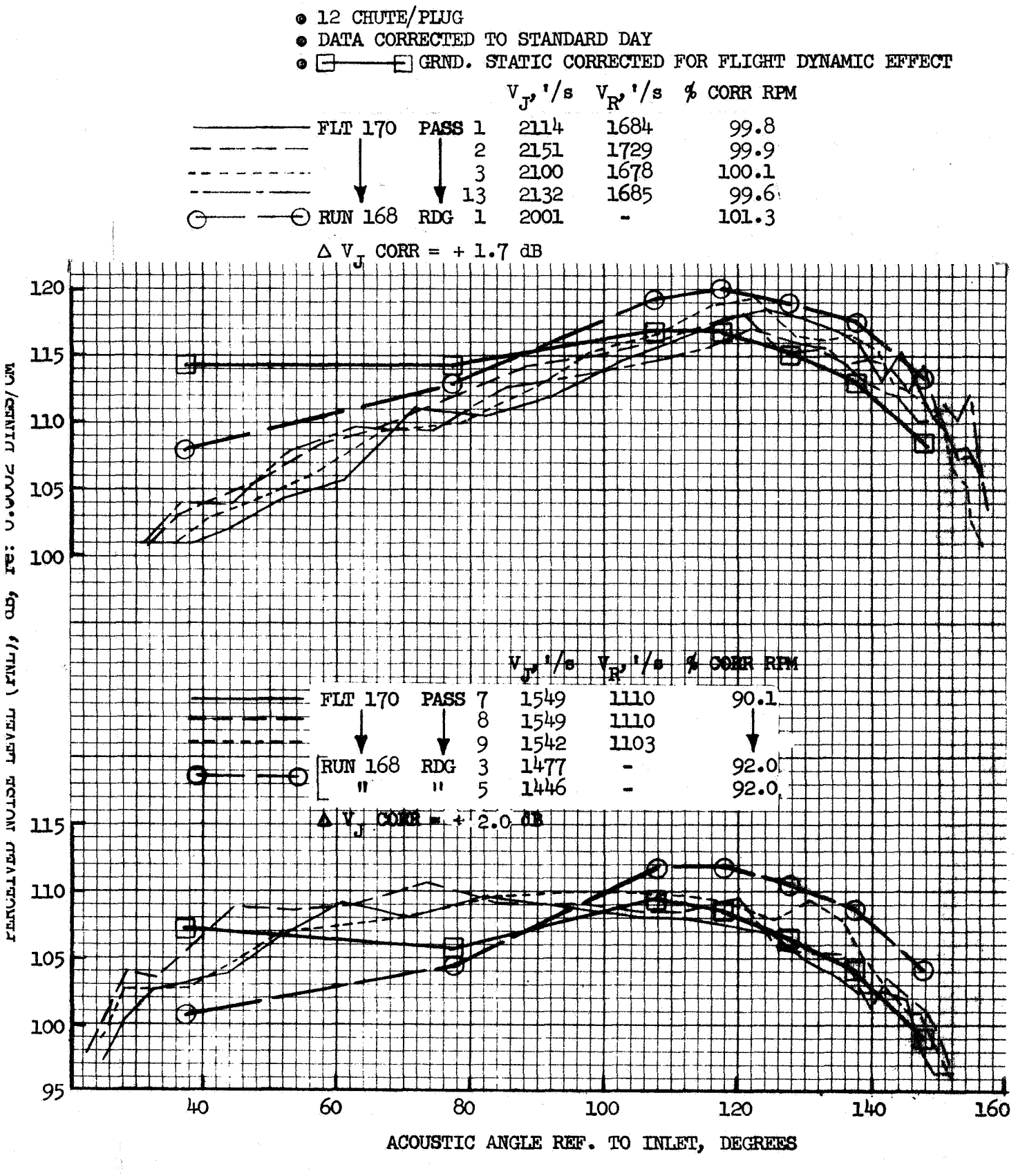

FIGURE 184 COMPARISON OF STATIC AND FLIGHT PNL DIRECTIVITY

- Change in noise levels from static to flight is very inconsistent between nozzles, between speed settings and even between angles at the same speed settings for each nozzle. If all changes from static to flight are considered as flight velocity effects no general conclusions, applicable to all nozzles, can be formed. The magnitudes of change vary considerably, in some instances indicating a flight velocity decrease in noise and in others indicating a reverse V_R effect or an increase in noise from static to flight.

- The conical ejector has a marked shift in directivity from ground to flight, the shift magnitude being about 20° closer to the jet exhaust. (See Figure 180). The ground static peak occurs near the SAE prescribed 135° location (actual about 130°) but is in the vicinity of 150° for flight. Static noise near the inlet is well above the flight noise indicating a substantial lowering of forward quadrant noise in flight. The trend holds for all speed settings indicating presence of flight velocity effect across all angles, and particularly so at inlet angles, but complicated by the shift in directivity.

- The plug nozzle static PNL levels and directivity agree much closer to the flight levels than did those of the conical ejector. Slight directivity shift is seen but it is not consistant in direction or amount. At high engine speed of 102 - 103% (upper half of Figure 181) flight PNL levels are lowered significantly at the exhaust angles and by several dB at the inlet angles, indicating presence of partial V_R effect. At the lower speed of 97 - 98% (lower half of Figure 181), PNL is lowered in flight by a smaller amount but the inlet PNL is increased in flight rather than decreased, indicating a reverse V_R effect.

- The 32 spoke nozzle shows very good agreement between static and flight PNL levels and directivity at the two high speed settings (top of Figure 182), indicating flight velocity influence is not present at high velocity. Only a slight shift in peak noise location occurs in flight, moving nearer to the exhaust axis. At the lower

speed of 89 - 92% (bottom of Figure 182) and at the lowest speed setting of 86 - 88% (not shown) the static data at the inlet are considerably under the flight data. The exhaust data match fairly well for the velocity shown but are under the flight by several dB at the lowest speed setting, indicating a reverse flight velocity effect required to raise the static levels to flight.

- The 64 spoke static data nearly parallel the flight data at the three higher speed settings, both in level and in directivity pattern. At the two highest speeds the static aft quadrant PNL's are several dB above the flight (top of Figure 183) and indicate small flight velocity effects. The inlet levels are consistent with flight and shown no V_R effect. At the lower speed, 91 - 93%, (bottom of Figure 183) the aft quadrant agree but the forward static are under the flight. At the lowest speed of 88 - 89% (not shown), static levels are considerably under flight indicating reverse V_R. No shift in peak angle noise locations is seen at any speed setting.

- The static PNL of the 12 chute nozzle are above the flight data at the two high speed settings, (top of Figure 184). At the lower 90 - 92% speed (bottom of Figure 184), the flight noise near the inlet is considerably above the static and is also above that of the higher speed settings. The exhaust levels match well. At the lowest speed of 87 - 88% (not shown), all static levels are under the flight. These comparisons indicate a partial flight velocity influence at the exhaust and inlet at high velocity, influence at the exhaust only at intermediate velocity and reverse V_R effect at low velocity. Directivity pattern shifts considerably at low velocity with peak noise angles moving closer to the point of closest approach.

Doppler Shift and Dynamic Effect

The magnitudes of change in subjective noise levels have been observed in Figures 180 through 184 by comparing ground static PNL to flight PNL. The observed changes were categorized under the general term of flight velocity effects without assigning specific reasons for the changes or being able to separate the total change into parts whose magnitudes could be assigned a specific cause. The mechanics of change are varied and complex, categorized into major areas of a) change in source noise generation - conventionally termed flight velocity or V_R effect, b) change in directivity, c) Doppler shift and d) dynamic effect.

A conventional method of analyzing the empirical data is to correct first for effects known to occur or theoretically predicted to occur, reevaluate the comparison after the alterations, then apply the remaining deltas to the non-predictable causes. Thus, to project the ground static data to flight it should be corrected to free field, Doppler shifted, altered by flight dynamics predictions, then compared to flight data at a similar reference plane. Any remaining differences would be assigned to source noise generation changes or directivity shift.

There is no general agreement on how static jet noise data should be adjusted for Doppler shift and dynamic effect for comparison to flyover data. Jet noise is not a point source of noise and the source does not move at the same velocity as the aircraft. Kobrynski gives an analytical and experimental treatment of the subject in references 14 and 15. Mangiarotty and Turner discuss the Doppler shift and bandwidth correction in reference 16. Morse and Ingard (ref. 10) and Appendix A of this report discuss the dynamic effect.

The Doppler shift is conventionally assigned as $f_R/f_E = 1/(1 - M \cos \theta)$ where f_R and f_E are received and emitted frequencies, respectively, M is Mach number of the moving source and θ is the acoustic angle. Figure 185a shows the variance of Doppler frequency shift with acoustic angle at the aircraft flight speed of M = 0.4. As the aircraft approaches the microphone the received frequencies are higher than those generated and the opposite occurs as the aircraft recedes from the microphone. Associated with the Doppler

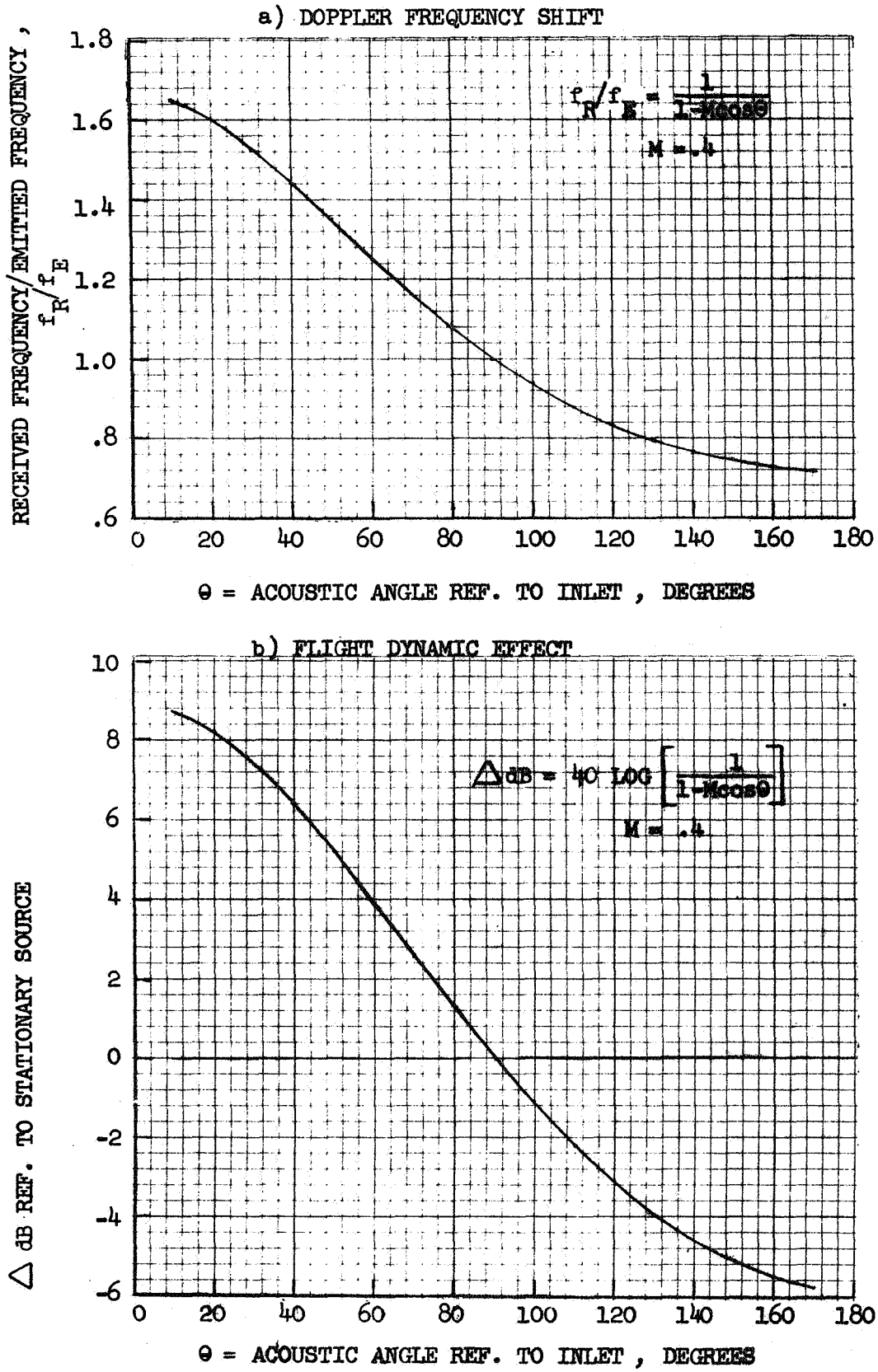

FIGURE 185 DOPPLER FREQUENCY SHIFT & FLIGHT DYNAMIC EFFECT AT M = .4

frequency shift, there is a bandwidth correction which has an effect on sound pressure level (ref. 16).

The flight dynamic effect suggests that, in addition to the Doppler shift and bandwidth correction, a change in sound pressure level will occur due to flight motion, as observed on the ground relative to the level at the source. The change is a function of acoustic angle and Mach number and is assigned the value $\Delta SPL = -40 \log (1 - M \cos \theta)$. This is based on reference 10 and Appendix A. Figure 185b shows the magnitude of suggested change versus acoustic angle at the flight speed of M = 0.4. Another approach to the subject is in references 14 and 15.

Application of the flight dynamic correction to the 300 ft. sideline PNL directivity is done in Figures 180 through 184 for the five nozzles. It is applied directly to the PNL values without going back to the original spectra for Doppler shifting, as the relative change in PNL level is normally small when Doppler shifted. The dynamic-corrected static PNL in some instances now closer approximate the flight. In others, particularly at inlet angles, they suggest that an even stronger V_R effect must now be present to compensate for the original mis-match plus the dynamic effect. At the exhaust angles, for most nozzles and speeds, it suggests that a stronger reverse V_R effect must be present to raise the static levels to flight measurements.

For purpose of comparing on a spectral basis, Figures 186 through 189 are included. Figures 186 and 187 are for the conical ejector and Figures 188 and 189 are the 64 spoke/plug, each set being at maximum engine speed. Ground static acoustic angles of 80, 120, 140, and 150° to the inlet are included. The ground static spectra, corrected for ground plane interference, are at the 300 ft sideline. They are Doppler shifted and dynamic effect corrected per the curves of Figure 185 for each particular acoustic angle. They are then compared to the flight as-measured and corrected spectra. The 1/8 second of integrated flight data was used which included the flight angle corresponding to the ground static angle after consideration of flight angle of attack and engine mount angle.

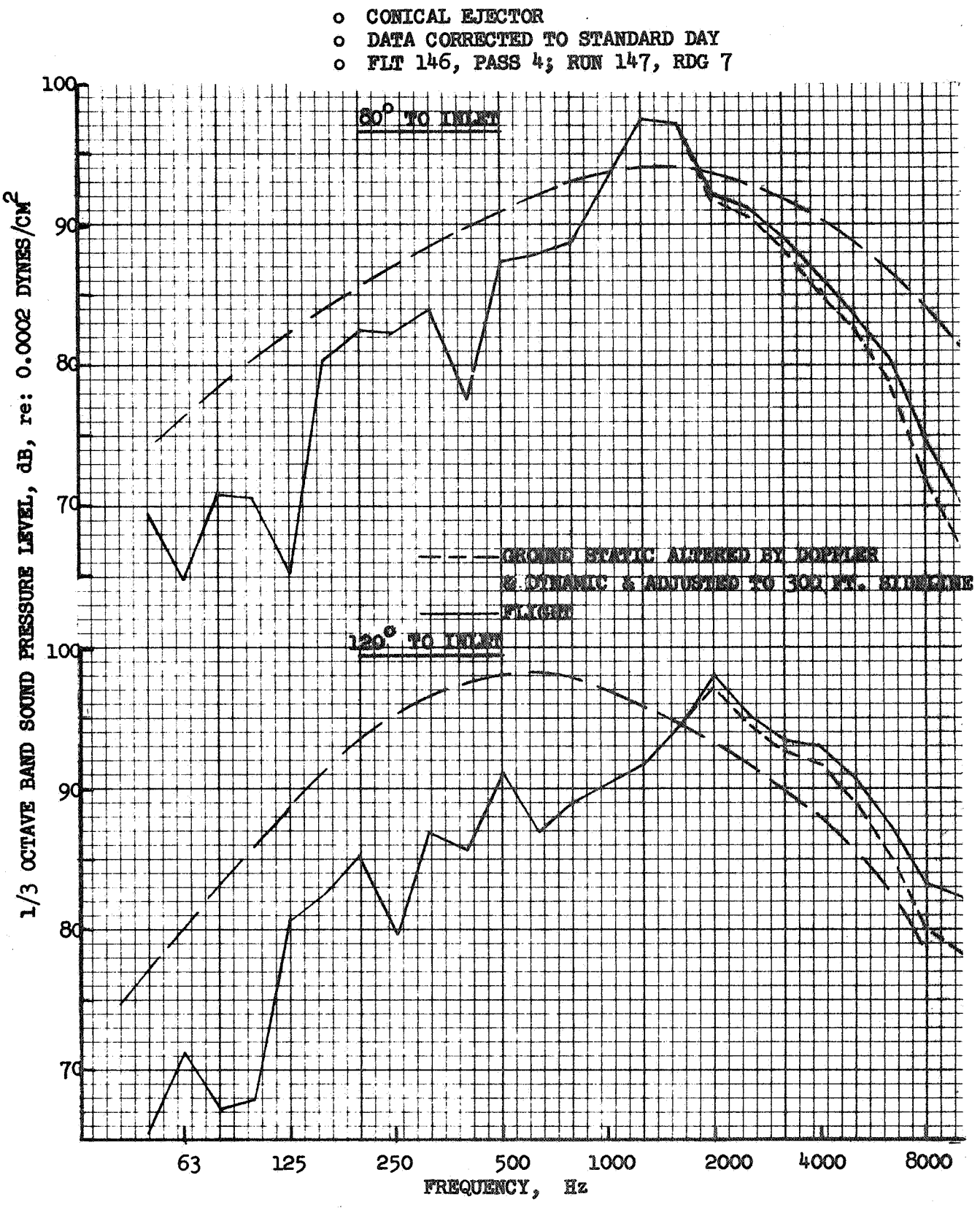

FIGURE 186 COMPARISON OF STATIC & FLIGHT SPECTRA, CONICAL EJECTOR

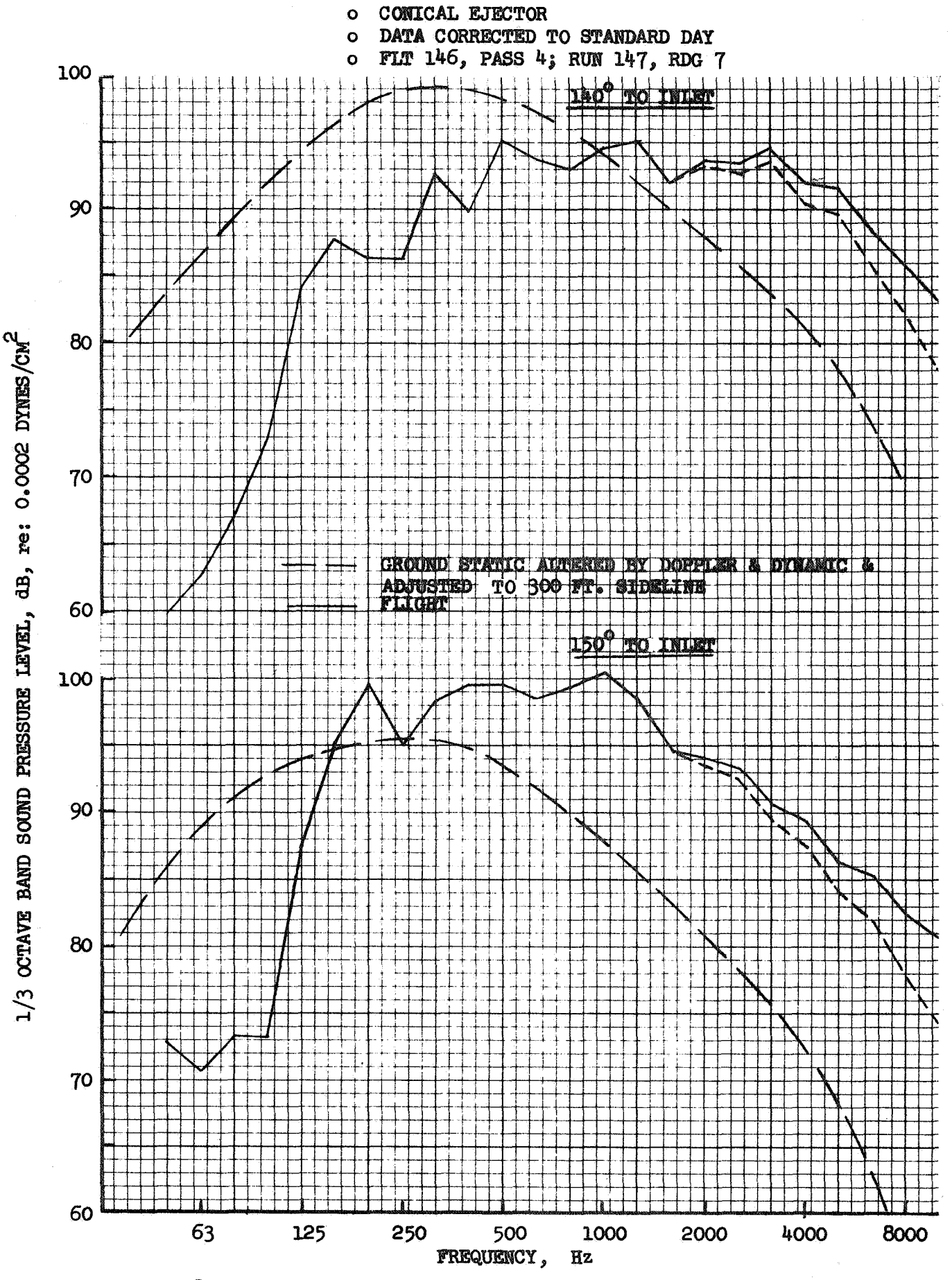

FIGURE 187 COMPARISON OF STATIC & FLIGHT SPECTRA, CONICAL EJECTOR

o 64 SPOKE/PLUG
o DATA CORRECTED TO STANDARD DAY
o FLT 155, PASS 2; RUN 150, RDG 1

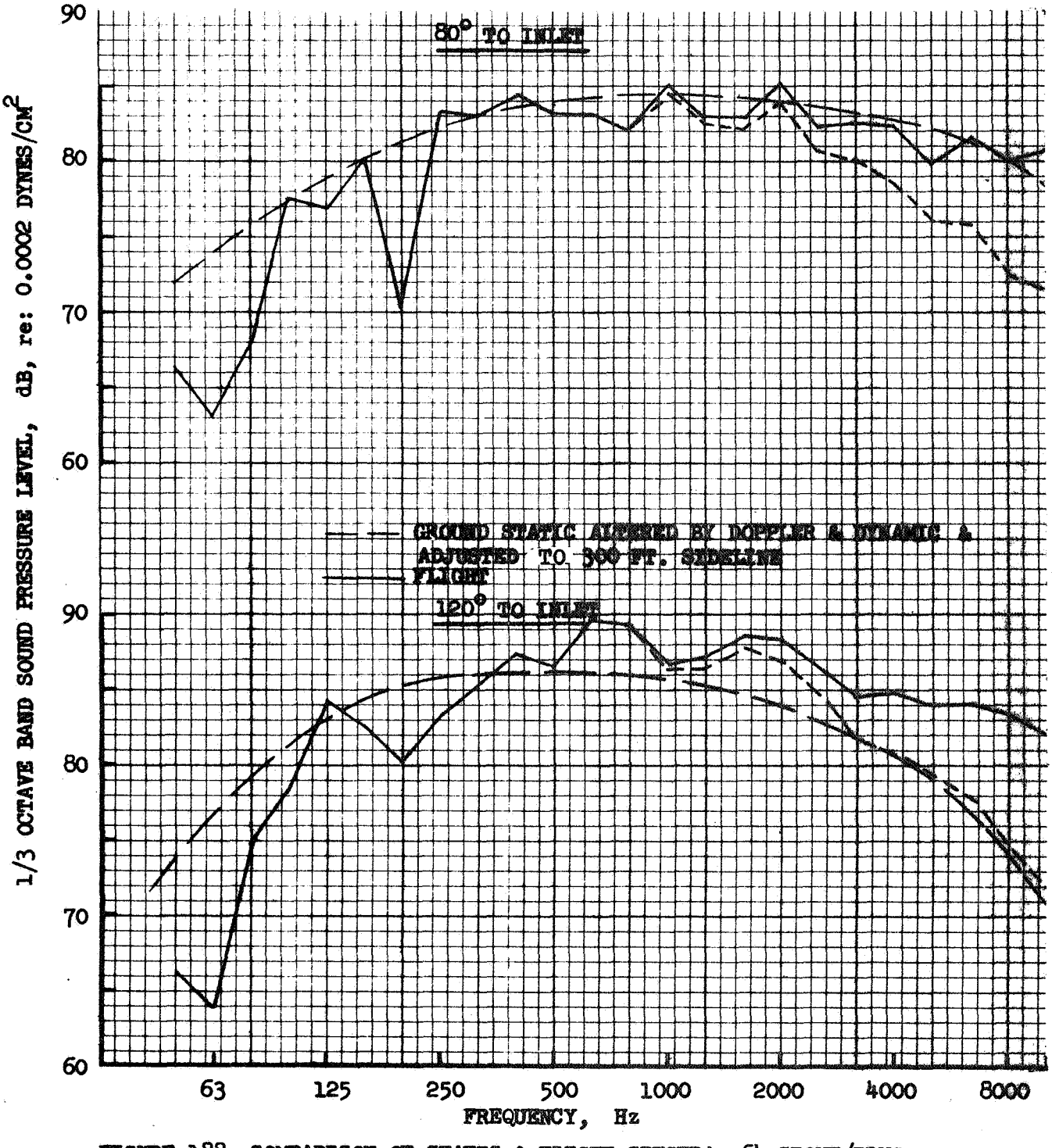

FIGURE 188 COMPARISON OF STATIC & FLIGHT SPECTRA, 64 SPOKE/PLUG

o 64 SPOKE/PLUG
o DATA CORRECTED TO STANDARD DAY
o FLT 155, PASS 2; RUN 150, RDG 1

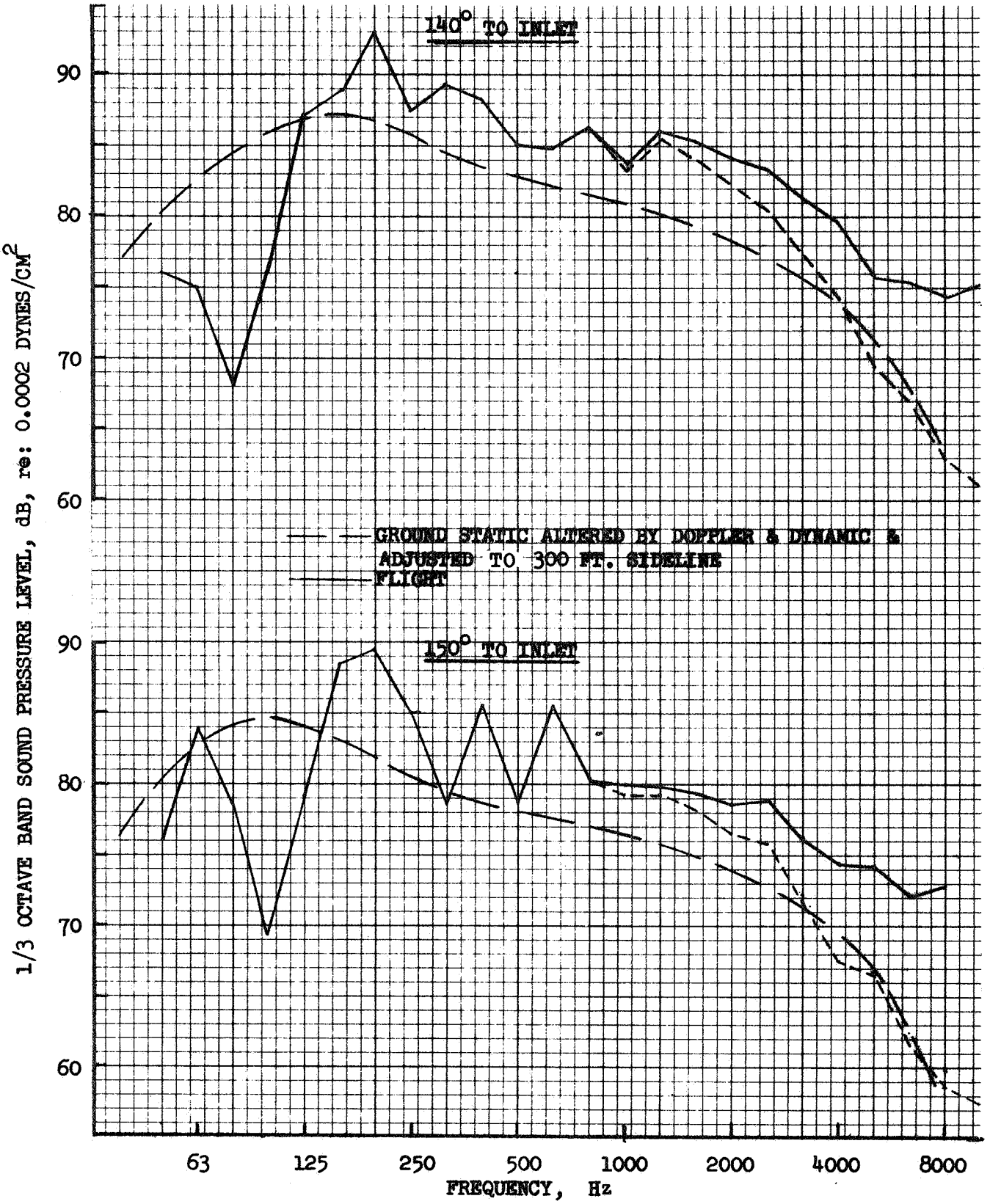

FIGURE 189 COMPARISON OF STATIC & FLIGHT SPECTRA, 64 SPOKE/PLUG

Figures 186 and 187 suggest that for the conical ejector, the ground static spectra approximate the flight spectra only near the overhead position. As the aircraft recedes from overhead, a strong shift to high frequency occurs. The low frequency static corrected spectra are considerably above the flight and the high frequency are well under. This possibly indicates a shift of energy to high frequency in flight which causes the large shift in PNL directivity as seen from the curves in Figure 180.

For the 64 spoke/plug nozzle, Figures 188 and 189, the Doppler shifted and dynamic corrected static spectra agree well near the overhead location and are somewhat under the flight spectra at angles toward the inlet. This is in agreement with the top curves of Figure 183 and would suggest that the change from static to flight at this velocity and angles is only a function of Doppler and dynamic. However, as considered previously from Figure 180 through 184, the application would only fully cover the flight velocity change in some instances. In others, higher divergence results.

CONCLUSIONS

For the purpose of investigating flight velocity influence on noise characteristics of unsuppressed and suppressed jets, an F106 aircraft with a wing mounted J85-13 engine was used for static and flight noise measurements. Five nozzles were tested, including a conical primary with a cylindrical ejector, baseline annular plug, 32 spoke/plug, 64 spoke/plug and 12 chute/plug; each over a speed range of 80 to 100% (max dry) statically and 88 to 100% in flight.

Ground Static

The ground static measurements produced a unique set of unsuppressed and suppressed jet engine noise data, after correcting where necessary for influence of a) conical ejector pure tone, b) J85 turbomachinery tones, c) J75 at idle noise and d) J85 cooling air noise. The data are believed to accurately represent jet noise except for measurements on several nozzles at low engine speed and at angles near the inlet. Here the J75 at idle pure tone predominated the mid-frequency range to where its influence could not be accurately removed. In some instances the J85 broadband turbomachinery noise also added to the total noise and could not be separated from the jet noise.

A comparison of the peak static PNL suppression to smaller hot flow model measurements scaled to J85 size shows similar results at high jet velocity and considerably higher suppression at low jet velocity. When compared to the SAE prediction method, ground static peak OASPL and peak PNL measurements suggest a shallower sloped curve than SAE for the conical ejector nozzle.

Flight

For flight measurements, repetitive fly-overs at the same engine speed produce quite consistent PNL histories, indicating the aircraft overhead location is adequately accurate for the study. Several of the flight measuring days varied considerably from a standard meteorological day. Magnitude of atmospheric absorption corrections to the standard day changed PNL of the conical ejector slightly and those of the 32 and 64 spoke suppressors by up to 3 and 4 dB.

Suppression levels are changed somewhat but study conclusions are not.

In general, for under the flight path measurements, there was no interference of the J75 at idle within the range of 10 dB down from peak noise and little interference at acoustic angles comparable to ground static locations. An exception was the conical ejector at low engine speed and then only at 60° and forward. For the sideline measurements, only minor interference within the 10 dB down range occurred. Each pass should be checked individually at the inlet angles.

At max dry engine setting, 7 to 13 ΔdB suppression was seen for the 32 and 64 spoke nozzles, depending on the parameter. The 12 chute/plug showed 3 to 6 ΔdB and the baseline plug had about 2 ΔdB. All nozzles experienced greater EPNL suppression than peak PNL suppression due to their more favorable PNL(T) directivity shortening noise duration.

Aerodynamic Performance

The static and flight aerodynamic performance losses were fairly high. This was anticipated since the nozzles were not refined for optimum aerodynamic performance. The 32 spoke performance is within $\pm$ 1% of results from model static and wind tunnel tests.

Flight Velocity Influence

Both peak OASPL and peak PNL agree fairly well with SAE predictions at max dry and 96% speeds, but are underpredicted at low velocity, particularly on PNL. Shallower slopes of peak OASPL and PNL curves are suggested than those predicted by SAE procedure.

The general trend was for lower peak PNL suppression in flight than statically when compared at similar jet velocities, particularly at low jet velocity. On a relative velocity basis the 64 and 32 spoke nozzles show only minor peak PNL suppression loss in flight.

Change in noise levels from static to flight is very inconsistent between nozzles, between speed settings and even between angles at the same speed setting for each nozzle. If all changes from static to flight are considered

as flight velocity effects, no general conclusions, applicable to all nozzles, can be formed. Individual nozzle conclusions, when comparing static to flight at the same jet velocity are as follows:

- The conical ejector has a marked shift in directivity from static to flight. Noise is lowered in flight for all speed settings indicating presence of flight velocity effect.
- The plug nozzle has a slight directivity shift from static to flight but direction of shift is not consistent. Flight velocity lowers PNL for all exhaust angles at all speeds but increases PNL at inlet angles for low engine speed.
- The 32 spoke nozzle shows good agreement between static and flight at high engine speed indicating no influence of flight velocity. A slight shift of peak noise toward the exhaust occurs. As speed is lowered, static exhaust angle PNL match flight and then drop under flight PNL, the inlet flight being considerably under the static. This indicates a reverse V_R effect in flight.
- The 64 spoke static PNL nearly parallel the flight at mid and high speed indicating only slight V_R effect. At the lowest speed both the front and rear quadrant static PNL are under the flight levels indicating a reverse V_R effect. No shift in peak noise location is seen.
- The 12 chute static PNL are above the flight levels at high speed and are all under at lowest speed. Directivity pattern shifts considerably at low speed, peak noise shifting closer to the sideline.

Application of the flight dynamic correction in some instances makes the static data more closely approximate the flight measurements. In others, particularly at inlet angles and at high speeds, it suggests an even stronger V_R effect must be present to compensate for the dynamic effect. At exhaust angles it suggests a reverse V_R effect must also be present at low jet velocity to raise the levels to the flight measurements.

APPENDIX A*

Effect of Source Motion on Free Field Sound Pressure Levels

The following is a physical description of why a moving source will have not only the well known Doppler shift of frequency but also a change in the SPL as seen by a stationary observer. The result of this analysis is the same as that given by Morse and Ingard in "Theoretical Acoustics"; however, this analysis gives a better "feel" for the physics of the problem (ref. 10).

When the source moves, the sound wave pattern is established by the combination of the velocity of sound in air and of the velocity of the source so as to result in a pattern like that sketched below:

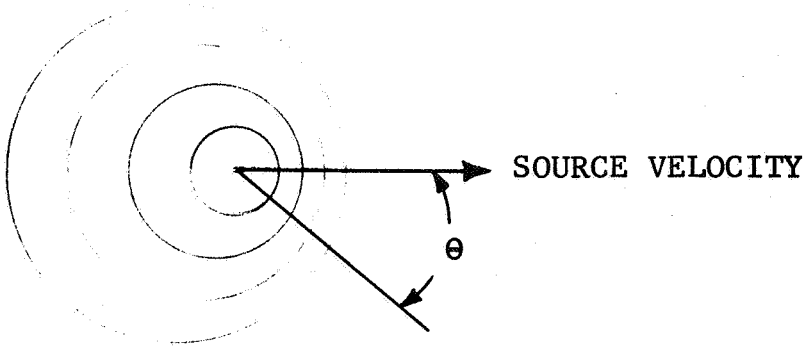

In the direction of source motion, the spacing between the waves is decreased and vice-versa. This effect causes not only the Doppler shift in frequency and associated bandwidth correction to pressure level but also a change in the sound pressure level described herein. The change occurs as a result of the change in the sound frequency and in the sound energy density caused by the crowding (or dilation) of adjacent wave fronts.

The sound energy density is determined by the time averages of the particle velocity squared according to:

* As originally published in internal General Electric letter by R.E. Motsinger, May 3, 1972.

1) $$E = \frac{1}{T} \int_0^T \rho_o u^2 dt$$

Where E = sound energy density per unit volume

T = the time period of averaging

ρ_o = air density

u = partical velocity due to acoustic vibration

This is analogous to the energy contained in the dynamic head of bulk fluid steady state flow, i.e.:

$$q = \frac{1}{2g} \rho V^2 \ \#/ft^2 \sim ft \ \#/ft^3$$

The point is that the sound energy density is dependent on the particle velocity squared. For a wave with an acoustic particle displacement given by:

$$\xi = A \cos (wt - kx),$$

the particle velocity depends on the frequency according to:

2) $$|u| = \left|\frac{d\xi}{dt}\right| = A w \sin (wt - kx)$$

This can be used in Equation (1) to show that the time averaged energy density is:

3) $$E = \frac{\rho_o w^2 A^2}{2}$$

So, the energy density is dependent upon frequency and amplitude of the particle displacement squared.

The energy density of the stationary source is then:

3a) $$E = \frac{\rho_o W_o^2 A_o^2}{2}$$

But for the moving source, the frequency the observer sees is given by the Doppler shift.

4) $$w = \frac{w_o}{1 - M \cos \theta}$$

where

w = frequency as seen by the observer

w_o = frequency emitted by the source

M = Mach number of the source relative to the observer

θ = angle between a line from the observer to the source and the engine centerline at the instant the observed sound was emitted

The amplitude of the particle displacement is also affected by the source motion. For a given periodic volumetric displacement, the product of the amplitude of the particle displacement and the wave length must remain constant, so:

$$A\lambda = A_o\lambda_o$$

then,

5) $$\frac{A}{A_o} = \frac{\lambda_o}{\lambda}$$

In the stationary medium, the speed of sound, c, is constant so that the wave length depends on frequency according to:

$$\lambda = \frac{2\pi C}{w}$$

then, using Equation (4) for the change in frequency:

6) $$\frac{\lambda_o}{\lambda} = \frac{w}{w_o} = \frac{1}{1 - M \cos \theta}$$

From Equation (3) and (3a):

$$\frac{E}{E_o} = \left(\frac{w}{w_o}\ \frac{A}{A_o}\right)^2$$

And, using Equation (4), (5), and (6), we get:

7) . . . . . $\frac{E}{E_o} = \frac{1}{(1 - M \cos \theta)^4}$

Thus, the change in energy density is determined. The acoustic intensity is the product of the energy density and the speed of sound:

$$I = EC, \text{ So } \frac{I}{I_o} = \frac{E}{E_o}$$

and $$\Delta \text{ SPL} = 10 \text{ Log } \frac{I}{I_o} = 10 \text{ Log } \frac{1}{(1 - M \cos \theta)^4}$$

$$= -40 \text{ Log } (1 - M \cos \theta)$$

NOMENCLATURE

M	Aircraft Mach Number
OASPL	Overall Sound Pressure Level; calculated by summation of sound pressure levels at each 1/3 octave.
PNL	Perceived Noise Level; a calculated, annoyance weighted sound level.
PNLT	Tone corrected PNL
EPNL	Effective Perceived Noise Level; PNL adjusted for both discrete frequencies and time history.
% RH	Ambient atmospheric relative humidity in percent.
Peak PNL	Highest Perceived Noise Level generated, usually referenced to a specific angle from the source.
Peak OASPL	Highest Overall Sound Pressure Level generated, usually referenced to a specific angle from the source.
dB	decible, re: 0.0002 dynes/cm^2
RPM	revolutions per minute
C_{f_g}	Gross Thrust Coefficient
Hz	Hertz (cycles per second)
V_J	Jet Velocity
m	meters
FT/SEC, '/s	feet per second
m/s	meters per second
T_5	Turbine exhaust temperature
T_{T8}	Total exhaust nozzle temperature
V_A	Aircraft velocity
V_R	Relative velocity, V_J-V_A
R	Radius
AFB	Air Force Base

IPS	inches per second
T_o	Ambient dry bulb temperature
P_o	Ambient pressure
P_{T8}/P_o	Exhaust nozzle pressure ratio
Wg	Engine weight flow
PPS	pounds per second.
EPNL-10 log ρ^2A	Normalized EPNL
PNL-10 log ρ^2 A	Normalized PNL
OASPL-10 log ρ^2A	Normalized OASPL
kg/s	kilograms per second
n/m	newtons per meter
$\frac{fD}{V}$	Strouhal Number; a calculated function of frequency, nozzle diameter and jet velocity.
θ	The angle between a straight line from source to microphone and engine centerline; referenced to inlet.
F_E	emitted frequency
F_R	received frequency
SPL	Sound Pressure Level; a level of sound pressure that occurs in a specified frequency range at any instant of time.

REFERENCES

1. Federal Aviation Regulation Volume III Part 36, "Noise Standards: Aircraft Type Certification," Department of Transportation, Federal Aviation Administration, Nov., 1969.

2. Society of Automotive Engineers, Inc., Aerospace Information Report 876, "Jet Noise Prediction," issued 7/10/65.

3. Society of Automotive Engineers, Inc., Aerospace Information Report 923, "Method for Calculating the Attenuation of Aircraft Ground to Ground Noise Propagation During Takeoff and Landing," issued 8/15/66.

4. Society of Automotive Engineers, Inc., Aerospace Recommended Practice 866," Standard Values of Atmospheric Absorption as a Function of Temperature and Humidity for use in Evaluating Aircraft Flyover Noise," issued 8/31/64.

5. Howes, W.L., "Ground Reflection of Jet Noise," NASA TR R-35, 1959.

6. Hoch, R. and Thomas, P. (S.N.E.C.M.A.), "The Effect of Reflections on Jet Sound Spectra," Translation from a paper presented at the First Symposium on Aeronautical Acoustics Organized by A.F.T.A.E. and G.A.L.F., Toulouse, March 6 - 8, 1968.

7. Thomas, P., "An Investigation of Acoustic Wave Interference Due to Reflections, Application to Jet Sound Pressure Spectra," Translation from a paper presented at the A.G.A.R.D. Congress on "Aircraft Engine Noise and Sonic Boom," Saint Louis, May 27-30, 1969.

8. Kraft, R.E., "Acoustic Ground Reflection Correction for Broadband Noise Based on Empirical Determination of Ground Impedence," T.M. 70-815, General Electric Company, Evendale, Ohio, 10/12/70.

9. Society of Automotive Engineers, Inc., Aerospace Recommended Practice 865A, "Definition and Procedure for Computing the Perceived Noise Levels of Aircraft Noise," issued 10/15/64, revised 8/15/69.

10. Morse, P.M. and Ingard, K.V., " Theoretical Acoustics," Chapter 11, McGraw-Hill Book Co., 1969.

REFERENCES (Concluded)

11. Groth, H.W., Samanich, N.E. and Blumenthal, P.Z., "Inflight Thrust Measuring System for Underwing Nacelles Installed on a Modified F106 Aircraft," NASA TMX-2356, 1971.

12. Samanich, N.E. and Chamberlin, R., "Flight Investigation of Installation Effects on a Plug Nozzle Installed on an Underwing Nacelle," NASA TMX-2295, 1971.

13. Groth, H.W., "Nozzle Performance Measurement on Underwing Nacelles of an F-106 Utilizing Calibrated Engines and Load Cells," NASA TMX-67816, 1971.

14. Kobrynski, M., "General Method for Calculating the Sound Pressure Field Emitted by Stationary or Moving Jets," Proceedings of A.F.O.S.R.-U.T.I.A.S. Symposium on Aerodynamic Noise, Toronto, May 1968.

15. Kobrynski, M., "Determination of the Field of Sound Produced by a Jet Aircraft in Motion," NASA TT F-13, 096, National Aeronautics and Space Administration, Washington, D.C., July, 1970.

16. Mangiarotty, R.A. and Turner, B.A., "Wave Radiation Doppler Effect Correction for Motion of a Source, Observer and the Surrounding Medium," Journal of Sound and Vibration, (1967) 6 (1), Pages 110-116.

REPORT DISTRIBUTION LIST

Addressee			Number of Copies
1.	NASA Lewis Research Center 21000 Brookpark Road Cleveland, Ohio 44135 Attention:		
	Report Control Office	MS: 5-5	1
	Library	MS: 60-3	2
	Dr. B. Lubarsky	MS: 3-3	1
	M. A. Beheim	MS: 86-1	26
	N. D. Sanders	MS: 501-5	1
	C. E. Feiler	MS: 501-5	1
	V. H. vonGlahn	MS: 501-5	1
	R. J. Rulis	MS: 501-2	1
	B. J. Clark	MS: 501-2	1
2.	NASA Headquarters 600 Independence Avenue, S. W. Washington, D. C. 20546 Attention:		
	N. F. Rekos (RL)		1
	James J. Kramer (RL)		1
3.	FAA Headquarters 800 Independence Avenue, S. W. Washington, D. C. 20553 Attention:		
	John Powers		1
	W. C. Sperry		1
4.	NASA Scientific & Technical Information Facility Attention: NASA Representative, Box 33 College Park, Maryland 20740		10
5.	NASA Langley Research Center Hampton, Virginia 23365 Attention:		
	Harvey Hubbard	MS: 239	1
	Mark Nichols	MS: 403	1
	I. E. Garrick	MS: 115	1
	D. J. Maglieri	MS: 239	1
6.	NASA Ames Research Center Moffett Field, California 94035 Attention:		
	David Hickey	MS: 221-2	1

Addressee			Number of Copies
7.	NASA Flight Research Center P. O. Box 273 Edwards, California 93523 Attention:		
	Norman McLeod	Room 2100	1
	Don Bellman	Room 2106	1
8.	Office of Secretary of Transportation 800 Independence Avenue, S. W. Washington, D. C. 20590 Attention:		
	Charles Foster	TRT-30	1
9.	Department of Transportation 400 7th Street, S. W. Washington, D. C. 20590 Attention:		
	W. F. Dankhoff	TST-50	1
10.	Naval Air Propulsion Test Center Aeronautical Engine Department Philadelphia, Pennsylvania 19112 Attention:		
	Robert Benham		1
11.	Naval Air Systems Command Washington, D. C. 20360 Attention:		
	Eugene Lichtman	Code Aer 330E	1
12.	Air Force Systems Command Wright-Patterson Air Force Base, Ohio 45433 Aero-Propulsion Laboratory Attention:		
	L. Obery, NASA Representative		1
13.	Headquarters, USAF Wright-Patterson AFB, Ohio 45433 Attention:		
	Zeke Gershon	Building 18	1
14.	Ministry of Technology National Gas Turbine Establishment Pyestock, Farnborough, Hants. England Attention:		
	Michael Neale		1

Addressee	Number of Copies
15. O.N.E.R.A. 92-Chatillon, France Attention: Dr. M. Kobrynski	1
16. Air Research Manufacturing Company 402 South 36th Street Phoenix, Arizona 85034 Attention: R. O. Bullock	1
17. Air Research Manufacturing Company 8951 Sepulveda Boulevard Los Angeles, California 90009 Attention: Linwood Wright	1
18. Allison Division, GMC P. O. Box 894 Indianapolis, Indiana 46206 Attention: L. Corrigan Dept. 8890	1
19. AVCO Corporation Lycoming Division 550 South Main Street Stratford, Connecticut 06497 Attention: David Knoblock	1
20. The Boeing Company 3801 South Oliver Street Whichita, Kansas 67210 Attention: Dean Nelson MS: 16-31	1
21. The Boeing Company Commercial Airplane Division Renton, Washington 89055 Attention: J. V. O'Keefe	1
22. The Boeing Company P. O. Box 3707 Seattle, Washington 98124 Attention: J. Little MS: 73-16	1

Addressee		Number of Copies
23. Bolt, Beranek and Newman, Inc. 15808 Wyandoffe Street Van Nuys, California 91406 Attention: Dr. T. D. Scharton		1
24. Curtiss-Wright Corporation Aeight Aeronautical Woodridge, New Jersey Attention: S. Lombardo		1
25. Douglas Aircraft Division McDonnel-Douglas Corporation 3855 Lakewood Boulevard Long Beach, California 90801 Attention: J. E. Merriman	CI-250	1
26. General Dynamics Corporation Convair Aerospace Division P. O. Box 748 Fort Worth, Texas 76101 Attention: Bob Matteson		1
27. Grumman Aerospace Corporation Bethpage, Long Island New York, 11714 Attention: Russ Goss		1
28. Hawker-Siddeley Aviation Ltd. Hatfield, Hertz. England Attention: E. D. G. Kemp		1
29. Lear Jet Industries, Inc. Aircraft Division Municipal Airport P. O. Box 1280 Wichita, Kansas 67201 Attention: Tom Reichenberger		1

Addressee			Number of Copies
30.	Lockheed Aircraft Corporation P. O. Box 551 Burbank, California 91503 Attention:		
	Harry Drell	Code 61-30	1
31.	Lockheed Georgia Company Marietta, Georgia 30060 Attention:		
	H. S. Sweet	Dept. 72-71	1
32.	Massport Aviation Technical Service Division 470 Atlantic Avenue Boston, Massachusetts 02210 Attention:		
	George Bender, Jr.		1
33.	North American Rockwell Corporation Los Angeles Division International Airport Los Angeles, California 90009 Attention:		
	Leonard Rose		1
34.	Northern Research and Engineering 219 Vassar Street Cambridge, Massachusetts Attention:		
	K. Ginwala		1
35.	Pratt and Whitney Aircraft Division, UAC East Hartford, Connecticut 06108 Attention:		
	C. W. Bristol		1
36.	Pratt and Whitney Aircraft Florida Research and Development Center West Palm Beach, Florida 33402 Attentin:		
	H. D. Stetson		1
37.	Rohr Corporation Riverside, California 92502 Attention:		
	R. Thielman		1

Addressee	Number of Copies
38. Rolls-Royce Limited Aero Engine Division P. O. Box 31 Derby, England Attention: L. G. Dawson	1
39. Rolls-Royce Limited Flight Test Establishment Hucknall, Nottingham, England Attention: J. S. B. Mather Dept. 428F	1
40. Wyle Laboratories 128 Maryland Street El Segundo, California 90245 Attention: Ed Grande	1
41. Brown University Physics Department Providence, Rhode Island Attention: Professor P. J. Westervelt	1
42. Dept. of Engineering and Applied Science University of California, Los Angeles Los Angeles, California 90024 Attention: Dr. W. C. Meecham	1
43. California Institute of Technology Pasadena, California 91109 Attention: Duncan Rannie	1
44. Cornell University Aerospace Engineering Department Ithaca, New York 14850 Attention: W. R. Sears	1
45. Iowa State University Dept. of Mechanical Engineering Ames, Iowa 50010 Attention: George Serovy	1

Addressee	Number of Copies
46. Massachusetts Institute of Technology Cambridge, Massachusetts 02139 Attention: J. L. Kerrebrock	1
47. University of Michigan Aerospace Engineering Department Ann Arbor, Michigan 48103 Attention: W. W. Willmarth	1
48. Princeton University Forrestal Research Center Princeton, New Jersey, 08540 Attention: Professor W. D. Hayes	1
49. Insititue of Sound and Vibration Research The University, Southampton S09 5NH England Attention: John Large	1
50. Syracuse University Mechanical Engineering Department Syracuse, New York 13200 Attention: Professor D. Dosanjh	1
51. University of Toronto Insititue of Aerospace Studies Toronto, Canada Attention: H. S. Ribner	1